THE UNIVERSITY *of* EDINBURGH

This thesis has been submitted in fulfilment of the requirements for a postgraduate degree (e. g. PhD, MPhil, DClinPsychol) at the University of Edinburgh. Please note the following terms and conditions of use:

- This work is protected by copyright and other intellectual property rights, which are retained by the thesis author, unless otherwise stated.
- A copy can be downloaded for personal non-commercial research or study, without prior permission or charge.
- This thesis cannot be reproduced or quoted extensively from without first obtaining permission in writing from the author.
- The content must not be changed in any way or sold commercially in any format or medium without the formal permission of the author.
- When referring to this work, full bibliographic details including the author, title, awarding institution and date of the thesis must be given.

Understanding the heat transfer, pyrolysis and ignition of wildland fuels

Carlos Walker-Ravena

Supervisor: Dr. Rory M. Hadden

A thesis presented for the degree of
Doctor of Philosophy

THE UNIVERSITY *of* EDINBURGH

Edinburgh Fire Research Centre
University of Edinburgh
UK
2021

Contents

Part I
Preface

1.1 Author's Note

Here is presented the work undertaken to address the topic of this PhD project. It is the result of four years thinking long and hard about wildland fuels and their ignition.

I want to dedicate this thesis to the next person who tackles the topic. In making this work, it was my dream to make a guide to the problem and have kept in my mind the question: 'what would I have wanted to know four years ago?'. I hope that the next person can take this work and get a head-start on making the next step in further understanding of the heat transfer, pyrolysis and ignition of wildland fuels.

It goes without saying that I have not conducted this work in a vacuum. I, like everyone else, am a product of my environment and I have been fortunate in my environment over the last four years. I would like to acknowledge every conversation and discussion I've had with my colleagues, whom I now call friends. I couldn't have done it without them (as cliche as that might sound). It is my belief that I did not build this on my own and that every idea shared and discussed has been another brick laid. My advice is to talk it out, as you never know how your ideas might be reflected in someone else.

Lastly, I want to say what the reader probably already knows... research is beautiful work. It is beautiful because it is the repeated attempt to uncover the truths of our environment and consequently our existence - and there is not many endeavours as pure as that. I was very fortunate to have this opportunity to wonder why? and how? and although it has been trying at times I would do it all again, and again, and again.

1.2 Abstract

This work provides an understanding of the heat transfer, pyrolysis and ignition of wildland fuels. To do so the wildland fuel morphology, thermal degradation and flammability were assessed through experimentation and literature review.

The burning of wildland fuels is a complex problem. They have a complex elemental structure, chemistry and bulk structure. The processes leading to the ignition depend on these properties and as such the ignition and consequently the flammability is also complex. In this work, pine needle fuel beds are used as typical wildland fuels.

To understand the role of the different processes leading to ignition of natural fuels a systematic experimental campaign was conducted. This covered both assessment of the differences in fuel chemistry and the structure of natural fuels. This involved evaluating the thermal decomposition using TGA and evaluating the flammability of different wildland fuel bed structures under well-defined heating conditions using a standardised testing apparatus (Fire Propagation Apparatus).

Different fuel chemistries were evaluated using different species of pine needles. The fuel bed structures were manipulated by changing the fuel element length to form low permeability (high solid fraction) and high permeability (low solid fraction) samples. A wide range of solid fractions are studied here compared to previously work - ranging from 0.03 to 0.51. This allows the flammability of wildland fuel beds to be understood as function of the fuel bed structure. Together this allows an assessment to be made of the relative importance of different fuel bed properties in determining the flammability of different fuel beds.

Initially, classical ignition theory is applied to the problem however, due to the large influence of fuel bed structure it is concluded that this approximation is not fit for purpose. Subsequently, a novel framework was employed whereby the ignition processes were interrogated using the experimentally measured sample mass. This involved the superposition of a 1-D heat diffusion equation and the use of thermal degradation chemistry. Using a Genetic Algorithm, the thermochemical model was fit to the experimental dataset. In this way changes to the effective heat transfer properties of fuel bed were analysed as a function of the fuel bed structure.

It was concluded that fuel bed structure has a dominating effect on the material flammability compared to the fuel chemistry and that the ignition of wildland fuels (and therefore porous fuels) requires a consideration of the heated depth as opposed to a surface temperature at ignition - as is assumed in classical ignition theory. The study also showed that the convective flow through a porous fuel has a large impact on determining the flammability as convective cooling of fine elements by entrained air delays the ignition time and may increase the burning rate. This finding is important for the design of future studies of the burning of wildland fuels as the fuel bed structure is generally not considered beyond the level of fuel loading or bulk density.

1.3 Structure

This work tackles the problem by providing understanding of the heat transfer, pyrolysis and ignition of wildland fuels. It does so in the following four parts:

1. Part II - Introduction
2. Part III - Thermal Degradation
3. Part IV - Ignition
4. Part V - Effective Fuel Bed Properties

In Part II, the tools and descriptions needed to understand the problem are presented. These include the mathematical descriptions of heat transfer mechanisms; a differential equation that describes the interaction between said mechanisms; an overview of fire and the nuances of wildfires; and an insight into the variation inherent to wildland fuels. The intention here is that, in order to understand wildland fuels in a fire context, it is necessary to appreciate the transport of energy they are subjected to and in what forms they exist.

In Part III, the material composition and thermal degradation of wildland fuels are presented. This includes understanding the reactions involved in fire; and the different methods used to characterise a material be that by elemental, molecular or proximate analysis. Experimental work is presented that establishes reaction temperatures and the fractions of the material available for each reaction. The intention here is that, although driven by heat energy, a fire requires chemical reactions to initiate and sustain itself.

In Part IV, the ignition of wildland fuel beds is presented. This includes understanding what defines ignition; how it occurs in solids; the differences involved when considering a porous fuel like wildland fuels; the approaches followed in previous work. Experimental work is presented that establishes the changes in flammability and burning as the fuel bed changes. The intention here is that, because wildland fuels are porous fuels, they cannot be understood solely in terms of their material properties. They do not exist as single fuel elements but as collections of said elements. As such it is necessary to understand the problem as a function of fuel structure.

In Part V, the a method for interrogating the ignition of wildland fuels is presented. This includes the combination of heat transfer and thermal degradation; the use of a genetic algorithm; and the fitting of experimental data. The intention here is that temperatures of a porous fuel cannot be measured experimentally with a satisfactory degree of certainty. As such the mass is used as a means to understand the temperature distribution of the effective solid. In this way quantification of the changes due to fuel bed structure can be made.

Nomenclature

Symbols

α	Thermal Diffusivity
Δ	Change in...
δ_x	Non-Dimensional Distance
ϕ	Void Fraction
ρ	Density
σ	Stefan-Boltzman Coefficient
τ	Non-Dimensional Time
θ	Temperature Difference from Reference
ε	Emissivity
φ	Angle
A	Area
a	Absorptivity
A_p	Mean Projected Area of Randomly Orientated Particles
c	Specific Heat Capacity
d	Mean Equivalent Diameter of Element
E	Radiation
e	Solid Fraction
h	Heat Loss Coefficient
k	Conductivity
L	Length of Individual Element
m	Mass
N_p	Number of Elements
q	Heat
R	Residual
T	Temperature
t	Time
t_c	Characteristic Time
V_P	Volume of All Elements
V_p	Volume of Individual Element
V_s	Volume of Sample
x	Distance

Subscripts

0	Initial
∞	Free Flowing Fluid
A	Constant
B	Constant
c	Convection
$conv$	Convection
e	Emitted
exp	Experiment
G	Generated
inc	Incident
$mean$	Mean
$model$	Model
r	Radiation
rad	Radiation
s	Surface
T	Total

Superscripts

$'''$	Per Volume
$''$	Per Area
$\dot{}$	Rate
$\tilde{}$	Garg Model Coefficient

Symbols Related to the Solution of Partial Differential Equations

$\mathcal{L}$	Laplace Operator
$A(s)$	General Solution Coefficient
$B(s)$	General Solution Coefficient
$F(s)$	Laplace Transform of f(t)
$f(t)$	General Function in time
H	Simplification Coefficient
s	Complex Number Frequency Parameter
Z	Simplification Coefficient

Part II
Introduction

Firstly, the tools and descriptions needed to understand the problem must be established. These include the definition of a wildfire and its drivers; mathematical descriptions of heat transfer mechanisms; a differential equation that describes the interaction between said mechanisms; an overview of fire and the nuances of wildfires; and an insight into the variation inherent to wildland fuels. The intention here is that, in order to understand wildland fuels in a fire context, it is necessary to appreciate the transport of energy they are subjected to and in what forms they exist.

2.1 Problem Statement

2.1.1 Wildfires - A Social-Ecological Disturbance

Wildfires are a natural phenomenon which have been part of the Earth's system for millions of years [1]. Wildfires are fires that occur in the natural environment and have vegetation as their fuel. Fire is the manifestation of the combustion process and is the result of a combination of physical phenomena. The initiation of this process is the ignition and this occurs under a suitable combination of heat, oxygen and fuel. The phenomena that underpin ignition, and the resulting fire behaviour, can be described using heat transfer, fluid mechanics and chemistry. By understanding the characteristics that influence the physics of these phenomena, we can gain a better understanding of the ignition and fire behaviour which we can then use to develop strategies to better manage the hazard posed by wildfires.

In recent times, wildfires are reported to be larger and more frequent as a consequence of the impact on humans being both larger and more frequent [2][3]. An increase in impact implies that the hazard and the probability of the hazard, affecting humans, has increased. It is the role for fire safety engineering to protect people, property and the environment and therefore, as the impact on humans has increased so has the remit of Fire Safety Engineering in the wildfire space. To manage the hazards brought on by wildfires it is important to establish its drivers and how we can interact with them. To do this we must first define what a wildfire is.

Although wildfires are a natural phenomena that cause hazards, it would be an oversimplification to define them as natural hazards. Wildfires occur in nature but are also induced by human activity [4][5]; that is to say, they are not always unavoidable acts of nature such as other natural hazards (earthquakes, hurricanes etc), quite the contrary, the interplay between natural components, socio-economic and political drivers means that humans, as sentient actors on the landscape, influence wildfire occurrence [6]. That is to say, the actions of society have consequences in regard to wildfires, and its definition should reflect this. Furthermore, the use of hazard implies that all wildfires are damaging. This disregards the beneficial role wildfires have in maintaining the ecological integrity of several ecosystems. Instead, the definition of wildfires as a social-ecological disturbance [6] best encapsulates its drivers and impacts. Thus, reflecting its human influence, its occurrence in the landscape and its capability for positive and negative impact.

As a long-standing disturbance, wildfire has led to adaptation of vegetation in fire-prone ecosystems. These include characteristics such as thick bark, serotiny, branch shedding, a juvenile grass stage and the capability to re-sprout [1]. Moreover, there are those who suggest that the flammability of some species is due to the evolutionary pressures present in fire prone environments [7]. This is because the characteristics of vegetation influence the drivers of fire and therefore, alter the fire behaviour. The implication is that plants favour characteristics that influence fire behaviour to their advantage. By understanding the influence that vegetative fuel has on fire behaviour, we can link the fuel with wildfire hazard and its probability of occurrence.

2.1.2 Contributing factors to wildfire hazard and fire risk

Wildfire hazard and probability can be summarised as changes in fire risk. To understand the drivers of fire risk we must establish what the basic requirements for a wildfire to occur are [8]:

1. Environmental conditions that favour fire.
2. Fuel available to burn and sustain fire spread.
3. Sources of ignition.

With these in mind, drivers of wildfire are stipulated as hotter/drier climate, tree dieback, land cover/use, and fire exclusion. These together form a positive feedback loop that further potential for wildfires to occur [9]. The interaction of the drivers on each of the basic requirements will be described in the following.

Environmental conditions are determined by climate and weather. Climate is the long-term weather conditions of a geographical area. The climate is changing as a result of the climate crisis which in itself is driven by human influence [10]. Climate change may impact on weather patterns [11] and as such can increase the potential for environmental conditions that encourage wildfires [12]. For example, hot, dry conditions cause fuels to dry out and therefore become easier to ignite. On the other hand, wet conditions can cause increased plant growth and therefore increased fuel availability which increases the potential fire once ignited. Once ignited, weather also plays a major role in fire spread, through changes to the combustion process and therefore that cause an increase in heat transfer to surrounding unburnt fuel which in turn facilitates the spread of the wildfire[13].

Therefore, weather affects the probability of ignition of a wildfires and changes the fire dynamics of it once ignited, altering the hazard. Moreover, changes in climate will consequently cause wildfires to occur in areas previously unaffected as the environmental conditions, in those geographical areas, have changed to promote wildfire. These areas may not have the capabilities to cope with these events and therefore, agency response will have to adapt in parallel to the changing fire risk [14]. By understanding the conditions that promote wildfires, these agencies can adapt in an informed way. This means understanding the risk imposed on the landscape due to the environmental conditions as well as how to manage the risk through alteration to the fuel conditions and sources of ignition.

Weather is not the only component influencing fire risk [12]. This is because wildfire occurrence is driven by the amount of vegetation available to burn, followed by hot, dry conditions [15]. Therefore, fuel availability determines fire risk; land cover and use contribute to this availability as well as the potential sources of ignition.

A 'natural' change in land cover may be tree dieback. This happens when vegetation dies and remains on the landscape. This can be due to insects or changes in climate that the vegetation cannot sustain. The presence of dead, dry vegetation changes what fuel is available and where it is distributed, therefore, altering the probability of ignition and the hazard once ignited – the fire risk. Moreover, changes to the land use and expansion of the Wildland-Urban Interface (WUI) are human factors that change the land cover and consequently, create potential for ignitions and damages. For example, the western United States has had a 60% expansion, of the WUI, since 1970 and it is predominantly here where the fire severity has been higher [16]. Furthermore, as humans have manipulated the landscape, the amount of managed land has increased. Land use change will change the fire risk posed by it. When managed land is abandoned, vegetation that would have previously been managed will accumulate therefore, increasing the available fuel on the landscape and potential for wildfires. As such, land cover and use is linked to fuel availability and ignition sources, both of which are important factors in determining wildfire risk [17].

The way in which land is managed affects the occurrence of wildfires as it changes the fuel available. Fire exclusion is a management technique that suppresses any fire on the landscape as a means to mitigate fire risk. It requires the application of an ideology that the hazard from fire is so high that any fire on the landscape is unacceptable. Consequently, understanding the relationship between fire behaviour and fuel availability does not need to be considered, as within this ideology, it is assumed all fire will be suppressed. However, suppression artificially

increases fuel loads in the landscape [18] and ultimately only provides a short term solution. In the long term, the hazard increases due to this increased fuel load [19]. As the hazard increases, so does the cost of fire exclusion. Ultimately, wildfires occur that are beyond the capability of the emergency services and disasters become inevitable. Therefore, fire suppression is not a sustainable practice as it compounds the problem. In addition, fire suppression neglects the fundamental role that fire has in sustaining biodiversity and ecosystem health [20]. Rather than conserving the landscape with fire exclusion, it would be more beneficial to preserve the natural phenomenon of wildfires. By utilising wildfires, the fuel availability can be managed which will in turn control the intensity of future wildfires. To achieve this, it requires developing an understanding of the relationship between fuel availability and fire behaviour.

2.1.3 Combating Wildfire Risk through Improvement of Physical Understanding of Risk Drivers

An alternative to fire suppression, is to instead use fire as a land management tool, this may be through prescribed burning and management of active wildfires. These practices acknowledges the positive impact fire can have on the landscape and may be the means to combat the drivers of wildfire risk. During prescribed burning, the conditions can be chosen and so the outcome of a fire can be used to the advantage of land managers [21]. However, in order to engineer wildfires in this way, we must understand how fire behaviour is affected by both environmental conditions and fuel availability. As ecosystems reflect the changes brought on by the climate crisis, inevitably experiential knowledge is challenged [21]. Instead an understanding of the physics principles underpinning wildfires is essential as these are flexible enough to account for the changes in conditions. That is to say, a physics based approach allows for flexibility in understanding the fire landscape which is important as the global fire risk changes both temporally and spatially.

The effects of environmental conditions are well documented [22][23][24][25][26][27][28][29] and so, in this work, the focus will instead be on the effect of fuel availability. Whereas, environmental conditions cannot be easily influenced, fuel availability can be managed. Hence, in order to be proactive rather than reactive in wildfire management, it would be beneficial to understand how fuel availability affects fire behaviour as we can manage this condition and as a consequence manage wildfires.

Fuel availability describes what fuel is available and the quantity of it. What fuel is available describes the fuel chemistry and the dimensions of individual components which in turn determine the fuel bed structure. Plant chemistry is dynamic and changes depending on multiple factors although it can be generalised/bounded. To this end, chemistry has a secondary effect compared to fuel bed structure [18] due to the fact that fuel bed structure is less likely to change significantly with time as it may be the case with plant chemistry.

Vegetative fuel is often arranged in a fuel bed structure made up of individual components. The quantity of fuel determines not only the mass but also the structure of the fuel. It is important to consider the fuel bed, rather than individual plant components, in understanding flammability [30], as descriptions of the flammability of individual plant components alone do not scale to fire behaviour [31]. Nevertheless, the individual components will determine how the bed will be structured. Hence, it is important to understand the fuel bed structures that result from characteristics of the individual plant components and how the flammability of these fuel beds change, as the characteristics of these individual components will vary not only across and within a species but also across environmental conditions [32]. In this way, environmental conditions affect fuel availability and the need to understand how fuel availability affects fire behaviour is underlined.

Previously, the effects of fuel availability on fire behaviour have been captured by describing the fuel bed structure using the packing ratio [33]. However, this work was supported by experiments using artificial fuel (excelsior, a type of wood shaving). Instead the work described in the following sections will focus on natural fuels, such as pine needles. The individual fuel elements will be cut to different sizes to generate an array of fuel bed structures with the same plant chemistry. The effects of the fuel bed structure on the physical parameters controlling

the heat transfer process can be found by analysing the ignition process,

Hence, to summarise, wildfires are a social-ecological disturbance which society directly influences and which in turn impacts both on society and nature. Due to our influence, there is a responsibility to ensure that we do not exacerbate the negative effects of wildfire. To do so, we must understand that wildfire is driven by both environmental conditions and fuel availability. We cannot effectively control environmental conditions, however, the fuel availability can be managed. One method of managing the fuel, is to consider fire as a tool, which can be engineered, and to actively introduce it onto the landscape, under conditions that are within the capabilities of the emergency services. In this way, the fire can alter the fuel availability in a controlled way and the landscape can be managed. In order to achieve this, we must understand how the fuel availability affects the fire behaviour.

The aim of this work is to investigate the influence of different fuel structures on flammability. This will be achieved by describing the physical phenomena leading to ignition with heat transfer, and analysing how the parameters that control the physics change with different fuel bed structures.

2.2 Heat Transfer

The transport of heat energy occurs due to certain mechanisms. Heat transfer is a description of the mechanisms that allow heat to change in time and in space. The mechanisms are conduction, convection, radiation. Heat transfer is used in conjunction with conservation of energy to describe the changes in energy of a system. Mass can store energy and chemical reactions can create or use up energy. Systems can be modelled by using the conservation of energy law and the descriptors of these mechanisms.

2.2.1 Descriptors of Heat Transfer Mechanisms

2.2.1.1 Conduction

Conduction is the transfer of energy from more energetic to less energetic particles of a substance due to interactions between the particles [34]. It is described by Fourier's law:

$$q'' = -k\frac{dT}{dx} \tag{1}$$

2.2.1.2 Convection

Convection is the transfer of energy, from a fluid to another phase, due to both the random molecular motion (diffusion) and bulk macroscopic motion of fluid (advection) [34]. It is described by Newton's law of cooling:

$$q''_{conv} = h_c(T_s - T_\infty) \tag{2}$$

2.2.1.3 Radiation

Thermal radiation is energy emitted by matter at non-zero temperatures. A surface can both emit and absorb radiation to and from the surroundings [34]. The net radiation from a surface is hence:

$$q''_{rad} = E_{emitted} - E_{absorbed} \tag{3}$$

Assuming the surface is a grey body (i.e. its absorbtivity = emissivity), radiation is described by the Stefan-Boltzman law:

$$q''_{rad} = \varepsilon\sigma(T_s^4 - T_\infty^4) \tag{4}$$

2.2.1.4 Energy Concentration

Energy concentration or heat stored is the amount of energy inherent to matter at a given temperature. That is to say that is is a total internal energy in a system [35]. It is approximated using the specific heat capacity:

$$q''' = c\rho T \tag{5}$$

2.2.2 Conduction in a 1D Uniform Rod

A canonical example of a system energy model is heat conduction in an one-dimensional uniform rod [36]. A schematic of the system is shown in Figure 1.

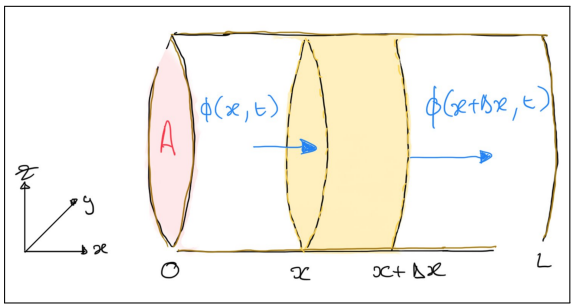

Figure 1: Schematic of uniform rod.

Creating an energy balance:

Rate of change of heat energy in time	+	Heat energy flowing across boundaries per unit time	=	Heat energy generated per unit time

(6)

Focusing on slice of the cylinder and rearranging in terms of the rate of change of heat energy this is written algebraically as:

$$\frac{\partial}{\partial t}[q'''(x,t)A\Delta x] = A(q''(x,t) - q''(x+\Delta x,t)) + q'''_G(x,t)A\Delta x \tag{7}$$

Dividing by $A\Delta x$:

$$\frac{\partial q'''(x,t)}{\partial t} = \frac{(q''(x,t) - q''(x+\Delta x,t))}{\Delta x} + q'''_G(x,t) \tag{8}$$

Taking the limit of $\Delta x \to 0$:

$$\frac{\partial q'''(x,t)}{\partial t} = -\frac{\partial q''(x,t)}{\partial x} + q'''_G(x,t) \tag{9}$$

The heat is related to the temperature (as in Section 2.2.1):

$$q'''(x,t) = c(x)\rho(x)T(x,t) \tag{10}$$

$$q''(x,t) = -k\frac{\partial T(x,t)}{\partial x} \tag{11}$$

$$q'''_G(x,t) = 0 \tag{12}$$

Substituting and rearranging and defining the thermal diffusivity $\alpha = \frac{k}{c\rho}$:

$$\frac{\partial T(x,t)}{\partial t} = \frac{k}{c\rho}\frac{\partial^2 T(x,t)}{\partial x^2} = \alpha\frac{\partial^2 T(x,t)}{\partial x^2} \tag{13}$$

2.3 Heat Diffusion Equation

Solution of the equation in Section 2.2 allows for the temperature (and therefore the energy) to be described in both time and space. This is necessary because the majority of problems in fire are transient, that is to say they change over time.

2.3.1 Semi-Infinite Solution

The model in Section 2.2 can be solved by applying boundary conditions. A common approximation used is that of the semi-infinite solid.

$$\frac{\partial T(x,t)}{\partial t} = \alpha \frac{\partial^2 T(x,t)}{\partial x^2} \tag{14}$$

To solve this an intial condition and two boundary conditions are needed. The initial condition is:

$$T(x,0) = T_0 \tag{15}$$

For the top boundary an energy balance is constructed:

$$-k\frac{\partial T(0,t)}{\partial t} = a\dot{q}''_e(t) - h_c[T(0,t) - T_\infty] - \epsilon\sigma[T(0,t)^4 - T_\infty^4] \tag{16}$$

This energy balance, from left to right, states that the energy conducted into the surface is equal to the heat absorbed on the surface, from a radiative source, less the heat lost from the surface due to convection, less the heat lost from the surface due to radiation plus the heat absorbed from the environment due to radiation.

This energy balance is non-linear and complicates the solution. So a simplification is made where the convective and radiative terms are combined and represented by a total heat transfer coefficient. The incident heat is defined as the heat absorbed by the surface, from a radiative source $\dot{q}''_{inc}(t) = a\dot{q}''_e(t)$:

$$-k\frac{\partial T(0,t)}{\partial t} = \dot{q}''_{inc}(t) - h_T[T(0,t) - T_\infty] \tag{17}$$

Assuming that the material is initially at thermal equilibrium with the environment then, $T_0 = T_\infty$. This results in the top surface boundary condition being:

$$-k\frac{\partial T(0,t)}{\partial t} = \dot{q}''_{inc}(t) - h_T[T(0,t) - T_0] \tag{18}$$

The back face boundary condition is simplified by assuming a semi-infinite solid. That is to say that $x \to \infty$ and so:

$$\frac{\partial T(\infty,t)}{\partial x} = 0 \tag{19}$$

2.3.1.1 Change in Variable

By substituting $\theta(x,t) = T(x,t) - T_0$, the set of equations can be rewritten as:

$$\frac{\partial \theta(x,t)}{\partial t} = \alpha \frac{\partial^2 \theta(x,t)}{\partial x^2} \tag{20}$$

$$\text{IC} \quad \theta(x,0) = 0, \qquad \theta\epsilon[0,\infty) \tag{21}$$

$$\text{BC} \quad \frac{\partial \theta(\infty,t)}{\partial x} = 0, \qquad x\epsilon[0,\infty) \tag{22}$$

$$\text{BC} \quad \frac{\partial \theta(0,t)}{\partial x} = \frac{h_T}{k}\theta(0,t) - \frac{\dot{q}''_{inc}(t)}{k} \qquad t\epsilon[0,\infty) \tag{23}$$

2.3.1.2 Characteristic Temperature

Using a constant heat flux, a further simplification can be made by establishing a characteristic temperature:

$$T_c = \frac{\dot{q}''_{inc}}{h_T} \tag{24}$$

Substitution in the surface boundary condition:

$$\frac{\partial\theta(0,t)}{\partial x} = \frac{h_T}{k}\left(\theta(0,t) - T_c\right) \tag{25}$$

2.3.1.3 Laplace Transform

This set of equations can be solved using the Laplace transform. The Laplace transform of a function, $f(t)$, for $t \geq 0$ can be defined as:

$$F(s) = \mathcal{L}\{f(t)\} = \int_0^\infty f(t)e^{-st}dt \tag{26}$$

Where s is a complex variable, $s = a + ib$. Applying the Laplace transform to equation 20, using the notation $\mathcal{L}\{\theta(x,t)\} = \Theta(x,s)$:

$$s\Theta(x,s) - \theta(x,0) = \alpha\frac{\partial^2\Theta(x,s)}{\partial x^2} \tag{27}$$

Substitution of the initial condition, $\theta(x,0) = 0$, and re-arranging:

$$\frac{\partial^2\Theta(x,s)}{\partial x^2} - \frac{s}{\alpha}\Theta(x,s) = 0 \tag{28}$$

2.3.1.4 General Solution

This is linear, homogenous second order ordinary differential equation. The general solution to which is:

$$\Theta(x,s) = A(s)e^{-\sqrt{\frac{s}{\alpha}}x} + B(s)e^{\sqrt{\frac{s}{\alpha}}x} \tag{29}$$

As $x\epsilon[0,\infty)$ and $\Theta(x,s)$ is finite then $B(s) = 0$. Hence the general solution to the ordinary differential equation is:

$$\Theta(x,s) = A(s)e^{-\sqrt{\frac{s}{\alpha}}x} \tag{30}$$

Differentiating the general solution:

$$\frac{\partial\Theta}{\partial x} = -\sqrt{\frac{s}{\alpha}}A(s)e^{-\sqrt{\frac{s}{\alpha}}x} \tag{31}$$

2.3.1.5 Particular Solution

The particular solution is found by applying the boundary conditions. Applying the Laplace transform to the surface boundary condition:

$$\frac{\partial\Theta(0,s)}{\partial x} = \frac{h_T}{k}\left(\Theta(0,s) - \frac{T_c}{s}\right) \tag{32}$$

Setting $x = 0$ in the general solution,

$$\Theta(0,s) = A(s) \tag{33}$$

and comparing to the surface boundary condition:

$$\frac{\partial\Theta(0,s)}{\partial x} = -\sqrt{\frac{s}{\alpha}}A(s) = \frac{h_T}{k}\left(A(s) - \frac{T_c}{s}\right) \tag{34}$$

Re-arranging:

$$A(s) = \frac{T_c}{s(1 + \frac{\sqrt{k\rho c}}{h_T}\sqrt{s})} \tag{35}$$

Hence, the particular solution:

$$\Theta(x,s) = T_c \frac{1}{s(1 + \frac{\sqrt{k\rho c}}{h_T}\sqrt{s})} e^{-\sqrt{\frac{s}{\alpha}}x} \tag{36}$$

Defining $H = \frac{x}{\sqrt{\alpha}}$ and $Z = \frac{h_T}{\sqrt{k\rho c}}$ this can be rewritten as:

$$\Theta(x,s) = T_c \frac{1}{s(1 + \frac{1}{Z}\sqrt{s})} e^{-H\sqrt{s}} \tag{37}$$

2.3.1.6 Inverse Laplace Transform

The solution for $\theta(x,t)$ can be found by taking the inverse Laplace transform. Re-arranging the equation:

$$\theta(x,t) = T_c \mathcal{L}^{-1}\left\{ \frac{Z e^{-H\sqrt{s}}}{s(Z + \sqrt{s})} \right\} \tag{38}$$

The inverse transform given by Luikov (item 56) [37] gives the solution as:

$$\theta(x,t) = T_c \left[erfc\left(\frac{H}{2\sqrt{t}} \right) - e^{(ZH + Z^2 t)} erfc\left(\frac{H}{2\sqrt{t}} + Z\sqrt{t} \right) \right] \tag{39}$$

By defining the following non-dimensional quantities:

$$\delta_x = \frac{x}{\sqrt{4\alpha t}} \tag{40}$$

$$t_c = \frac{k\rho c}{h_T^2} \tag{41}$$

$$\tau = \frac{t}{t_c} = \frac{h_T^2 t}{k\rho c} \tag{42}$$

The solution can then be written:

$$\theta(x,t) = \frac{\dot{q}''_{inc}}{h_T} \left[erfc(\delta_x) - e^{(2\delta_x\sqrt{\tau} + \tau)} erfc(\sqrt{\tau} + \delta_x) \right] \tag{43}$$

Or in other words the temperature of the solid is controlled by the heat transfer parameters of the system:

$$T(x,t) = \frac{a\dot{q}''_e}{h_T} \left[erfc(\delta_x) - e^{(2\delta_x\sqrt{\tau} + \tau)} erfc(\sqrt{\tau} + \delta_x) \right] + T_0 \tag{44}$$

2.4 Fire

Fire safety engineering is concerned with a set of processes that result in combustion and a sustained diffusion flame. The sustained flame is a mixture of oxygen and gaseous fuel that must mix and ignite before burning. In the case of solid fuel, the flame necessitates its pyrolysis into a gaseous fuel. the anchor for the flame is the region from which gaseous fuel is generated by the pyrolysis reaction. As the pyrolysing region spreads across the solid fuel, a series of ignitions of the gaseous fuel are perceived as flame spread. This is because the flame heats up the surrounding material, causing more gaseous fuel to be produced and the fire to spread. As the material continues to burn, the amount of fuel available, in the solid, decreases to the point where the flame cannot be sustained and the flame is extinguished. Fire is therefore a collection of interconnected processes rather than a single process and can be visualised as in Figure 2.

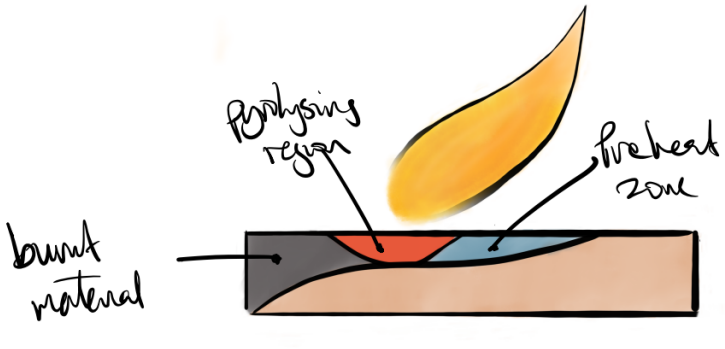

Figure 2: Illustration of flame spread over a solid surface. The brown region represents virgin material whereas the red region represents the material currently producing enough flammable gases to fuel the flame. The blue region represents the material being heated by the flame which will in turn become red once producing enough flammable gases to fuel the flame. The black region is material which has been spent and so it can no longer fuel the flame

2.4.1 Wildfires

Wildfires are fires that occur in the natural environment. Even more so than fires in the built environment these are subjected to an increased uncertainty principally in length and timescales. Weather and topography are key parameters in wildfires [13][27]. The wind and moisture content of the fuel are both influenced by the weather, which modifies the fuel's physical characteristics and the environmental conditions, impacting how the fire behaves. Additionally, because weather affects plant growth, it also plays a role in the fuel's natural variation [38]. Therefore, variation in the weather leads to both variation in the environmental conditions and fuel availability, which impacts the fire behaviour. Topography is also important as it dictates spatially the way in which the flame can heat and ignite subsequent fuel. Furthermore topography can locally interact with the weather, such as in the case of canyons, causing particular fire behaviour [39]. However, these effects are not considered in the present work and the focus will instead be on the effects of the fuel bed structure.

Wildfires can be classed as surface fires or canopy fires depending on the location of the fuel. Where the surface fires occur on the forest floor and canopy fires in the forest overstorey. Examples of surface fires are shown in Figure 4. A wildfire can transition between a surface and a canopy fire by ladder fuels or firebrands. This is because ladder fuels form a connection between the forest floor and the tree canopy [40] and firebrands are particles that are transported, from a fire, to a remote location where they cause a new ignition to occur [41]. Figure 3a, illustrates how the fuel density might vary spatially with more open porous fuels in

the canopy and less porous fuels on the forest floor. Whilst Figure 3b and c show examples of ecosystems with pine trees.

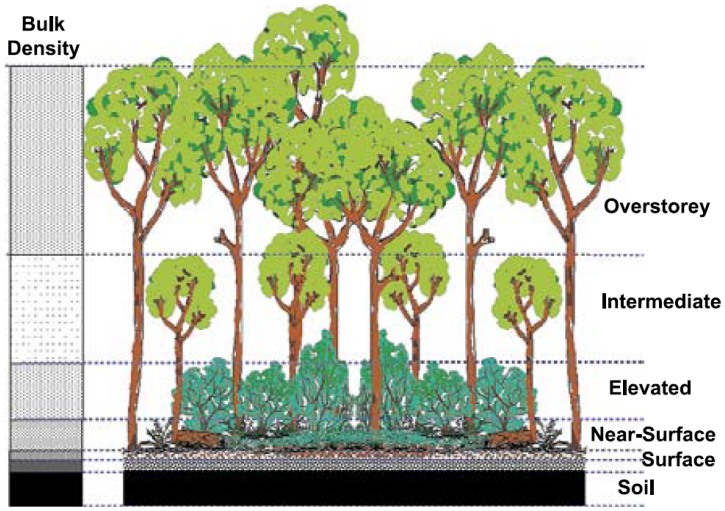

(a) Illustration of fuel density spatial variation, with more open porous fuels in the canopy and less porous fuels on the forest floor. Extracted from Gould et al.[42].

(b) Pinus Halepensis ecosystem in Eastern Spain (Alicante)

(c) Pinus Rigida ecosystem in Eastern USA (New Jersey)

Figure 3: Examples of the different fuel strata involved in wildfires.

(a) Experimental burn in Pinus Rigida ecosystem in Eastern USA (New Jersey)

(b) Management burn in Pinus Rigida ecosystem in Eastern USA (New Jersey)

(c) Management burn in a heathland ecosystem in Scotland

Figure 4: Examples of flame spread in wildfires.

Figure 5: 2015 Tree Cover composite image made using Google Maps and Sexton et al.[43].

2.5 Natural Fuels

Through the lens of fire safety engineering, vegetation are reduced to fuels. Nevertheless, the context of these fuels is important as, contrary to the majority of fuels in the built environment, wildland fuels can be porous. This is because wildland fuel beds are collections of individual fuel elements arranged in a fuel structure. This fuel structure is determined by the fuel loading and the fuel element morphology. As such there is a spectrum of fuel beds, ranging from an open porous bed to a closed solid-like bed. In order to understand wildland fuels it is necessary to understand where they exist and the bounds of their morphology.

2.5.1 Global Tree Cover

There are many distinct ecosystems where wildfires can occur, including savannas, grasslands, and heathlands. Forest fires, also referred to as wildfires that start in forests or woodlands, are a notorious example. These happen in habitats where trees predominate and, due to the fuel distribution in this ecosystem, wildfires might be surface or canopy fires.

Figure 5, shows that all continents used for human habitation are covered in trees. Under the correct conditions, wildfires might can anywhere there is vegetation and therefore the potential for wildfire occurrence is global. The largest risks are often at the Wildland-Urban Interface as it is here that a wildfire can cause the most damage to society and it is often here that fatal disasters occur. However, the presence of humans not only increases the potential damage but also the increases the frequency of occurrence. This is because their increased occurrence is often attributed to the expansion of the Wildland-Urban Interface, climate change and mismanagement of property [3].

One approach to mitigate human-caused wildfire catastrophes is to incorporate fire safety engineering into the wildfire response. This is appropriate as the remit of fire safety engineering is the protection of people, property and environment. However, fire safety engineering was born out of the built environment and is not wildfire science. Therefore, steps must be taken to understand the differences when considering natural fuels over engineered materials. The goal of this work is to understand natural fuels and their response to fire, and this will be done using vegetation such as pine needles.

2.5.2 Pinus Distribution

Pine needles are the leaves of the pine tree. Pine trees are evergreen coniferous that originated 150 million years ago during the mid-Mezoic Era. They are distributed across the northern

hemisphere due to their presence on the Laurasian continent which subsequently broke into North America, Europe and Asia [44]. They belong to the pinus genus which is divided into two subgenera - Pinus and Strobus. These are known as hard pines and soft pines. The global distribution of the pinus genus is shown in Figure 6. Whereas those species tested in this work are shown in Figure 7.

Figure 6: Global Distribution of Pinus (Pine Trees) Genus. Extracted from Little et al. [45].

2.5.3 Pine needle Morphology

Pine needle morphology determines the fuel bed structure. Pine trees exhibit plasticity, this means they are adaptable to their environment. One adaptation is changes in pine needle morphology. This plasticity is what facilitates the extension of the Pinus genus across the northern hemisphere. The extent of the genus is illustrated in Figure 6.

2.5.3.1 Genus and Species Plasticity

The morphology of a pine needle can vary within the genus and within a species. The variation within the genus can be see in Figure 8. This shows the pine needle morphology of 103 species plotted against the average latitude of each species. In general, morphological trends follow subgenera (Pinus and Strobus). Furthermore, as the latitude changes, the needle length is subject to larger variations than the needle width. The latitude can be taken as a climatic pseudo parameter. This suggests that the needle width is a species dominated quantity whereas the needle length is more heavily influenced by climate with longer needles occurring at lower latitudes [48].

On the other hand, Figure 9 shows that pine needle morphology can vary within a species due to the environmental conditions in which they are produced. These data indicate that main drivers of the needle length is environmental conditions whilst the needle width is predetermined by the species.

The pine needles tested in this thesis come from latitudes between 30-45°. Pine species in these latitudes have a varied morphology, as seen in Figure 8. Additionally, Figure 9 illustrates

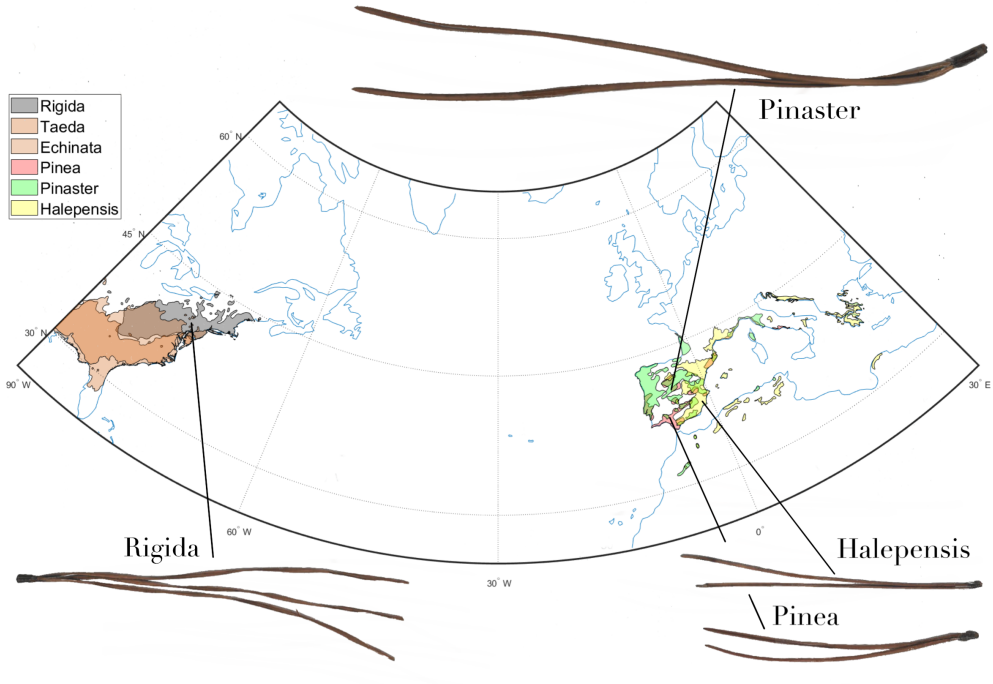

Figure 7: Distribution of main Pine needles tested in the present work. Extracted from [46] [47]

that morphology is not only influenced by species but also by environmental and climatic factors. As pine needle fuel beds are composed of individual pine needles, it follows that pine needle fuel beds are determined by the morphology of individual pine needles. Hence, to understand pine needle fuel beds varied pine needle morphology should be considered.

2.5.4 Fuel Bed

Figure 10 shows how collections of individual fuel elements (pine needles) transition to a fuel bed as the density (or fuel load) increases. It is clear that there is a spectrum of fuel beds, ranging from individual elements to a porous open fuel bed to a dense solid-like bed. It is this transition from a discontinuous to a continuous fuel which is of interest as it leads to a change in the phenomena underpinning a resultant fire. These changes occur as for example, an open porous fuel bed will be more susceptible convective flows and radiation will penetrate further into the bed than in the case of a dense solid-like bed.

In nature, the fuel bed density will change over time as a function of the longevity of the pine needles - that is to say how frequently does are leaves shed? Other factors such as rot will also have a role to play in affecting the fuel bed density. This reinforces the idea that wildland fuels cannot be considered in material terms but must be analysed at various fuel structures. One way that this could be simplified would be to understand the bounds of the different fuel structure regimes. In lay-mans' terms this would mean knowing: *when is a clump, a clump?*

2.5.5 Microscopic Pine Needle Structure

Pine needles are a functional part of a pine tree. Scanning electron microscope images are presented here to illustrate the inhomogenity and complexity of the interior of a pine needle.

Qualitatively, Figure 11,12,13,14 and 15 shows that a pine needle is not a material but it is a composite. This is due to its functionality whereby different functions require different plant structures. Plants are complex. The question to ask then is, what level of simplicity captures this complexity satisfactorily?

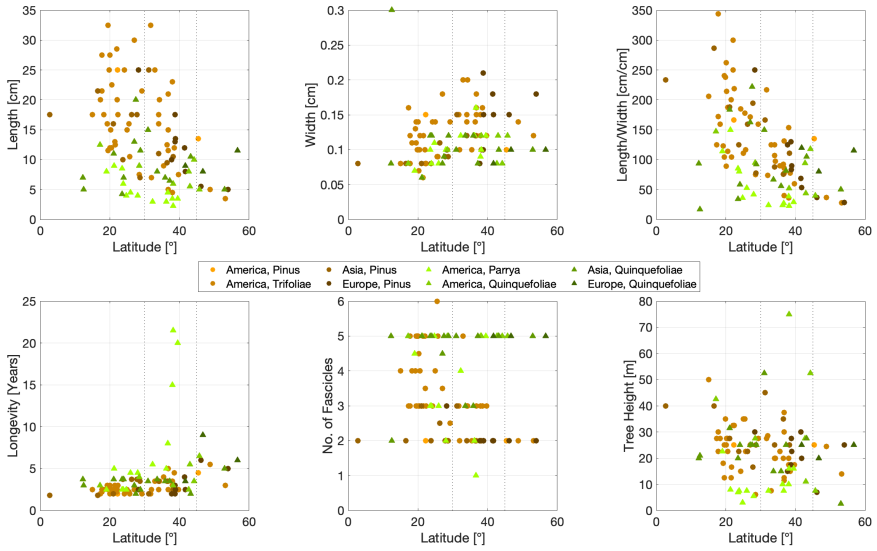

Figure 8: Variation of Pinus species needle morphology versus average latitude of natural distribuition range. Vertical lines show the bounds of the spatial distribution of the pine needles tested in this study. The yellow tones are pines belonging to Pinus Pinus. The green tones are pines belonging to Pinus Strobus. Extracted from Nobis et al. [48].

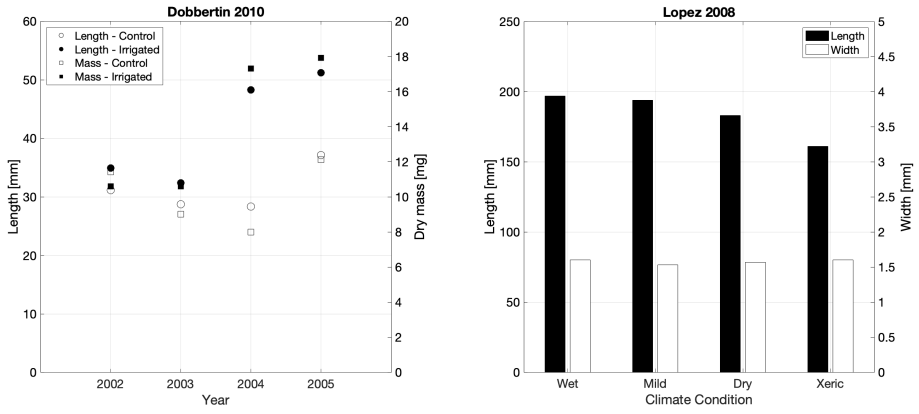

Figure 9: Left: Variation of Pinus Sylvestris needle morphology due to changes in irrigation. Extracted from Dobbertin et al. [49]. Right: Variation of Pinus Canariensis needle morphology due to differences in climate. Extracted from Lopez et al. [50].

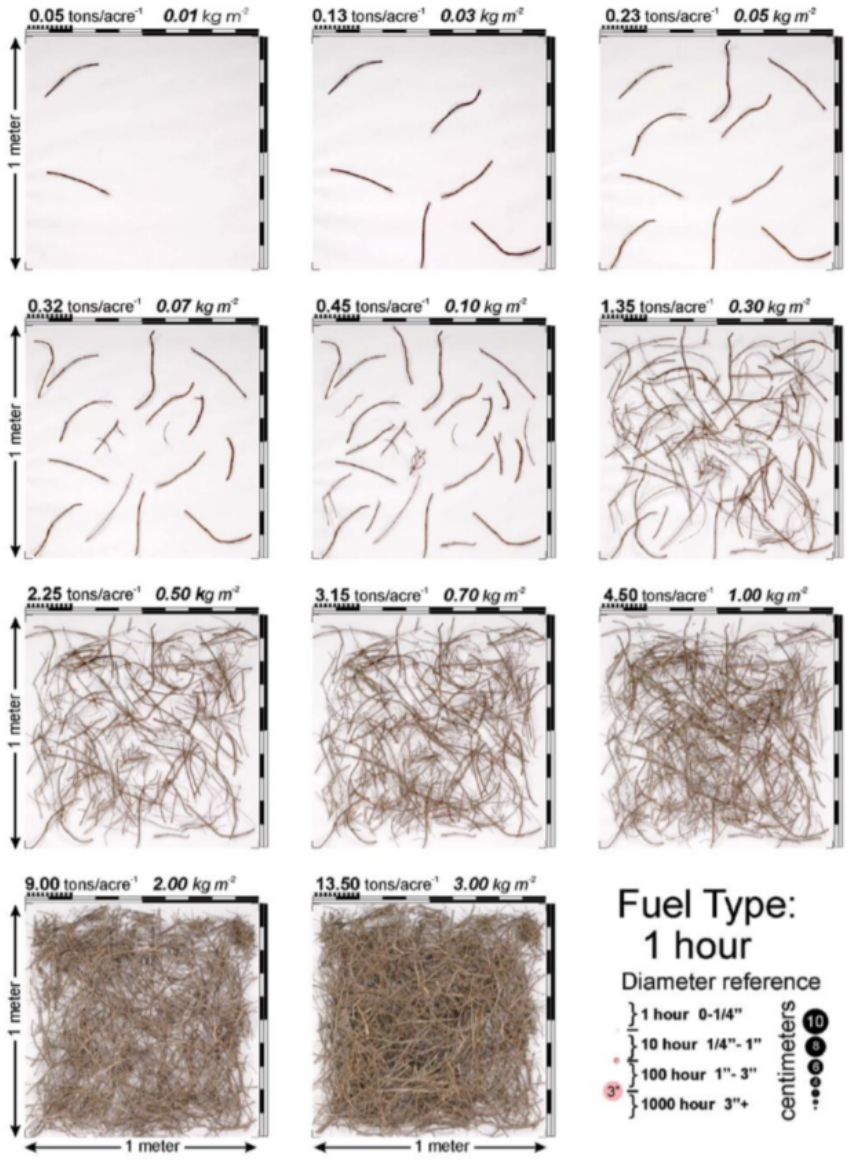

Figure 10: Photoload Sequences for Northern Rocky Mountain Fuelbeds. Extracted from Keane et al. [51].

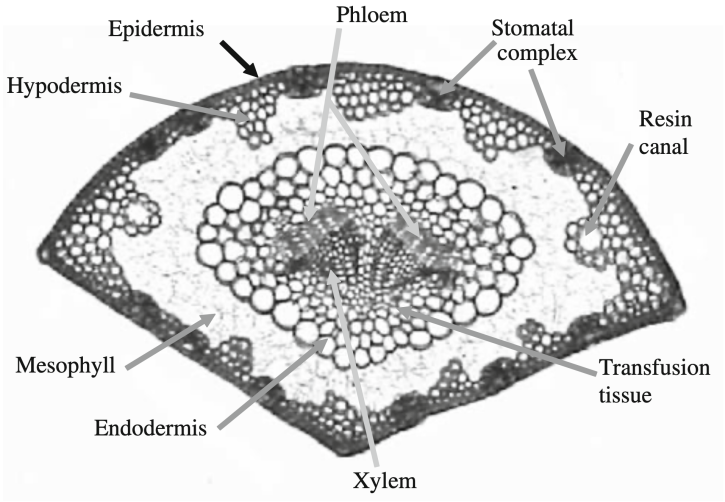

Figure 11: Cross-Section of Pinus Canariensis. Extracted from Lopez et al. [50]

The idea of reducing complexity is paramount within fire safety engineering. It is not practical to consider every aspect of reality. Instead a simplified reality that captures the most important qualities is more appropriate. In this way it is possible to traverse impassable complexities present in the science. The solution of problems through the application of a concise perception of reality is engineering. Hence, in this work ,despite the complexity at the micro-scale, homogeneous properties at the scale of the needle are assumed.

2.6 Conclusion

In this part it has been shown that natural fuels expand over a large area and are plastic in their morphology. This has consequences for wildfires as natural fuels make up the fuel bed that constitutes the principal fuel for a wildfire. The fuel bed is made up of individual fuel elements whose elemental structure and composition is dictated by the species plasticity. Changes in the morphology of the fuel elements will change the structure of the fuel bed and therefore the bulk properties. Consequently this affects the processes leading to ignition and these changes are what are of interest in this work. Since pine trees are a widespread genus, their needles serve as an example of a common natural fuel and will be used in this study to better understand heat transfer, pyrolysis, and ignition of wildland fuels. It is important to know not only the morphology of the fuel but also what it is made from. In the next part the thermal degradation of natural fuels will be explored.

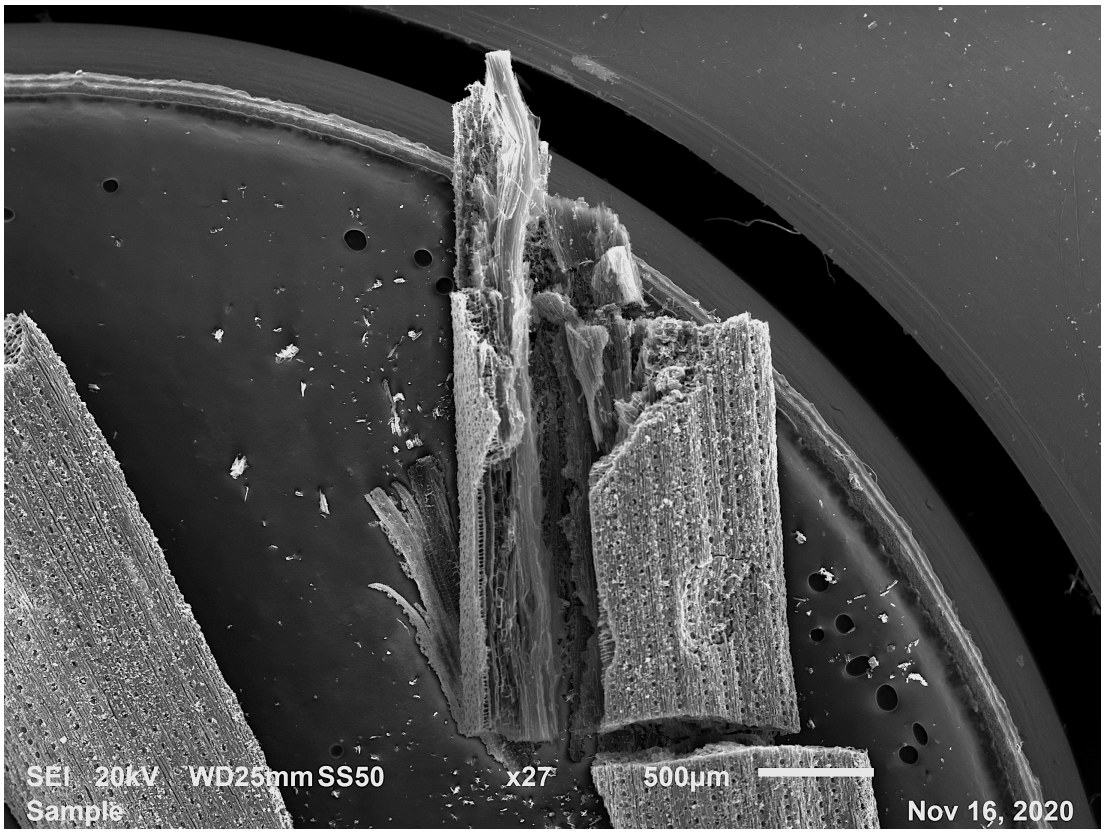

Figure 12: Charred Pinus Rigida needle broken along its length. Curved face facing up.

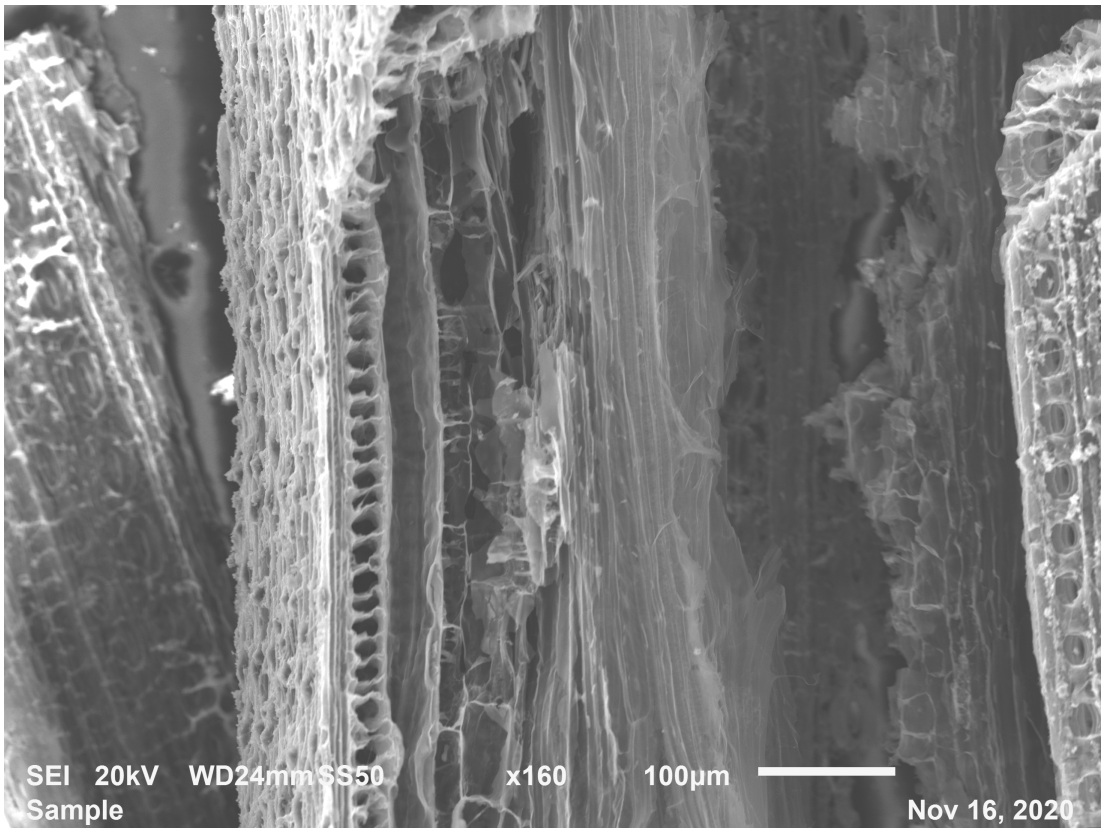

Figure 13: Charred Pinus Rigida needle broken along its length. Curved face facing up. - Zoomed in

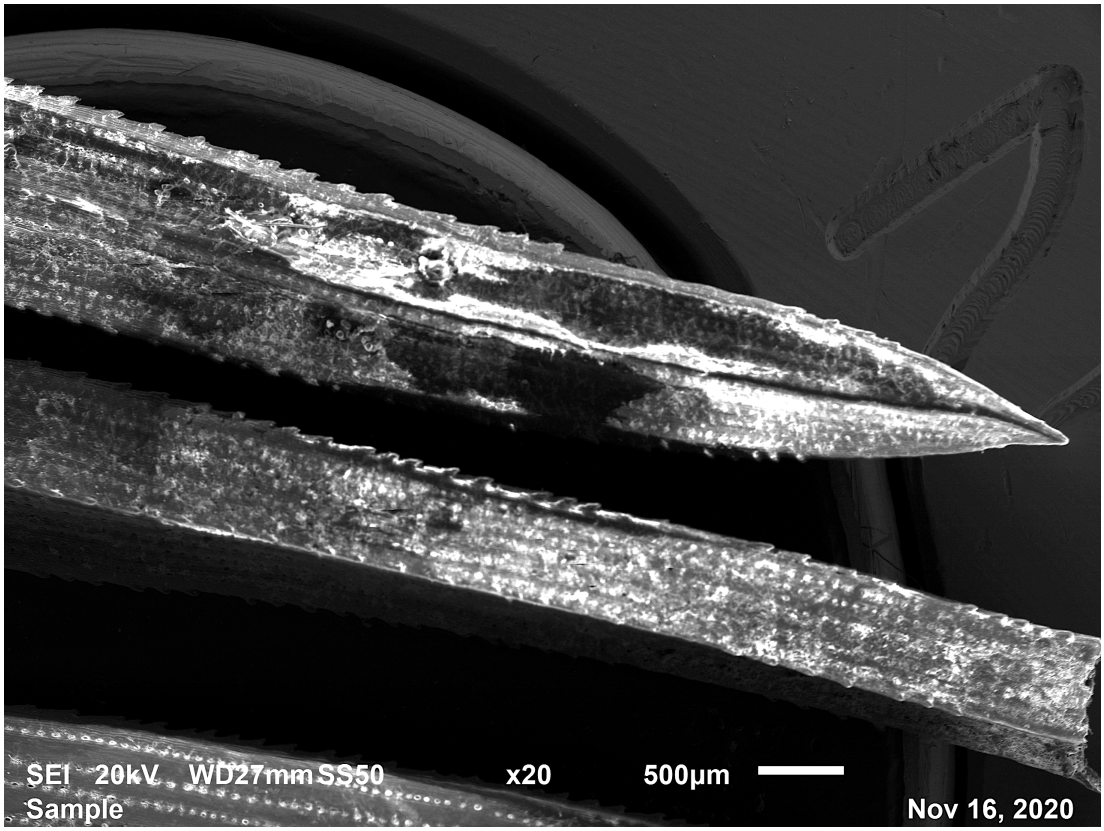

Figure 14: Virgin Pinus Rigida needle. Curved face facing down.

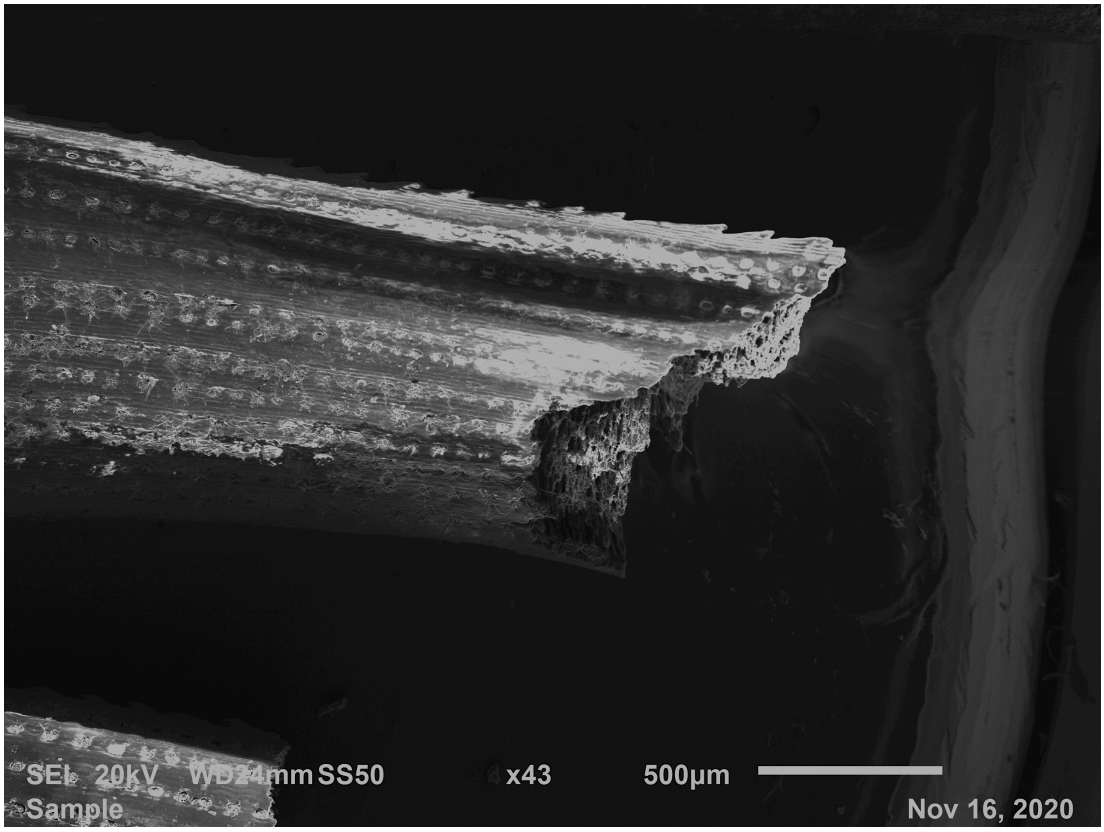

Figure 15: Virgin Pinus Rigida needle. Curved face facing up.

Part III
Thermal Degradation

The first question to ask is how do changes in species affect the ignition process? Species can differ in what they are made from and how they look - their chemistry and morphology. In Section 2.5.3, the plasticity of pine needle morphology was highlighted. The following work is interested in the variation in plant chemistry as a function of species. The change in chemistry will affect the thermal degradation of the material whereas the morphology will primarily affect the heat transfer. Thermal degradation is the process by which a material breaks down into smaller chemical species due to heat. This is sometimes called pyrolysis and is the mechanism that converts solid material to gaseous fuel. It is therefore an integral part of the ignition process. Although diversified for specific phytological uses, plant chemistry will have its limits in response when presented to high energy environments. This is fundamentally because plant chemistry is defined by similar organic species which have similar bonds that require similar energies to break them. In this part the thermal degradation will be understood in terms of how much material is available for the reactions and at what temperatures do they start and peak at.

3.1 Introduction

3.1.1 Thermogravimetric Analysis

Thermogravimetric analysis (TGA) is the technique used to interrogate the thermal degradation. This has been widely applied in wildfire science and also in related topics. for example in exploration of feed-stocks for combustion/pyrolysis reactors in process engineering [52] [53].

TGA focuses on characterising fuels by the response of the reactants to a change in thermal conditions, this is done by measuring the mass of the fuel in an oven. In a TGA experiment, the thermal conditions are assumed to be zero-dimensional [54]. The temperature is assumed uniform in the fuel and in equilibrium with the oven temperature. The output, of the experiment, is therefore a description of the mass of the fuel as a function of its temperature.

3.1.2 Processes

During burning three general processes occur, these are drying, pyrolysis and char oxidation.

These general processes are defined by the characteristics of the pathways that make them therefore rooting the practicality in theory.

1. Drying - dehydration or the removal of water. This can be in the form of free or bonded water. Where free water is liquid within the pores of the material and bounded water is chemically bonded to the material [55]

2. Pyrolysis - breaking of larger molecules to smaller molecules. This occurs as random and end-chain scission and chain stripping [35].

3. Char Oxidation - heterogenous oxidation reactions at the interface of solid fuel and oxidiser [35].

Using TGA, reactions can be defined to occur within a temperature range. Here the temperature is a lens to the energy of the material. At the reaction temperature there is enough energy to overcome the activation energy and the reaction can proceed. Sustained reaction requires consideration of the system energy this is discussed further in Section 3.1.4.

3.1.3 Hess' Law and Bond Energies

Reactions can be defined as either exothermic or endothermic, that is they either produce heat or require it. Chemically these can be defined as reactions that generate products that are either more or less stable than the starting reactants. Stability is linked to energy where lower energy leads to increased stability. This energy can be estimated using the first law of thermodynamics better known as the conservation of energy. This is expressed in chemistry as Hess' law:

'The total enthalpy change during the complete course of a chemical reaction is the same whether the reaction is made in one step or in several steps' [56]

By Hess' law the heat of reaction of molecules can be estimated using the bond energies and within the molecules and the heat of formations of molecules. The heat of formation is the heat required to form that molecule while the bond-dissociation energy is the heat required to break the bonds. The sign of the heat of reaction describes whether the reaction is endothermic or exothermic.

Bond	**Bond**	**Bond-dissociation energy at 298K [kJ/mol]**
H_3C–H	Methyl C–H bond	439
C_2H_5–H	Ethyl C–H bond	423
$(CH_3)_2CH$–H	Isopropyl C–H bond	414
$(CH_3)_3C$–H	t-Butyl C–H bond	404
$(CH_3)_2NCH_2$–H	C–H bond α to amine	381
$(CH_2)_3OCH$–H	C–H bond α to ether	385
$CH_3C(=O)CH_2$–H	C–H bond α to ketone	402
CH_2CH–H	Vinyl C–H bond	464
HCC–H	Acetylenic C–H bond	556
C_6H_5–H	Phenyl C–H bond	473
CH_2CHCH_2–H	Allylic C–H bond	372
$C_6H_5CH_2$–H	Benzylic C–H bond	377
H_3C–CH_3	Alkane C–C bond	347–377
H_2C=CH_2	Alkene C=C bond	∼710
HC≡CH	Alkyne C≡C triple bond	∼960
O–H	in methanol	440
O–H	in α-tocopherol (a phenol)	323
O–H	in water	497
O=O	in oxygen	498
O=CO	in carbon dioxide	532
C≡O	in carbon monoxide	1077

Table 1: Bond Dissociation Energies for bonds in variety of organic compounds and combustion-related molecules[57]

Table 1 shows bond energies have a certain range. Naturally it would follow that our measure of energy, temperature, would also follow a similar range. The outliers are the double and triple bonds which occur in unsaturated compounds. As temperature is a measure of energy we would expect the reaction temperatures to also occur over a certain range. Carbon dioxide, carbon monoxide and water have been included as these are often the products of combustion and their formation are the cause of energy release.

3.1.4 Chain reaction

Energy is not the only aspect controlling a reaction. A reaction cannot occur without reactants and so clearly the concentrations of reactants is an additional controlling factor. However if the reactants are sufficient then the limitation to reaction is the energy of the system. The system must have enough energy to overcome particle forces. Temperature is a surrogate measure for the energy of collisions and the reaction temperature is when we define the collisions to be successful in initiating the reaction.

Naturally, as they produce heat, it follows that exothermic reactions may be self-sustaining on the contrary endothermic reactions, that require heat, tend towards not occurring. It follows that external heat must be added for endothermic reactions to occur. Nevertheless being exothermic is not the sole prerequisite for a self-sustaining reaction. This is clear when one thinks beyond the chemical scale. The chemistry is occurring in a system and, as dictated by the second law of thermodynamics, heat will dissipate towards the colder regions of that system. A self sustaining reaction must be above the reaction temperature and the net energy of the system must be positive meaning that the heat generated is greater than the heat lost through dissipation. This manifests in two ways, it can be through the energy owing to the exothermic reaction or it can be due to additional external heating - for example from a flame.

Drying and pyrolysis are endothermic reactions and char oxidation is exothermic. One thing all three of these reactions have in common is that they result in a change of phase from the reactants to the products. In the TGA the solid reactants mass is measured and so a mass loss is observed as the products are created and removed from the system.

As an aside and for the completeness it is necessary to mention that the oxidation/combustion of pyrolysis products is exothermic. This is clear from the observation of a flame. This is a homogeneous reaction as all the products and reactants are in the same phase. However in the TGA the products are removed as they are produced and so the reaction is limited by the concentration of reactants and so its effect is mitigated. This concentration limitation in gas phase combustion is defined by the flammability limits this is not addressed here but it is an integral part of fire science and safety engineering [58].

3.1.5 Summary

TGA can be used to observe the mass signature of the reactions by computing the derivative of the mass of the reactants. The processes involved in fire are drying, pyrolysis and char oxidation. Drying and pyrolysis are endothermic and char oxidation is exothermic. This is a consequence of bonds being broken and made in the reactions.

Reactions are initiated after overcoming an activation energy and energy is required to break bonds whilst energy is given off in making them. Temperature is a measure of energy and as such reaction temperatures can be defined to characterise the reactions. If the bonds in different material have similar bond energies then it follows that the reaction temperatures should also be similar.

3.2 Material Composition

To understand the reactants it is best to understand what they are made from. Initially, this is done through literature review by looking at elemental, molecular and proximate analysis.

3.2.1 Elemental Analysis

Natural fuels are organic compounds and therefore are made of carbon and hydrogen. This can be verified through elemental analysis. Elemental analysis is a laboratory procedure where the elements in material are measured. Usually oxygen is found by subtraction [59]. As not all authors look for sulphur the literature data has been harmonised by adding sulphur to the oxygen values. This allows for the different literature values presented in Table 2 to be compared. This

highlights an inherent problem with material characterisation, where the material is defined by the components which have been assumed to occur a-prioi.

Elemental analysis does not give us an insight into the modes of burning but instead gives an overall picture of the variability in the plant chemistry. The similar values for the different natural fuels suggests that potentially similar bonds underpin their chemistry. Nevertheless, this does not distinguish between the different fire processes - drying, flaming/pyrolysis and char oxidation. A more useful approach would involve understanding how much of the material is available to each process.

	Carbon [%]	Hydrogen [%]	Oxygen [%]	Nitrogen [%]	Ref.
Arbutus unedo	48.24	6.15	40.33	5.28	[60]
Cistus monspeliensis	46.58	6.22	37.68	9.52	[60]
Dwarf palmetto	47.36	5.93	44.57	2.14	[61]
Erica arborea	52.43	6.98	35.92	4.63	[60]
Fetterbush	54.36	5.81	39.03	0.8	[61]
Inkberry	54.63	6.42	38.08	0.87	[61]
Live oak	49.57	6.01	42.12	2.3	[61]
Little bluestem	51.22	5.66	40.9	2.22	[61]
Longleaf pine foliage	51.37	3.00	44.42	1.21	[61]
Longleaf pine litter	52.31	6.09	39.29	2.31	[61]
Pinus halepensis	49.17	6.75	39.14	1.19	[62]
Pinus laricio	50.39	6.72	39.65	0.3	[62]
Pinus pinaster	49.87	6.72	40.16	0.26	[62]
Pinus pinaster	50.64	6.76	41.53	1.7	[60]
Saw palmetto	49.49	5.48	44.13	0.9	[61]
Sparkleberry	52.49	7.71	39.06	0.74	[61]
Swamp bay	52.48	6.11	40.05	1.36	[61]
Water oak	50.06	5.57	42.9	1.47	[61]
Wax myrtle	50.65	5.44	41.6	2.31	[61]
Wiregrass	47.42	6.34	42.93	3.31	[61]
Yaupon	51.34	6.28	40.92	1.46	[61]
Mean	**50.57**	**6.10**	**40.69**	**2.20**	

Table 2: Percentage mass elemental composition of wildland fuels and representative feedstocks. Extracted from [60] [62] [61].

3.2.1.1 Oxygen consumption and modified Huggett's constant

From this we can see similarities on an elemental level. In fire safety engineering gas calorimetry measurements make use of the similarity of material bonds in defining Huggett's constant[63]. Here the assumption is that energy produced by oxidation of the material is the same per unit of oxygen. Bartoli suggests the use of a modified Huggett's constant that is an average of different wildland fuels [64]. This is a powerful idea as it reduces the complexity of plant chemistry. The reality is that plants do have different chemistry but it would be preferable if it could be considered the same as otherwise we must characterise every species. This is not feasible and therefore undesirable.

3.2.2 Molecular Analysis

Molecular analysis of natural fuels is used to estimate the proportions of constituent components of natural fuels. Principal plant components can be extracted chemically [65].

In order of stability representative principal plant components are hemicellulose, cellulose and lignin. Often holocellulose is used to encompass both hemicellulose and cellulose [60]. They are natural polymers and are representative as they are subject to variation depending on species or phenological function. Representations of these polymers are shown in Figure 16.

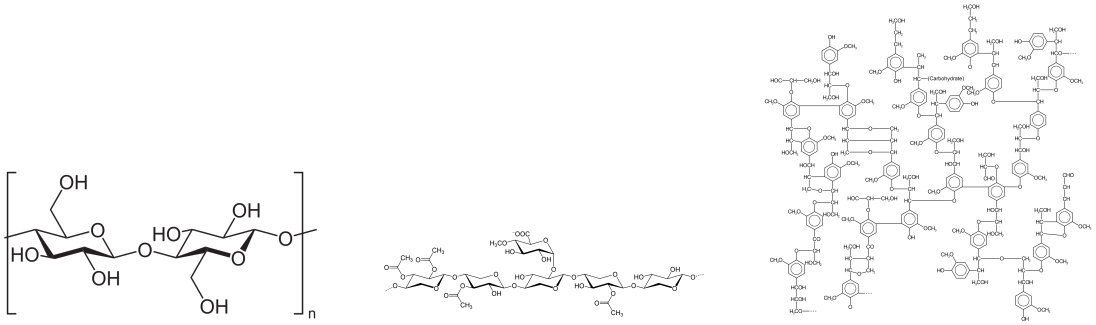

Figure 16: Skeletal diagrams - Each joint represents a methyl group whereas the hexagons are benzene rings. left to right: Cellulose monomer (Cellulose) [68], Xylan (Hemicellulose)[69], Lignin (Lignin)[70]

	Cellulose [%]	Hemi. [%]	Lignin [%]	Extr. [%]	Ash [%]	
Arbutus unedo	39	5	43	13	-	[60]
Erica arborea	41	14	40	6	-	[60]
Cistus monspeliensis	41	13	36	10	-	[60]
Pinus pinaster	40	5	41	14	-	[60]
Cotton linter	90	1	3	6	0	[71]
Flax	80	13	2	4	1	[71]
Hemp	74	8	2	16	0	[71]
Sugar cane	52	28	11	9	1	[71]
Bamboo	55	11	22	11	2	[71]
Coconut	51	12	31	6	1	[71]
Mean	**56**	**11**	**23**	**9**	**1**	

Table 3: Molecular composition (cellulose, hemicellulose, lignin, extractives and ash) of wildland fuels and representative feedstocks found using chemical extraction. Values extracted and summarised as percentages from [60] and [71].

Additionally to polymers, plants contain other organic compounds, such as oils or aromatics, that are soluble in water and organic solvents. These can be extracted in this way and so these compounds are called extractives. Different vegetation can be characterised using the percentage mass of these molecules and extracted literature values are given in Table 3.

A more in-depth approach, as shown in Table 4, can be followed for understanding plant composition where other components such as lipids or sugars are included. This is more precise but as a consequence it is more complex. Such analysis allows for the snapshot of the plant species to be very well defined. Alas, this is a snapshot nonetheless as plants are dynamic and so naturally as are their chemical compositions. That is to say a newly produced leaf will be different to a mature one and freshly fallen leaf will not be the same as a rotted one.

To use the information in Table 4 we would have to model each component of every plant in a known forest floor mixture. That is an unobtainable goal and even using the simpler breakdown of Table 3 stretches the field to its limits [55] [66] [67]. Research into this is limited to the laboratory where information is more precise. At this point in time it would be inappropriate to extend this to the field.

Dry basis	**lipids** (%)	**gluc.** (%)	**fruct.** (%)	**protein** (%)	**pectin** (%)	**hemi.** (%)	**cell.** (%)	**starch** (%)	**phenols** (%)	**lignin** (%)	**minerals** (%)	**silicates** (%)	**total** (%)
Saw palmetto	11.9	0.7	0.6	5.4	0.7	18.6	11.0	1.0	4.8	29.8	1.8	4.8	91.2
Dwarf palmetto	6.8	1.3	1.0	12.9	2.0	18.0	28.0	0.6	7.9	17.1	3.3	1.1	100.0
Swamp bay	11.3	2.2	1.9	8.3	1.8	10.5	18.3	0.8	5.3	32.9	1.9	0.0	95.2
Yaupon	31.3	3.4	0.3	8.7	1.9	7.3	8.8	0.0	6.6	25.2	4.5	0.4	98.4
Inkberry	28.1	3.4	0.8	5.3	2.6	5.4	11.1	2.2	9.0	25.0	1.9	0.0	94.9
Wax myrtle	15.6	0.9	0.8	14.1	2.7	10.5	17.6	0.3	2.4	28.1	2.5	0.2	95.7
Fetterbush	30.0	3.5	0.5	4.9	1.8	6.9	16.6	0.0	3.4	30.3	2.2	0.3	100.6
Live oak	9.9	1.5	1.1	14.0	1.7	10.9	19.2	0.7	5.8	23.7	2.9	0.0	91.4
Water oak	15.1	1.6	1.3	8.8	2.9	5.8	15.7	0.9	13.5	25.3	3.1	4.3	98.2
Longleaf pine	22.3	1.4	0.8	7.4	2.0	15.0	19.0	0.7	3.1	23.5	2.0	0.6	97.9
Wiregrass	3.8	1.0	0.1	9.5	0.0	22.8	34.8	0.0	2.8	18.7	2.2	0.0	95.7
Little bluestem	4.8	0.7	0.4	12.5	0.5	21.5	31.3	0.1	3.1	21.2	2.3	0.0	98.4

Table 4: Molecular composition (lipids, glucose, fructose, protein, pectin, hemicellulose, cellulose, starch, phenols, lignin, lignin, minerals, silicates) of some wildland fuels extracted from Matt el al. [65].

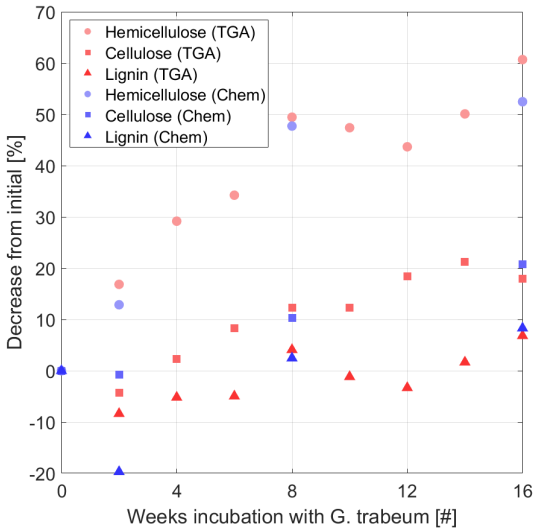

Figure 17: Effect of brown rot on the molecular composition of pinus sylvestris sapwood. Extracted from Alfredsen et al. [72]

3.2.2.1 Forest floor degradation

In Section 3.2.2, Table 3 and 4 are given as a snapshot of the molecular composition of wildland fuels. However the forest floor is not only a mixture of species but also of different degrees of senescence. Senescence is dynamic and occurs due to natural processes such as rotting. One study, by Alfredsen et al. [72], shows that molecular degradation occurs due to rotting. In this study both TGA and wet chemistry were used to investigate the effect of brown rot fungus on wood composition. They found that after 16 weeks incubation hemicellulose, cellulose and lignin had decreased in mass 50, 20 and 10% respectively. This data is shown in Figure 17.

The change in molecular composition, illustrated in Section 3.2.2.1, will affect the fire processes. Fire processes can be quantified by comparing oxygen consumption occurring in the combustion of pyrolysis products. Susott reports experimental data for different Douglas fir (pseudotsuga menziesii) specimens. Figure 18 shows the comparison of virgin stems and rotted wood [73] and shows differences in the temperature range over which thermal degradation occurs. Changes due to the fuel chemistry are demonstrated in Figure 19. In the left figure the rotted sample is shown to produce less pyrolysis gases compared to virgin samples. The virgin specimens on the other hand show a general trend at low temperatures where less structural specimens, such as foliage, are at one end of the distribution and more structural specimens, such as bark, are on the other end. However at 500°C all specimens, except the rotted wood, have produced similar amounts of pyrolysis gases.

The right hand in Figure 19 underlines the previous point. In Figure 19 the specimens are shown to have similar heats of combustion as a complete fuel. Whereas distinguishing between the volatiles and the char reveals that rot affects the material composition and therefore flammability of wildland fuels by shifting availability from volatiles to char.

The literature indicates that plant element function determines material composition and therefore combustion behaviour. Additionally there is indication that biological degradation has a role to play in the subsequent thermal degradation. Molecular analysis would have to be coupled with knowledge of each molecule rot degradation mechanisms as well as their respective thermal degradation mechanisms. The result would be a complex model where a simpler one is more desirable.

3.2.2.2 Conclusion

Considering the forest floor variation and the limitation in terms of thermal degradation modelling. Questions are raised about the practicality of molecular analysis in a context outside of

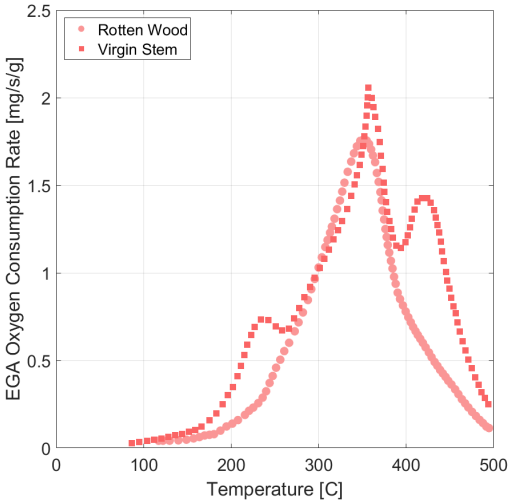

Figure 18: Comparison of oxygen consumption for virgin and rotted specimens of a Douglas Fir. Extracted from Susott et al. [73].

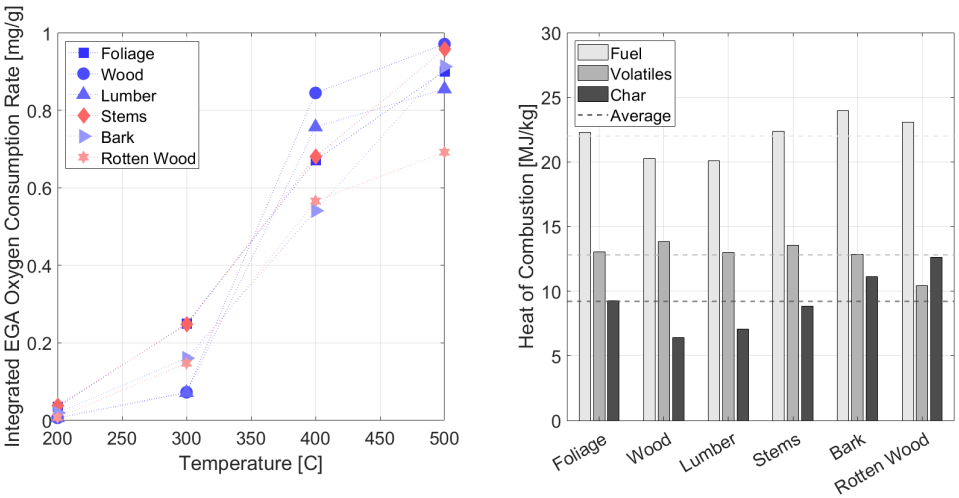

Figure 19: Comparison of Douglas Fir specimens. (left) Integrated Oxygen consumption. (right) Heat of Combustion. Extracted from Susott et al. [73].

	Volatile Matter [%]	Fixed Carbon [%]	Ash [%]	Ref.
Dwarf palmetto	89.8	10.2	3.26	[61]
Fetterbush	77.7	22.3	2.24	[61]
Inkberry	80.2	19.8	1.88	[61]
Live oak	80.9	19.1	2.71	[61]
Little bluestem	84.9	15.1	4.12	[61]
Longleaf pine foliage	79.7	20.3	2.02	[61]
Longleaf pine litter	78.3	21.7	1.77	[61]
Saw palmetto	76.4	23.6	3.19	[61]
Sparkleberry	79.0	21.0	3.1	[61]
Swamp bay	79.6	20.4	1.84	[61]
Water oak	80.6	19.4	4.18	[61]
Wax myrtle	77.4	22.6	2.41	[61]
Wiregrass	81.7	18.3	4.34	[61]
Yaupon	86.2	13.8	4.89	[61]
Mean	**80.9**	**19.1**	**3.0**	

Table 5: Proximate composition of wildland fuels. Volatile matter and fixed carbon are on a dry and ash free basis. Values extracted from Safardi et al. [61]

botany such as wildfires. In terms of fire processes, knowing precisely the molecular components brings us no closer to knowing how they will contribute to the fire processes as we do not know the mechanisms by which they degrade thermally or biologically nor is this level of complexity welcome. A more pragmatic analysis would be one that had the fire processes at the centre of it.

3.2.3 Proximate Analysis

Proximate analysis is a material analysis based on the thermal degradation itself. Here the material is characterised using the proportion of material involved in each process. The proportions are termed volatile matter, fixed carbon and ash. Volatile matter is the maximum proportion of the material available for pyrolysis and therefore flaming combustion. Whilst fixed carbon is available for char oxidation and therefore smouldering combustion. Table 5 shows that using this characterisation the wildland fuels are reduced in their complexity. The ranges in each value are small and thus wildland fuels can provide ≈80% mass as volatile matter and ≈20% as fixed carbon.

From Table 4 it can be appreciated that is a diverse set of plant molecules owing from plants being complex organisms, as illustrated in Section 2.5.5, Figure 11. Nevertheless, Table 2 shows that in terms of elemental composition there is not a wide variety between different plants. Elements are constituent parts of molecules and determine bond energies of the material. As discussed in Section 3.1.3, the bond energies determine the energy required for certain reactions to occur. As such it is safe to assume that similar bonds will break when confronted with similar energies this translates to similar reaction temperatures. If this is the case then wildland fuel composition could be defined by the different reactions underpinning the thermal degradation of th material

The proximate analysis approach is rooted in the fire process and moves the lens away from the specificity of plant chemistry. In the context of wildfires it seems the most practical approach. There are three main reasons why it is the most practical.

1. Firstly, plant composition is not a static quantity. It is influence by the seasons and by other forms of degradation such as rot.

2. Secondly, even if we did know these details, we cannot use that information in a practical way.

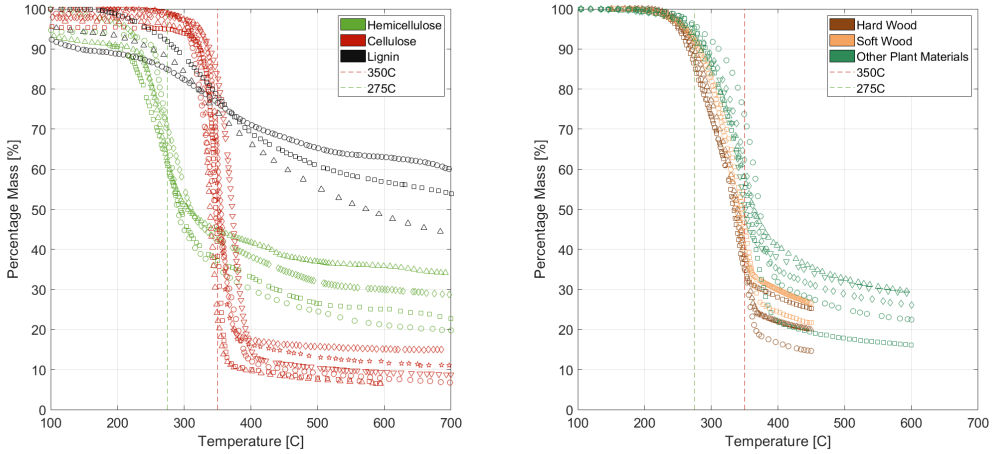

Figure 20: Thermal degradation of different natural components in non-oxidative environment. a)[71][74][75][76][77] b)[71][78]

3. Thirdly, this knowledge does not translate to the knowledge of the forest floor. No wildland is homogeneous and this approach either requires it is or that we are omniscient. Neither is practical nor possible.

Hence, the knowledge of plant chemistry is useful in understanding plants however is it necessary when considering fire? As when considering high energy environments they are likely to degrade at similar temperatures? Instead the focus should be on the proportions available to the different processes that constitute a fire. As such the proximate analysis approach is followed in this work as it provides a simple and interpretable method of characterising wildland fuel composition. As wildland fuels are complex by nature, the goal here is to reduce said complexity rather than be restricted by it.

3.3 Literature on Pyrolysis and Char Oxidation Experimental Works

As we are considering flaming combustion we will focus on the process that generates the necessary gaseous fuel, this process is called pyrolysis. However the role of drying and the char oxidation cannot be underestimated. Primarily, because the drying of a fuel is endothermic and therefore amount of fuel moisture is important as it acts as a heat sink - counterbalancing any heat input. On the other hand, char oxidation is exothermic and so it is a heat source and increases the heat in the system.

3.3.1 Pyrolysis

Although the inclusion of molecular composition complicates thermal degradation modelling it is still useful to understand the composite material. By measuring representative component degradation the extremes of the composite material is observed. The pyrolysis of these representative component parts has been studied in literature.

From Figure 20, it can be seen that hemicellulose and lignin both begin degrading before cellulose. Cellulose has a narrow reaction temperature range (300-400°C) after which only <20% mass is remaining. Higher final masses are found for hemicellulose and lignin (≈30% and ≈50% respectively). However hemicellulose will have degraded almost completely by the end of the cellulose reaction temperature range. As a first approximation the temperatures at the midpoint of the reactions would give 275°C and 350°C for hemicellulose and cellulose respectively.

Although natural fuels will vary in their constituent components, they are observed to degrade in the temperature range of their constituent parts.

	PP	PH	PL	EA	CM	AU	**Mean**
CO_2 [%]	64	66	62	72	59	69	**65**
H_2O [%]	9	7	7	5	14	8	**8**
CO [%]	17	15	14	14	13	13	**14**
VOCs [%]	10	12	17	9	15	9	**12**

Table 6: Products of pyrolysis (280 and 430°C in nitrogen) of some crushed wildland fuels: pinus pinaster (PP), pinus halepensis (PH), pinus laricio (PL), erica arborea (EA), arbutus unedo (AU). Under the same conditions. Extracted and condensed from Tihay et al. [79].

	PH	PL	PP	**Mean**
CO [%]	48	40	49	**46**
CH_4 [%]	16	15	14	**15**
C_2H_6 [%]	13	15	13	**14**
CHOH [%]	12	11	10	**11**
C_6H_{14} [%]	7	7	5	**6**
C_6H_6 [%]	2	3	3	**3**
C_8H_{10} [%]	2	9	6	**6**

Table 7: Products of pyrolysis of Pinus species: pinus halepensis (PH), pinus laricio (PL), pinus pinaster (PP). Conducted in Fire Propagation Apparatus under nitrogen conditions. Extracted and repurposed from Bartoli et al. [80].

Further support of similarity in chemistry can be found when looking at the products of pyrolysis measured for a certain heating condition, as shown in Table 6and Table 7. The values are similar within each author's results however there are discrepancies when comparing the authors. The discrepancy between the two authors are both in the percentages recorded for the same species and in the components measured by each author. The former underlines how the products of combustion are dependent on the environmental conditions whilst the latter how the results depend on the experimental methodologies used. This highlights the impracticality of focusing on the products of combustion and suggests the reactant-based analysis followed in this work is the most appropriate.

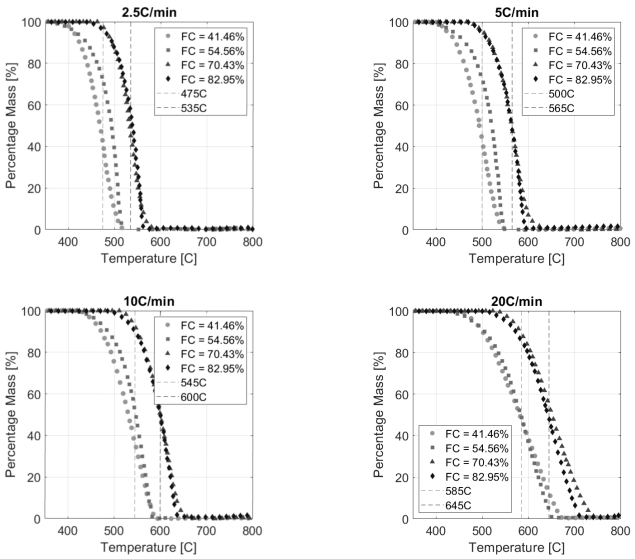

Figure 21: Oxidation of anthracite and bituminous coal chars at 2.5, 5, 10, 20°C/min. Vertical lines indicate the temperature where approximately 50% of the mass has been lost. Extracted from Wang et al. [81].

3.3.2 Char Oxidation

Char oxidation is the heterogenous oxidation reaction occurring between gaseous oxidiser and solid carbonaceous fuel. Clearly then the reaction cannot be controlled predominately by heat transfer, as pyrolysis and drying are. Oxygen must be present in the reaction and so the mass transfer of oxidiser is additionally important.

Here is presented literature work on the oxidation of chars made from different coal char samples. The char was produced by heating the coal to 1000°C in a nitrogen environment. Coal is an organic compound, it has a higher fixed carbon value and a lower volatile matter value compared to natural fuels. Nevertheless it is worthwhile to look at coal char data as it is first pyrolised to produce the char. Therefore the differences in volatile matter are no longer relevant as they are removed in the pyrolysis process. Nevertheless the differences in the fixed carbon do remain. The data in Figure 21 suggests that higher fixed carbon leads to higher reaction temperatures. The reaction temperature at 2.5°C/min ranges between 475-535°C.

Additionally the application of different heating rates shows how the reaction temperature measured using the TGA is affected by the heating rate. The reaction temperature is seen to increase with increasing heating rate. Additionally the shape of the degradation is changed with the mass loss spread over a larger temperature range at higher heating rate. This suggests that either the temperature of the char lags behind the oven temperature and/or that there is an oxygen deficit leading to a delayed and smeared reaction. Hence, char oxidation process is subject to both heat transfer and mass transfer effects.

	Proximate Analysis [%]			Ultimate Analysis [%]				
Coal	VM	FC	Ash	C	H	O	N	S
Bituminous A	48.14	41.46	10.4	60.76	2.76	13.87	0.64	0.19
Bituminous B	36.08	54.56	9.36	66.35	4.57	17.84	0.77	0.44
Anthracite A	14.88	70.43	14.69	75.23	2.5	1.61	0.93	0.85
Anthracite B	10.31	82.95	6.74	84.97	3.21	3.64	0.69	0.14

Table 8: Proximate (volatile matter (VM), fixed carbon (FC), ash) and Ultimate analysis of bituminous and anthracite coals used to form the chars that were subsequently oxidised and presented in Figure 21. Extracted from Wang et al. [81].

3.4 Experimental Work

To investigate wildland fuels, experiments were conducted. Two thermogravimetric analysis methodologies were conducted. These are proximate analysis and controlled combustion.Additionally, heat of combustion was measured using a bomb calorimeter.

3.4.1 TGA Experimental Matrix

Table 9 shows the different experiments conducted and the number of repetitions for each one. All data recorded can be found in Appendix A and B.

Heat Rate [K/min]			5	5	15	15	25	25	25	35	50	70	100	100
Gas [50 mL/min]			Air	Air	Air	N_2	Air	Air	N_2	Air	Air	Air	Air	N_2
T_{end} [°C]			900	400	900	900	900	900	900	900	900	900	900	900
Condition							Dry							
Species	Blueberry	Leaves		3					3					
	Blueberry	Wood		3					3					
	Maple	Red Leaves	1					1	3				1	
	Oak	Black Jack Leaves		3					3					
	Oak	Black Jack Wood		3					3					
	Oak	Chestnut Leaves	1					1	3				1	
	Oak	Mixed Leaves	3	3					3					
	Oak	Post Leaves	1						1					
	Oak	White Leaves		3					3					
	Pinus	Echinata	3	3	3				3	3				
	Pinus	Halepensis	1						1					
	Pinus	Pinea	1						1					
	Pinus	Rigida	3	3	3	3	3	6	3	6	3	3	3	3
	Pinus	TaedaX	6	6	6			6	6	6			3	

Table 9: Experimental matrix of TGA experiments

3.4.2 Proximate Analysis

In proximate analysis, the goal is to isolate the different reactions (defined below) and characterise how much of the initial mass is available for each general reaction. This method uses the characteristics of the reactions as a means to isolate them.

1. Drying occurs at low temperature ($T < 110$°C). Irrespective of the environment
2. Pyrolysis occurs at medium-high temperature ($T > 110$°C). The response of the reactants is similar irrespective of the environment. (N.B. That does not exclude the products being different however.)
3. Char oxidation cannot occur without oxygen.

3.4.2.1 Method

3.4.2.1.1 Proximate Analysis Method

The characteristics of the reactions directly influences the testing methodology. Proximate analysis was conducted as follows [82]:

1. Gas flow of N_2 at 50 mL/min. Increase T from 25°C to $110C$ at a rate of 25°C/min. In this step the sample is dried.
2. After holding for $t = 5$ min increase T to 900°C at 25°C/min. In this step the sample is pyrolysed.
3. at 900°C change gas flow to air at 50 mL/min. In this step the sample is oxidised.

The temperature profile is shown in Appendix A in Figure 75, 76 and 77. The repeat tests were used to create an average result by averaging the data at each test time.

3.4.2.1.2 Reaction Temperatures Method

Establishing reaction temperatures is a method to quantify the thermal degradation. Here the maximum mass loss rate temperature and onset temperature are defined for each reaction.

The maximum mass loss rate temperature is relevant when considering the burning rate. The fastest burning rate will occur in the idealised scenario where the material is at this temperature. This was found by defining the reaction bounds (onset and offset), computing derivative of the mass and finding the maximum mass loss rate within the bounds. To define the temperature bounds, a value was chosen that showed the derivative being close to zero. A simplifying assumption made was that the reactions are sequential and so do not overlap.

The onset temperature is relevant when considering the ignition. Ignition is the attainment of the minimum concentration of flammable gases and so an earlier onset leads to the potential of an earlier ignition. To ensure the same treatment of all samples, this was defined as the temperature at which there is a mass loss rate of 20% of the max mass loss rate.

There are two reactions observed dynamically during proximate analysis: drying and pyrolysis. These will be referred to as reaction 1 (R1) and reaction 2 (R2) in the following section. The bounds chosen for these reactions as to capture the reactions. These are shown in Table 10.

Reaction	T_{start} [°C]	T_{end} [°C]
Drying	25	115
Pyrolysis	115	900

Table 10: Reaction bounds for proximate analysis.

3.4.2.2 Proximate Analysis and Reaction Temperature Results

The proximate analysis results are shown in Figure 22, 23 and 24 and are tabulated in Table 11, 12 and 13. Further Figures can be found in Appendix A.

3.4.2.2.1 Pinus Species

Pinus species results for proximate analysis are presented in Figure 22 and Table 11. The volatile matter, char and ash ranges between 69-78%, 19-26% and 2-5% respectively. The onset and maximum temperatures for reaction 1 and reaction 2 range between 29-40°C, 72-77°C, 216-254°C and 350-371°C respectively.

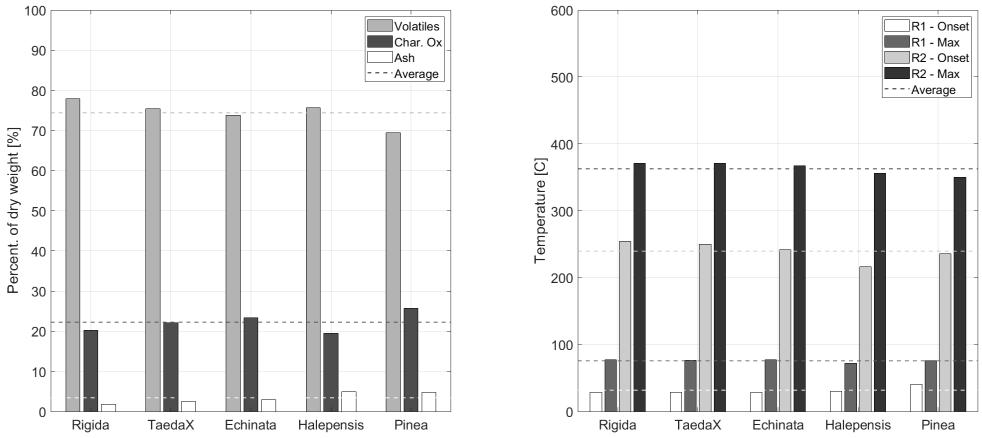

Figure 22: Proximate analysis of pinus species. Left: Percentage mass of components. Right: Reaction temperatures.

	Percentage [%]			Temperature [°C]			
Pinus	Volatile Matter	Char	Ash	R1 Onset	R1 Max	R2 Onset	R2 Max
Rigida	77.90	20.30	1.80	28.80	77.34	254.29	371.30
TaedaX	75.38	22.07	2.55	28.88	76.79	249.88	370.80
Echinata	73.77	23.31	2.92	29.05	77.35	241.46	367.23
Halepensis	75.66	19.44	4.90	30.50	72.15	216.28	356.18
Pinea	69.40	25.78	4.83	40.39	76.20	235.94	349.70
Mean	74.42	22.18	3.40	31.52	75.96	239.57	363.04

Table 11: Proximate analysis percentage and reaction temperature results for pinus species.

3.4.2.2.2 Broad Leaves

Broad leaf results for proximate analysis are presented in Figure 23 and Table 12. The volatile matter, char and ash ranges between 69-72%, 24-28% and 3-5% respectively. The onset and maximum temperatures for reaction 1 and reaction 2 range between 28-31°C, 77-81°C, 234-243°C and 298-365°C respectively.

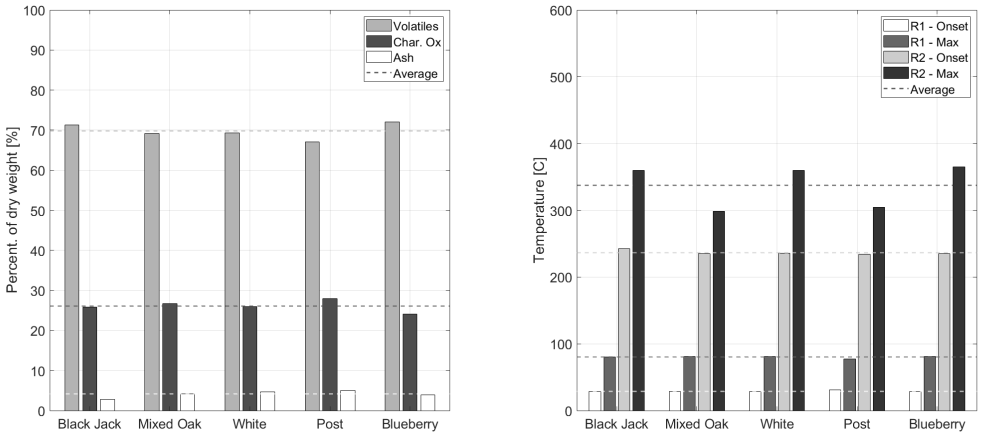

Figure 23: Proximate analysis of broad leaf species. Left: Percentage mass of components. Right: Reaction temperatures.

	Percentage [%]			Temperature [°C]			
Broad	Volatile Matter	Char	Ash	R1 Onset	R1 Max	R2 Onset	R2 Max
Black Jack	71.35	25.84	2.81	28.76	80.41	242.73	359.62
Mixed Oak	69.13	26.69	4.17	28.49	81.29	234.63	298.30
White	69.32	26.00	4.68	29.02	81.01	235.66	359.57
Post	67.04	27.95	5.01	30.84	77.00	234.27	304.66
Blueberry	72.05	24.04	3.92	28.41	81.36	235.08	365.11
Mean	69.78	26.10	4.12	29.10	80.21	236.48	337.45

Table 12: Proximate analysis percentage and reaction temperature results for broad leaf species.

3.4.2.2.3 Stems

Stems results for proximate analysis are presented in Figure 24 and Table 13. The volatile matter, char and ash ranges between 74-76%, 20-23% and 3-4% respectively. The onset and maximum temperatures for reaction 1 and reaction 2 range between 29-35°C, 76-77°C, 249-258°C and 366-372°C respectively.

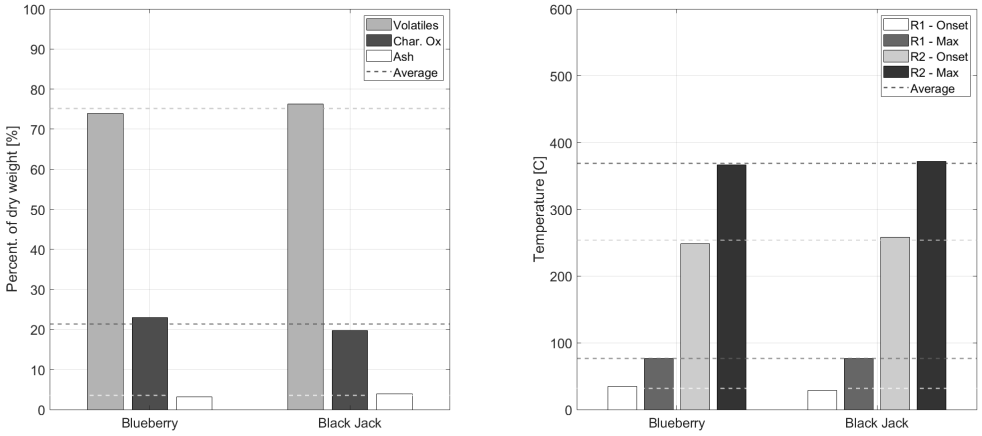

Figure 24: Proximate analysis of stem samples. Left: Percentage mass of components. Right: Reaction temperatures.

	Percentage [%]			Temperature [°C]			
Wood	Volatile Matter	Char	Ash	R1 Onset	R1 Max	R2 Onset	R2 Max
Blueberry	73.89	22.98	3.13	34.67	76.79	248.63	366.26
Black Jack	76.31	19.75	3.94	29.05	76.96	258.10	371.56
Mean	75.10	21.37	3.53	31.86	76.87	253.36	368.91

Table 13: Proximate analysis percentage and reaction temperature results for stem samples.

3.4.2.3 Discussion

3.4.2.3.1 Volatile Matter, Char and Ash fractions

The volatile matter ranges from 69-78% with Pinus Rigida containing the largest volatile matter fraction. Averaging the functional groups, the stems contain the most followed by the pinus species and then the broad leaf species. The char percentage ranges from 19-28% with Post Oak containing the largest char fraction. Averaging the functional groups, the broad leaf species contain the most followed by pinus species and the stems. This is the opposite to the volatile matter trend. The ash percentage ranges from 2-5% with Post Oak containing the largest ash fraction. Averaging the functional groups,the broad leaf species contain the most followed by stems and then the pinus species.

In general the functional group (pinus, broad leaf, stem) samples are similar when compared within their group. There is a difference in the ash percentage between the European and American pinus species where the European species have a higher ash content. In a study using 2022 leaf samples it was found that ash content was related to mean annual precipitation. It was reported that higher precipitation lead to lower ash content [83]. The mean annual precipitation in the area of collection of the the European and American pinus species is 279mm and 1119mm respectively [84]. Hence, potentially explaining the higher ash content in the European species.

3.4.2.3.2 Reaction Temperature Ranges

The first reaction is drying and its onset was recorded between 28-40°C. This range is due to some initial destabilisation in the mass signal and because the onset is defined as the temperature when a fraction of the maximum mass loss rate is being lost. Hence, differences in the total mass of water in the sample will affect the maximum mass loss rate and therefore this fraction. The temperature of maximum mass loss rate during drying was recorded between 72-81°C.

The second reaction is pyrolysis and its onset was recorded between 216-258°C. The average for the broad leaf, pinus and stem samples was 236°C, 240°C and 253°C respectively. This trend in increasing onset temperature follows the trend in total amount of volatile matter. This means that although there is more to pyrolyse the temperature required to start that process is higher.

The temperature of maximum mass loss was recorded between 298-372°C. The average for the broad leaf, pinus and stem samples was 337°C, 363°C and 369°C respectively. This trend in increasing maximum mass loss temperature follows the trend in total amount of volatile matter. Comparing these to the average onset temperature indicates that there is more than 100°C between these.

3.4.2.3.3 Shape of Pyrolysis Reaction

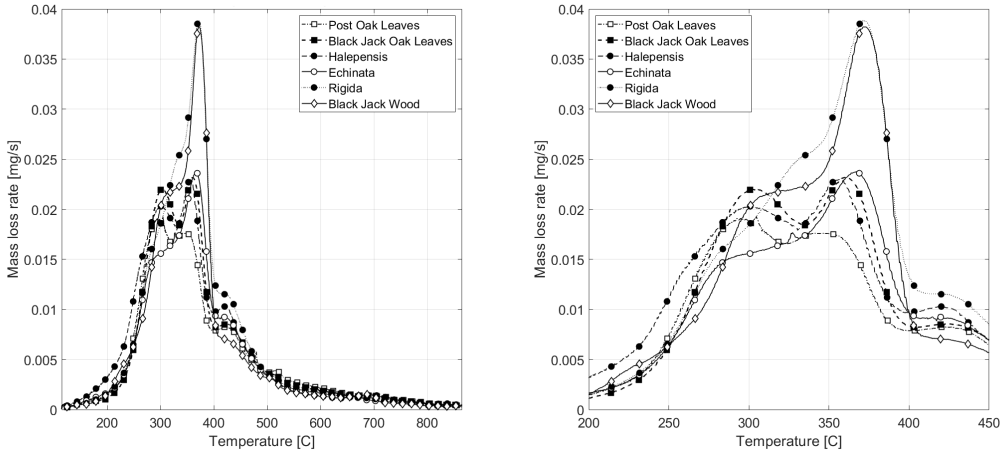

Figure 25: Proximate analysis mass loss rate for selected samples. Left: 115-900°C. Right: 200-450°C.

The thermal degradation has been characterised by proportions of volatile matter, char and ash and the onset and maximum mass loss rate temperatures. This resulted in a pyrolysis range of more than 100°C. Taking a closer look at the mass loss rate curves in Figure 25 it is clear that the pyrolysis reaction is composed of, at least, two peaks. This is likely to be due to the pyrolysis of a range of plant components, such as those in Table 3 and Table 4, as was shown in Figure 16. The lower temperature peak is more pronounced in the broad leaf samples whilst the higher temperature is more pronounced in the pinus and stem species.

3.4.2.3.4 Summary

Pinus has largest volatile fraction whilst broad leaf have largest char fraction. Nevertheless the difference is only 5% and 4% respectively. There is some indication that ash content is a function of the growing environment where higher rainfall leads to lower ash content.

Temperature range of pyrolysis was observed to be more than 100°C with the broad leaf species on average pyrolysing before the pinus and stem species. The shape of the curve suggest that there are at least two peaks that make up the pyrolysis reaction. The structure of the vegetation seems to relate to a greater contribuiton of one peak over the other. Broad leaves are observed to have a more pronounced lower peak whilst pinus and stems have a more pronounced higher peak. This suggests that plant morphology may indicate the chemical make up.

3.4.2.4 Conclusion

Here we have shown that the proportions of the material active in the different fire processes is similar for the natural fuels. Comparison with other plant-based fuels shows similarity however there is a scale of similarity. This scale ranges from structural plant materials, such as wood, and other functional plant materials, such as leaves. This is clearly due to different plant chemistry being optimised for different functions. Nevertheless the temperature range of reactions is similar regardless of function as fundamentally the plant building blocks are themselves made of a small set of chemical bonds. These chemical bonds determine the energy needed for pyrolysis and therefore measured mass loss of reactants at a given temperature. The next step is to understand if the same is true in an oxidative environment.

3.4.3 Controlled Combustion

Controlled combustion experiments investigate the thermal response of a material in an oxidative environment. In proximate analysis it was assumed that the material, and therefore the reactant, response is the same regardless of environment. Here comparable oxidative conditions were tested and are presented. Additional tests at higher and lower heating rates are conducted as a means to further validate the assumption and investigate any effects due to the heating rate.

The effects of conditioning is investigated by testing material that has been treated at 60°C for 24hrs in an exterior oven. Low heating rate experiments are conducted to understand the thermal degradation of the natural materials tested. Higher heating rates are found in real fires however, as mentioned in Section 3.1.1, the underlying assumption in TGA experiments is a 0-D experiment. Higher heating rates challenge this assumption as the materials thermal inertia begins to play a significant role. The consequence of this is that there are thermal gradients in the sample. The exterior of the sample is at a higher temperature than the interior. As such the sample temperature measured is no longer representative of the whole material. Nevertheless high heating rates are the reality in fire, and so medium and high heating rate experiments are conducted.

Due to the presence of oxidiser the degradation as a function of temperature is found for all general reactions. In the proximate analysis this is not possible as the oxidiser is introduced at 900°C. The data is analysed and characterised using the onset temperature of each reaction and the temperature at the peak mass loss rate. These experiments were conducted after the proximate analysis. As such the nature of these experiments are related to and inspired by the proximate analysis. To summarise, the controlled combustion experiments were conducted with 15 mg and can be characterised as follows:

1. Change in Environment - Air vs N_2
2. Conditioning
3. Low Heating Rates
4. All Heating Rates

3.4.3.1 Method

Controlled combustion is conducted at different heating rates to see how the material responds. Controlled combustion consists of increasing the TGA oven temperature at a given linear heating rate of 5-100°C/min with a mass of 15 mg. Each experimental set was averaged as in the proximate analysis case. Furthermore, experiments were normalised by their dry mass. This was taken as the mass at 115°C. Normalised mass was differentiated with respect to time. Experiments were conducted at 1 Hz. Therefore the difference between successive measurements gives the mass loss rate. Division by the heating rate allows for the effect of the heating rate on magnitude to be mitigated and is used when comparing different heating rate experiments. This units here are then kg/°C.

Unlike proximate analysis the method does not automatically separate the material components. The volatile matter is defined as the mass lost up to 400°C and the char mass is the mass lost up to 900°C and the remaining mass is the residue. The volatile matter cut off temperature was chosen as the proximate analysis showed that the pyrolysis reaction peaks before 400°C, as shown in Figure 25.

Reaction temperatures are found in a similar way to that described in Section 3.4.2.1.2. That is to say that the maximum mass loss rate is found between certain temperature bounds and the onset as a fraction of the mass loss rate. Additionally, the reaction temperature of the char oxidation reaction is found. This is found in a slightly different way as this reaction overlaps with the volitisation reaction and so finding the maximum is not an effective technique. Instead, starting from 900°C, the mass loss rate is compared to successive temperatures until it starts to decrease, in this way establishing the peak. The onset temperature is similarly

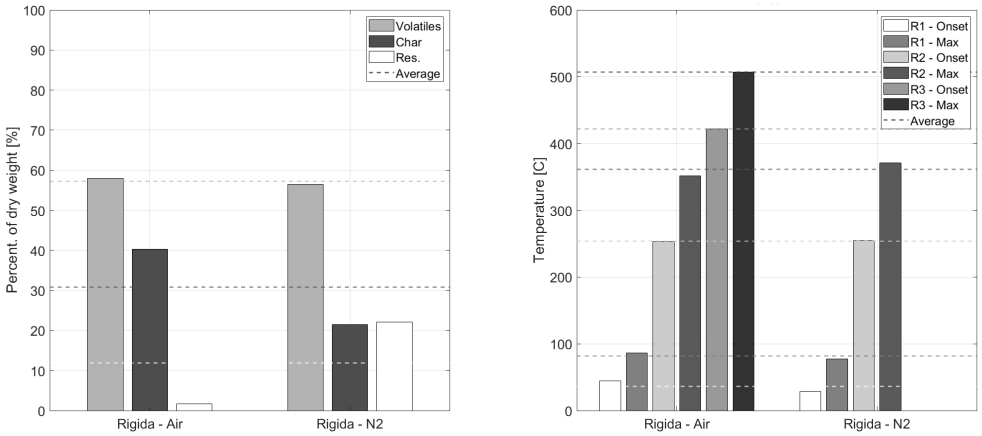

Figure 26: Results for air and nitrogen experiments at 25°C/min. Left: Percentage mass. Right: Reaction temperature.

found but instead successive temperature are compared until there is an increase. This gives the minimum that exists between the two reactions.

3.4.3.2 Results

In the following sections the results of the controlled combustion experiments are presented with further Figures presented in Appendix B. The experiments presented include:

1. Change in Environment - Air vs N_2 - 25°C/min
2. Conditioning
3. Low Heating Rate
4. All Heating rates

3.4.3.2.1 Change in Environment - Air vs N_2 - 25°C/min

The intention of these experiments is to understand how the environment affects the thermal degradation of wildland fuels. This was done by conducting experiments in both air and nitrogen at the same heating rates with the results presented in Figure 26 and Table 14 and 15.

On average the mass lost before 400°C in air is 70% whilst in N_2 68% is recorded. The mass lost after 400°C in air is on average 28% whilst in N_2 it is 11%. The recorded average residue is 3% in air and 20% in nitrogen. The difference between the mass lost after 400°C in air and N_2 is 16%. This is less than the mass attributed to char in the proximate analysis (20% see Table 11) which suggests that in an oxidative environment ≈4% is lost before 400°C.

Reaction temperatures are observed to vary due to heating rate and environment. Reaction 1 is drying. Its onset and maximum mass loss rate temperature ranges between 25-65°C and 59-118°C respectively. Reaction 2 is pyrolysis. Its onset and maximum mass loss rate temperature ranges between 240-258°C and 334-373°C respectively. Reaction 3 is char oxidation. Its onset and maximum mass loss rate temperature ranges between 396-457°C and 475-503°C respectively.

3.4.3.2.2 Conditioning

The intention of these experiments is to understand how the conditioning (60°C in an oven for 24 hr) affects the thermal degradation of wildland fuels. This was done by conducting experiments with conditioned and unconditioned pinus rigida with the results presented in Figure 27 and Table 16 and 17.

		15°C/min	25°C/min	100°C/min	Mean
Volatile Matter [%]	Air	72.31	69.34	68.00	69.16
	N_2	69.42	66.71	69.17	
Char [%]	Air	26.40	28.61	27.74	19.43
	N_2	10.89	11.24	11.68	
Residue [%]	Air	1.30	2.05	4.25	11.10
	N_2	19.68	22.05	19.15	

Table 14: Mass percentages for pinus rigida in different heating and environment conditions (Air and N_2).

			15°C/min	25°C/min	100°C/min	Mean
Temperature [°C]	R1	Air	38.25	40.83	70.00	44.33
		N_2	25.25	26.67	65.00	
	R1 max	Air	82.00	86.67	118.30	91.31
		N_2	59.25	83.33	118.30	
	R2	Air	242.00	245.40	258.30	248.48
		N_2	239.80	247.10	258.30	
	R2 max	Air	334.00	338.80	355.00	353.03
		N_2	356.30	360.80	373.30	
	R3	Air	395.80	406.30	456.70	419.60
		N_2	-	-	-	
	R3 max	Air	474.50	491.30	503.30	489.70
		N_2	-	-	-	

Table 15: Reaction temperatures for pinus rigida in different heating and environment conditions (Air and N_2)

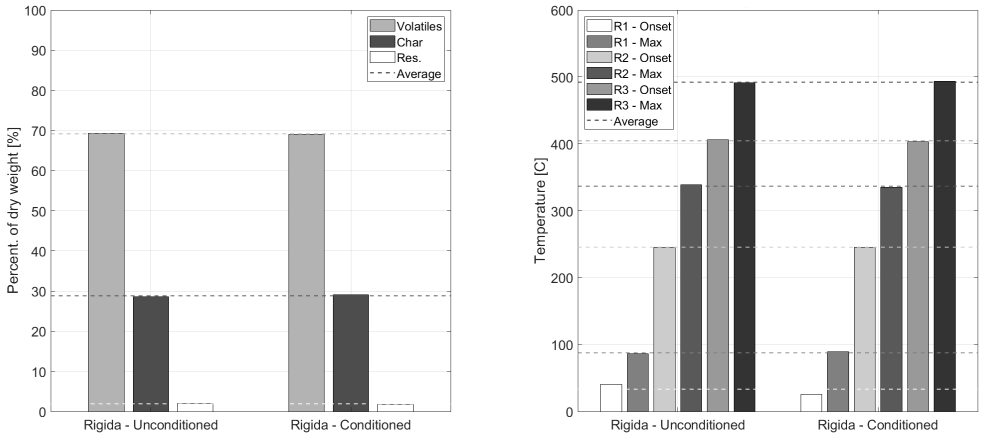

Figure 27: Controlled combustion results for unconditioned and conditioned pinus rigida at 25°C/min. Left: Percentage mass. Right: Reaction temperature.

	Percentage [%]		
	Volatile Matter	Char	Residue
Unconditioned	69.34	28.61	2.05
Conditioned	69.09	29.09	1.82

Table 16: Controlled combustion mass percentages for unconditioned and conditioned pinus rigida at 25°C/min.

	Temperature [°C]					
	R1	R1 max	R2	R2 max	R3	R3 max
Unconditioned	40.83	86.67	245.4	338.8	406.3	491.3
Conditioned	25.42	89.17	245.4	335	402.9	493.3

Table 17: Controlled combustion reaction temperatures for unconditioned and conditioned pinus rigida at 25°C/min.

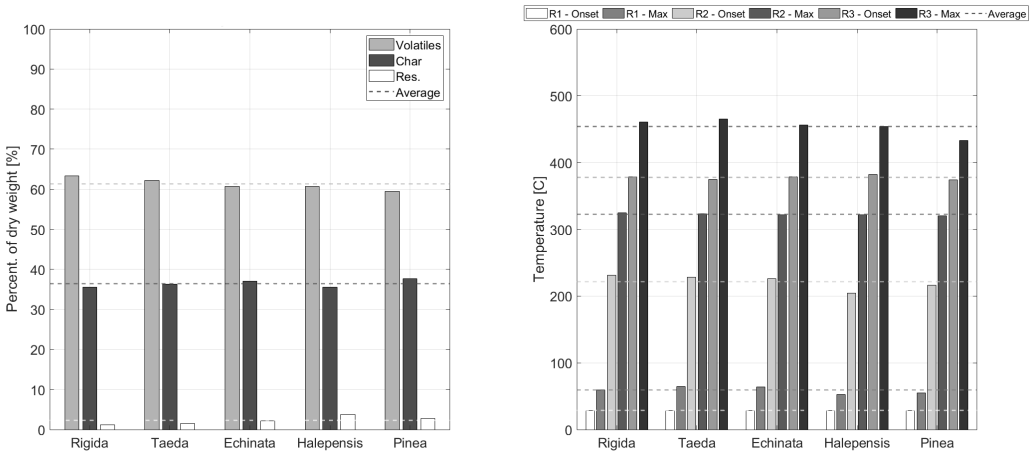

Figure 28: Controlled combustion results for pinus species at 5°C/min. Left: Percentage mass. Right: Reaction temperatures.

3.4.3.2.3 Low Heating Rate

The intention of these experiments is to understand how thermal degradation of wildland fuels proceeds at a low heating rate of 5°C/min. This was done by conducting experiments where the final temperature was 400°C and 900°C.

3.4.3.2.3.1 Pinus Species

Here are the volatile matter, char and ash fractions results for the Pinus species along with the reaction temperatures are presented in Figure 28 and Table 18 and 19.

For the pinus species the mass lost before 400°C ranges from 61-67%. The mass lost after 400°C ranges from 34-36%. The residue ranges from 1-4%. Reaction 1 is drying and its maximum mass loss rate temperature ranges between 51-67°C. Reaction 2 is pyrolysis and its onset and maximum mass loss rate temperature ranges between 202-230°C and 311-320°C respectively. Reaction 3 is the char oxidation reaction and its onset and maximum mass loss rate temperature ranges between 362-382°C and 424-457°C respectively.

Species - End Temperature	Volatile Matter [%]	Char [%]	Residue [%]
Rigida - 400°C	67.31	-	-
Taeda - 400°C	65.93	-	-
Echinata - 400°C	65.41	-	-
Rigida - 900°C	64.63	34.26	1.114
Taeda - 900°C	63.59	34.91	1.504
Echinata - 900°C	62.34	35.51	2.148
Halepensis - 900°C	62.05	34.18	3.766
Pinea - 900°C	61.24	35.89	2.869

Table 18: Controlled combustion mass percentages for pinus species at 5°C/min.

Species - End Temperature	R1 [°C]	R1 max [°C]	R2 [°C]	R2 max [°C]	R3 [°C]	R3 max [°C]
Rigida - 400	25.08	65.33	229.7	314.9	382.1	-
Taeda - 400	25.08	66.92	225.5	313.9	362.3	-
Echinata - 400	25.08	67.08	223.9	310.9	382.2	-
Rigida - 900	25.08	59.5	229.7	319.6	372.3	452.4
Taeda - 900	25.08	64	226.3	318.1	368.2	457.2
Echinata - 900	25.08	62.83	223.6	316.3	372.3	447.8
Halepensis - 900	25.08	51	202.3	316	375.1	443.9
Pinea - 900	25.08	52.67	214	314	366.9	424

Table 19: Controlled combustion reaction temperatures for pinus species at 5°C/min.

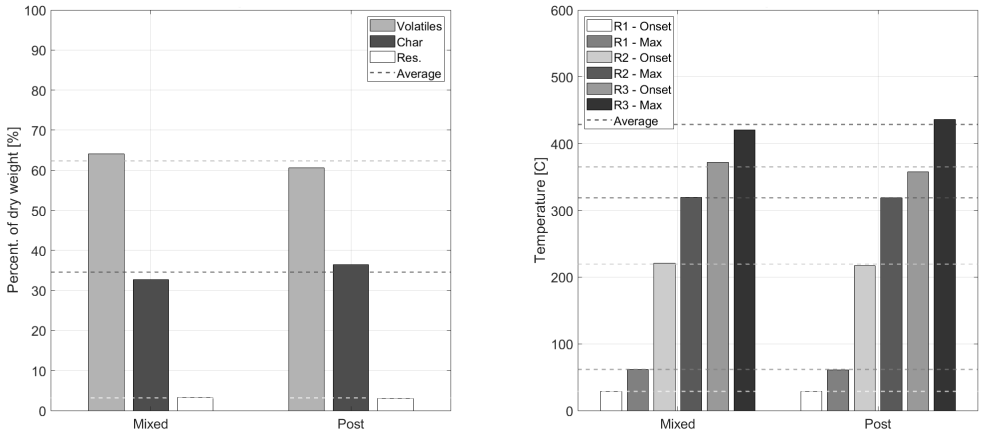

Figure 29: Controlled combustion results for broad leaf species at 5°C/min. Left: Percentage mass. Right: Reaction temperatures.

3.4.3.2.3.2 Broad Leaves

Here are the volatile matter, char and ash fractions results for the broad leaf species along with the reaction temperatures are presented in Figure 29 and Table 20 and 21.

For the non-pinus species the mass lost before 400°C ranges from 55-68%. The mass lost after 400°C ranges from 38-42% and the residue is 3%. Reaction 1 is drying and its maximum mass loss rate temperature ranges between 52-67°C. Reaction 2 is pyrolysis and its onset and maximum mass loss rate temperature ranges between 215-228°C and 298-315°C respectively. Reaction 3 is the char oxidation reaction and its onset and maximum mass loss rate temperature ranges between 366-347°C and 417-426°C respectively.

Species - End Temperature	Volatile Matter [%]	Char [%]	Residue [%]
Mixed - 400°C	60.21	-	-
Black Jack - 400°C	63.49	-	-
Jam Bush - 400°C	68.23	-	-
White - 400°C	58.45	-	-
Mixed - 900°C	57.41	39.43	3.165
Chestnut - 900°C	59.06	37.75	3.19
Post - 900°C	54.6	42.39	3.014

Table 20: Controlled combustion mass percentages for broad leaf species at 5°C/min

Species - End Temperature	R1 [°C]	R1 max [°C]	R2 [°C]	R2 max [°C]	R3 [°C]	R3 max [°C]
Mixed - 400°C	25.08	66.83	220.3	308.5	347.3	-
Black Jack - 400°C	25.08	67.25	227.6	307.1	347.3	-
Blueberry - 400°C	25.08	66.75	221.2	298	347.3	-
White - 400°C	25.08	67.08	221.2	310.1	347.3	-
Mixed - 900°C	25.08	51.83	217.3	314.5	365.8	417.3
Chestnut - 900°C	25.08	57.42	220.8	310.3	362.3	425.3
Post - 900°C	25.08	60.08	215	312.6	350.7	426.3

Table 21: Controlled combustion reaction temperatures for non-pinus species at 5°C/min

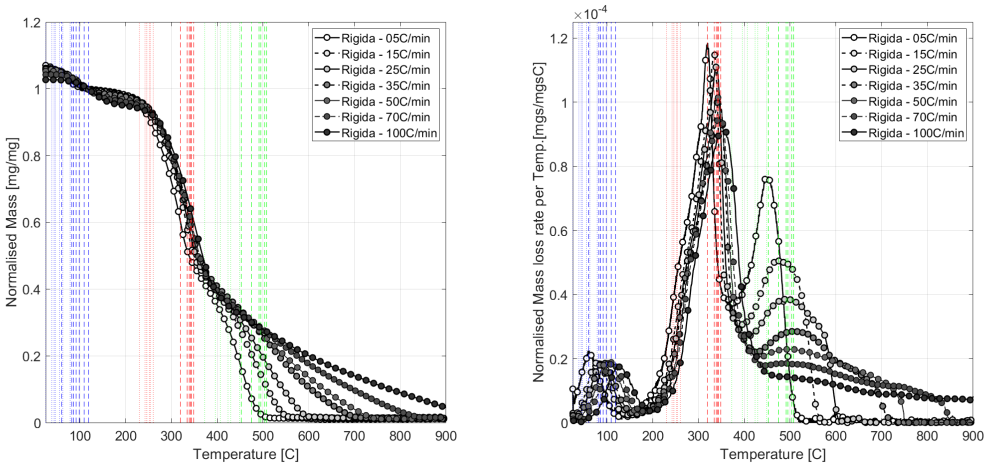

Figure 30: Controlled combustion results for pinus rigida at all heating rates. The dotted line indicates the onset temperatures and the dashed line the maximum temperature. Left: Normalised mass. Right: normalised mass loss rate per temperature rate

3.4.3.2.4 All Heating Rates

Here all the results for the different heating rates are presented in Figure 30, 31 and 32 and in Table 22 and 23. The intention of these experiments is to understand how thermal degradation of wildland fuels proceeds at different heating rates ranging from 5-100°C/min. This was done by conducting experiments with pinus rigida where the final temperature was 900°C.

	Percentage [%]		
Heat Rate [°C/min]	Volatile Matter	Char	Residue
5	63.3	35.57	1.127
15	58.98	39.68	1.34
25	58.01	40.31	1.673
35	56.87	41.74	1.39
50	57.8	41.1	1.101
70	56.98	41.5	1.521
100	56.5	38.2	5.488

Table 22: Controlled combustion mass percentages for pinus rigida at all heating rates.

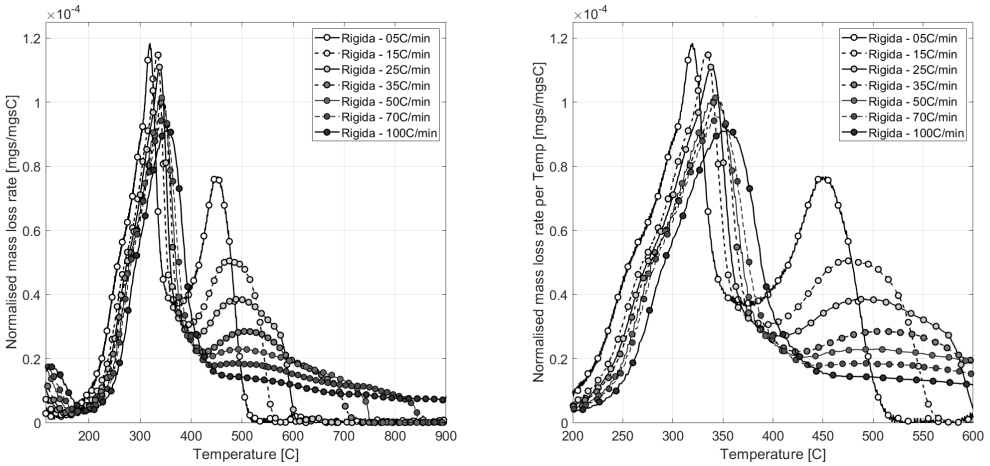

Figure 31: Controlled combustion normalised mass loss rate per temperature rate for pinus rigida at all heating rates. Left: 115-900°C. Right: 200-600°C.

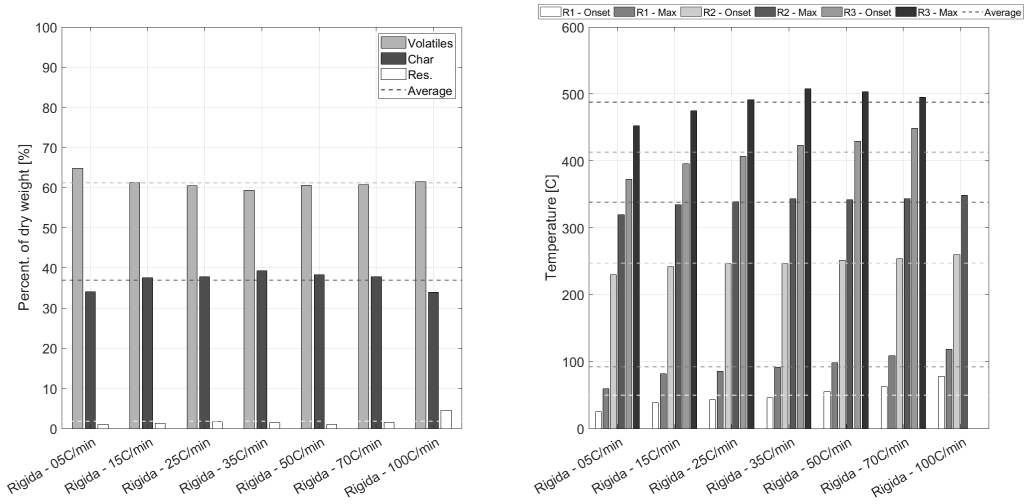

Figure 32: Controlled combustion results for pinus rigida at all heating rates. Left: Percentage mass. Right: Reaction temperatures.

	Temperature [°C]					
Heat Rate [°C/min]	R1	R1 max	R2	R2 max	R3	R3 max
5	28.84	59.40	231.6	324.6	378.4	460.5
15	39.54	82.65	247.3	344	7407.6	487.9
25	44.29	86.60	253	351.3	421.9	507.3
35	46.53	93.23	254.2	356.8	439.2	523.6
50	53.02	98.26	259.5	356.2	447.6	521.9
70	56.97	108.2	262.8	3600	470.2	517
100	62.87	117.7	266.6	363.3	-	-

Table 23: Controlled combustion reaction temperature for pinus rigida at all heating rates

3.4.3.3 Discussion

3.4.3.3.1 Change in Environment

3.4.3.3.1.1 Volatile Matter, Char and Ash fractions

Table 14 shows the average over both environments in 69.16%, the difference in average mass lost as volatile matter (i.e.before 400°C) in the two environments is 1.45%. This indicates that the pyrolysis reaction, in terms of mass loss, can be considered independent of the environment.

The difference between the mass lost after 400°C in air and N_2 is 16.31%. This is less than the mass attributed to char in the proximate analysis (20.30% see Table 11) which suggests that in an oxidative environment 4% is lost before 400°C. This underlines the need for an oxidative environment for oxidation to occur. This may seem like a redundant statement but it does show that the oxygen within the material (Table 2) is not available for char oxidation.

3.4.3.3.1.2 Reaction Temperatures

Table 15 shows the reaction temperatures recorded increase with heating rate. This is often attributed to a break down in the experimental assumptions. Where the sample has a large Biot number and is subject to temperature gradients, thereby invalidating the assumption of the TGA method. Consequently the interior of the sample is at a lower temperature than exterior of the sample. This causes the perception of higher reaction temperatures as it is the exterior sample temperature is measured.

Reaction 2 is the pyrolysis. The onset of pyrolysis is similar regardless of the environment and ranges between 240-258°C. This further supports the idea that pyrolysis can be considered independent of environment. Occurring predominantly due to heat transfer.

On the other hand the temperature of maximum mass loss rate of reaction 2 is reduced in air compared with N_2 ranging between 356-373°C and 334-355°C respectively. In general there is approximately a 20°C reduction. Potentially char oxidation occurring before 400°C is interacting with the pyrolysis reaction.

3.4.3.3.2 Conditioning

Conditioning of the sample has no effect on the the thermal degradation of dead Pinus Rigida. Previous authors suggested that volatiles may be lost from a sample during drying [85]. This may still be true for live or recently fallen needles which may have a larger volatile profile. Nevertheless the results here suggest otherwise.

3.4.3.3.3 Low Heating Rate

3.4.3.3.3.1 Volatile Matter, Char and Ash fractions

Pinus rigida is shown to have the most mass lost before 400°C which is similar to the trend in volatile matter percentage found in proximate analysis. Pinus pinea has the largest mass lost after 400°C this is similar to the result for the percentage char content found in the proximate analysis. Pinus halepensis shows the largest residue content this is similar to the ash result shown in proximate analysis.

The non-pinus species show the same results as the proximate analysis results. Blueberry is shown to have the most mass lost before 400°C a result analogous to the having the most volatile matter. Furthermore post oak is shown to have the most mass lost after 400°C. This is analogous to the measuring of the char fraction.

3.4.3.3.3.2 Reaction Temperature

The reaction temperatures are observed to exist in a smaller range for the oxidative experiments compared to the nitrogen ones. For example the maximum mass loss rate temperature range for reaction 2 for the pinus species is 311-320°C and for non-pinus species it is 298-314°C. On the other hand, the nitrogen experiments the range was 350-371°C and 298-365°C. This indicates

that the non-oxidative environment allows the different components to be distilled whilst in oxygen they act more homogeneously.

Unlike in Section 3.3.2 the increased char content of the non-pinus species did not translate to higher reaction temperatures. Pinus char content was measured as 19-26% whilst non-pinus species contained 24-28%. Instead the pinus species maximum mass loss rate temperature for reaction 3 was 424-457°C compared to the non-pinus species ranging 417-426°C.

3.4.3.3.4 All Heating Rates

Figure 31 shows the effect of changing the heating rate. Increasing the heating rate shifts the mass loss rate curve to higher temperatures.

As suggested in Section 3.4.2.1.2 this has been attributed to the formation of temperature gradients within the sample and therefore the assumption of a homogeneous sample temperature. Conducting the experiments in an oxidative environment showcases how the heating rate affects the char oxidation process. It is shifted to higher temperatures but also its shape undergoes a more dramatic change than the pyrolysis peak.

Over an increase from 5 to 70°C/min, the peak reaction temperature is shifted 36°C and 57°C for the pyrolysis and char oxidation peaks respectively. The shape of the char oxidation peak is altered as the process requires oxygen and so at higher heating rates the flow rate of oxidiser to the char oxidation zone is too slow compared to the heating. This change in shape was also observed in the similar process undergone by coal char in Section 3.3.2.

3.4.3.4 Conclusion

Pyrolysis reaction is practically independent of the environment when considering the percentage mass and the onset temperature. Differences are observed in the temperature of maximum mass loss rate where samples in air are observed to reach their maximum mass loss rate 20°C before their N_2 counterpart. This is attributed to the char oxidation reaction which overlaps with the pyrolysis peak. Comparison of the proximate analysis and controlled combustion results suggest that char oxidation occurs before 400°C.

Species trends in mass content are replicated in both environments. However reaction temperatures are observed to become more consistent in an oxidative environment. That is to say there are less differences between species in an oxidative environment than in a nitrogen one.

Increasing heating rate shifts the mass loss rate to higher temperatures. Nevertheless the effect is less substantial when considering the pyrolysis curve compared to the char oxidation. This is because the char oxidation requires not just that the heating rate is adequate but also the flow rate of oxidiser.

3.4.4 Heat of Combustion

The bomb calorimeter is used to measure the heat of combustion of a material. This is done by burning the material and recording the rise in temperature of the surrounding fluid. This can be used to calculate the change in energy which is then normalised by the initial mass. The output of the device is then the energy per unit mass.

3.4.4.1 Method

For these experiments an IKA bomb calorimeter was used. Before testing, the bomb calorimeter was calibrated using benzoic acid. The tests involved using a crucible containing 0.15g of wildland fuel sample. Once filled the crucible was placed inside the chamber of the bomb calorimeter and a cotton thread was used to connect the crucible and a hot wire, also within the chamber. Once the chamber is closed, the wire was heated causing ignition of the thread and the sample. Concurrently, the chamber was flooded with oxygen ensuring complete combustion of the sample leaving behind a incombustible residue. The energy output is measured and used to give the heat of combustion of the sample using th initial mass.

3.4.4.2 Results

The heats of combustion are presented in Figure 24 amd were observed to vary from 17.07 to 19.67 J/g. Averaging the different groups the pinus, stems and broad leaf species have a heat of combustion of 19.51, 18.21 and 17.25 J/g respectively.

	Species	Hc [J/kg]	Mean [J/kg]
Pinus	Rigida	19.67	19.51
	Taeda	19.56	
	TaedaX	19.67	
	Echinata	19.12	
Broad Leaf	Red Maple	17.69	17.25
	Blueberry	17.40	
	White Oak	16.95	
	Chestnut Oak	17.16	
	Black Jack Oak	17.07	
Stems	Black Jack Oak Stems	17.65	18.21
	Blueberry Stems	18.77	

Table 24: Results from bomb calorimeter for different wildland fuel samples.

3.4.5 Intra-Experiment Discussion

3.4.5.1 Proximate Analysis and Controlled Combustion

Comparing the two techniques similar trends are found. Nevertheless, the comparison of the techniques leads to the following observations:

1. High heating rates shift the curve to higher temperatures and in the case of the char oxidation curve also changes its shape. Most likely due to lack of optimum mass flow rate of oxygen.

2. Reaction temperatures are more consistent for the different species in oxidative environments. Most likely due to interaction with the char oxidation reaction.

3. Proximate analysis allows the different process to be considered independently and gives a similar pyrolysis peak as in an oxidative environment.

4. Controlled combustion allows for considering the char oxidation process which underpins smouldering.

3.4.5.2 Empirical Relations

3.4.5.2.1 Higher Heating Value

Similar literature data has been used in empirical correlations for determining the higher heating value (HHV). The higher heating value is analogous to the heat of combustion as both describe the total available thermal energy of a sample whose products have been brought back to pre-combustion temperature. In these works the idea is that the composition determines the heat. Correlations are given below - where VM is the volatile matter fraction, FC is the fixed carbon fraction and ASH is the ash fraction:

$$HHV = 0.1905VM + 0.2521FC \quad [86] \tag{45}$$

$$HHV = 0.1559VM + 0.3536FC - 0.0078ASH \quad [87] \tag{46}$$

They suggest that the weight of the fixed carbon is higher than the volatile matter when determining the higher heating value. Using the values from the proximate analysis the calculated values would be as in Table 25. Also shown are the values measured using the bomb calorimeter.

		HHV [J/kg]		Hc [J/kg]
	Species	Yin [86]	Parikh [87]	
Pinus	Rigida	19.96	19.31	19.67
	TaedaX	19.92	19.54	19.67
	Echinata	19.93	19.72	19.12
	Halepensis	19.31	18.63	-
	Pinea	19.72	19.90	-
Broad	Black Jack	20.11	20.24	17.07
	Mixed Oak	19.90	20.18	17.85
	White	19.76	19.97	16.95
	Post	19.82	20.30	-
	Blueberry	19.78	19.70	17.40
Wood	Blueberry	19.87	19.62	18.77
	Black Jack	19.52	18.85	17.65

Table 25: Estimated HHV and measured heat of combustion.

The calculated values are consistent for the experimental values for the pinus samples. However the heat of combustion of non-pinus species are overestimated. As the initial mass is more than two thirds volatile mass and shows more variation across the species it is assumed that the heat of combustion is most affected by the volatile matter. This is contrary to the relations just mentioned but they are meant for a broader sample space than just wildland fuels. As such it is postulated that the volatile matter of pinus species is different to the non-pinus species.

This can be supported by considering the thermal degradation curves of these materials (Section 3.4.2.3.3). Pinus species are observed to have a larger second peak compared to the non-pinus samples. The volatiles released in these two peaks will most likely be different. This can be underlined by considering the thermal degradation parameters measured in the proximate analysis. Figure 33 highlights this difference with the non-pinus species being grouped in the lower left corner and the pinus species grouping in the top right.

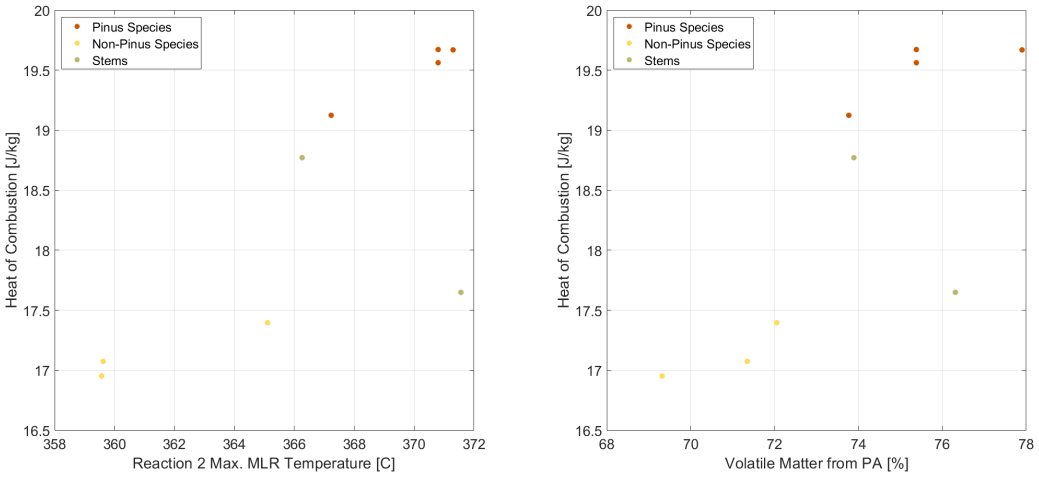

Figure 33: Measured heat of combustion as a function of measured thermal degradation parameters

3.5 Conclusion

The TGA can be used to observe the mass signature of the reactions by computing the derivative of the mass of the reactants. The reactions involved in fire are drying, pyrolysis and char oxidation. Drying and pyrolysis are endothermic and char oxidation is exothermic. This is a consequence of bonds being broken and made in the reactions.

Reactions are initiated after overcoming an activation energy and energy is required to break bonds whilst energy is given off in making them. Temperature is a measure of energy and as such reaction temperatures can be defined to characterise the reactions. If the bonds in different material have similar bond energies, then it follows that the reaction temperatures should also be similar.

The literature indicates that plant element function (e.g. leaf, stem, bark, wood) determines material composition and therefore combustion behaviour. Additionally, there is indication that biological degradation has a role to play in the subsequent thermal degradation.

Elemental analysis does not give us an insight into the modes of burning but instead gives an overall picture. The similar values for the different natural fuels suggests that potentially similar bonds underpin their chemistry. Nevertheless, this does not distinguish between the different fire processes - drying, flaming/pyrolysis and char oxidation. A more useful approach would involve understanding how much of the material is available to each process.

In terms of fire processes, knowing precisely the molecular components brings us no closer to knowing how they will contribute to the fire processes as we do not know the mechanisms by which they degrade thermally or biologically nor is this level of complexity welcome. Nevertheless, investigating individual representative molecular components does set bounds for the degradation but not necessarily how they will contribute the different modes of burning. A more pragmatic analysis would be one that had the fire processes at the centre of it.

The proximate analysis approach is rooted in the fire process and moves the lens away from the specificity of plant chemistry. In the context of wildfires, it seems the most practical approach. However, it must be coupled with controlled combustion as char oxidation must occur in an oxidative environment. This was the approach taken here.

It was found that:

1. Pyrolysis is independent of environment under TGA conditions.
2. Char oxidation requires consideration of oxygen flow rates at high heating rates
3. Pyrolysis is made up of at least two peaks. High and low temperature pyrolysis. Contribution of each peak depends on plant structure.
4. Samples with a more pronounced higher temperature pyrolysis had a higher heat of combustion.
5. Experiments in oxidative environments had narrow reaction temperature range and the different samples were more consistent.
6. Pyrolysis and therefore flaming combustion occurs between 250°C and 350°C.
7. A maximum of 70% of the original dry mass is available for pyrolysis.

Part IV
Ignition

4.1 Introduction

In the previous Parts, wildland fuel morphology and thermal degradation were highlighted. These both have their role in the ignition of fuel beds. Morphology will determine the fuel bed structure and the way it heats up whilst thermal degradation will determine the material response to that heat. In this part the effect of both are tested experimentally using the fire propagation apparatus (FPA). Fuel beds were made using different species of Pinus and non-natural pine needle lengths were manufactured from Pinus Rigida needles. In this way the flammability of wildland fuel beds is understood as a function of species and fuel bed structure.

4.1.1 Ignition

The ignition of a material is defined as the appearance of a flame. This phenomenon is observed independent of the initial state of fuel - be that solid, liquid or gas. Ultimately the presence of a flame signifies a gas phase reaction. However the route to that gas phase reaction is dependent on how the fuel exists initially and particularly how it responds to heating.

In solid ignition the solid fuel must be transformed to a gaseous fuel. This requires heat transfer, pyrolysis (chemical reaction) and mass transfer to occur. In fire safety engineering, charring solid is considered as an archetype along with the melting/bubbling solid [35][88]. Wildland fuels undergo charring and so here the charring solid will be considered in the following sections.

4.1.2 Solid Ignition Process

Ignition is a transition event where a combustion reaction is initiated, usually followed by a period of sustained burning. The processes preceding ignition are the heating of the solid, the pyrolysis of the solid to form volatile components and the migration and mixing of those gases to produce a flammable mixture. Finally, the air-fuel mixture must have enough energy that the gas phase flame reaction occurs.

4.1.2.1 Heat transfer

Ignition is the point when we observe a gas phase reaction due a series of processes occurring in the solid (or condensed) phase. These are driven by changes in the temperature of the solid. The ignition process is an umbrella term and it is worth remembering that it involves a number of sub-process. If we subject a solid, initially at ambient temperature, to an external source of energy we will observe some of the processes leading to ignition and, if conditions are satisfied, witness ignition.

For this discussion and for simplicity we will assume that the heat input is restricted to the top face of the solid. This allows for the ignition process to be considered one-dimensional. That is to say, because energy enters the solid through the top surface, it is here where we should see the highest temperatures. In depth there is a decrease in temperature, away from the top surface, towards the back surface of the solid. In other words, the top face defines the heat transfer into the system the back face defines the energy leaving the system. As time progresses the thermal wave penetrates through the solid resulting in the temperature being a function of both depth, x, and time, t. The dominant mechanism of heat transfer occurring through an impermeable, opaque solid is due to conduction.

The heat transfer can be evaluated using the solid temperature. Through the application of the heat equation and some simplifications, an analytical solution to the heating process can be established to develop relationships between the ignition and the thermal exposure. This is discussed in Section 2.3.1.6.

4.1.2.2 Chemistry

Ignition as defined previously is a gas phase reaction and as such the ignition process requires the solid to be converted to the gas phase. The increase in solid temperature causes thermal decomposition of the solid and the molecules break up to form smaller gaseous components. This process is called pyrolysis.

The solid fuel constitutes a finite source of gaseous components. Not all the material is consumed and a solid residue is formed (ash). Ash is the non-combustible residue and char is a carbonaceous residue. Charring materials (such as timber and many natural fuels) will additionally form a char after pyrolysis. The char formed can then undergo a secondary reaction at high solid temperatures and in the presence of oxygen. This is called char oxidation. It occurs at the interface of the solid and the gas and may be observed as a red glow on the surface.

Some of the gaseous products emanating from the solid degradation reactions will be fully-oxidised and/or inert. That is to say not all the mass lost, as gaseous components, is gaseous fuel. These fully oxidised/inert gases can dilute the fuel mixture shifting it away from the flammability limit and therefore ignition. A common example of this would be in fuels with a moisture content e.g. wood. As they degrade the moisture is evaporated and released as gaseous components. These cannot contribute to flammable mixture and as such serve only to dilute the fuel mixture. The different components produced can be defined for a material using product yields which define the proportions of each product given off per unit mass.

As the gaseous mass production is a direct consequence of the solid temperature distribution the production of gases is maximum at the top surface and decreases in depth. Therefore both the temperature of the solid and the mass flux of pyrolysis gases are defined by the heat transfer. However the mass production draws from a finite source and so converse to the temperature depends on the remaining solid mass. What this means is gaseous mass production zone occurs within the heated zone but fluctuates depending on the remaining solid available to produce gaseous components.

The production of gases is a consequence of the thermal degradation of the solid fuel. Naturally it follows that an increase in gaseous production is due to an increase in solid fuel consumption. As such the amount of solid fuel is minimum at the surface and increases towards the back face.

We can interpret the chemistry process by constructing it on top of the heat transfer process. That is to say the production of gaseous fuel is due to a change in the composition of the original solid fuel. This is manifested as a loss of mass fraction of the original solid fuel.

4.1.2.3 Mass Transfer and Gas Chemistry

Ignition is the observance of a gas phase reaction and as such the gaseous fuel must mix with the ambient air and be heated up such that we have the ideal conditions for gas phase combustion reaction. Remember that the gaseous fuel is a part of the pyrolysis gases produced during thermal degradation of the solid.

Piloted ignition occurs in the presence of a pilot flame. The pilot flame is a localised region of high temperature which promotes conditions for ignition of the gas phase reaction. This reduces the problem to only requiring that the correct mixture of gas fuel and air is present in this location. Without a pilot flame the gas mixture must have sufficient energy to initiate the combustion reaction - that is to say it must be at a high enough temperature.

The mixing of the gaseous fuel and the air is a consequence of the buoyant flow resulting from a density gradient in the gaseous phase. Low density gas will rise above high density gas. In the wake of this rising plume ambient air is drawn into the pyrolysis gases creating a fuel-air mixture. The changes in gas density are due to the temperature field resulting from the heated solid surface and the temperature of the gaseous pyrolysis products being produced. That is to say the hot solid surface heats the gas above it that the pyrolysis gases are produced at the temperature of the solid. An illustration of the ignition process is shown in Figure 34.

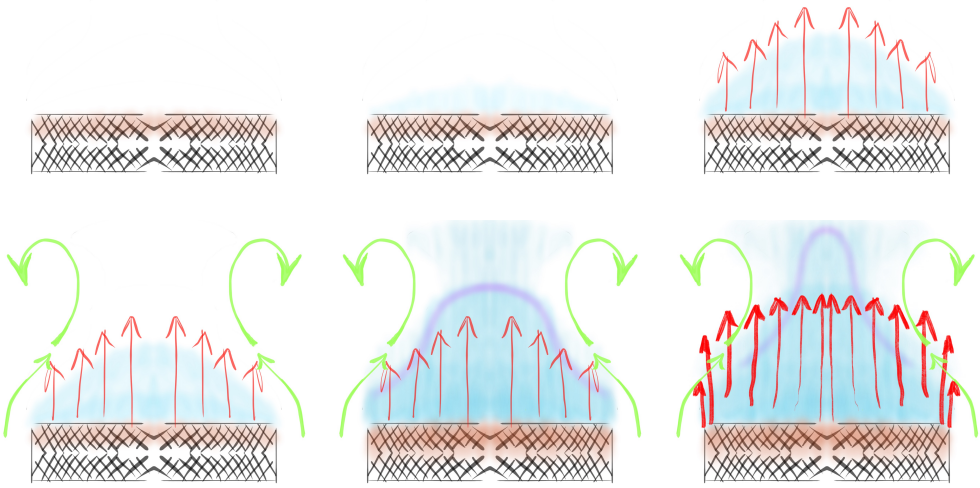

Figure 34: Illustration of the ignition process. Where the brown heated region produces the blue pyrolysis gases. As a convective current is established ambient air is drawn into the pyrolysis gases resulting in a mixture within the flammability limits. This is shown as the purple region.

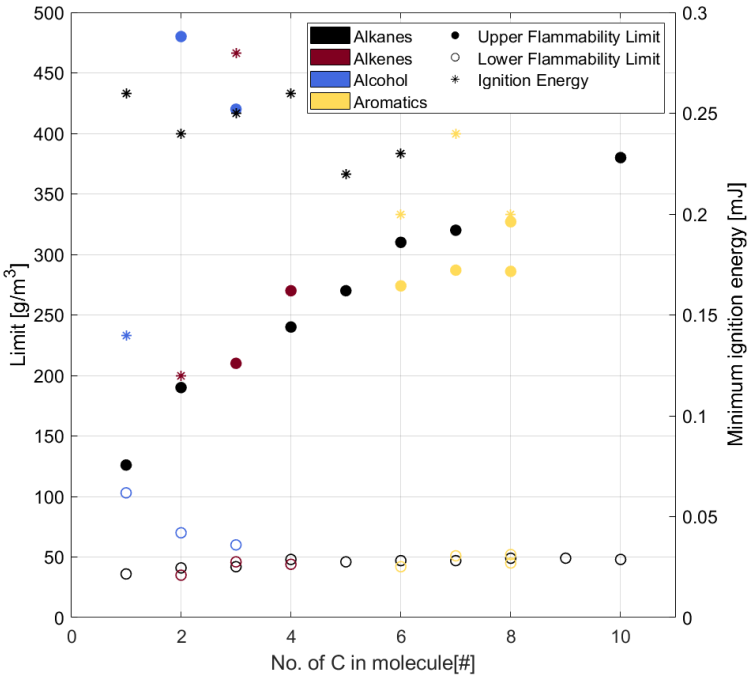

Figure 35: Flammability of organic compounds. Extracted and re-plotted [58][89].

4.1.2.4 Flammability Limits

The gas phase flame reaction is an oxidation reaction. This requires non-oxidised gaseous products to mix with oxygen through mixing with ambient air. The mixtures required for a flame exist within flammability limits which are dictated by the gaseous fuel mixture. Figure 35 shows the flammability limits for a number of organic compounds. When there is more oxygen than required by stoichiometry, the mixture is lean conversely when there is more fuel than required by stoichiometry, the mixture is fuel rich. Here we can see that the lower flammability limit is consistent at approximately 50 g/m^3. In the course of ignition we are expecting to be on the lower flammability limit. Hence, Figure 35 suggests that concentration of fuel at ignition should be similar for different flammable mixtures. We can interpret the mass transfer process by constructing it on top of the solid chemistry and heat transfer processes. That is to say the mass transfer is driven by a buoyant flow in turn driven by the solid temperature. The production of gaseous fuel is due to a fraction of the solid fuel consumption owing to a change in the temperature of a solid finite mass.

4.1.3 Porous Considerations

Ignition is a gas phase phenomenon where a sustained exothermic oxidation reaction occurs in a gaseous fuel/oxidiser system. Ignition occurs when gaseous fuel is supplied at a sufficient rate to, and mixed with, an appropriate quantity of gaseous oxidiser either at a threshold temperature or in the presence of a pilot flame. This process is therefore governed by mass transfer and heat transfer.

However, often the fuel is not initially in the gaseous state and must undergo a phase transformation. In liquids this may be solely due to evaporation whilst in solids pyrolysis often takes place. Evaporation is the change from liquid to gas phase of a material. Pyrolysis is the breaking of a material into smaller parts, leading to the production of liquid and gaseous fractions. This is governed by heat transfer and the decomposition chemistry.

When the fuel in question is porous both mass and heat transfer are controlled by the structure of the fuel. Porous fuels often have high permeability, allowing gaseous components to move more freely within and around the fuel. This can be beneficial to ignition as the mixing of fuel and oxidiser can occur more easily. On the other hand, it can delay ignition as the gaseous fuel is diluted.

Additionally, the heat transfer process is altered due to the increase in gas movement and decrease in the (bulk) conductivity and increase in inter-particle radiation. Consequently, the relative importance of convection as a heat transfer mechanism is increased.

Similarly, the heat transfer processes at the boundaries change. In particular the radiative heating of the fuel in increased in depth either due to a lack of attenuation or the presence of pores that open up to the interior of the fuel bed.

Both of these potential properties of the solid alter the ignition process in different ways but the general result is similar - the actively heated region is no longer a moving surface but instead a volume. In other words they affect the thermal penetration depth, which is anticipated to have a significant impact on the ignition process. The thermal depth is defined as the distance from the free surface through which the incident heat flux has influence. It must be noted that the thermal depth is a function of time as it is the depth through which the thermal wave has travelled.

Wildland fuels form porous fuel beds composed of vegetative fuel elements. To understand the processes involved in the ignition of these fuels, the fuel bed is characterised and modified to alter its mass transfer, heat transfer and thermal degradation characteristics. Hence we can analyse each of these processes within the ignition response.

The fuel bed can be characterised using global parameters, such as bulk density, but also by local parameters such as the dimensions of the fuel element. Altering the fuel element will change the packing efficiency of the fuel bed. As such, the fuel element will change the mass transfer and heat transfer in the fuel bed. This can be done by choosing a different material or species however this would not only alter the the fuel element dimensions but also the thermal degradation.

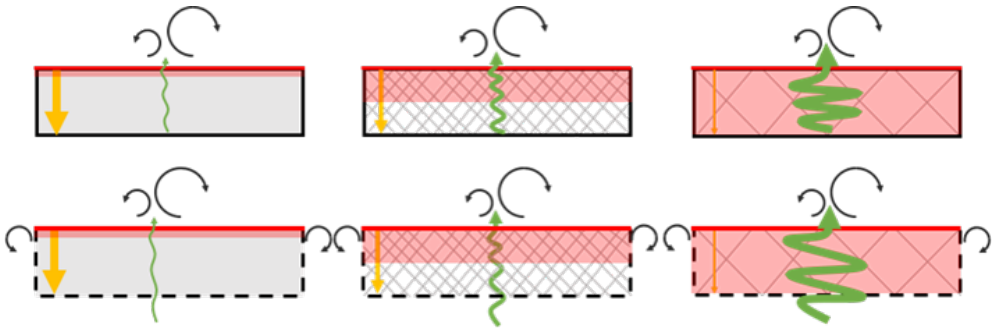

Figure 36: Illustration of the changes in heat transfer mechanisms as the material becomes more porous from left to right. Red is radiation, yellow is conduction, green is convection.

4.1.3.1 Ignition Temperature

In solids the ignition process is driven by the surface temperature of the solid. The complexity of ignition is reduced by assigning a surface temperature where all the processes should be proceeding in such a way that ignition occurs. This is the termed the ignition temperature.

Figure 36 illustrates that the heated region is not restricted to the top surface, in porous fuels, and as such the question becomes what is the meaning of the ignition temperature when considering a porous fuel? As such this is one of the core questions of this work. In response to the question an alternative framework is presented in Part V which instead of temperature as mass at its centre.

4.2 Literature

Previous work has been conducted in order to understand the thermal processes of porous fuel. A large portion of this work has been conducted using the Fire Propagation Apparatus (FPA).

A time line of the research undertaken to study the ignition of porous fuels is presented below. A discussion of this is given in the following section. .

4.2.1 FPA Timeline

2008 — Paper and Thesis
Schemel et al. [90] [91]
Explored the problem experimentally by investigating the effect of the permeability of the experimental control volume. This was done by using sample baskets made of perforated steel with open fraction 0,26,63%. Here a heat flux of 25 kW/m^2 was used and a mass of 15g. The species of pine used was Pinus halepensis and Pinus pinaster.

2009 — Conference Paper
Bartoli et al. [92]

2010 — Conference Paper
Jervis et al. [93]

2010 — Paper
Torero et al. [94]
Compared the inert solid model to experimental work conducted by Schemel and preliminary work conducted by Bartoli (conf) and Jervis (conf). Agreement was found with impermeable baskets where the fuel bed was described as having effective properties. However permeable baskets saw a deviation from model trends. The deviation here showing the assumptions underpinning the model are not appropriate. Most notably that the control volume can be considered impermeable bar the exposed face is not appropriate when the bed is permeable. Here the ignition criteria is a critical surface temperature.

2011 — Paper
Bartoli et al. [80]
Extended the experimental work of Schemel. They tested the same mass of three different species of pine under different basket and airflow conditions. This results in changing both the fuel element geometry (surface to volume) and chemistry, and the relative effect of convection on the reaction system. Additionally, Bartoli found the LHV using ultimate analysis. Pyrolysis experiments were conducted in nitrogen and the pyrolysis products were defined using FTIR. The LHV and the calorific value of the pyrolysis products were compared and a new coefficient for oxygen calorimetry was calculated. Here a heat flux of 25 kW/m^2 and a mass of 15 g was used. The species of pine used was Pinus halepensis, Pinus pinaster and Pinus laricio

2011 — Thesis
Bartoli et al. [95]
Attributed the changes in the flammability of their previous work to changes in the fuel bed permeability. They defined the permeability by conducting experiments to find the pressure drop through the fuel bed. Correlation between fuel bed parameters and the permeability was conducted. By altering the bulk density (10-20 g) and surface to volume of fuel elements they were able to vary the permeability of their fuel beds. Time to ignition was found to increase with decreasing surface to volume ratio, at a given permeability. Time to ignition was also found to increase with decreasing bulk density, for a given surface to volume ratio.

2011 — Paper
Simeoni et al. [62]
Reports the work of Bartoli with a focus on the HRR characteristics with respect to permeability. They report that more pemermeable beds release more energy during burning. Due to the similarity in the LHV, differences between species are suggested to be due to particle geometry. Here the idea of radiation incident in-depth is put forward.

2011

Paper

Mindykowski et al. [96]

Conducted experimental work similar to Bartoli varying the bulk densities(5-20 g) and heat fluxes(12.5-30 kW/m^2) applied to fuel beds made of Pinus Pinaster. They extended the work by including Oak leaves which represent a change in the aspect ratio of the fuel element. Here solid fraction and surface to volume is used to describe the fuel bed. Their data shows a good linear agreement between the inverse time to ignition and the heat flux. They suggested that the results are similar to the results of a thermally thin solid. Through dimensional analysis of the energy equation averaged over the radiation depth they showed that this trend would also be followed by a homogenous equivalent medium. This suggests the fuel beds are acting as a thermally thin solid or a homogenous equivalent medium. Here the ignition criteria is a critical average temperature.

2011

Paper

Consalvi et al. [97]

Applied a multiphase finite volume numerical scheme to the experimental work conducted by Mindykowski. Here the criterion for ignition is the thermal runaway in the gas phase. Their simulations suggested that char oxidation becomes an important factor when considering low heat fluxes. Furthermore, they found that a simplified criterion for ignition was achieved by considering a critical mass flux of pyrolzate rather than considering the gas phase temperature. This suggests that the ignition process is controlled by the response of the solid phase rather than the gas phase.

2012

Conference Paper

Thomas et al. [98]

2012

Thesis

Jervis et al. [99]

Conducted experimental work similar to Bartoli varying the bulk densities (3-20 g) and heat fluxes(25, 35, 50 kW/m^2). The species tested were Pinus halepensis, Pinus nigra and Pinus pinaster. They concluded that the time to ignition decreases with increased bulk density and that flow increased the combustion process.

2012

Paper

Simeoni et al. [100]

Presents radiation attenuation experiments suggesting the radiation depth is less than that calculated using the isotropic medium assumption. Presentation of results for airflow and heat flux (20-60 kW/m^2) experiments with 15 g of dead pinus strobus needles. Presents previous work by Bartoli and Schemel. Suggests that previous experiments with forced flow are mischaracterised as the flux measured does not necessarily pass through the fuel bed but around it instead. Proposal of a porous fuel model that explicitly distinguishes between the solid fraction and gaseous fraction in the control volume. In depth radiation is accounted for and a conductive term is used to represent radiative transfers within the bed (across pores) which are assumed to be diffusive. Due to the high gas fraction radiation dominates over conduction and so the latter is neglected. The radiative term is linearised using the Rosseland approximation. Porous model was solved using a finite volume approach. The model was found to be very sensitive to input parameters. However the experimental tendency was reproduced suggesting that the formulation used captures the phenomena well.

2013

Paper

Fuentes et al. [101]

Repeated some of the work by Mindykowski with an increased focus on the burning dynamics.

2013

Conference Paper
Thomas et al. [102]
Here experimental work was presented investigating the effect of airflow and moisture content. They introduced a blockage device to the FPA to ensure that all the flow was conducted through the sample. Experiments presented by Simeoni (2012) extended to include Pinus resinosa. These were experiments with airflow and heat flux (20-60 kW/m^2) experiments with 15g of dead pine needles. The moisture content experiments were done at 25 kW/m^2 with live Pinus rigida (7%-180%). Comparisons were done within a species. They found that time to ignition increases with air flow and moisture content. They suggest that closed baskets should follow the inert solid model however the use of permeable baskets allows convection to occur in the bed this is exacerbated by introducing forced flow. They show that as the radiation is increased it becomes dominant and the fuel bed can then comply with the assumptions made in the solid inert model.

2014

Conference Paper
Thomas et al. [103]
Here the focus is on Pinus Rigida. The work conducted in 2013 is extended by adding an additional heat flux of 50 kW/m^2.

2015

Paper
Lamorlette et al. [104]
Lamorlette used experimental results from Schemel, Torero amd Mindykowski to conduct dimensional analysis of a porous fuel ignition model. Additional new experiments involving Pinus Strobus were included. They concluded that the problem is mainly dictated by the product of the drag coefficient and the leaf area index when considering natural convection.

2016

Paper
Jervis et al. [85]
Tested both live, dead and aged needles. He compared the results of unconditioned and oven-dried samples and found that drying caused the three types of needles to respond similarly. He asserts that the chemistry of the samples has changed through the desorption of volatiles. This highlights the phenological effects that intersect the ignition problem.

2016

Paper
El Houssami et al. [105]
Experimental work modelled numerically using Fire Foam.

2017

Thesis
El Houssami et al. [106]
Conducted experiments on Pinus Rigida and Pinus Strobus at different bulk densities (6.4-15g) at different heat fluxes (20, 50 kW/m^2) under natural convection. This work includes some preliminary work conducted by Thomas (2013). A multiphase model, firefoam, was used to reproduce the work and analyse the role of each component of the conservation equations. Additionally, work understanding the role of pine needle absorbtivity is presented. Furthermore char oxidation found not to be represented by simplistic one-step model routinely used. They also found that derivation of the convective coefficient is overestimated when using Reynolds correlations and that instead correlations based on the Grashof number are more appropriate.

2017

Thesis
Thomas et al. [107]
Similarly to Simeoni (2012) he discusses the competing effects of convective cooling and fuel dilution leading to different trends for high and low fluxes in the time to ignition under imposed flow conditions. He also investigated the influence of increasing the flow temperature with the time to ignition decreasing with the increase in flow temperature.

2017

Paper
Thomas et al. [108]
They found that there was an increased time to ignition after decreasing below 15% O_2, otherwise it is relatively stable even at elevated O_2 concentrations. This indicates the influence of gas mixing phenomena however the large deviation from ambient suggests that the O_2 needed from mixing is not that high. Furthermore, they conducted flammability experiments throughout the year on live needles leading to an assessment of the periods of the year when the needles are most prone to fire. This bolsters the phenological importance highlighted by Jervis.

2018

Paper
El Houssami et al. [109]
They continue the work from 2016 and extends the work of Thomas (2014) by including forced flow experiments on dead pinus rigida. Three different bulk densities (8.7-15g) are tested at 50 kW/m^2. Contrary to Thomas (2014), the fuel bed is dried before testing. Found that the convective coefficient can be computed as a function of the reynolds number if a specific correlation is used. Contrary to natural convection, char oxidation can be described by a 1-step reaction under forced flow conditions. This suggests that the forced flow dominates the natural convection and so the concentration of oxygen does not depend on the burning reaction but is predefined and steady.

2018

Paper
Lamorlette et al. [110]
Proposes a multiphase model where there is a thermal disequillibrium between phases. Uses the work of Schemel, El Houssami (2016) and Thomas (2017). Finds that high moisture samples require this to be reproduced.

2019

Conference Paper
Walker-Ravena et al. [111]
Conducted experiments at different bulk densities using Pinus Rigida. The fuel elements were cut to nominal sizes to preserve the surface to volume ratio and the chemistry of the material whilst allowing for a change in the packing efficiency. Fuel beds were defined by their void fraction. Experiments were conducted with non-permeable baskets. A non-monotonic relationship between time to ignition and void fraction was found. This indicates competing processes that are controlled by the bed properties.

4.2.2 Literature Summary

4.2.2.1 Experimental Literature

Previous experiments mostly centre on influencing the fluid flow in the fuel bed. Experiments have consisted of applying impermeable and permeable boundary condition and subjecting the fuel bed to different flow conditions [90][80][95][99][105][107].

Recognising its importance in wildland fuels, some authors have investigated different fuel moisture contents and the differences between live and dead material [85][107]. Nevertheless the majority of experiments are conducted with dead fuels that are at laboratory moisture content (8-12%) or they are oven dried at 60°C for 24hr. On the other hand, Jervis [85], El Houssami[106] and Thomas [107] have conducted experiments with live fuels.

Meanwhile the fuel bed has been described by either the bulk density [85],the solid fraction [96][101], the void fraction [109] or the bed permeability [62][80]. Nevertheless this previous work is conducted over a small range of fuel bed conditions focusing instead on capturing a large range of different materials. Typical porosities are in the range 0.9-0.99, where the porosity is the fraction of the sample that is not solid.

It is likely that this small range of fuel bed conditions may not lead to fully realising the influences of the fuel bed structure on the igntion processes. Therefore, the experiments conducted in this work are conducted over a large range of fuel bed structures using a single material. Experimental conditions of previous work are summarised in Table 26:

Reference [-]	**Heat Flux** [$\mathbf{kW/m^2}$]	**Flow** [**L/min**]	**Basket Porosity** [%]	**Material** [-]	**Mass** [**g**]
Schemel	25	Air: 0, 200	0, 26, 63	Halepensis, Pinaster	15
Bartoli	25, 30, 35, 40	Air: 0, 100, 200. N_2: 60.	0, 26, 63	Halepensis, Pinaster Laricio	4, 10, 11, 12,13, 15, 17, 20
Jervis	25, 35, 50	Air: 0, 200	63	Halepensis Nigra Pinaster	3,5,8, 10,12,15, 20
Mindykowski	12.5, 15, 17.5, 20, 22.5, 25, 27.5, 30	Air: 0	63	Pinaster	5, 10, 20
El Houssami	20, 50	Air: 0, 200		Strobus, Rigida	6.4-15
Thomas	10-60	14-23% O_2: 0, 50, 100, 200	0, 63	Strobus, Resinosa, Rigida	15

Table 26: Experimental work present in the literature.

4.2.2.2 Modelling Literature

Analytical solutions of the heat equation arise from imposing simplified behaviour on the problem whilst numerical solutions are necessary when more complex phenomena are to be included. The analytical solution used in classical ignition theory is found by making simplifications on a semi infinite domain [94].

Numerical solutions of the heat equation have been developed when, for example, gas phase advection was included or the constants of the heat equation were not constant [100] or when solid phase chemistry or gas phase transport equations were included [97][104][105][109][110]. The difference in the two methods comes down to complexity. Complexity of representation and complexity of input parameters. The present work opts for a simpler approach.

4.2.3 Analytical Solution

The simplest way of interpreting ignition is by reducing it to heat transfer. Often the material is idealised as a semi-infinite solid. That is to the say the material is so thick the thermal wave does not affect the back face - it is infinitely far from the top surface.

4.2.3.1 Torero Model

Here the classical ignition model is expressed as in literature [35]. This will be referred to as the Torero model. The classical ignition model is the diffusion equation on a semi-infinite domain with an initial condition and an inhomogenous boundary condition. Coefficients are constant with respect to temperature, time and space.

$$\frac{\partial T}{\partial t} = \alpha \frac{\partial^2 T}{\partial x^2} \tag{14}$$

The initial and inhomogenous boundary conditions are expressed as in equation

$$\text{IC} \quad T(x,0) = T_0 \quad = T_\infty, \qquad T\epsilon[0,\infty) \tag{47}$$

$$\text{BC} \quad -k\frac{\partial T(\infty,t)}{\partial x} = 0, \qquad x\epsilon[0,\infty) \tag{48}$$

$$\text{BC} \quad -k\frac{\partial T(0,t)}{\partial x} \quad = \dot{q}''_s(0,t) \qquad t\epsilon[0,\infty) \tag{49}$$

where the total surface flux is given by

$$\dot{q}''_s(0,t) = \dot{q}''_{inc}(0,t) + \dot{q}''_{rad}(0,t) + \dot{q}''_{conv}(0,t) \tag{50}$$

The convective and radiative losses are defined as and approximated by

$$\dot{q}''_{conv}(0,t) = h_c(T(0,t), -T_\infty) \tag{51}$$

$$\dot{q}''_{rad}(0,t) \quad = \varepsilon\sigma(T(0,t)^4 - T_\infty^4) = h_r(T(0,t), -T_\infty) \tag{52}$$

The radiative heat loss is simplified by assuming a radiative heat transfer coefficient. The total surface flux can then be given in terms of an overall heat transfer coefficient

$$h_T = h_c + h_r \tag{53}$$

$$\dot{q}''_{inc}(t) = a\dot{q}''_e(t) \tag{54}$$

$$\dot{q}''_s(0,t) = a\dot{q}''_e(0,t) + h_T(T(0,t) - T_\infty) \tag{55}$$

The surface temperature is given by Torero as

$$T_s = T_\infty + \frac{a\dot{q}''_e}{h_T}\left[1 - \exp\left(\frac{h_T^2}{k\rho c}t\right) erfc\left(\sqrt{\frac{h_T^2}{k\rho c}}\sqrt{t}\right)\right] \tag{56}$$

Due to the inert solid simplification ignition is defined to occur at a certain surface temperature. This allows us to model the ignition behaviour of certain fuels.

4.2.3.2 Garg Model

Experimental ignition of porous fuels is mostly conducted in the FPA however an example of a similar situation is the work by Garg [112]. They explored the radiant ignition of excelsior fuel bed of different voidages and proposed their own solution to the heat equation. Their experimental results are shown in Figure 37.

They analyse their results with the diffusion-source heat equation on a semi-infinite domain. This is an inhomogenous second order partial differential equation with homogenous boundary conditions.

$$\frac{\partial^2 T}{\partial x^2} + \frac{\tilde{a}\dot{q}_e''(0,t)}{\tilde{k}}\exp\{-\tilde{a}x\} = \frac{1}{\alpha}\frac{\partial T}{\partial t} \tag{57}$$

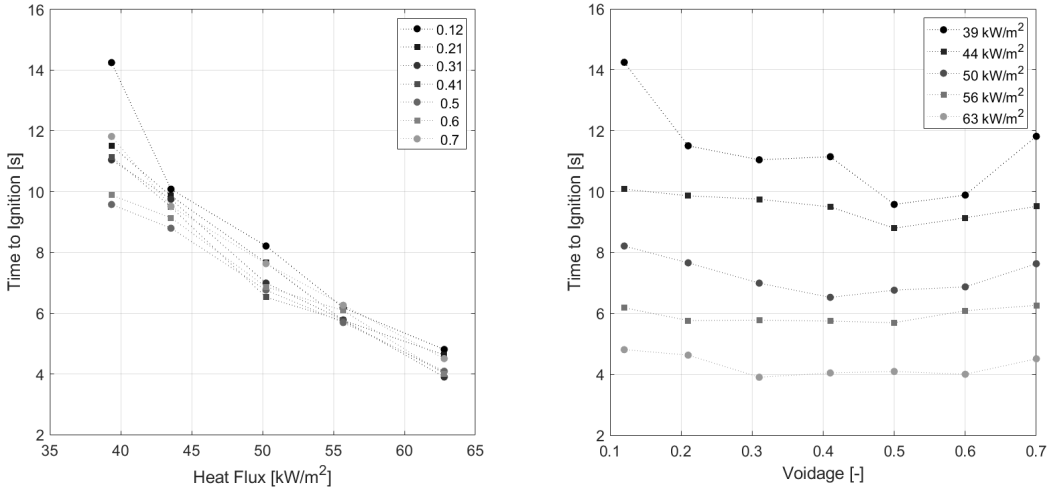

Figure 37: Experimental ignition results extracted from Garg et al. [112].

$$\text{IC} \quad T(x,0) = T_\infty, \qquad T\epsilon[0,\infty] \tag{58}$$

$$\text{BC} \quad T(\infty,t) = T_\infty, \qquad x\epsilon[0,\infty] \tag{59}$$

$$\text{BC} \quad -\tilde{k}\frac{\partial T}{\partial x} = \dot{\tilde{q}}_s''(0,t) \tag{60}$$

The surface heat flux is defined as in the Torero model with the exception of the incident heat flux. Garg introduces the incident radiation through the source term in the governing differential equation.

$$\dot{\tilde{q}}_s''(0,t) = \dot{q}_{rad}''(0,t) + \dot{q}_{conv}''(0,t) \tag{61}$$

$$\dot{\tilde{q}}_s''(0,t) = h_T(T(0,t) - T_\infty) \tag{62}$$

Garg gives the following solution for the surface temperature

$$T_s = T_\infty + \frac{\tilde{a}\dot{q}_e''}{h_T - \tilde{a}\tilde{k}}\left[\frac{1}{\tilde{a}}\left(1 - \exp\left(\frac{\tilde{a}^2\tilde{k}}{\tilde{c}\tilde{\rho}}t\right)erfc\left(\sqrt{\frac{\tilde{a}^2\tilde{k}}{\tilde{c}\tilde{\rho}}}\sqrt{t}\right)\right)\right. \tag{63}$$

$$\left. - \frac{\tilde{k}}{h_T}\left(1 - \exp\left(\frac{h_T^2}{\tilde{k}\tilde{c}\tilde{\rho}}\right)erfc\left(\sqrt{\frac{h_T^2}{\tilde{k}\tilde{c}\tilde{\rho}}}\sqrt{t}\right)\right)\right] \tag{64}$$

The source term accounts for the change in the incident absorption as the fuel bed changes. This is done by first determining the mean projected area on a hemisphere surrounding the particle. This is equivalent to determining the mean radiation on a large number of randomly orientated particles.

$$A_p = \frac{\int_0^{2\pi}\int_0^{\pi/2} Ld\sin^2\varphi_1 d\varphi_1 d\varphi_2}{\int_0^{2\pi}\int_0^{\pi/2}\sin\varphi_1 d\varphi_1 d\varphi_2} = \frac{Ld\pi}{4} \tag{65}$$

Defining the absorption coefficient as

$$\tilde{a} = \frac{N_p A_p}{V_s} = \frac{N_p Ld\pi}{4V_s} \tag{66}$$

Taking the definition for the void fraction.

$$\phi = \frac{V_s - V_P}{V_s} = 1 - \frac{N_p V_p}{V_s} = 1 - \frac{N_p Ld^2\pi}{4V_s} = 1 - \tilde{a}d \tag{67}$$

Rearranging to produce the absorption coefficient as a function of the bed and element properties.

$$\tilde{a} = (1 - \phi)/d \tag{68}$$

The conduction coefficient and thermal density is altered to account for the fuel bed changes.

$$\tilde{k} = k(1 - \phi) \tag{69}$$

$$\tilde{c\rho} = c\rho(1 - \phi) \tag{70}$$

4.3 Method

4.3.1 Apparatus

For this study the Fire Propagation Apparatus (FPA)[113] was used. The FPA is a standard testing equipment consisting of a set of tungsten lamps, pilot flame, load cell and extraction hood. The extraction hood is connected to a gas analyser measuring oxygen, carbon dioxide and carbon monoxide. It allows for well-defined heating conditions to be applied to samples and for the ignition and burning behaviour to be studied through analysis of mass and gas results. By subjecting different fuel beds to well-defined heating conditions then the flammability as a function of the fuel bed can be studied and this is the approach followed here.

4.3.2 Experimental Conditions

Pilot flame was located 20 mm above the centre of the fuel bed surface this was done to avoid false ignitions caused by expansion of the fuel bed surface upon heating where the surface moves in the upwards direction towards the pilot flame. Photographs from an example ignition test are shown in Figure 38.

In this work heat fluxes of 25, 35 and 50 kW/m^2 are applied to fuel beds made from pinus rigida, pinus halpensis, pinus pinea and pinus pinaster. This procedure is similar to previous work discussed in Section 4.2. A summary of experimental conditions presented in this work is detailed in Table 27.

Heat Flux [kW/m^2]	**Pilot [-]**	**Flow [-]**	**Basket Porosity [%]**	**Material [-]**	**FMC [-]**	**Mass [g]**
25	20 mm	Natural	0	Rigida	∼1%	7.5, 15, 25, 35, 60, 95, 120
25	20 mm	Natural	63	Rigida	∼1%	15, 20, 25, 35, 60, 90
25	20 mm	Natural	63	Halepensis	∼1%	10, 15, 20
25	20 mm	Natural	63	Pinea	∼1%	10, 15
25	20 mm	Natural	63	Pinaster	∼1%	10, 15
35	20 mm	Natural	63	Rigida	∼1%	15, 35, 90
50	20 mm	Natural	63	Rigida	∼1%	15, 35, 90

Table 27: Experimental conditions used in the present work

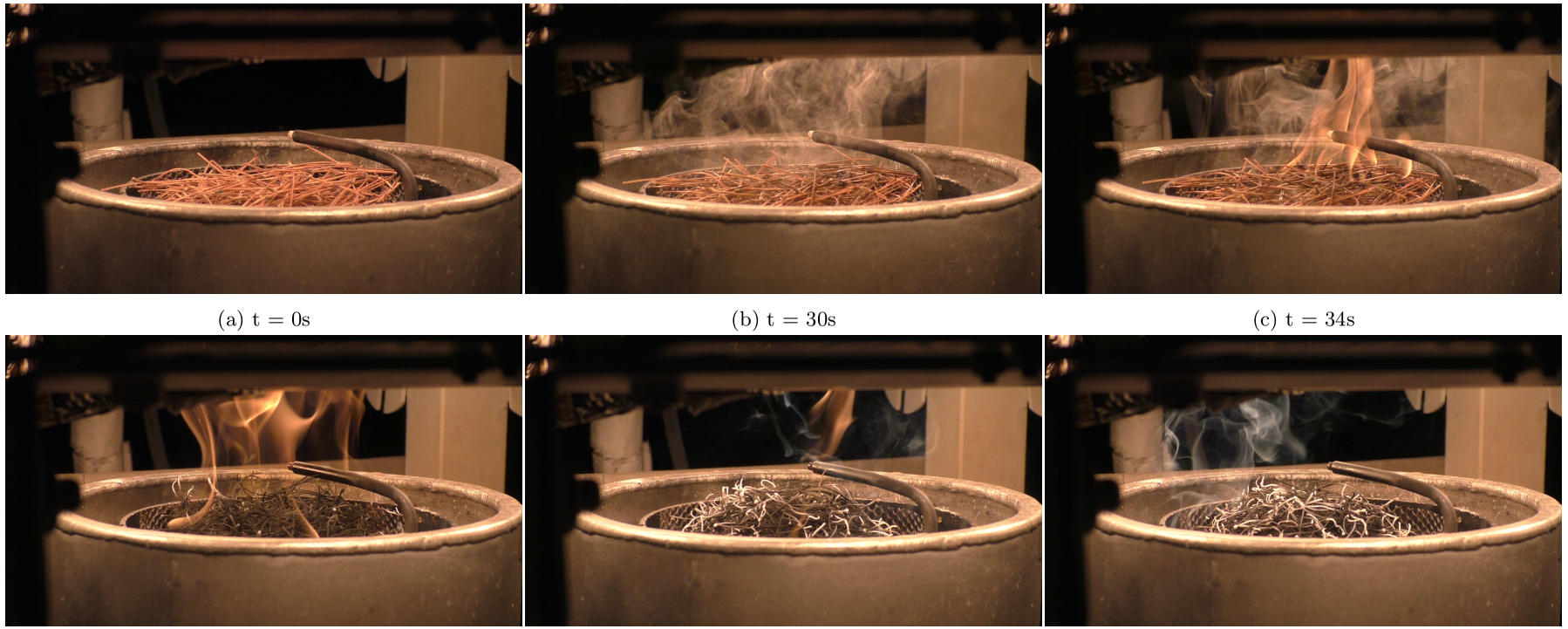

(a) t = 0s (b) t = 30s (c) t = 34s

(d) t = 45s (e) t = 60s (f) t = 65s

Figure 38: Stills from ignition experiment of Pinus Halepensis

4.3.3 Materials

4.3.3.1 Pine Needle Morphology

Table 28 shows the morphology reported by Nobis et al. [48]. However as detailed in Section 2.5.3 pine needles are plastic in their morphology. To check this a sample of pinus rigida needles were measured. This is in Appendix D. The average results were length 97.2 mm, width 1.2 mm, thickness 0.5 mm and mass 0.028 g. As discussed in Section 2.5.3, the width is consistent whilst the length is not.

Species	**no. fas [#]**	**len [cm]**	**wid [cm]**	**l/w [-]**	**lon [years]**
Pinus rigida	3	7.5	0.12	60	2.5
Pinus halepensis	2	10	0.08	125	2
Pinus pinaster	2	17.5	0.21	83.33	3
Pinus pinea	2	13.5	0.15	90	2.5

Table 28: Literature morphological values: Number of fascicles; Length; Width; Length/Width; Longevity. Longevity being number of years before the needle is dropped. Extracted from Nobis et al.[48].

4.3.3.2 Manufactured pine needle fuel beds

To make the applicability of the results more extensive. Pine needles were processed to create a samples of known nominal lengths. This allowed for the sample baskets to be filled completely and for the fuel loads to be changed. Once prepared, samples were subsequently dried for 24 hours at 60°C therefore homogenising the fuel moisture contents. In this way different fuel bed structures were created whilst retaining a constant species chemistry.

The different fuel loads shown in Figure 39 are created by cutting the original pinus rigida needles to nominal lengths. The procedure for this is detailed in Table 29. The effect of changing the length of the pine needle can be appreciated in Figure 40. As the needle length is decreased the packing efficiency of the fuel bed increases with more mass filling the sample volume. The most interesting aspect is that at lengths smaller than 3-4 cm (fuel load of 35 g) the mass per pine needle length increases sharply. It is hypothesised that this sharp increase is due to the element lengths being a similar size to the fuel bed pores.

Wet Mass [g]	**Average Dry Mass [g]**	**Average Dry Bulk density [kgm-3]**	**Sample Preparation**
7.5	7	19	Natural needles dropped into the sample holder.
			Lengths extending beyond its volume were cut.
10	9	24	Natural needles dropped into the sample holder.
			Lengths extending beyond its volume were cut.
15	14	37	Natural needles packed into the sample holder.
			Lengths extending beyond its volume were cut.
20	18	48	Needles cut to 7cm lengths.
			Dropped into the sample holder.
25	23	62	Needles cut to 7cm lengths.
			Laid flat in the sample holder.
35	32	86	Needles cut to 3-4cm lengths.
			Dropped into the sample holder.
60	56	150	Needles cut to 1-2.5cm lengths.
			Dropped into the sample holder.
95	88	230	Needles cut to <1.5cm lengths.
			Dropped into the sample holder.
120	110	300	Needles ground to a powder.
			Sample holder filled.

Table 29: Manufactured fuel bed methodology

Figure 39: Photos of some of the fuel beds tested. Left to right and top to bottom - Rigida 7.5 g, 15 g, 25 g, 35 g, 60 g, 95 g; Halepensis 15 g; Pinea 15 g; Pinaster 15 g.

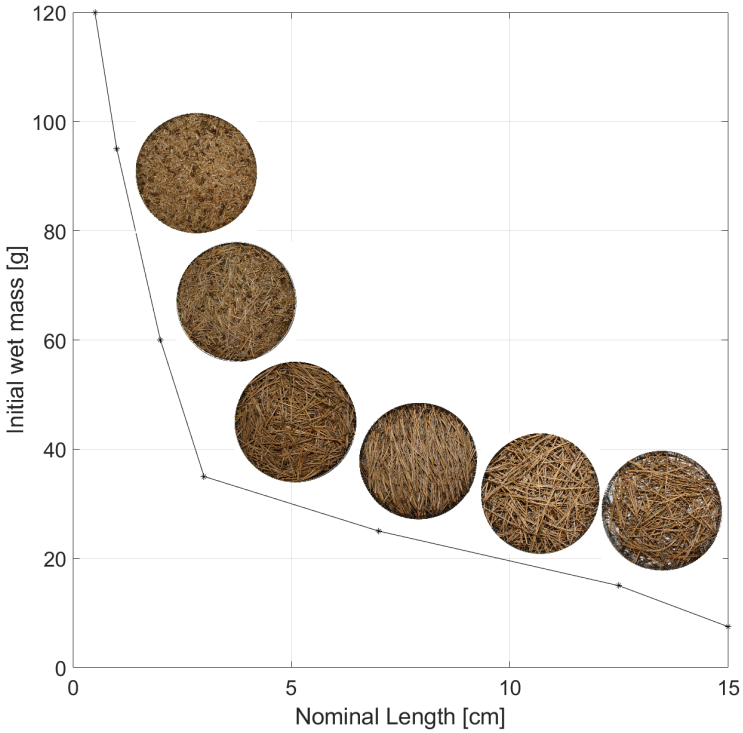

Figure 40: Wet mass of fuel bed as a function of the approximate cut length of the Pinus Rigida needle

4.3.4 Experiment Characterisation

4.3.4.1 Data Processing

Data from a typical experiment are presented in Figure 41. The data show the mass lost (left) and the mass loss rate (right) for four experiments, the average of these curves (and max-min range) as well as the windows observed for ignition and flame out. Complete results for all experiments can be found in Appendix C.

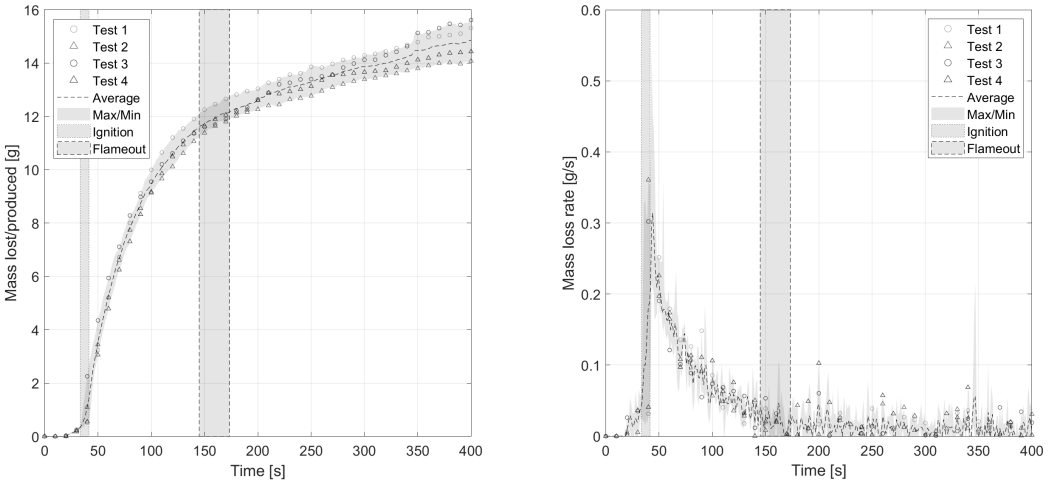

Figure 41: Average mass results for 15 g Pinus Rigida in closed baskets. Maximum and minimum experimental values shown by shaded area around dotted line. Time to ignition and flameout experimental values shown by vertical shaded regions.

4.3.4.1.1 Averaging

Each test condition was repeated at least twice. In this work individual tests are averaged to create a representative curve for each experiment. However, due to variation in the data this means is that similar features of the curve may not occur at the same time. Therefore averaging the data can create unrepresentative data. An example would be that if the time to ignition varies between two tests then the peak mass loss rate will also occur at two distinct times. Averaging the data when the peaks are not aligned causes the average peak mass loss rate to be lower than if the average of the individual peaks was taken. To ensure that the data presented is representative, the figures will include the a shaded region, around the average representative curve, that shows the maximum and minimum values of the experiments. Furthermore, each test will shown using its own set of markers.

4.3.4.2 Experimental Parameters

4.3.4.2.1 Time to ignition

Time to ignition is recorded as the time taken from exposure to the appearance of a flame. This is recorded during the experiment and compared with video data. An example of this event is shown in Figure 38c.

4.3.4.2.2 Duration of Flaming

Time to flameout is recorded during the experiment as the time taken from the flame to disappear. An example of this is shown in Figure 38e-f. The duration of flaming is the difference between the time to flameout and the time to ignition.

4.3.4.2.3 Mass lost at ignition

The mass lost at ignition is the integral of the mass loss rate between initial exposure and the time to ignition. This would be the mass lost between Figure 38a and c.

4.3.4.2.4 Mass lost during flaming

The mass during flaming is the integral of the mass loss rate between the time to ignition and the time to flameout. This would be the mass lost between Figure 38c and e.

4.3.4.2.5 Mass loss rate at ignition

Ignition is the transition to flaming. The mass loss rate at ignition represents the minimum mass flux of pyrolysis gases needed to sustain a flame for the given conditions. This would be the rate of mass loss at Figure 38c.

4.3.4.2.6 Mass loss rate at flameout

Mass loss rate at flameout, similarly to that at ignition, represents a transition between two states. Contrary to ignition, at flameout the sample is moving from flaming to not flaming. Nevertheless the value can be interpreted as the minimum mass flux to maintain a flame. This would be the rate of mass being lost at Figure 38e. However, this can be difficult to define, as unlike ignition, this can be a drawn out process where the fuel can extinguish and reignite. Additionally, it is not uncommon to see localised flaming.

4.3.4.2.7 Peak mass loss rate

The peak mass loss rate represents the point at which the greatest amount of solid fuel is being converted to gaseous components.

4.3.4.2.8 Average Mass Loss Rate during flaming

This is the mass lost during flaming divided by the duration of flaming.

4.3.4.2.9 Peak heat release rate

Heat release data is a secondary measurement. That is to say that it is not directly measured but is inferred from oxygen, carbon dioxide and carbon monoxide concentration measurements in the exhaust gases emanating from the burning sample. The idea is that the oxidation of pyrolysis gases produces a fixed amount of energy, on average. The average heat per unit oxygen is called Hugget's constant [63] and was described in Section 3.2.1.1. Hugget's constant is used on the basis of the assumption that: materials with similar constituent bond energies will release similar amount of energy when oxidised. Bartoli [64] suggested a modified constant that used only wildland fuels to create this average. In this work the general value suggested

by Hugget is used as this is the most commonly used among experimentalists in literature (see Section 4.2).

Calorimetry works on the basis that in most cases oxidation requires gaseous oxygen and as such the reduction in oxygen from the ambient allows us to evaluate how much has been consumed. Using Huggett's constant the heat produced due to this consumption can be computed. A layer of correction is added by considering the carbon dioxide and carbon monoxide produced. This is because these gas species can be considered markers for complete and incomplete combustion respectively. Incomplete combustion gives off less heat than complete combustion and as such its consideration allows for the correction of the heat calculated from the oxygen deficit. On its own the oxygen deficit assumed complete combustion at all times.

For completeness it is worth mentioning that a simpler approach to calculation of the heat release rate is possible - but as always simpleness comes at the cost of accuracy. In this approach the mass loss rate is used in conjunction with the heat of combustion. Where the heat of combustion represents the heat released per unit mass. The approach assumes that all the mass burns in the same way. That is to say there is no consideration for how complete the combustion reaction is. Furthermore the heat of combustion is usually evaluated using a bomb calorimeter. In the bomb calorimeter, as detailed in Section 3.4.4, the material is burned in a pure oxygen environment and so the heat of combustion evaluated is a maximum possible value. In reality, the combustion is likely to be constrained by other factors and the actual energy release will be lower than by this method.

4.4 Results and Discussion

In the following section the results for the experiments conducted in the FPA are presented. They consist of critical heat flux; open/closed basket; change of heat flux and change of species. Detailed tabulated data from the present work and from literature can be found in Appendix C. Additional figures created for the present work can also be found in Appendix C.

Changing the Closed/Open condition affects the fluid flow in the fuel bed. As convection is the heat transfer mechanism that is associated with fluid flow it will be affected. Not only is heat transfer affected but changes in the fluid flow will affect the mass transfer and mixing of the volatile components. On the other hand, changing the heat flux alters the balance of heat transfer mechanisms within the system. Increasing the heat flux allows for an indication of the relative magnitude of the inherent heat transfer.

Change in the species changes the morphology of the individual pine needles that make up the fuel bed. The individual element morphology dictates the structure of the fuel bed. Hence the different species should be subject to different fluid flows and effective fuel bed heat transfer properties. The change in morphology can be quantified by looking a the the values given by Nobis [48] and presented in Table 28. This gives the species length in decreasing order as Pinaster, Pinea, Halpensis and Rigida. The species width in decreasing order is given as Pinaster, Pinea, Rigida, Halepensis. The ratio of the length and the width in decreasing order is given as Halepensis, Pinea, Pinaster and Rigida. Changing the species will also mean changing the thermal degradation. As these are all from related species, their chemistry should exist within relatively narrow bounds (see Part III).

The results will be grouped in terms of time, mass, mass loss rate and heat release rate. Current work is plotted along-side data extracted from literature. In this way a wider picture of the experimental space can be appreciated. Colour is used to denote the experimentalist whilst symbol is used to denote the pinus species used. Symbols are detailed in Table 30. Colour is detailed in the individual Figures. Additionally dry or wet fuel is denoted by either filled or unfilled markers.

4.4.1 Critical Radiant Heat Flux Results

Critical radiant heat flux experiments are conducted to understand the change in the time to ignition as a function of the heat flux. The goal is to understand what is the minimum incident radiant heat flux at which ignition will occur.

Symbol	Pinus Species
□	Halepensis
△	Nigra
◇	Pinaster
▽	Laricio
○	Rigida
⋆	Strobus
▷	Pinea

Table 30: Symbols used to denote the Pinus species used

Figure 42 shows the results from previous critical radiant heat flux experiments and those produced in the present work. At 25 kW/m^2 there is a spread of ≈50 s between the different experiments. Additionally, as expected, the lower the heat flux the longer the time to ignition. The radiant heat flux at which this exponential increase is observed is different depending on the boundary conditions of the sample. When there is a flow imposed this value is ≈10 kW/m^2 higher than when there is no flow. This is expected as in the case where there is flow, the convective heat loss is increased. The incident radiant heat flux must compensate for the increased heat loss. That is to say that at a given incident radiant heat flux the net heat flux is less in the case of imposed flow than the case without flow.

From Table 26 and Figure 42 it is clear that the most common incident heat flux, in past testing, is 25 kW/m^2. This is a relatively low heat flux. It is common for the heat flux in a wildfire to be in excess of 100 kW/m^2 [114]. Nevertheless lower heat flux allows for the differences in the samples to be observed. Whereas high heat fluxes mask any differences - all samples will ignite quickly. The spread illustrated in the experiments in Figure 42 is what is investigated in this work.

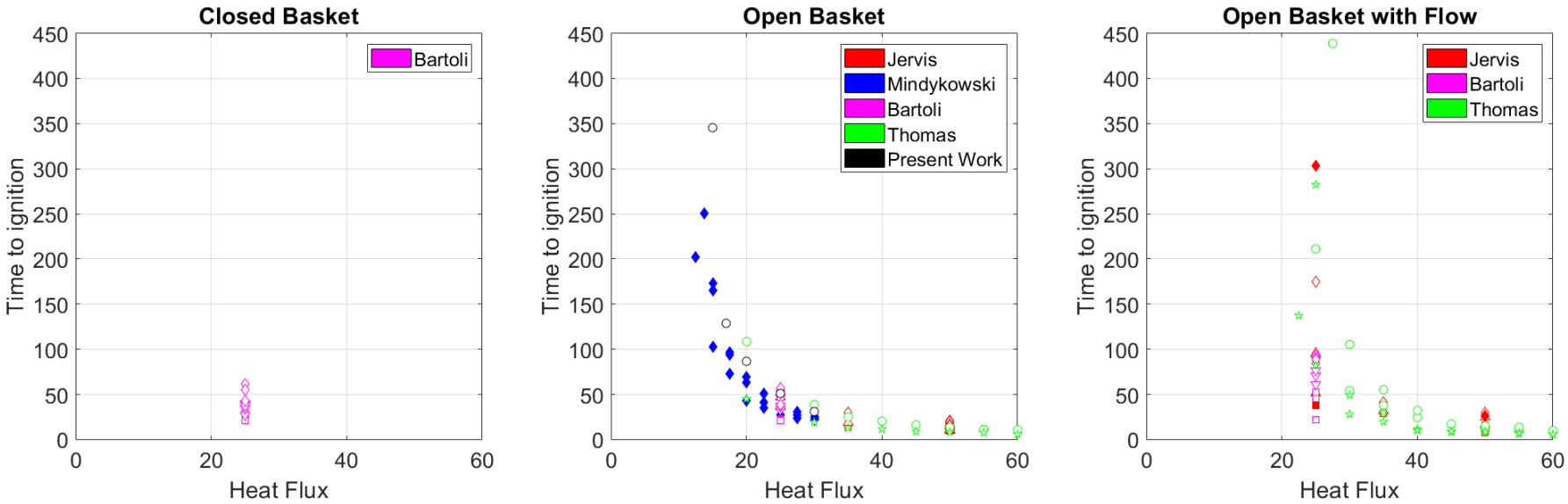

Figure 42: Critical radiant heat flux experiments

4.4.2 Time Results

The mean time results for the different FPA experiments conducted are presented in the following Tables 31, 32, 33, 34 and 35 and in Figures 43 and 44.

Closed	Ignition [s]	Flameout [s]	Duration of Flaming [s]	End [s]
7.5 g	51.21	96.84	45.63	470.00
15 g	38.28	157.43	119.15	518.16
25 g	30.42	223.08	192.66	604.35
35 g	29.07	370.46	341.39	601.98
60 g	30.76	-	-	603.00
95 g	47.66	549.08	501.42	605.86
120 g	37.18	235.51	198.33	604.35

Table 31: Mean time results for pinus rigida closed 25 kW/m^2

Open	Ignition [s]	Flameout [s]	Duration of Flaming [s]	End [s]
10 g	70.98	91.26	20.28	409.16
15 g	67.94	109.51	41.57	457.32
20 g	45.12	88.22	43.10	332.09
25 g	44.62	165.96	121.34	581.03
35 g	42.40	206.26	163.86	677.35
60 g	41.34	464.92	423.58	2007.75
90 g	54.42	322.12	267.70	2961.98

Table 32: Mean time results for pinus rigida open 25 kW/m^2

35 kW/m^2	Ignition [s]	Flameout [s]	Duration of Flaming [s]	End [s]
15 g	20.80	61.86	41.07	683.96
35 g	20.79	171.37	150.58	1376.01
90 g	24.95	270.85	245.90	3607.84

Table 33: Mean time results for pinus rigida open 35 kW/m^2

50 kW/m^2	Ignition [s]	Flameout [s]	Duration of Flaming [s]	End [s]
15 g	12.95	43.60	30.65	400.54
35 g	11.37	160.72	149.35	862.40
90 g	11.15	509.94	498.79	2386.43

Table 34: Mean time results for pinus rigida open 50 kW/m^2

Halepensis	Ignition [s]	Flameout [s]	Duration of Flaming [s]	End [s]
10 g	44.11	65.91	21.80	332.60
15 g	28.90	62.87	33.97	566.83
20 g	23.85	82.66	58.80	483.68
Pinea				
10 g	57.29	77.57	20.28	316.89
15 g	40.57	73.02	32.45	512.60
Pinaster				
10 g	137.90	161.23	23.32	391.91
15 g	87.71	112.56	24.84	536.91

Table 35: Mean time results for pinus halepensis, pinea, pinaster open 25 kW/m^2

4.4.2.1 Time to ignition

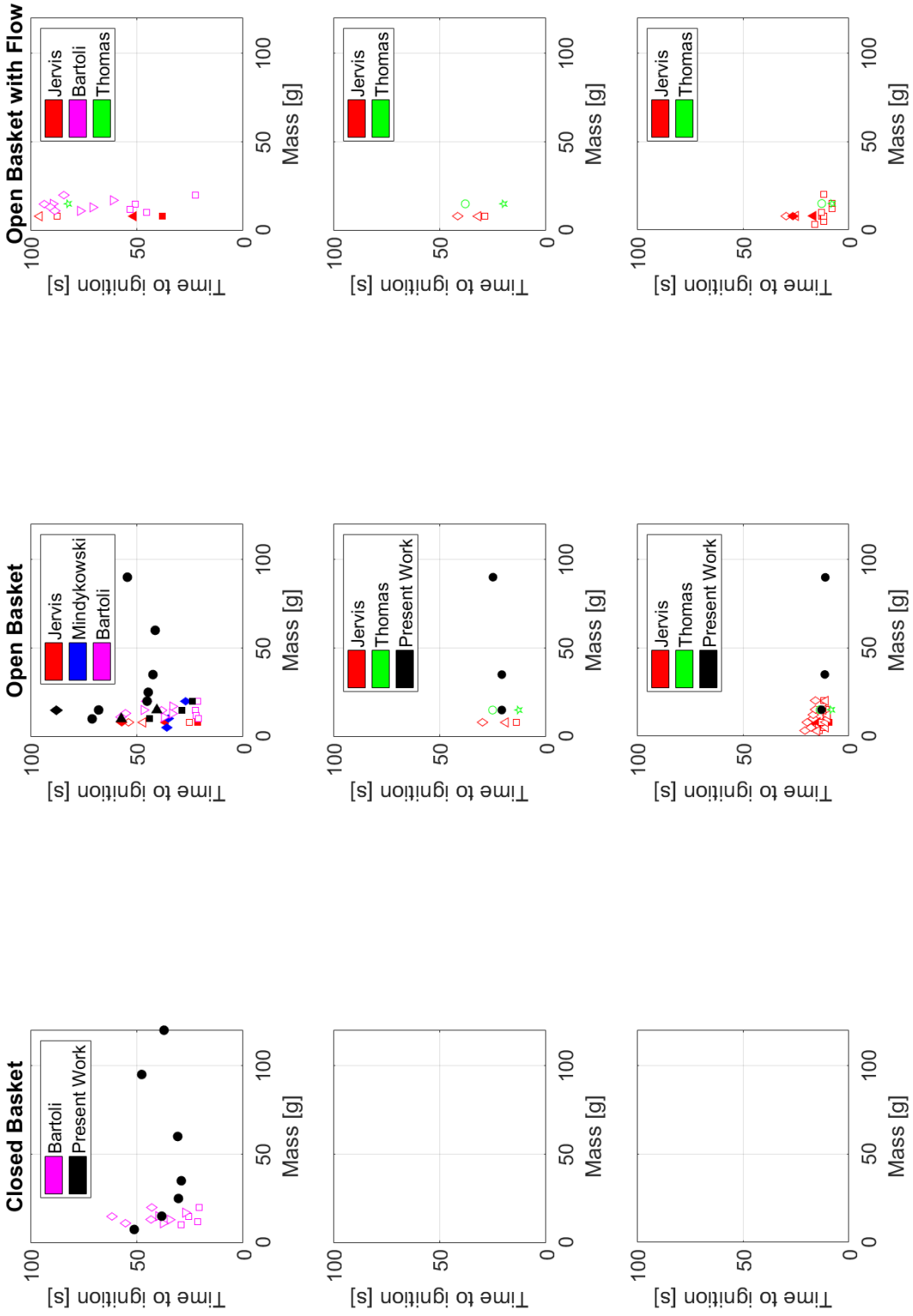

Figure 43: Mean time to ignition experimental data. Each row is a heat flux: 25, 35, 50 kW/m^2.

4.4.2.1.1 Pinus Rigida - Close/Open - 25 kW/m^2

Time to ignition for closed baskets at 25 kW/m^2 decreased from a maximum of 51.21 s at 7.5 g to a minimum of 29.07 s at 35 g. It was observed to increase again to a value of 46.66 s at 95 g. The powder case at 120 g was observed to ignite quicker than the 95 g case with ignition occurring after 37.18 s. Compared to the minimum time to ignition this is a difference of approximately 20 s and 17 s respectively.

For open baskets at 25 kW/m^2 the maximum time to ignition was at 10 g with a value of 70.98 s. This decreased with increasing mass to a minimum of 41.34 s at 60 g however further increase in mass lead to an increase to 54.42 s. Compared to the minimum time to ignition this is a difference of approximately 30 s and 13 s respectively.

4.4.2.1.1.1 Discussion

The trend for both open and closed baskets at 25 kW/m^2 is that the fuel beds are more difficult to ignite at low fuel loads; at intermediate fuel loads they become easier and at high fuels loads they become more difficult to ignite. The trend is more pronounced in the open basket low mass cases. Closed baskets ignite quicker than the open baskets.

The same trend regardless of boundary condition indicates that there are influences other than fluid flow that discriminate between the fuel beds. However the trend becoming more pronounced in the open basket case indicates that fluid flow is a dominant influence in the low mass cases. At high mass loads the fluid flow is not as important as the fuel bed is less permeable.

The decrease in ignitability at high fuel loads is explained in the same way that it is for a solid fuel. Whereby the additional mass increases the energy required to increase the temperature of the solid. This is because there is more solid to heat up and energy is conducted into the solid resulting in a temperature distribution and on average lower temperatures.

There is a decrease in the time to ignition when comparing the closed to the open cases. This is due to the change in fluid flow. In the low mass cases this results in a change in the heat transfer. With the increase fluid flow there is an increase in the convective heat losses which increase the time to ignition.

Additionally, at low mass loads the separation between individual pine needles becomes important. This is because, instead of acting like a continuous surface, the individual pine needles are sources of pyrolysis products. If they have a large separation then the the products are more likely to be diluted than accumulated at the surface. As such, low fuel loads are likely to see longer times to ignition as more needles must reach a pyrolysis production rate to overcome the dilution owing to their separation.

4.4.2.1.2 Pinus Rigida - Open - 35 kW/m^2 and 50 kW/m^2

At 35 kW/m^2 the maximum time to ignition was at the maximum fuel load of 90 g and had a value of 24.95 s. The minimum was at 35 g with a value of 20.79 s. This is a difference of 3 s. At 50 kW/m^2 the maximum time to ignition was at the minimum fuel load of 15 g and had a value of 12.95 s whilst the minimum was at 90 g with a value of 11.15 s. This is a difference of 2 s.

4.4.2.1.2.1 Discussion

Comparison of the different open basket experiments shows that higher heat fluxes cause quicker times to ignition. The more heat input into the system the faster the degradation process.

Furthermore, the differences observed between the fuel beds, at 25 kW/m^2, are homogenised under higher heat fluxes. At 35 kW/m^2, time to ignition is observed to be delayed for the high mass fuel bed while the low mass fuel bed is observed to be at the minimum value. This implies that the low fuel bed is more affected by the increase in the heat flux. The convective heat losses the low mass fuel beds are subjected to are less than the heat losses caused by the increase mass in the high mass cases.

At 50 kW/m^2 these difference become unimportant as all fuel beds ignite after a similar time. This means that the time to ignition in real fires (≈100 kW/m^2) should not be greatly affected by the fuel structure (under no flow conditions). However ignition is not burning and as such the fuel structure still has its part to play.

4.4.2.1.3 Pinus Halepensis, Pinea, Pinaster - Open - 25 kW/m^2

For the European pine needles the time to ignition decreased from a maximum at the lowest fuel load. Comparing the 15 g samples of all 4 species the time to ignition increases from Halepensis, Rigida (C), Pinea, Rigida (O), Pinaster. The corresponding values of 28.90 s, 38.28 s, 40.57 s, 67.94 s and 87.71 s.

4.4.2.1.3.1 Discussion

The time to ignition has similarities with the trend in the pine needle width. Halepensis is the thinnest pine needle and ignites quickest. Whilst Pinaster is the thickest pine needles and ignites the slowest. This is because mass of each needle is less and so it takes less energy to raise the temperature of the individual needles. This results in the effective temperature of fuel bed increasing more quickly and the ignition condition being reached sooner.

The thinner the pine needle the larger the number in a given fuel load. The greater the number of elements the less porous the fuel bed or in other words the more closed the fuel bed. There is also an increase in the solid surface area when there are more elements. This is beneficial in decreasing the time to ignition as the decrease in openness decreases the possible heat loss by convection and the increase in solid surface area increases the heat gain by radiation.

4.4.2.2 Duration of Flaming

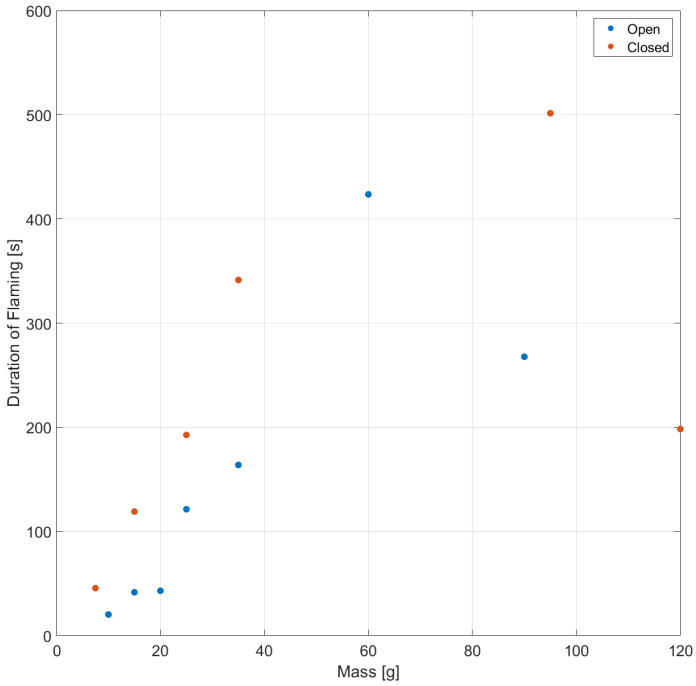

Figure 44: Duration of Flaming for Pinus Rigida in open and closed conditions at 25 kW/m^2

4.4.2.2.1 Pinus Rigida - Close/Open - 25 kW/m^2

Duration of flaming for closed baskets at 25 kW/m^2 increased from a minimum at 45.63 s at 7.5 g to a maximum at 60 g where the sample did not extinguish for the duration of the test. Most of these tests were stopped after 600 s however an experiment was conducted to assess the total duration of flaming for the 60 g case. This test lasted 2000 s. At higher fuel loads the duration of flaming decreases. The powder case was observed to burn for a much shorter time compared to its closest porous case. The difference between these was 300 s.

For open baskets at 25 kW/m^2 the duration of flaming increased from a minimum of 20.28 s at 10g to a maximum of 423.58 s at 60 g. At higher mass loads the flaming time decreased to 267.70 s. The difference between minimum and maximum value is 403 s.

4.4.2.2.1.1 Discussion

In both cases is the duration of flaming increases with mass up until a point. This is because there is more mass to supply the flame with pyrolysis products for a longer time. However, at a point the increase in mass decreases the duration of flaming. This is because the increase in mass causes the fuel bed to act more like a charring solid. The material undergoes charring and so a protective layer is formed on the top surface. This top surface reduces the heat transfer to the lower layers and hence the production of pyrolysis gases.

In both open and closed baskets the 60 g samples gave the longest flaming duration. This is the fuel bed where the layer is permeable enough to not protect the deeper layers. The importance of the fluid flow and the permeability of the sample in affecting the flaming duration is highlighted when the open baskets are compared to the closed baskets. Open baskets are seen to have a shorter flaming duration in general. This is because oxidiser is readily available and so char oxidation can occur. This is a localised heat source and so increases the heat in the system and consequently reduces the flaming time. More information can be garnered from the percentage mass lost during flaming.

4.4.2.2.2 Pinus Rigida - Open - 35 kW/m^2 and 50 kW/m^2

At 35 kW/m^2 the flaming time increased from a minimum of 41.07 s at 15 g to a maximum of 245.90 s at 90 g. The difference between minimum and maximum is 205 s. At 50 kW/m^2 the flaming time increased from a minimum of 30.65 s at 15 g to a maximum of 498.75 s at 90 g. This is larger than the corresponding open basket values at lower heat fluxes and comparable to the value in the closed basket case.

4.4.2.2.2.1 Discussion

For the duration of flaming the change in heat flux does not result in a big change between 25 kW/m^2 and 35 kW/m^2. This implies that during flaming the heat flux from the flame is the dominant heat source rather than the incident radiation. At 50 kW/m^2 the duration of flaming is reduced at low mass loads and increase at high mass loads. This is because the incident heat flux is greater than the heat flux produced by the flame. This accelerates the burning process at low mass loads. At high mass loads the increased heat flux overcomes the residue layer that is formed during burning. Therefore the fuel bed is able to flame for longer.

4.4.2.2.3 Pinus Halepensis, Pinea, Pinaster - Open - 25 kW/m^2

For the European pine needles the duration of flaming increased with increasing fuel load. Comparing the 15g samples of all 4 species the duration of flaming increased from Pinaster, Pinea, Halepensis, Rigida (O), Rigida (C). The corresponding values 24.84 s, 32.45 s, 33.97 s, 41.57 s, 119.15 s.

4.4.2.2.3.1 Discussion

The duration of flaming has similarities with the trend in pine needle size. Where larger pine needles have a shorter duration of flaming. This indicates that once burning the duration of flaming is proportional to the number of pine needles in the fuel bed. The less pine needles the more open the fuel bed and the burning front has to traverse fewer solid-gas interfaces. That is to say that with larger individual elements, for a given fuel load, the pores will be larger than one with smaller elements. A more porous fuel bed results in larger surface areas to receive radiation from the flame and there are less pine needles that need to have their temperature raised. The importance of the openness of the fuel bed is highlighted by the comparison to the close basket case.

4.4.3 Mass Loss Results

The mean mass loss results for the different FPA experiments conducted are presented in the following Tables 36, 37, 38, 39 and 40 and in Figures 45 and 46.

Closed	Ignition [g]	Flameout [g]	at 300 s [g]	Flaming [g]	Normalised Flaming [-]
7.5 g	1.23	6.72	10.11	5.49	0.79
15 g	0.49	11.87	13.86	11.38	0.82
25 g	0.46	19.49	21.02	19.03	0.82
35 g	0.30	25.26	23.22	24.95	0.77
60 g	0.40	-	23.52	-	-
95 g	1.03	35.52	21.64	34.50	0.39
120 g	0.50	14.87	18.12	14.37	0.13

Table 36: Mass loss results for pinus rigida closed 25 kW/m^2.

Open	Ignition [g]	Flameout [g]	at 300s [g]	Flaming [g]	Normalised Flaming [-]
10 g	0.45	7.37	9.84	6.92	0.74
15 g	1.11	11.03	12.77	9.92	0.71
20 g	0.39	13.17	17.036	12.78	0.69
25 g	0.52	21.18	23.85	20.66	0.89
35 g	0.39	26.07	29.24	25.69	0.79
60 g	0.64	38.68	28.48	38.03	0.68
90 g	0.96	25.26	23.85	24.30	0.29

Table 37: Mass loss results for pinus rigida open 25 kW/m^2.

35 kW/m^2	Ignition [g]	Flameout [g]	at 300s [g]	Flaming [g]	Normalised Flaming [-]
15 g	0.46	12.29	17.32	11.83	0.85
35 g	0.54	25.11	28.66	24.57	0.75
90 g	0.66	27.44	29.57	26.79	0.32

Table 38: Mass loss results for pinus rigida open 35 kW/m^2.

50 kW/m^2	Ignition [g]	Flameout [g]	at 300s [g]	Flaming [g]	Normalised Flaming [-]
15 g	0.88	11.02	15.76	10.14	0.73
35 g	0.32	24.28	27.73	23.96	0.74
90 g	0.59	50.15	36.78	49.55	0.59

Table 39: Mass loss results for pinus rigida open 50 kW/m^2.

Halepensis	Ignition [g]	Flameout [g]	at 300s [g]	Flaming [g]	Normalised Flaming [-]
10 g	0.73	7.45	12.02	6.72	0.67
15 g	0.29	10.12	12.16	9.84	0.66
20 g	0.57	12.70	16.25	12.12	0.61
Pinea					
10 g	1.00	7.77	9.44	6.774	0.68
15 g	0.60	10.41	13.57	9.81	0.65
Pinaster					
10 g	1.08	8.43	9.02	7.35	0.74
15 g	1.06	9.90	11.41	8.84	0.59

Table 40: Mass loss results for Pinus Halepensis, Pinea, Pinaster open 25 kW/m^2.

4.4.3.1 Mass Lost at Ignition

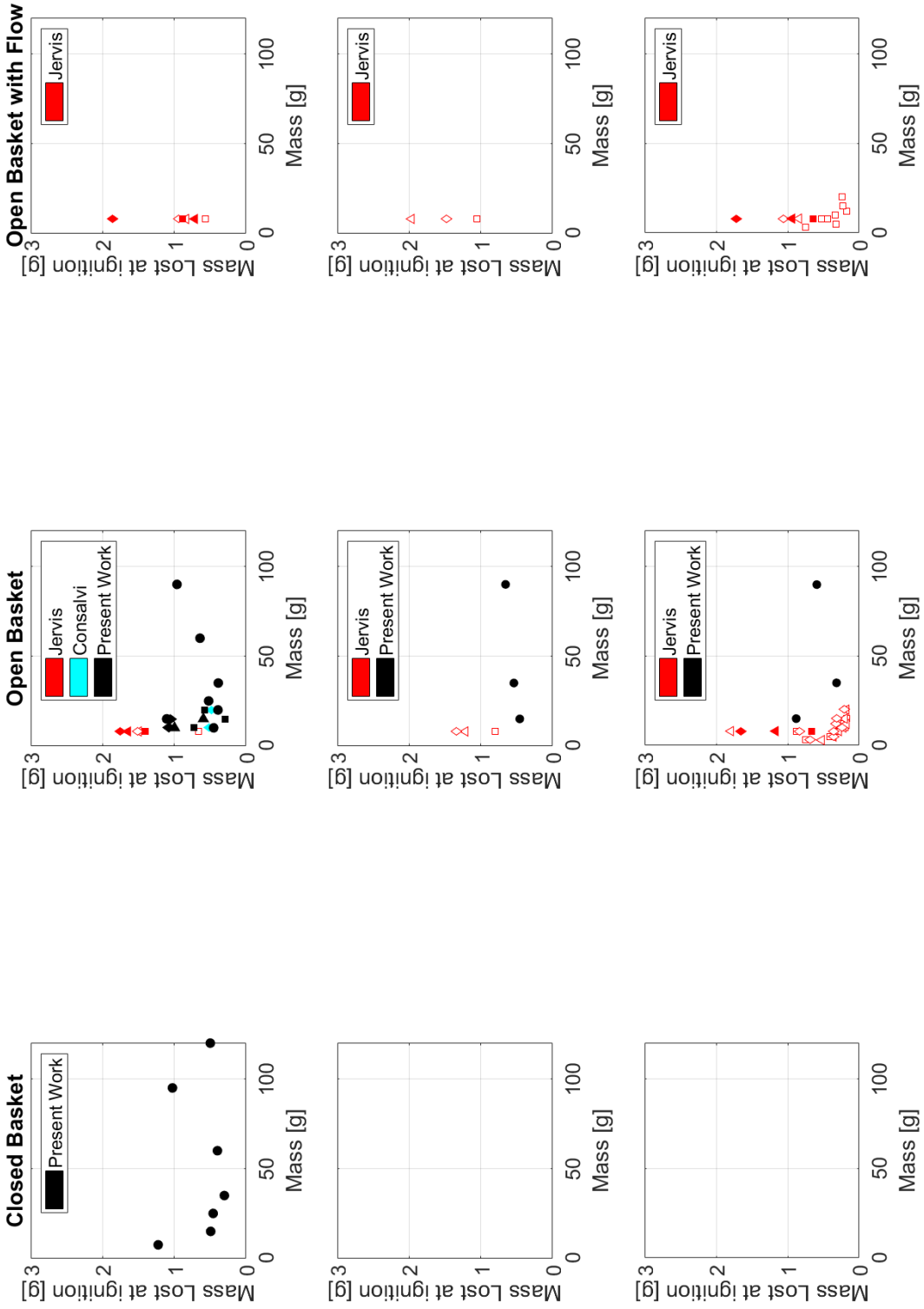

Figure 45: Mass lost at ignition experimental data. Each row is a heat flux: 25, 35, 50 kW/m^2.

4.4.3.1.1 Pinus Rigida - Close/Open - 25 kW/m^2

Mass lost at ignition for closed baskets at 25 kW/m^2 decreases from a maximum of 1.23 g at 7.5 g to a minimum of 0.30 g at 35 g. It was observed to increase again to a value of 1.03 g at 95 g. The powder case at 120 g was observed to lose 0.5 g which is less than the 95 g which represents the closest porous case.

For the open baskets case at 25 kW/m^2 the trend is less smooth. Nevertheless a decrease from a maximum of 1.11 g at 15 g to a minimum of 0.39 g at both 20 g at 35 g is observed. At higher fuels loads the mass lost increases to the extent of 0.96 g at 90 g.

4.4.3.1.1.1 Discussion

Mass lost at ignition follows the time to ignition. Those fuel beds that are slower to ignite lose more mass prior to ignition. In general the closed baskets lose less mass as they ignite faster. This is because the closed baskets reduce the convective cooling in the fuel bed by reducing the fluid flow through it. Additionally the accumulation of gases at the pilot is facilitated by the closed nature of the baskets.

At low mass loads there are some instances where the mass lost at ignition is high. In these cases some of the needles may have begun to smoulder before flaming ignition was able to occur. In terms of thermal degradation, that is to say that, the needle has undergone pyrolysis but has not produced enough pyrolysis gases to cause ignition, subsequently it has begun to undergo char oxidation. As such the needles may have begun to lose mass , through char oxidation, that does not have contribute to the accumulation of flammable gases needed for ignition.

The lack of a trend here suggests that the random packing of the fuel bed may be playing a part. The suggestion being made is that smouldering of pine needles might be occurring in sections of the fuel bed where there is clumping of the needles and that this clumping is something that occurs due to the way the needles are packed and it is not necessarily always packed in the same way.

4.4.3.1.2 Pinus Rigida - Open - 35 kW/m^2 and 50 kW/m^2

At 35 kW/m^2 the maximum mass lost at ignition was at the maximum fuel load of 90 g and had a value of 0.66 g. The minimum value was at 15g with a value of 0.46 g. At 50 kW/m^2 the maximum mass lost at ignition is 0.88 g at the minimum fuel load of 15 g. The minimum value is at 0.32 g at a fuel load of 35 g.

4.4.3.1.2.1 Discussion

As the heat flux is increased there is variation in the mass lost at ignition however there is not a discernible trend and more data point are needed. Nevertheless the results indicate that ignition can occur after less than ≈1g has degraded.

4.4.3.1.3 Pinus Halepensis, Pinea, Pinaster - Open - 25 kW/m^2

For the European pines the mass lost at ignition was highest at the lowest fuel loads. Comparing the 15g samples of all four species the mass lost at ignition increases from Halepensis, Rigida (C), Pinea, Pinaster, Rigida (O). The corresponding values are 0.29 g, 0.49 g, 0.60 g, 1.06 g, 1.11 g.

4.4.3.1.3.1 Discussion

The mass lost at ignition follows the ratio of the length and the width. Halepensis has the highest ratio and loses the least mass whilst Rigida has the lowest ratio and loses the most mass. The closed basket loses less compared to its open counterpart. This suggests that the mass lost at ignition is related to the permeability of the fuel bed. Whereby fuel beds which are more closed more easily accumulate a flammable mixture and so ignite quicker and as such do not lose as much mass before ignition.

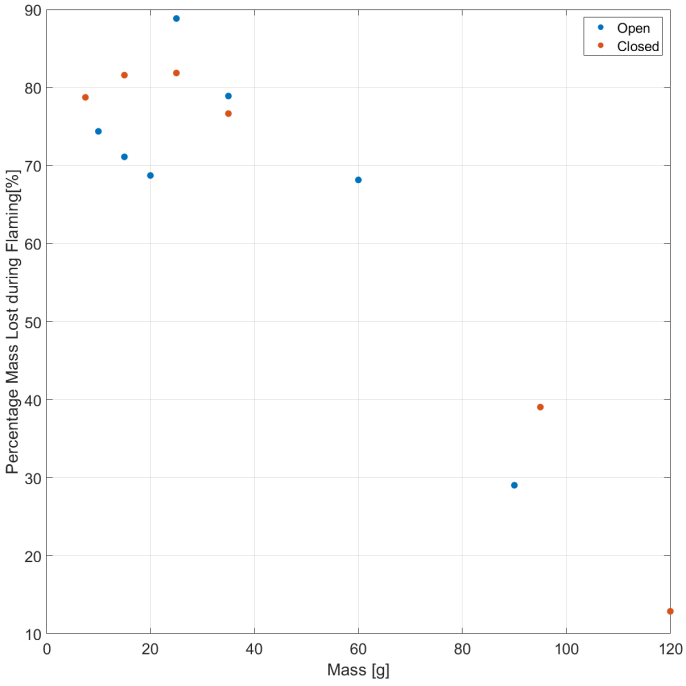

Figure 46: Percentage Mass Lost during flaming for Pinus Rigida, under a heat flux of 25 kW/m^2

4.4.3.2 Mass Lost and Percentage loss during flaming

4.4.3.2.1 Pinus Rigida - Close/Open - 25 kW/m^2

The mass lost during flaming for closed baskets at 25 kW/m^2 increases from a minimum of 5.49 g at 7.5 g to a maximum of 34.50 g at 95 g. It is important to note that at 60 g the flame did not extinguish. As a fraction of the initial mass the maximum is at 15 g with a value of 0.82 and this decreases to a value of 0.39 at 95 g.

The powder case at 120 g was observed to burn much less than its closest porous case of 95 g. The amount lost was 14.37 g which corresponds to a fraction of 0.13. There is a difference of 20.13 g when compared to the 95 g case.

For open baskets the mass burnt during flaming increases from a minimum of 6.92 g at 10 g to a maximum of 38.03 g at 60 g. At higher fuel loads the flaming mass decreases to 24.30 g for an initial mass of 90 g. As a fraction of the initial mass the maximum is 0.89 at 25 g and decreases with both increasing and decreasing fuel load. The minimum value is at 90 g with a value of 0.29.

4.4.3.2.1.1 Discussion

The amount of mass lost during flaming is best analysed by considering the percentage lost. This is because the work in Section 3 indicates that the percentage available to be pyrolysed is around 70%. Anything less than this indicates that not all the mass available to sustain the flame has been used. Anything more than this indicates that char oxidation has also occurred.

The trend for both open and closed baskets is that as the fuel load was increased, the percentage mass lost during flaming decreased. This means that the change in fuel structure is detrimental to the flame. The turning point for this is 60 g. As discussed in the time to ignition, at mass loads higher than 60 g the sample forms a layer on the top surface that protects the deeper layers from thermal exposure.

4.4.3.2.2 Pinus Rigida - Open - 35 kW/m^2 and 50 kW/m^2

At the 35 kW/m^2 the flaming mass increased from a minimum of 11.83 at 15g to a maximum of 26.79 g at 90 g. As a fraction of the initial mass this is 0.85 at 15 g to 0.32 at 90 g. At 50 kW/m^2 the flaming mass increased from a minimum of 10.14 g at 15 g to a maximum of 49.55 at 90 g. As a fraction of the initial mass, this was maximum at 35 g with 0.74 and a minimum at 90 g with 0.59. This is more than the corresponding open basket values at lower heat fluxes.

4.4.3.2.2.1 Discussion

The mass lost during flaming reflects the same results as the duration of flaming. The high fuel load is seen to increase in percentage mass lost during flaming from 29%,to 32% to 59%. This further indicates how the increase in heat flux is enough to overcome the protective layer ensuring that the mass is removed by flaming rather than by smouldering.

4.4.3.2.3 Pinus Halepensis, Pinea, Pinaster - Open - 25 kW/m^2

For the European pines the mass lost during flaming increased with fuel load. Comparing the 15 g samples of all the species the mass lost during flaming increased from Pinaster, Pinea, Halepensis, Rigida (O), Rigida (C). The corresponding value are 8.84 g, 9.81 g, 9.84 g, 9.92 g, 11.38 g. As a fraction of the initial mass these are 0.59, 0.65, 0.66, 0.71 and 0.82.

4.4.3.2.3.1 Discussion

The mass lost during flaming seems to be related to the size of the individual elements. Pinaster are the longest and widest elements whilst the shortest and thinnest elements are Rigida and Halepensis respectively. The most mass lost during flaming was Pinaster and the least mass was Rigida (C), followed by Rigida (O) and Halepensis. The largest the element the bigger the spacing between elements and so the fuel bed is more open and therefore more permeable for a give fuel load. A more open fuel bed promotes burning. This is supported by the close basket case losing the least amount of mass during flaming.

An interesting point is that the trend does not follow the available volatile matter found in proximate analysis. In Section 3.4.2.2.1, out of the species tested, it was found that Rigida had the most volatile matter whilst Pinea the least. This suggests that element size is a bigger factor than the thermal degradation.

4.4.4 Mass Loss Rate Results

The mean mass loss rate results for the different FPA experiments conducted are presented in the following Tables 41, 42, 43, 44 and 45 and Figures 47, 48, 49 and 50.

Closed	Ignition [g/s]	Flameout [g/s]	Peak [g/s]	Average [g/s]	Average/Peak[-]
7.5	0.050	0.049	0.34	0.12	0.35
15	0.054	0.016	0.43	0.096	0.22
25	0.074	0.014	0.36	0.099	0.27
35	0.054	0.025	0.36	0.073	0.20
60	0.072	-	0.29	-	-
95	0.095	0.025	0.27	0.069	0.26
120	0.079	0.059	0.26	0.072	0.28

Table 41: Mass loss rate results for pinus rigida closed 25 kW/m^2.

Open	Ignition [g/s]	Flameout [g/s]	Peak [g/s]	Average [g/s]	Average/Peak[-]
10 g	0.020	0.076	0.62	0.34	0.55
15 g	0.020	0.046	0.63	0.24	0.38
20 g	0.036	0.087	0.53	0.30	0.56
25 g	0.036	0.059	0.43	0.17	0.40
35 g	0.041	0.060	0.44	0.16	0.36
60 g	0.053	0.031	0.36	0.090	0.25
90 g	0.045	0.055	0.27	0.091	0.34

Table 42: Mass loss rate results for pinus rigida open 25 kW/m^2.

35 kW/m^2	Ignition [g/s]	Flameout [g/s]	Peak [g/s]	Average [g/s]	Average/Peak[-]
15 g	0.035	0.066	0.66	0.29	0.43
35 g	0.089	0.026	0.39	0.16	0.42
90 g	0.076	0.089	0.36	0.11	0.30

Table 43: Mass loss rate results for pinus rigida open 35 kW/m^2.

50 kW/m^2	Ignition [g/s]	Flameout [g/s]	Peak [g/s]	Average [g/s]	Average/Peak[-]
15 g	0.48	0.099	0.72	0.33	0.46
35 g	0.13	0.044	0.53	0.16	0.30
90 g	0.21	0.045	0.39	0.099	0.26

Table 44: Mass loss rate results for pinus rigida open 50 kW/m^2.

Halepensis	Ignition [g/s]	Flameout [g/s]	Peak [g/s]	Average [g/s]	Average/Peak[-]
10 g	0.11	0.12	0.58	0.31	0.53
15 g	0.036	0.071	0.58	0.29	0.50
20 g	0.025	0.094	0.46	0.21	0.45
Pinea					
10 g	0.032	0.13	0.68	0.33	0.017
15 g	0.038	0.17	0.79	0.30	0.015
Pinaster					
10 g	0.0064	0.11	0.75	0.32	0.42
15 g	0.022	0.073	0.77	0.36	0.46

Table 45: Mass loss rate results for Pinus Halepensis, Pinea, Pinaster open 25 kW/m^2.

4.4.4.1 Mass Loss Rate at Ignition and Flameout

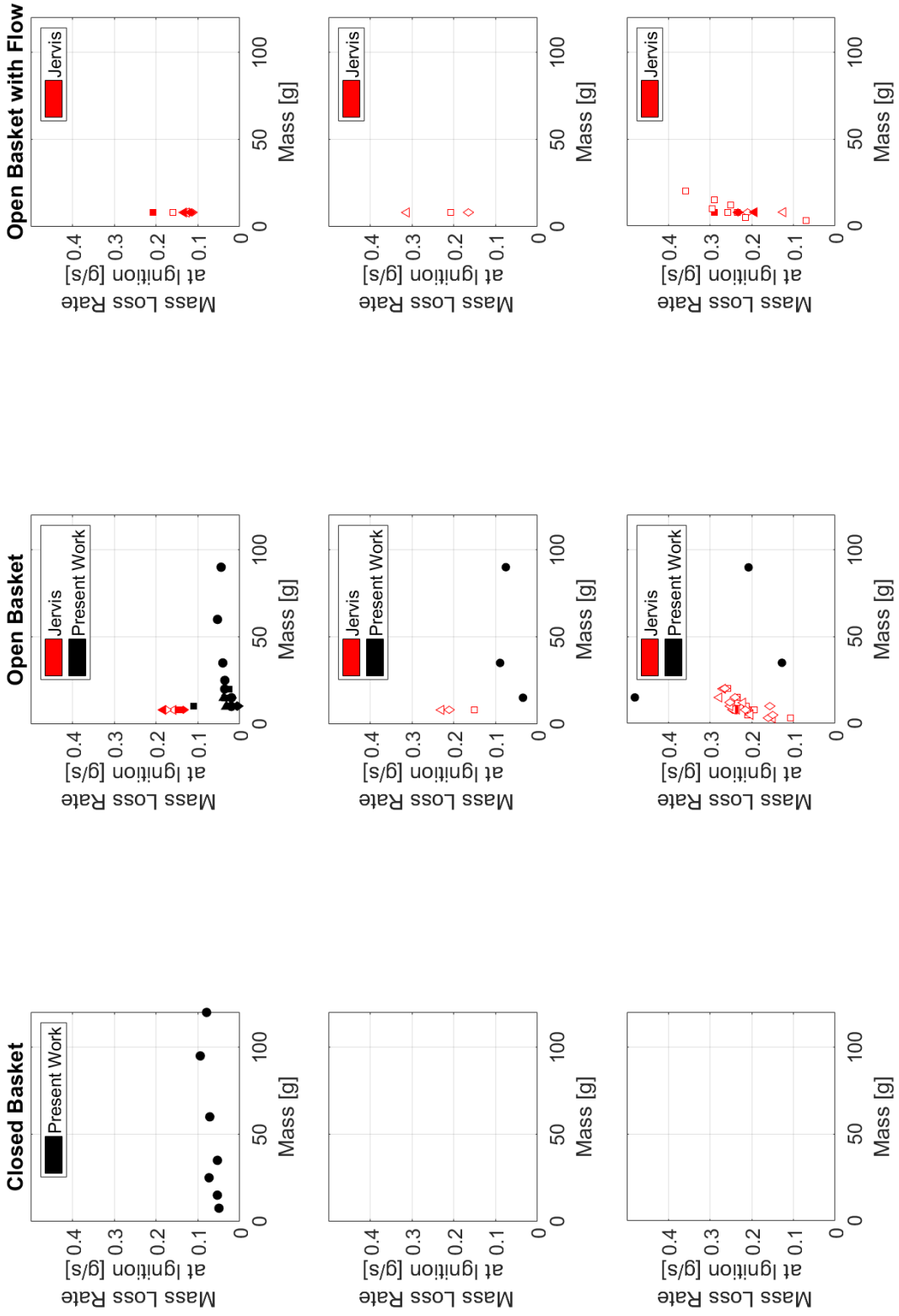

Figure 47: Mass loss rate at ignition experimental data. Each row is a heat flux: 25, 35, 50 kW/m^2.

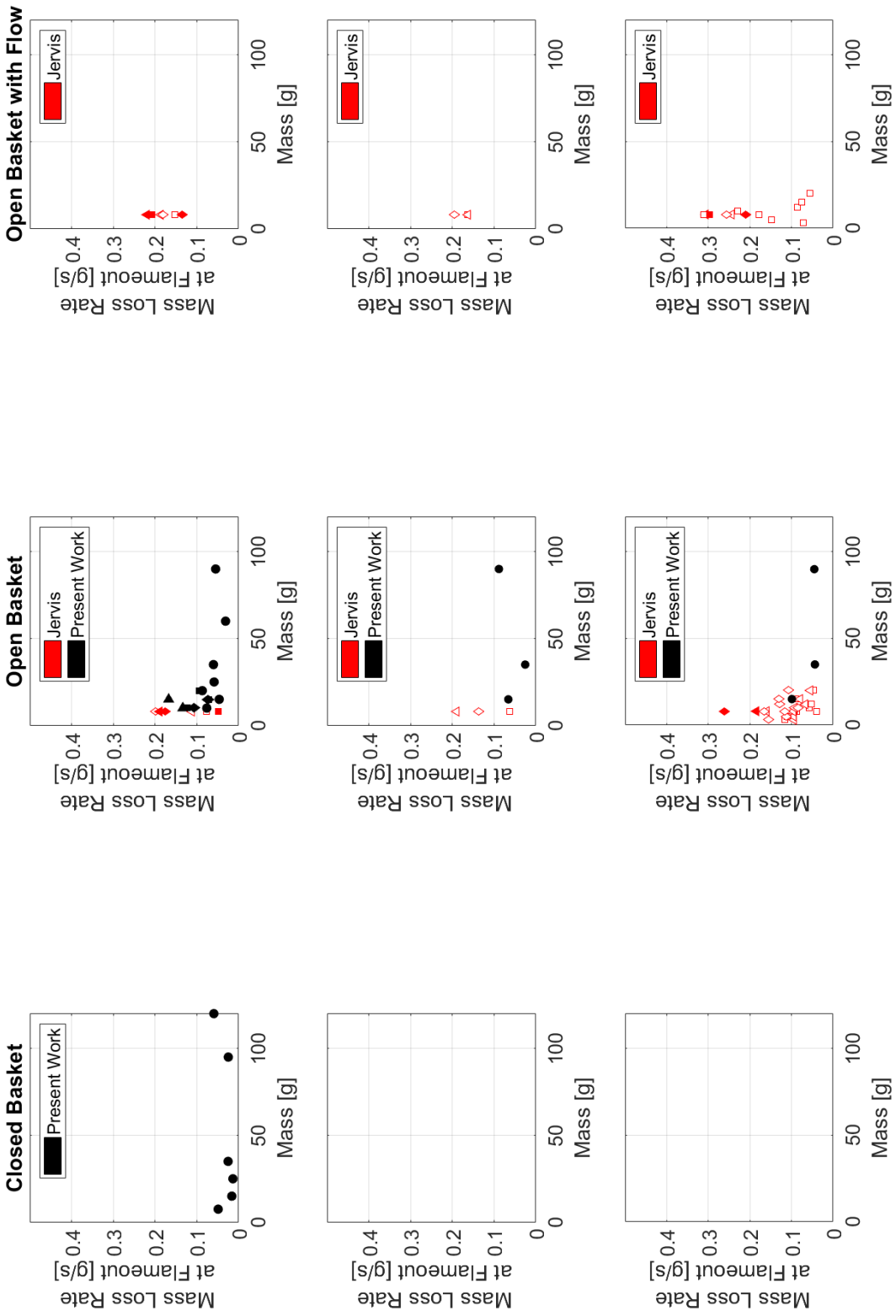

Figure 48: Mass loss rate at flameout experimental data. Each row is a heat flux: 25, 35, 50 kW/m^2.

4.4.4.1.1 Pinus Rigida - Close/Open - 25 kW/m^2

For closed baskets at 25 kW/m^2 the mass loss rate at ignition ranges from 0.050 g/s to 0.095 g/s with the minimum value at 7.5 g and maximum at 95 g. The mass loss rate at flame out ranges from 0.014 g/s to 0.059 g/s with the minimum value at 25 g. The value increases with both increasing and decreasing fuel load.

For open baskets at 25 kW/m^2 the mass loss rate at ignition ranges from 0.020 g/s to 0.053 g/s with the minimum value at 10 g and the maximum at 60 g. The mass loss rate at flameout ranges from 0.031 g/s to 0.087 g/s with the minimum at 60 g and the maximum at 20 g.

4.4.4.1.1.1 Discussion

Ignition and flameout are the limit cases for the flame and so represent the minimum mass flux needed to sustain a flame. Ideally this data would reflect the heat transfer in the fuel bed. Where a fuel bed with greater heat losses would require a higher mass loss rate at ignition/flameout. This is because a greater mass loss rate produces a bigger flame, needed to overcome the increased losses. However the results are inconclusive but future work should try and take advantage of these data points.

4.4.4.1.2 Pinus Rigida - Open - 35 kW/m^2 and 50 kW/m^2

At 35 kW/m^2 the mass loss rate at ignition ranges from 0.035 g/s to 0.089 g/s with the minimum at 15 g and the maximum at 35 g. The mass loss rate at flameout ranges from 0.026 g/s to 0.089 g/s with the minimum at 35 g and maximum at 90 g.

At 50 kW/m^2 the mass loss rate at ignition ranges from 0.13 g/s to 0.48 g/s with the minimum at 35 g and the maximum at 15 g. The mass loss rate at flameout on the other hand ranges from 0.044 g/s to 0.099 g/s with the minimum at 35 g and the maximum at 15 g.

4.4.4.1.2.1 Discussion

The mass loss rate at ignition increases with heat flux. However the trend with the fuel loading does not change consistently with the change in heat flux. The increase in mass loss rate at ignition at a given fuel loading is explained by an increased active volume of reaction due to the increase in penetration of the incident heat flux.

The mass loss rate at flame out is another measure of the limiting case of the flame. However the experimental results do not vary consistently making it difficult to analyse the results further.

4.4.4.1.3 Pinus Halepensis, Pinea, Pinaster - Open - 25 kW/m^2

For the European pines the mass loss rate at ignition ranges from 0.0064 g/s to 0.11 g/s whilst the mass loss rate at flameout ranges from 0.071 g/s to 0.17 g/s. Comparing the 15g samples in increasing order the mass loss rate at ignition is Rigida (O), Pinaster, Halepensis, Pinea and Rigida (C) with corresponding values 0.020 g/s, 0.022 g/s, 0.036 g/s, 0.038 g/s and 0.054 g/s. The mass loss rate at flame out increase from Rigida (C), Rigida (O), Halepensis, Pinaster and Pinea with corresponding values 0.016 g/s, 0.046 g/s, 0.071 g/s, 0.073 g/s and 0.17 g/s.

4.4.4.1.3.1 Discussion

The mass loss rate at ignition doesn't have a discernible trend however the mass loss rate at flameout does. It seems that the mass loss rate at flameout is highest in the cases where burning is least promoted. That is to say in the cases with more closed fuel beds i.e. where the elements are smaller and the bed is more compact as a result. This is because the burning occurs more in the earlier stages and as such at flameout there is not the same capability to lose mass.

4.4.4.2 Peak and Average Mass Loss Rate during Flaming

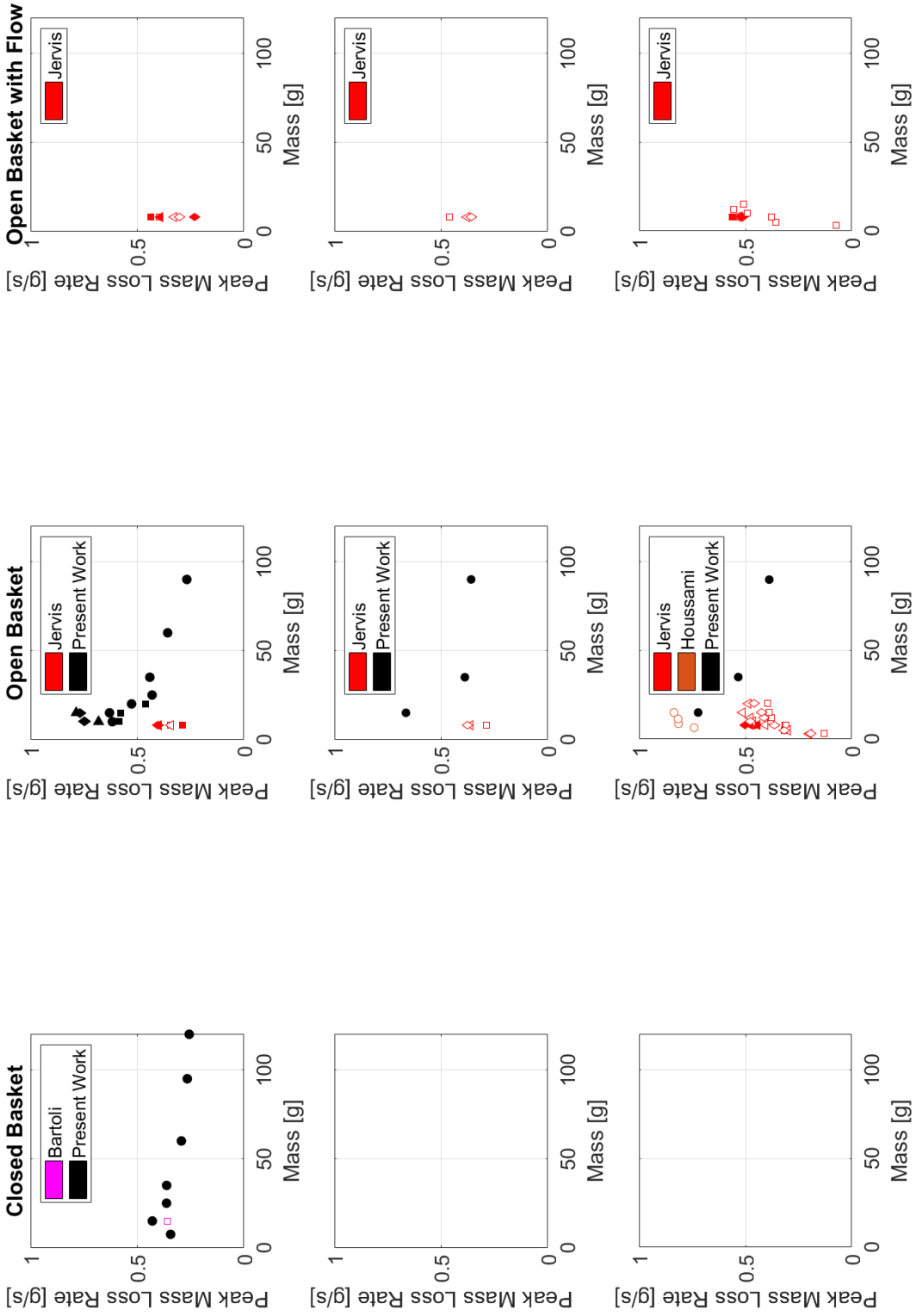

Figure 49: Peak mass loss rate experimental data. Each row is a heat flux: 25, 35, 50 kW/m^2.

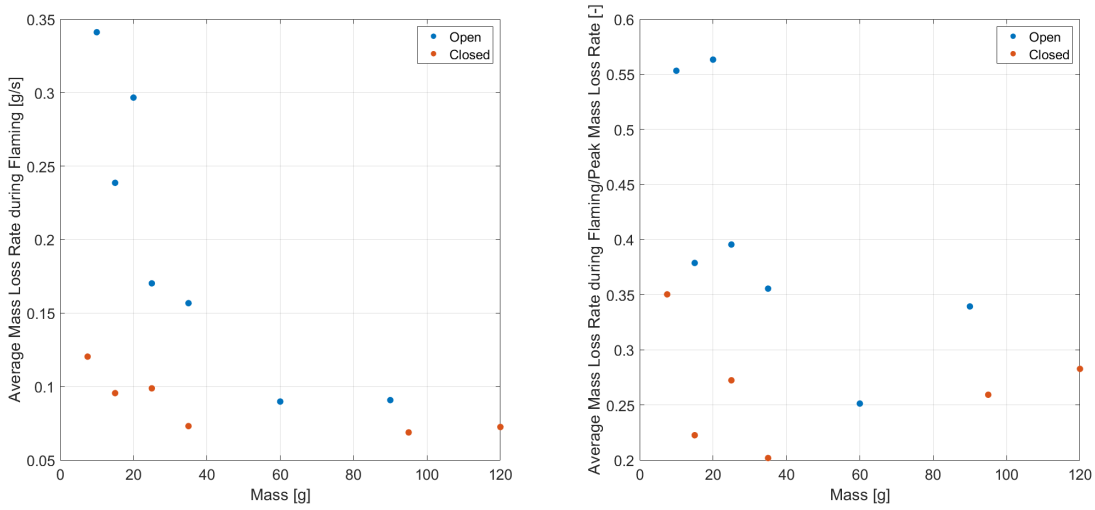

Figure 50: Left: average mass loss Rate during flaming for Pinus Rigida. Right: Normalised by the peak mass loss rate

4.4.4.2.1 Pinus Rigida - Close/Open - 25 kW/m^2

The peak mass loss rate for closed baskets at 25 kW/m^2 increases from a minimum of 0.26 g/s at a fuel load of 120 g to a maximum of 0.43 g/s at 15 g. Decreasing the fuel load further decreases the peak mass loss rate observed. The average mass loss rate during flaming increases from a minimum of 0.072 g/s at 120 g to a maximum of 0.12 at 7.5 g. As a fraction of the peak mass loss rate the maximum is 0.35 at 7.5 g and the minimum is 0.20 at 35 g. However the value increases as the fuel load increases from 35 to 120 g.

For open baskets the minimum peak mass loss rate is 0.27 g/s at 90 g increases to a maximum of 0.63 g/s at 15 g. The average increases from a minimum of 0.090 g/s at 60 g to a maximum of 0.34 g/s at 10 g. As a fraction of the peak the minimum is at 60 g increasing to a value of 0.56 at 20 g.

4.4.4.2.1.1 Discussion

The general trend is that as the mass increases the peak and average mass loss rate decreases. Comparison of the open and closed baskets highlights how influential fluid flow is to the burning process. The maximum peak value for closed baskets is 0.43 g/s whereas the open baskets are 0.62 g/s. The open baskets decrease to below 0.43 g/s after 25 g. This indicates that those baskets at fuel loads greater than 25 g burn as if they were in closed baskets. The average mass loss rate shows a similar trend. Where the open baskets burn on average like a closed basket at mass loads of 60 g or greater. This is because the lower permeability of the fuel bed minimises the effect of the boundary.

Dividing the average mass loss rate by the peak mass loss rate quantifies how representative the peak mass loss rate is of the burning process. The closed baskets have low values and this represents how after ignition the flame is immediately chocked by the lack of fluid flow. On the other hand the open baskets have higher values that represent how the ability of the fluid to flow and mix is beneficial to the combustion process.

4.4.4.2.2 Pinus Rigida - Open - 35 kW/m^2 and 50 kW/m^2

At 35 kW/m^2 the peak mass loss rate is minimum at 90g with a value of 0.36 g/s increasing to a maximum value of 0.66 g/s at 15 g. The average mass loss rate during flaming is minimum

at 90 g with a value of 0.11 g/s and maximum at 15 g with a value of 0.29 g/s. As a fraction the minimum is at 90 g with 0.30 and is maximum at 0.43 at 15 g.

At 50 kW/m^2 the peak mass loss rate is minimum at 90 g with 0.39 g/s and increases to a maximum of 0.72 g/s at 15 g. The average is minimum at 90g with a value of 0.099 g/s and increases to a maximum of 0.33 g/s at 15 g. As a fraction of the peak mass loss rate this is a minimum at 90 g with a value of 0.26 and maximum of 0.46 at 15 g.

4.4.4.2.2.1 Discussion

The peak mass loss rate is observed to, in general, increase with increasing heat flux and to decrease with increasing fuel load. This is because of an increase in active volume due to greater heat into the system. The most porous case is seen to have biggest change with increase in heat flux indicating that the fuel beds with greatest exposed surface are most affected by changes in radiative heat flux.

An increase in the fuel load may increase the fuel load per unit depth and the fuel load per unit area but it reduces the depth the heat flux can penetrate. These are competing effects that will alter the amount of fuel active in the reaction. The amount of fuel available is not the only aspect that will affect the peak mass loss rate. As the fuel load increases the fuel bed becomes more dense and less porous. As such the increase in fuel loading reduces the the permeability of the fuel bed and so the mixing of oxygen and fuel is not as effective and the result is a fuel bed that burns less efficiently.

The average mass loss rate increases with the increase in the heat flux for the 15 g but stays relatively the same in the higher mass cases. If this is expressed as a fraction of the peak mass loss rate the lowest fuel load is observed to increase with heat flux whilst the higher fuel loads are seen to decrease. This indicates that the average mass loss rate is affected by the fuel loading more than the heat flux. This is explained that the peak mass loss rate is about how much volatile components are present at ignition or shortly thereafter. On the contrary the average mass loss rate describes the process of sustaining the flame. This requires the continuous mixing of the oxygen with the produced volatile components. Therefore the fuel structure dictates the way in which oxygen can mix with the produced volatile components.

4.4.4.2.3 Pinus Halepensis, Pinea, Pinaster - Open - 25 kW/m^2

For the European pines, comparing the 15g samples the peak mass loss rate increases from Rigida (C), Halepensis, Rigida (O), Pinaster and Pinea with corresponding values 0.43 g/s, 0.58 g/s, 0.63 g/s, 0.77 g/s and 0.79 g/s. The average mass loss rate increases Rigida (C), Rigida (O), Halepensis, Pinea and Pinaster with corresponding values 0.096 g/s, 0.24 g/s, 0.29 g/s, 0.30 g/s and 0.36 g/s. As a fraction of the peak mass loss these increase from Rigida (C), Rigida (O), Pinea, Pinaster and Halepensis with value 0.22, 0.38, 0.38, 0.46 and 0.50.

4.4.4.2.3.1 Discussion

Closed basket show the minimum values suggesting that an increase is due to a more open fuel bed. The is consistent with the thicker needles having higher values as these will have bigger pores for a given fuel loading. As such more open fuel beds have their burning promoted.

4.4.5 Heat Release Rate Results

The mean heat release rate results for the different FPA experiments conducted are presented in the following Tables 46, 47, 48, 49 and 50 and in Figure 51.

Closed	Peak HRR - O_2 [kW]	Peak HRR - CO_2 [kW]
7.5 g	2.87	1.80
15 g	3.04	1.60
25 g	3.40	2.51
35 g	2.67	2.48
60 g	3.14	1.77
95 g	3.07	1.16
120 g	2.05	1.32

Table 46: Heat release rate results for Pinus rigida closed 25 kW/m^2.

Open	Peak HRR - O_2 [kW]	Peak HRR - CO_2 [kW]
10 g	6.14	0.96
15 g	5.05	1.11
20 g	6.31	2.12
25 g	4.13	1.73
35 g	3.94	1.94
60 g	2.88	1.23
90 g	2.62	0.97

Table 47: Heat release rate results for Pinus rigida open 25 kW/m^2.

35 kW/m^2	Peak HRR - O_2 [kW]	Peak HRR - CO_2 [kW]
15 g	4.93	1.19
35 g	3.61	1.49
90 g	2.50	0.93

Table 48: Heat release rate results for Pinus rigida open 35 kW/m^2.

50 kW/m^2	Peak HRR - O_2 [kW]	Peak HRR - CO_2 [kW]
15 g	5.35	1.46
35 g	3.95	1.98
90 g	4.16	1.51

Table 49: Heat release rate results for Pinus rigida open 50 kW/m^2.

Halepensis	Peak HRR - O_2 [kW]	Peak HRR - CO_2 [kW]
10 g	5.65	1.27
15 g	5.79	0.98
20 g	5.00	2.66
Pinea		
10 g	6.12	1.49
15 g	4.59	0.96
Pinaster		
10 g	6.64	2.07
15 g	6.81	1.05

Table 50: Heat release rate results for Pinus Halepensis, Pinea, Pinaster open 25 kW/m^2.

4.4.5.1 Peak Heat Release Rate

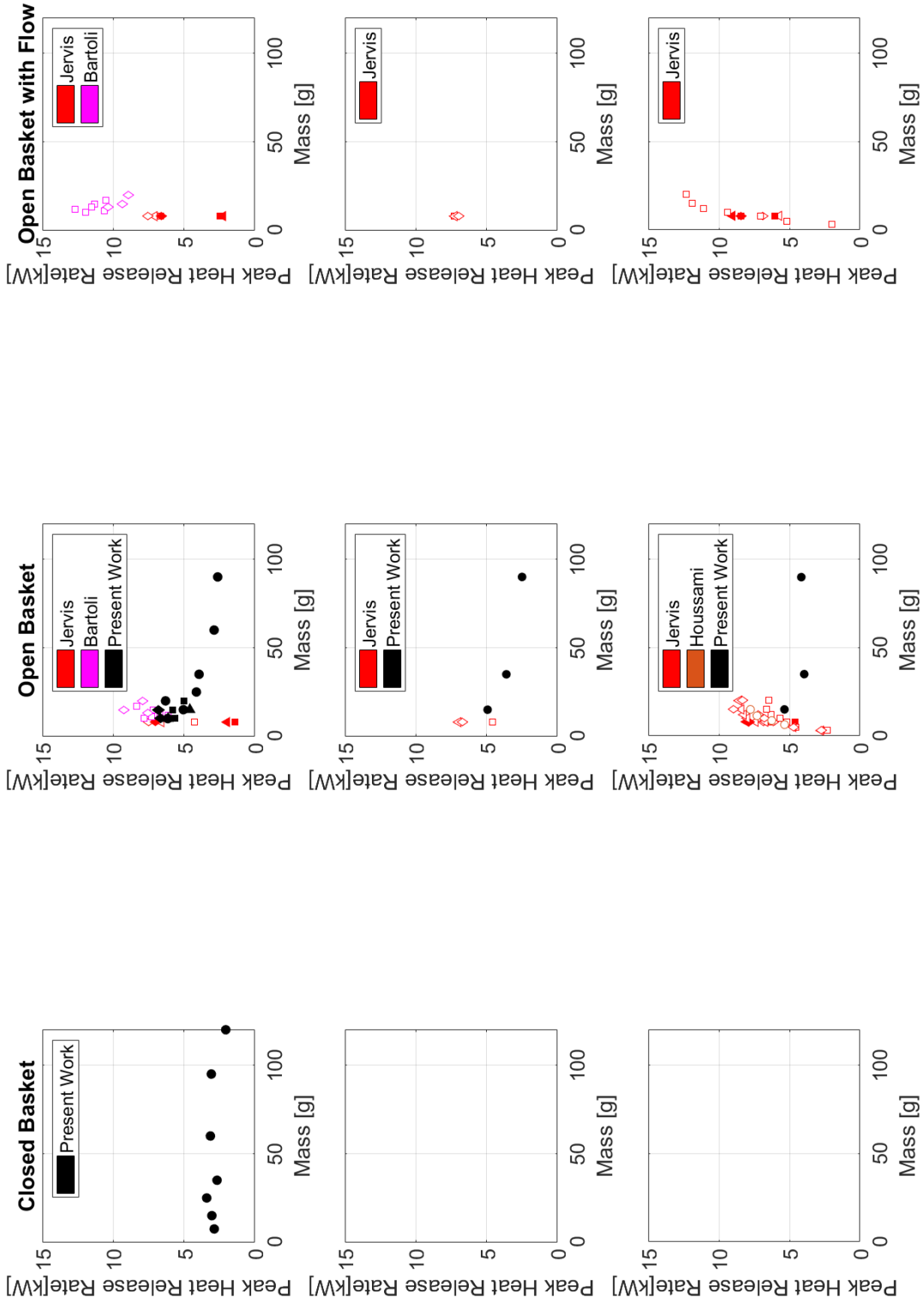

Figure 51: Peak heat release rate experimental data. Each row is a heat flux: 25, 35, 50 kW/m^2.

4.4.5.1.1 Pinus Rigida - Close/Open - 25 kW/m^2

For closed baskets at 25 kW/m^2 the peak heat release rate is maximum at 25 g with a value of 3.40 kW decreasing with both increasing and decreasing fuel load. The minimum value of for the powder case at 120 g with 2.05 kW. For open baskets at 25 kW/m^2 the peak heat release rate is maximum at 20 g with 6.31 kW with increasing fuel load decreasing the value to a minimum of 2.62 kW at 90 g.

4.4.5.1.1.1 Discussion

The peak heat release rate shows the same trend as the mass loss rate as they quantify the same phenomena.

4.4.5.1.2 Pinus Rigida - Open - 35 kW/m^2 and 50 kW/m^2

At 35 kW/m^2 the peak heat release rate is maximum at 15 g with 4.93 kW and decreases to 2.50 kW at 90 g. At 50 kW/m^2 the peak heat release rate is maximum at 15 g with 5.35 kW and minimum at 35 g with 3.95.

4.4.5.1.2.1 Discussion

The peak heat release rate increases with decreasing fuel load. Increasing the heat flux increases the peak heat release rate in the highest fuel load the most.

From these results it is appreciable that the peak heat release rate is mostly affected by the fuel structure where the increase in porous structure allows for greater mixing and a higher heat release rate. The increase in penetration owing to the increased heat flux is seen to greatly increase the peak heat release rate in the highest fuel load case. This indicates that at the lowest two fuel loads the depth of fuel bed must be quite high even at the lowest heat flux.

4.4.5.1.3 Pinus Halepensis, Pinea, Pinaster - Open - 25 kW/m^2

For the European pines, comparing the 15g samples the heat release rate increases from Rigida (C), Pinea, Rigida (O), Halepensis, Pinaster with corresponding values 3.04kW, 4.59kW, 5.05kW, 5.79kW, 6.81kW.

4.5 Surface Temperature Models

To interrogate the physics of the problem, one technique is to model the system. In classical ignition the ignition is modelled by using the time to ignition. Where the model ignition is denoted by the surface of the material reaching the ignition temperature. Here the different models are applied to the experimental results. To improve the model fit the input parameters are varied and this is also presented. The question arises as to how appropriate this ignition definition is when the reality of the experiments is that more than the top surface of the fuel bed is active in the ignition processes.

4.5.1 Unmodified Models Comparison

Further analysis involves comparing the present work with the models detailed in Section 4.2.3. These models represent the heat transfer in different ways in order to model the ignition. Whereby the ignition is denoted by the surface of the material reaching the ignition temperature. The two models are formulated differently (see Section 4.2.3) and include different sub-models:

1. Torero uses the classic semi-infinite equation with the solution presented in Section 2.3.1.6. This considers the conduction heat transfer through a semi-infinite volume. Heat is input through incident radiation on the surface and heat losses are accounted for using a heat loss coefficient at the surface.

2. Garg also considers a semi-infinite formulation. Here heat is input through radiation incident at the surface and into the depth of the volume. An additional sub-model is included whereby the material thermal properties are a function of the fuel bed and the fuel structure. Specifically the fuel element size and consequently the porosity.

4.5.1.1 Model Inputs

4.5.1.1.1 Equivalent Diameter

For the Garg model a value for the fuel element diameter is needed. This is approximated from the surface to volume ratio of a cylinder

$$S = 2\pi rL + 4\pi r^2 \tag{71}$$

$$V = \pi r^2 L \tag{72}$$

Since $L >> r$, the majority of the surface area will be from the length of the cylinder and so the surface area can be approximated by:

$$S \approx 2\pi rL \tag{73}$$

$$\sigma = \frac{S}{V} \approx \frac{2}{r} \tag{74}$$

The mean equivalent diameter is then approximately:

$$d \approx \frac{4}{\sigma} \tag{75}$$

4.5.1.1.2 Unmodified Heat Transfer Model Inputs

The model inputs were as in Table 51 and shown as a function of solid fraction in Figure 52. These were taken from literature [107] [79] [106]. However, the convective heat loss used had to be increased compared to the value reported in experimental literature [107].

Mass [g]	7.5	15	25	35	60	90	120
Solid Fraction [-]	0.06	0.12	0.19	0.27	0.47	0.70	0.93
Conv. Coeff. [W/mm2K]	3.30E-05	3.30E-05	3.30E-05	3.30E-05	3.30E-05	3.30E-05	3.30E-05
Absoptivity Torero [-]	0.8	0.8	0.8	0.8	0.8	0.8	0.8
Absoptivity Garg [-]	0.07	0.14	0.23	0.33	0.56	0.84	1.12
Conductivity Torero [W/mmK]	1.20E-04	1.20E-04	1.20E-04	1.20E-04	1.20E-04	1.20E-04	1.20E-04
Conductivity Garg [W/mmK]	7.01E-06	1.40E-05	2.34E-05	3.27E-05	5.61E-05	8.41E-05	1.12E-04
Specific Heat Torero [J/g°C]	2.07	2.07	2.07	2.07	2.07	2.07	2.07
Specific Heat Garg [J/g°C]	0.12	0.24	0.40	0.56	0.97	1.45	1.93

Table 51: Model inputs for a set of porous fuel beds made with pinus rigida.

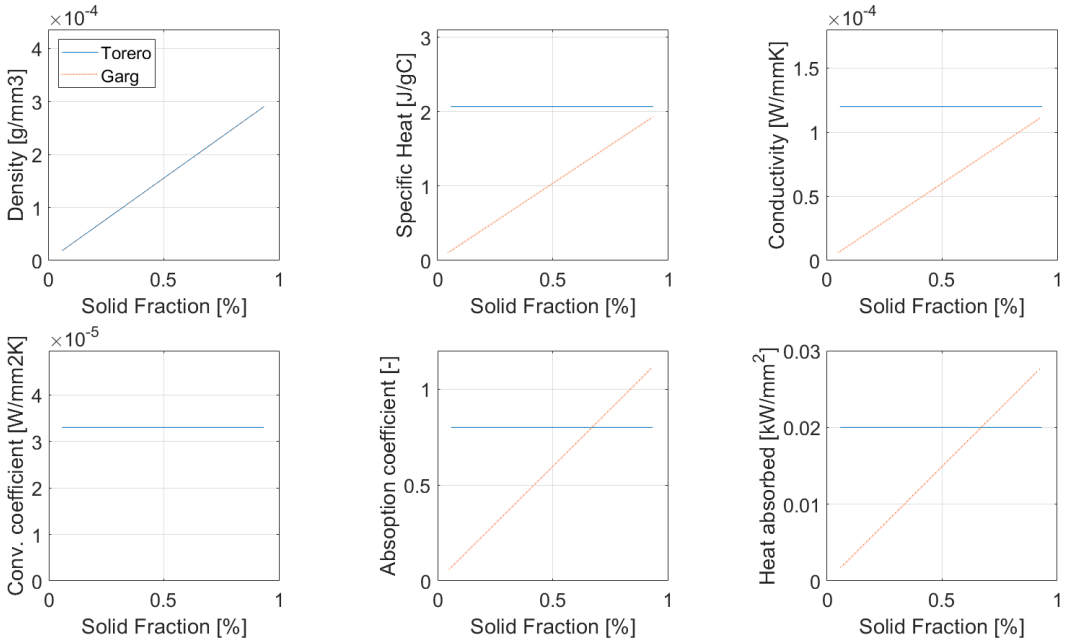

Figure 52: Unmodified input for the Garg and Torero models of the time to ignition using the surface temperature.

4.5.1.1.3 Ignition Temperature

In these models ignition is taken as the point as which the material surface temperature reaches the ignition temperature. The ignition temperature is taken as 340°C. This is the temperature used previously for wood [115] and corresponds to the temperature ranges found in Section 3.4.2.1.2.

4.5.1.2 Model Outputs

The time to ignition for each model is found using the solutions of the two models. That is to say by using the input parameters, the time required to reach the ignition temperature is found. The results of this are shown in Figure 53.

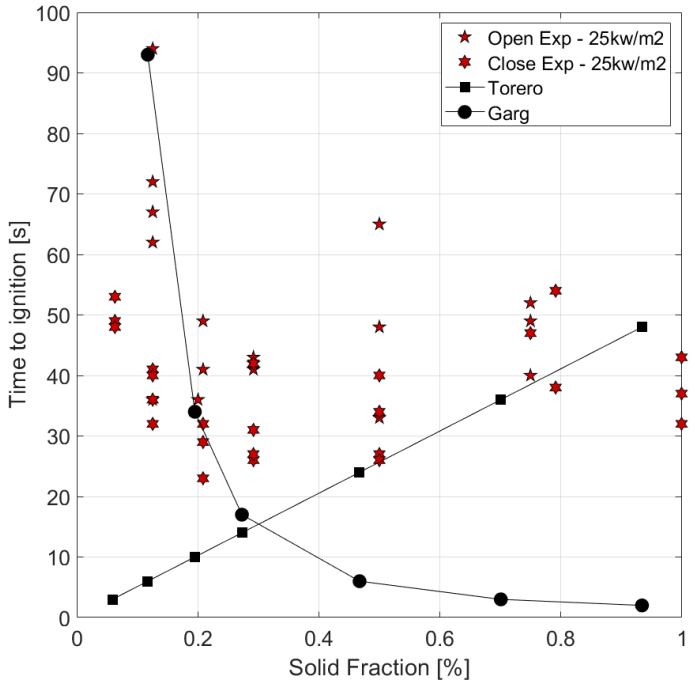

Figure 53: Results for Garg and unmodifed Torero modelling of the time to ignition with experimental values.

4.5.1.3 Discussion

Figure 53 shows that neither model represents the full range of fuel beds studied. Torero's model reproduces the more solid cases. The model only controlled by the bulk density as all other parameters stay the same regardless of fuel bed structure. Furthermore, this model was proposed with solid materials in mind and so it is reasonable that it is representative of the more solid cases. On the other hand, Garg's model reproduces the more porous cases by altering the heat transfer properties of the fuel as a function of the fuel bed structure. However there are some values where the input values go beyond what it physically possible specifically the absorptivity being greater than 1. Hence, although it fits the more porous data, there are questions about how representative of the physical phenomena it is.

4.5.1.4 Conclusion

The models reproduce different fuel loads but it is not possible to combine the two as the underlying material properties of the individual fuel beds are different. So in order to reproduce the experimental results with a single model the effective fuel bed properties of the Torero model are changed. This leads to the effective fuel bed properties being a function of the fuel bed structure.

4.5.2 Modified Torero Model Comparison

The Torero model was used as the Garg model resulted in unreal input parameters. To find the effective fuel bed properties that best fit the experimental data a genetic algorithm was

used. This meant fitting each experiment individually and resulted in the model inputs being a function of the fuel structure.

4.5.2.1 Modified Heat Transfer Model Inputs

The model inputs were optimised for each experiment and the resultant values are given in Table 52 and shown as a function of solid fraction in Figure 54.

Mass [g]	7.5	15	25	35	60	90	120
Solid Fraction [-]	0.06	0.12	0.19	0.27	0.47	0.70	0.93
Conv. Coeff. [W/mm2K]	3.20E-05	2.70E-05	2.10E-05	2.10E-05	2.00E-05	2.00E-05	2.00E-05
Absorptivity [-]	0.44	0.46	0.5	0.52	0.6	0.62	0.72
Conductivity [W/mmK]	1.40E-04	1.50E-04	1.50E-04	1.50E-04	1.50E-04	1.50E-04	1.50E-04
Specific Heat [J/g°C]	2.07	2.07	2.07	2.07	2.07	2.07	2.07

Table 52: Heat transfer inputs optimised for each experiment so that they are a function of the solid fraction

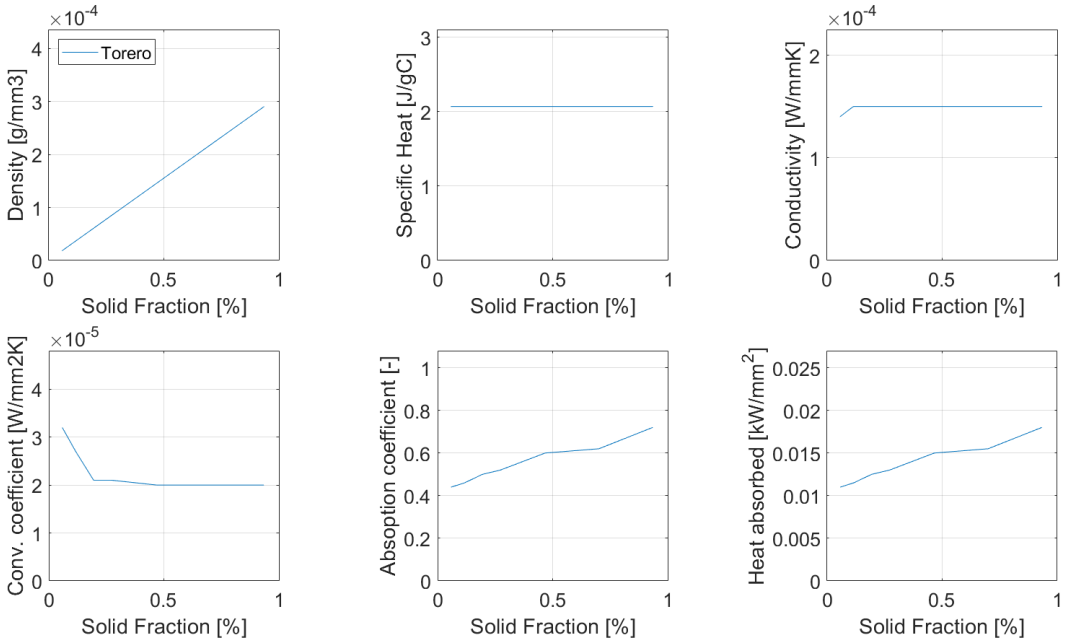

Figure 54: Optimised effective fuel bed properties as a function of solid fraction for the Torero model using the surface temperature to model the time to ignition of the different fuel beds.

The optimisation of the input parameters shows that optimum input parameters are a function of the fuel bed structure. It is interesting to see that the convective coefficient is seen to vary for the low fuel (low solid fraction and high porosity cases) and then become relatively constant. This suggests that the convective coefficient is a function of the fuel bed structure when it is porous but it becomes constant when it is solid. This follows from the idea that the fuel bed becomes less permeable as the fuel load increases - that is to say it is less affected by fluid flows and therefore convection.

4.5.2.2 Model Outputs

The model outputs for the fitted parameters are shown in Figure 55. This shows how the change in heat transfer inputs can allow the model to recreate the experimental data. However, the way in which the model inputs change as a function of the fuel structure, as shown in Figure 54, is the focus of this work.

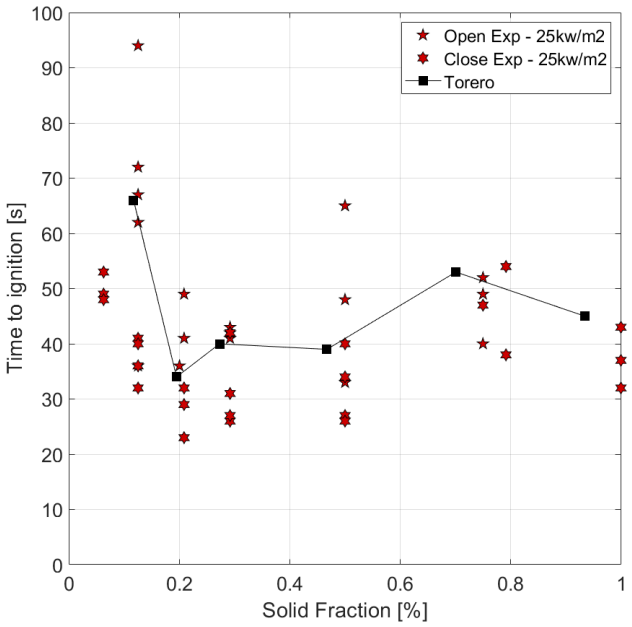

Figure 55: Model outputs when input parameters are optimised for the experiments

4.5.2.3 Conclusion

Using input parameters that are a function of the fuel bed structure works well however what does it really mean? and how does one verify the model? The answer to both of these questions is evident when you consider that we do not have a continuous surface and so the surface temperature is not a relevant parameter and the models are not sufficient to represent the phenomenon. As such, although it might fit the data, a more nuanced approach is needed.

To remedy this we add more information to our model and our optimisation. A quantity that we do measure is the mass. Hence, in the next section we extend the work here to compute the mass. Furthermore, we can leverage the benefits of the two models presented. We use the Torero model but borrow, from the Garg model, the idea that the input parameters are a function of the fuel structure.

4.6 Conclusion

Changing the boundary condition affects the fluid flow in the fuel bed. Convection is the heat transfer mechanism that is associated with fluid flow. Not only is heat transfer affected but changes in the fluid flow will affect the mass transfer and mixing of the volatile components.

The trend for both open and closed baskets at 25 kW/m^2 is that the fuel beds are more difficult to ignite at low fuel loads; at intermediate fuel loads they become easier and at high fuels loads they become more difficult to ignite. Furthermore, the increase in fuel load decreases the ability of the fuel bed to burn. A similar effect is seen when comparing the open to close baskets. This suggests that the increase in fuel load affects the fluid flow in a similar way to using a close basket and it is this effect that is behind the decrease in burning.

Changing the heat flux alters the balance of heat transfer mechanisms within the system. Increasing the heat flux allowed for an indication of the relative magnitude of the inherent heat transfer. Comparison of the different open basket experiments shows that higher heat fluxes cause quicker times to ignition. The more heat input into the system the faster the degradation process. This results in all the fuel beds igniting at similar times at high heat flux – removing any differences due to fuel structure. In terms of burning, the increase in heat flux allows for flaming to happen more quickly at lower fuels load and for longer at high fuel loads. This is due to increased heating and penetration that accelerates the low fuel loads, and which penetrates past any protective char layer that occurs at high fuel loads.

Change in the species changes the morphology of the individual pine needles that make up the fuel bed. The individual element morphology dictates the structure of the fuel bed. Hence the different species should be subject to different fluid flows and effective fuel bed heat transfer properties.

The thinner the pine needle the larger the number in a given fuel load. The greater the number of elements the less porous the fuel bed or in other words the more closed the fuel bed. There is also an increase in the solid surface area when there are more elements. This is beneficial in decreasing the time to ignition as the decrease in openness decreases the possible heat loss by convection and the increase in solid surface area increases the heat gain by radiation. Halepensis is the thinnest pine needle and ignites quickest. Whilst Pinaster is the thickest pine needle and ignites the slowest. This is because mass of each needle is less and so it takes less energy to raise the temperature of the individual needles. This results in the effective temperature of fuel bed increasing more quickly and the ignition condition being reached sooner.

The converse effect is true for the burning where larger pine needles have a shorter duration of flaming. The fewer pine needles the more open the fuel bed and the burning front has to traverse fewer solid-gas interfaces. That is to say that with larger individual elements, for a given fuel load, the pores will be larger than one with smaller elements. A more porous fuel bed results in larger surface areas to receive radiation from the flame and there are fewer pine needles that need to have their temperature raised.

Time to ignition results were compared with two models from literature. Neither model represented the results entirely but they did fit over two corresponding regimes – a high porosity and a low porosity. This indicates changes in the processes, underpinning ignition, that are due to changes in the fuel bed structure. Nevertheless, analysis of the models put into question their applicability. The ignition temperature approximation assumes that the region active in the ignition process is restricted to the top surface. Whereas, in the case of the more porous fuel beds the penetration of the incident heat flux will surely involve a volume of fuel bed rather than only its top surface.

Part V
Effective Fuel Bed Properties

5.1 Introduction

In Part IV the temperature of the fuel bed was modelled using the classical approach where ignition is denoted as the surface reaching a predetermined ignition temperature. This methodology assumes that the region involved in the ignition reaction is confined to the top surface and does not take into account the pyrolysis occurring in the depth of the sample. Due to the porous nature of the fuel it is sensible to assume the ignition processes are not confined to the top surface. This is principally due to radiation being absorbed in depth meaning that heat is received over a volume of the sample rather than just the top surface.

Furthermore, the verification of any ignition temperature is made difficult due to the porous nature of the samples. This is because of the uncertainty in temperature measurements in a porous fuel. Using a thermocouple, it is difficult to know what its measurement means as it is not known whether it is in contact with a solid element, a open pore or something in between. Additionally, even if the thermocouple were in contact with a solid element, their small thermal mass would result in the thermocouple creating large disturbances in the measurement e.g. it would draw heat from the element. Lastly, we cannot quantify any convective cooling the thermocouple itself would be subject to. As a result a method based on a different non-invasive measurement is sought. In this Part a mass-based approach is taken. This is achieved by superimposing a 1-D heat diffusion equation on the samples from Part IV and using the thermal degradation measured in Part III to model the mass. This thermo-chemical model is then fit to the experimental pre-ignition results of Part IV using a genetic algorithm. This is done by changing the effective fuel bed properties, which are assumed to be functions of the solid fraction of each sample. In this way the effective heat transfer properties of the fuel beds as a function of the fuel bed structure are analysed

5.2 Mass Method

The fuel bed temperature can be interrogated by direct measurement and a method for doing so can be found in Appendix E. However, this is an invasive measurement and uncertainty in the measurement brings its adequacy into question. Another method to interrogate the fuel bed temperature is to use the experimental mass measurement. As discussed in Section 4.1 the change in mass is a function of the mass temperature.

To model this requires knowledge of the temperature and the thermal degradation. The closed basket experimental data is used as this allows the use of Torero's model [94]. The temperature distribution within the effective volume can be modelled given a set of effective thermal properties. Using the thermal degradation the temperature can be used to map to the mass and in this way, we can compute the change in mass. Here the experimental thermal degradation is used as a look-up table. This is a simplification that has been used before [116]. Nevertheless, it does disregard the effect that heating rate has on the chemical kinetics.

5.2.1 Temperature to Mass mapping

In order to map from the temperature to the mass, the thermal degradation of the material must be known. Here, the experimental thermal degradation from Part III is used. However, to match the experimental conditions of Part IV the fuel moisture content was artificially reduced to 1%. This was done by scaling the mass loss rate during the drying phase and then reconstructing the mass curve. The resultant curve that was subsequently used to map the temperature the mass is shown in Figure 56.

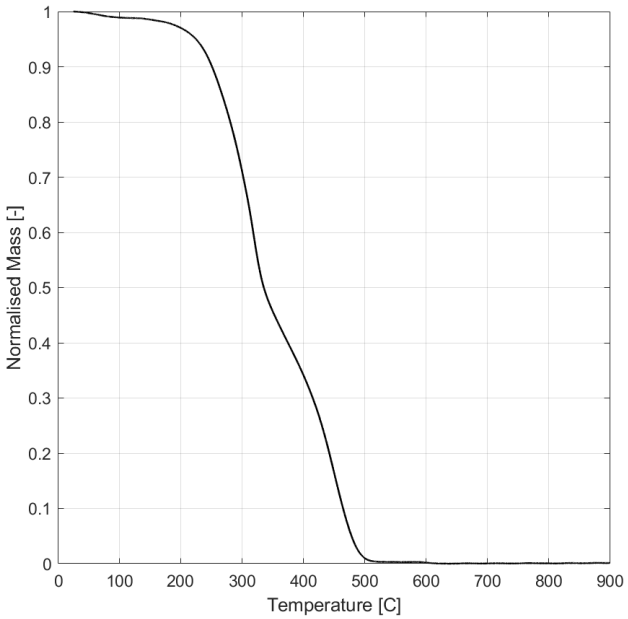

Figure 56: Average thermal degradation of Pinus Rigida at 5°C/min where the fuel moisture content has been artificially reduced to 1%

5.2.2 Temperature Distribution

To use the mapping the temperature must be known in the fuel bed. Here the solution presented in Section 2.3.1.6 is used. This allows the temperature of the fuel bed to be known spatially and temporally as a function of the effective fuel bed properties.

$$T(x,t) = \frac{a\dot{q}''_{rad}}{h_T}\left[erfc\big(\delta_x\big) - e^{(2\delta_x\sqrt{\tau}+\tau)}erfc\big(\sqrt{\tau}+\delta_x\big)\right] + T_0 \tag{44}$$

5.2.3 Mass Distribution

Combining the temperature distribution with the temperature to mass mapping, the mass distribution in the fuel bed can be modelled as a function of the effective fuel bed properties.

To implement the model a function was developed using Matlab. This had two types of input. Those that were shared between all experimental conditions:

1. x is the discrete values of the depth. This was 150 points evenly spaced between the top surface to the back surface.
2. t is the discrete values of the time. This was every 0.5 s from 0.5 s to the average time to ignition.
3. $dVol$ is the volume of each cell at the depths given by x. This was the product of the sample basket top face area and the difference between the x values.
4. q is the heat flux of the radiant source. This was set to 25 kW/m^2.
5. $Tamb$ is the ambient temperature. This was set to 25°C.

And those that could change between the different experimental conditions:

1. ρ is the density of the fuel bed i.e. the bulk density (as opposed to the material density). This is the fuel mass divided by the sample volume.

2. c is the effective specific heat capacity. This determined by the user.

3. k is the effective conductivity. This determined by the user.

4. h is the effective heat loss coefficient. This determined by the user.

5. a is the effective absorbtivity. This determined by the user.

The outputs of this function, m and T, are functions of time and space. The experimental measurement made is the mass. However, from the experiments, it is not known how the changes are spatially distributed. It is only known as a spatially integrated quantity as a function of time. To be able to compare the model with the experiment, the information provided by the model must therefore be spatially integrated to allow comparison with experiments. This means that a sum across the spatial dimension is made at each time step.

5.2.3.1 Implementation

An illustration of the propcedure used to implement the model is shown in Figure 57. The code used to implement the thermo-chemical model described previously was as follows:

```
function [T, m] = SimmsDist(x, t, dVol, q, Tamb, rho, c, k, h, a )
    load TGA_average_05.mat % Thermal degradation for 5C/min. T[25,900]
                            % The FMC has been corrected to 1%

    alpha = k/(rho*c);      % Thermal diffusivity
    q_a = q*a;              % Incident heat flux

    x_c = sqrt(4*alpha*t);  % Characteristic length
    t_c = (k*rho*c)/h^2;    % Characteristic time
    T_c = q_a/h;            % Characteristic temperature

    chi = x./x_c;           %Non-dimensional length
    tau = t./t_c;           %Non-dimensional time

    theta = T_c.*(erfc(chi)- exp(2.*chi.*sqrt(tau)+tau).*erfc(sqrt(tau)+chi));

    T = theta + Tamb;       % Conversion from theta to temperature

    T(isnan(T)) = Tamb;     % Correcting any NaN values to ambient temp.
    T(T<25)  = 25;          % Restricting lowest temp. to 25C
    T(T>900) = 900;         % Restricting highest temp. to 900C

    m_n = f(T);             % Conversion from temp. to normalised mass.
                            % f(T) is a spline function fitted to the TGA curve.
    m_n = reshape(m_n,size(T));
    m_n(m_n>1) = 1;         % Restriction of maximum normalised mass to 1

    m = rho*dVol*m_n;       % Conversion from normalised mass to mass.
                            % This is the mass in each cell of the discretised ...
                                volume

end
```

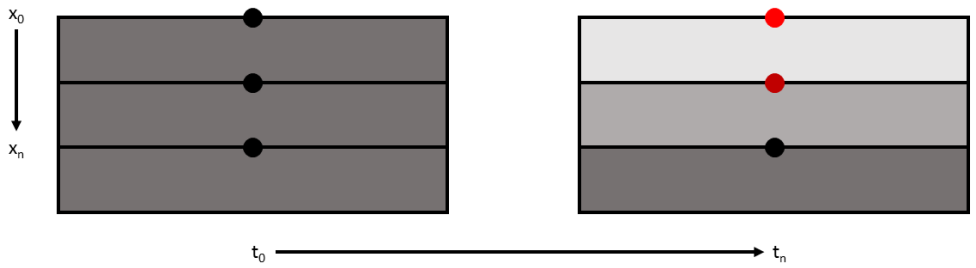

Figure 57: Illustration of the procedure used to model the mass distribution in the fuel bed using effective properties. The lighter shades of grey indicate the loss of mass whereas the more red dots indicate higher temperatures.

5.2.4 Genetic Algorithm

The heat transfer characteristics of each fuel bed structure must be identified before using this method. Inverse modelling, which uses experimental data as the modelling objective and optimises the model input parameters to best mimic the experimental data, makes this possible. The input parameters are found using optimisation methods. Due to the complexity and high non-linearity of the phenomenon, local search methods are not applicable. Instead, it is necessary to use global methods that can address the challenge of high-dimensional phenomena (eg local optima, multiple attraction basins, discontinuities)[117]. Genetic algorithms have been used in the past to find input parameters like chemical kinetics [67][118] or material properties [119]. So, in this work, a genetic algorithm is used as previously described [119]. However, instead of optimising the input parameters directly, the relationship between effective material properties and fuel bed structure is optimised. The Matlab code used for this Part can be found in Appendix F.

5.2.4.1 Experimental Inputs

Experimental measurements are needed as an objective for the genetic algorithm. The analytical solution used has been deemed appropriate in literature in the case of closed basket experiments [94] and as such those conducted in Part III are used. These were cleaned-up by taking the derivative and removing noise and anomalies in the mass loss signal caused by vibrations in the equipment. Subsequently, repeat tests were used to create an mean curve that reached the mean time to ignition. The resultant experimental inputs are shown in Figure 58.

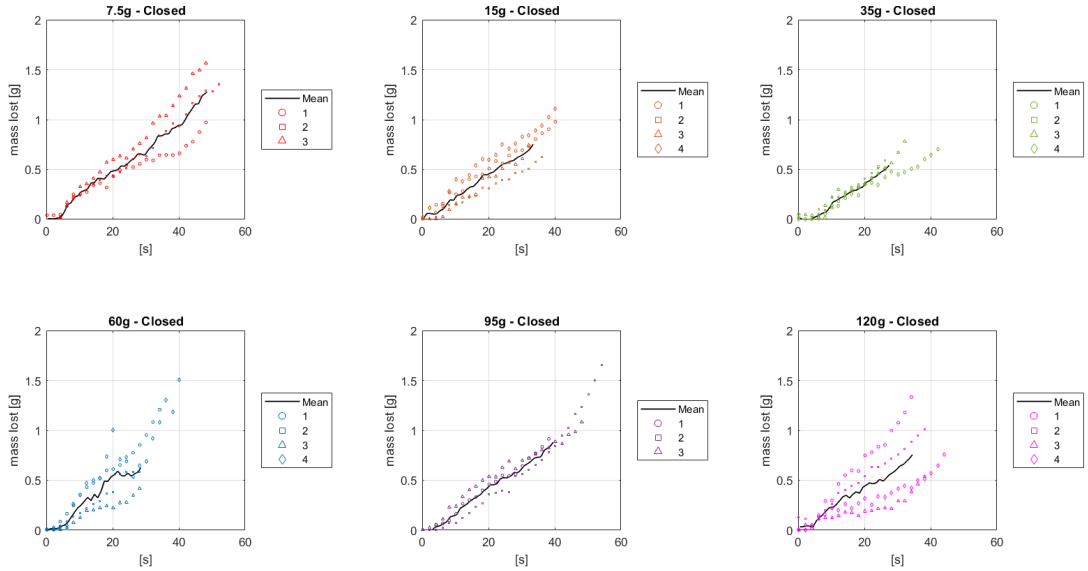

Figure 58: Closed basket pinus rigida experiments used in the genetic algorithm. Mean experiment values are taken up to the mean time to ignition for each condition

5.2.4.2 Effective Property functions

In this paper, all of the experiments are optimised simultaneously, and instead of a single parameter for each fuel bed, a relationship as a function of solid fraction is found. The solid fraction is used to describe the structure of the fuel bed because it is obvious that a higher value indicates a greater mass of fuel. The void fraction is the fraction's remainder and could have been used instead. Nonetheless, the effective properties are mathematically described as follows:

$$k = k_A + k_B e(m) \tag{76}$$
$$H = H_A + H_B e(m) \tag{77}$$
$$a = a_A + a_B e(m) \tag{78}$$
$$c = c_A + c_B e(m) \tag{79}$$

These functions describe the intrinsic value and the change due to the change in solid fraction of each heat transfer parameter. As part of the genetic algorithm the ranges of each of the eight parameters are defined.

Another method would be to optimise the individual experiments. This would require optimising twenty-four parameters whereas considering all the experiments at once and instead optimising for the function requires optimisation of only eight parameters. It is inherent to this latter method that the heat transfer parameters are assumed to be continuous functions of the solid fraction.

5.2.4.3 Objective function

In order to optimise the models, so that they fit the experiments, there must be an objective function. The objective function is used within the genetic algorithm to assess the 'fitness' of each candidate. Using the 'fitness' the algorithm selects optimal candidates and therefore definition of the objective function is integral to the optimisation process. The function in this case compares both the experimental mass and derivative with the model value as below:

$$R_1 = \sum \frac{\sum (m_{exp} - m_{mean})^2 - \sum (m_{exp} - m_{model})^2}{\sum (m_{exp} - m_{mean})^2} \tag{80}$$

$$R_2 = \sum \frac{\sum (\Delta m_{exp} - \Delta m_{mean})^2 - \sum (\Delta m_{exp} - \Delta m_{model})^2}{\sum (\Delta m_{exp} - \Delta m_{mean})^2} \tag{81}$$

$$R = R_1 + 0.5 R_2 x \tag{82}$$

R_1 is the residual that quantifies how similar, per time-step, the modelled measurement is to the experimental measurements. However, due to experimental noise it cannot be expected that the model reproduce the exact values at a given time. Therefore the rate of mass loss rate is also considered as an objective.

R_2 is the residual that quantifies how similar, per time-step, the modelled mass loss rate is to the mean experimental mass loss rate. The mean mass loss rate is used because the modelled data cannot reproduce the noise present in the experimental data. Therefore it is not sensible to use it as an objective.

R is the sum of the two residuals. Here R_2 has been subjected to a weighting of 0.5. This means that it is half as important compared to R_1. Using the residuals, the set of input parameters that give the best results are selected. Using this approach all the experiments are considered simultaneously and the functional form of the fuel bed effective properties is constrained to linear function of the fuel bed solid fraction. This allows the effective fuel bed properties to be found as the 'best' function of the fuel bed structure.

5.2.5 Results

In order to appreciate the potential changes in the heat transfer each of the parameters was changed systematically. The following functions were assumed:

1. Positive Linear Conductivity
2. Positive Linear Convection
3. Negative Linear Convection
4. Positive Linear Storage
5. Positive Linear Absorptivity
6. Positive Linear Conductivity and Negative Linear Convection
7. Positive Linear Absorptivity and Negative Linear Convection

The input parameters used by El Houssami et al.[106] were used as the baseline case. Figure 59 shows how using these inputs the model output does not represent the low fuel load experiments.

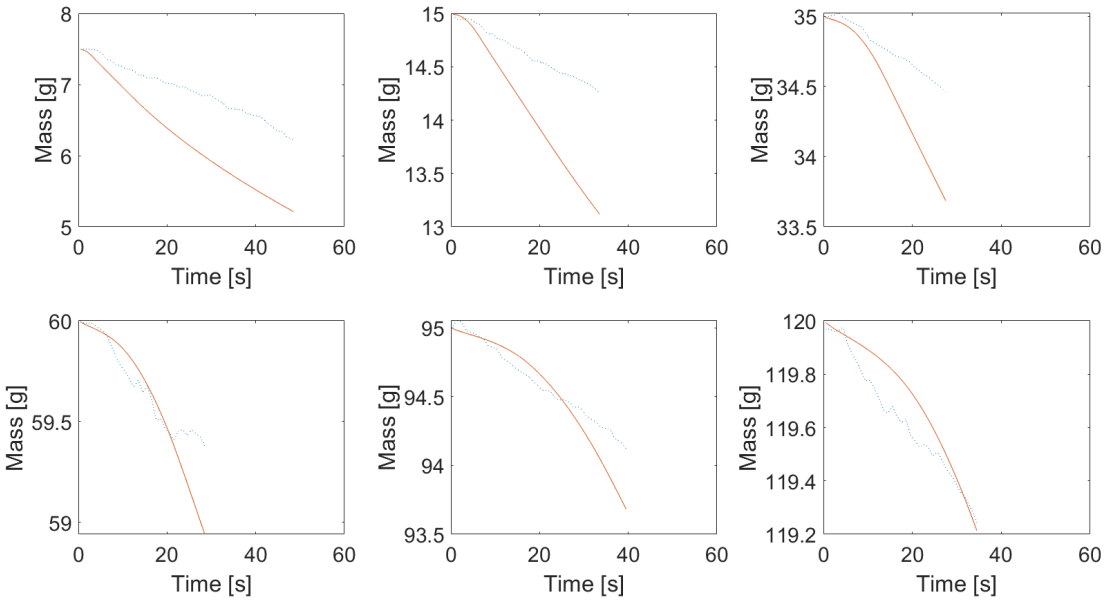

Figure 59: Results using baseline input parameters. Blue line shows experimental mean whilst red line shows the model output. From left to right, top to bottom, the fuel loads shown are 7.5 g, 15 g, 35 g, 60 g, 95 g, 120 g.

In Figure 59, the model outputs are concordant with the higher fuel loads. However, they over predict the mass loss in the low fuel load cases. This would indicate that the temperature distributions in the low fuel cases is too high i.e. the net energy of the system is too high. Therefore the heat transfer to the bed is too high or the heat losses are too low.

5.2.5.1 Positive Linear Conductivity

The first case is positive linear conductivity. The intention here was to represent the increase in conductivity that is assumed to occur with a decrease in the porosity of the fuel bed. That is to say smaller spacing between needles is assumed to lead to an easier conduction of heat through the fuel bed. Optimisation gave the values for k_A and k_B as 2.41e-6 W/mmK and 8.96e-5 W/mmK respectively and the model inputs as function of the solid fraction are shown in Figure 60.

The model output values are shown in Figure 61 and do not show good agreement with the experimental data. The lowest fuel beds were adequate but the high fuel loads were over estimated. Low values of conductivity have the effect of reducing the heat transfer through the fuel bed and as a result concentrating the heat at the surface and therefore surface temperature increases. In the low fuel load beds this cannot be the case as the radiation penetrates into the depth of the fuel bed and so the heat should be more distributed.

Another discussion point is that this may be because the conduction in the model does not represent pure conduction instead it may also represent the heat transferred through the fuel bed due to needle-to-needle radiation. This has been suggested previously in similar studies, where it was suggested that these two types of conduction will be affected by the fuel bed structure [100] however, the optimisation here suggests that they may compensate one another.

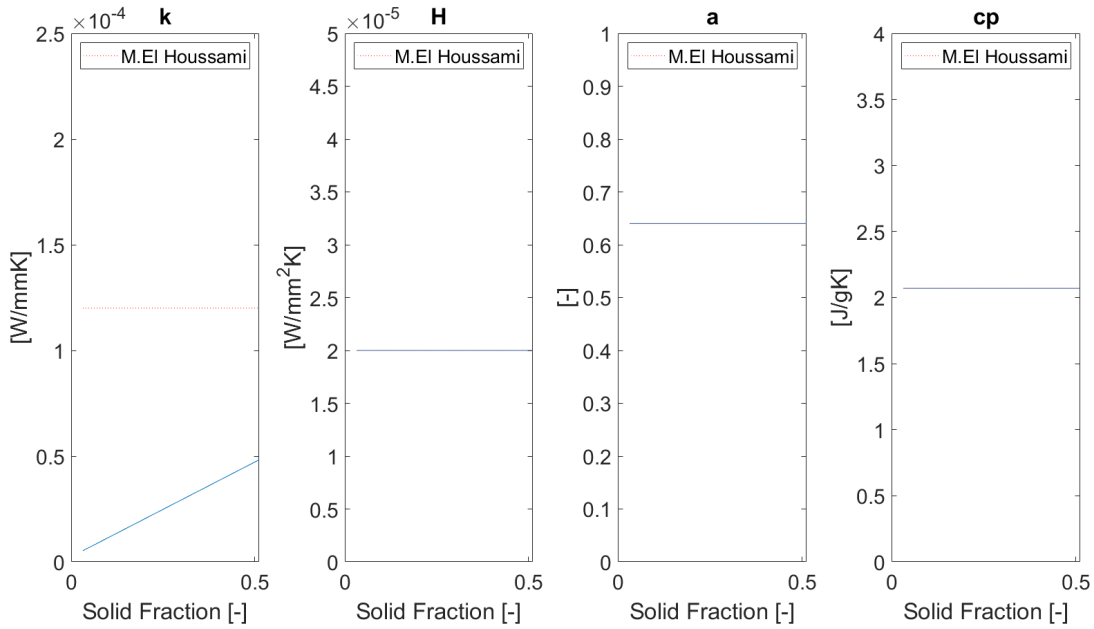

Figure 60: Positive Linear Conductivity model inputs. Showing, from left to right, the conductivity, total heat transfer coefficient, absorptivity and specific heat capacity as a function of the solid fraction

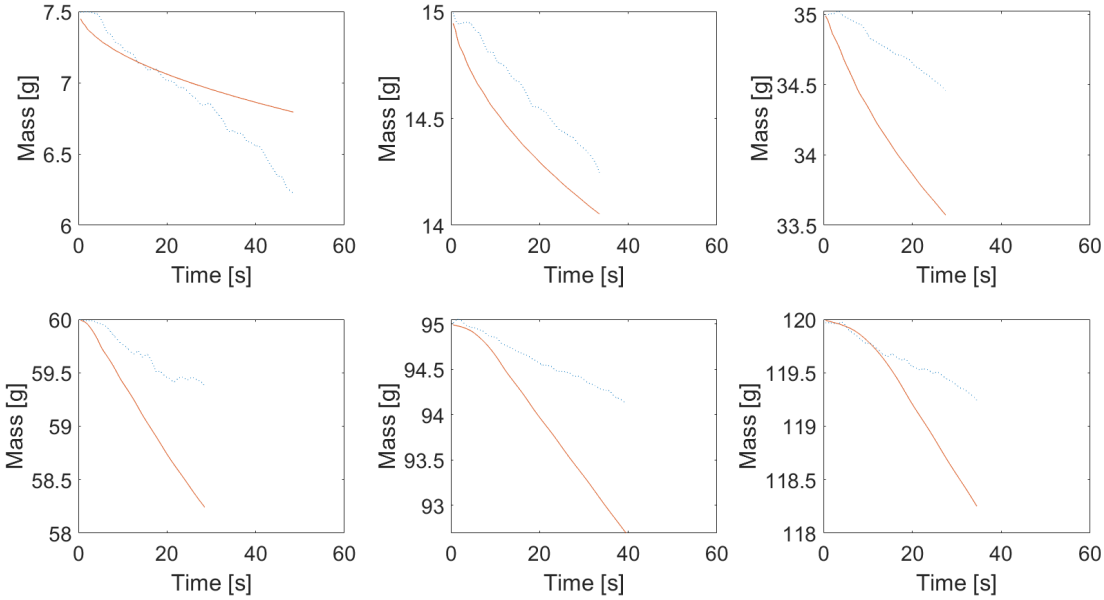

Figure 61: Positive Linear Conductivity model outputs. Blue line shows experimental mean whilst red line shows the model output. From left to right, top to bottom, the fuel loads shown are 7.5 g, 15 g, 35 g, 60 g, 95 g, 120 g.

5.2.5.2 Positive Linear Convection

The next case is positive linear convection. This case is illogical as the fuel bed should not be subject to higher convective losses as the fuel bed becomes less porous (and therefore more dense). However, it is included for completeness. Optimisation gave the values for H_A and H_B

as 3.23e-5 W/mm$_2$K and 3.01e-5 W/mm$_2$K respectively and the model inputs as function of the solid fraction are shown in Figure 62.

The model outputs are shown in Figure 63 and show improved agreement with the low fuel loads but, at high fuel loads the mass lost is under estimated. This indicates that the higher-than-baseline values in the low fuel loads case is suitable but that the increase in the value with solid fraction is not appropriate. This was expected as the relationship is non-physical in nature. The results however, do suggest that the opposite trend may be more appropriate.

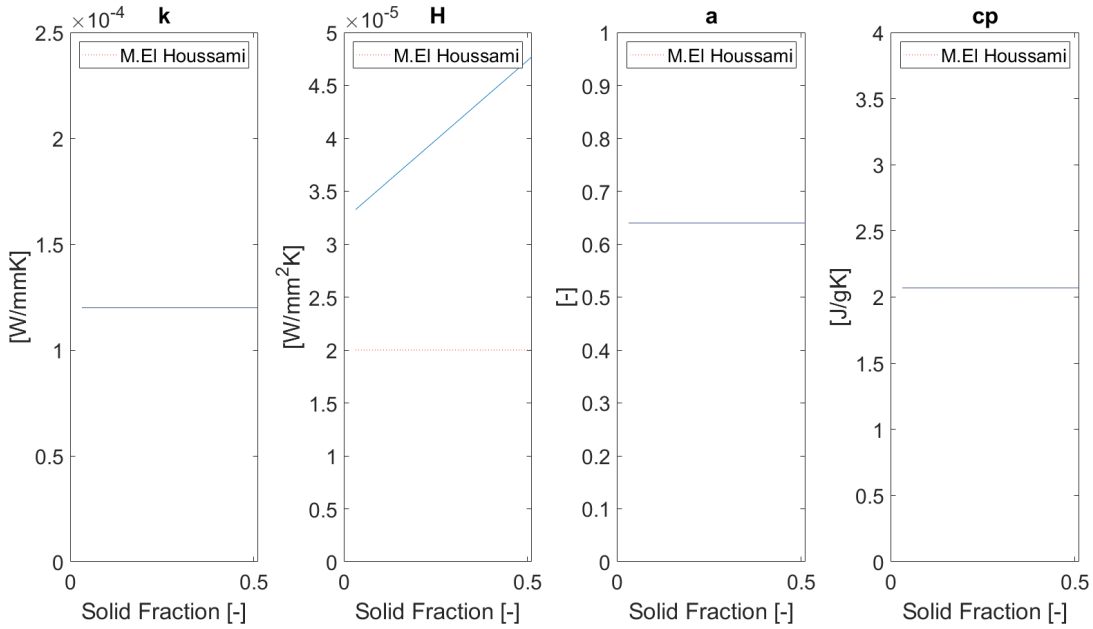

Figure 62: Positive Linear Convection model inputs. Showing, from left to right, the conductivity, total heat transfer coefficient, absorptivity and specific heat capacity as a function of the solid fraction.

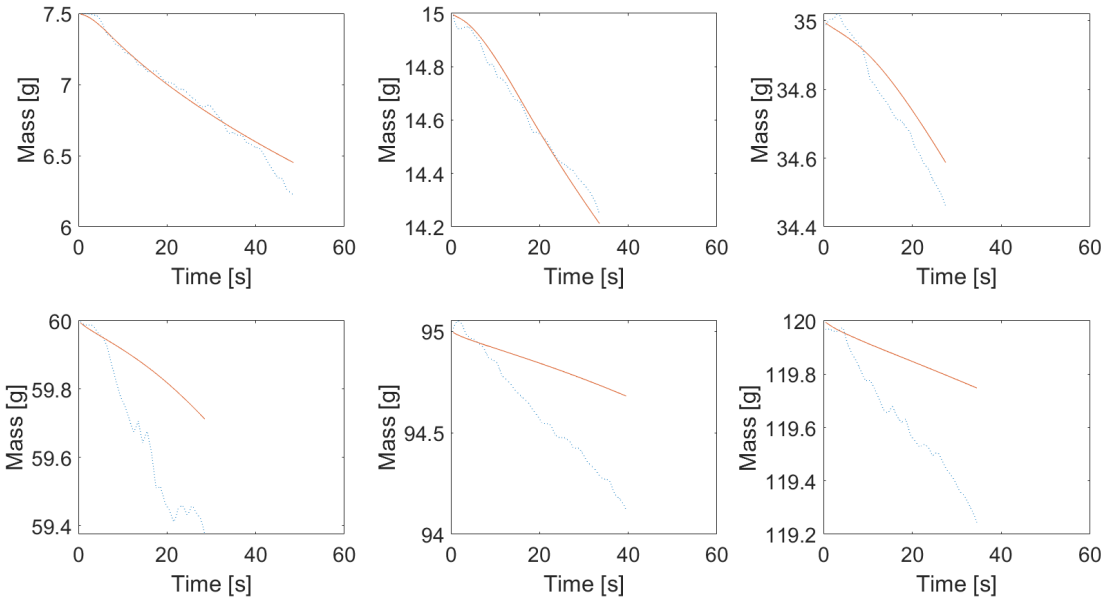

Figure 63: Positive Linear Convection model outputs. Blue line shows experimental mean whilst red line shows the model output. From left to right, top to bottom, the fuel loads shown are 7.5 g, 15 g, 35 g, 60 g, 95 g, 120 g.

5.2.5.3 Negative Linear Convection

The next case is negative linear convection. This intention here is to represent the increase in convective heat loss that is assumed to occur as the bed becomes more porous. That the increase in the porosity of fuel bed leads to an increase in its permeability and so it is more susceptible to fluid flows and therefore convective losses [64]. Optimisation gave the values for H_A and H_B as 3.35e-5 W/mm$_2$K and -8.54e-5 W/mm$_2$K respectively and the model inputs are shown in Figure 64.

The output is shown in Figure 65 and shows an improved representation of the experimental results in both the low and high fuel load cases. Although the lines do not overlap in the high fuel cases, a similar gradient is found at long time . This indicates that the rates of degradation are similar and as such some of the experiment physics are being captured. A decrease in the convective heat loss coefficient means that more energy is entering the system.

Another point to discuss is that these are closed basket experiments and therefore fluid flows through the bed are minimised. Therefore, the effect captured here instead could be that porous fuels are not subject convective losses only at the top surface but also throughout bed.

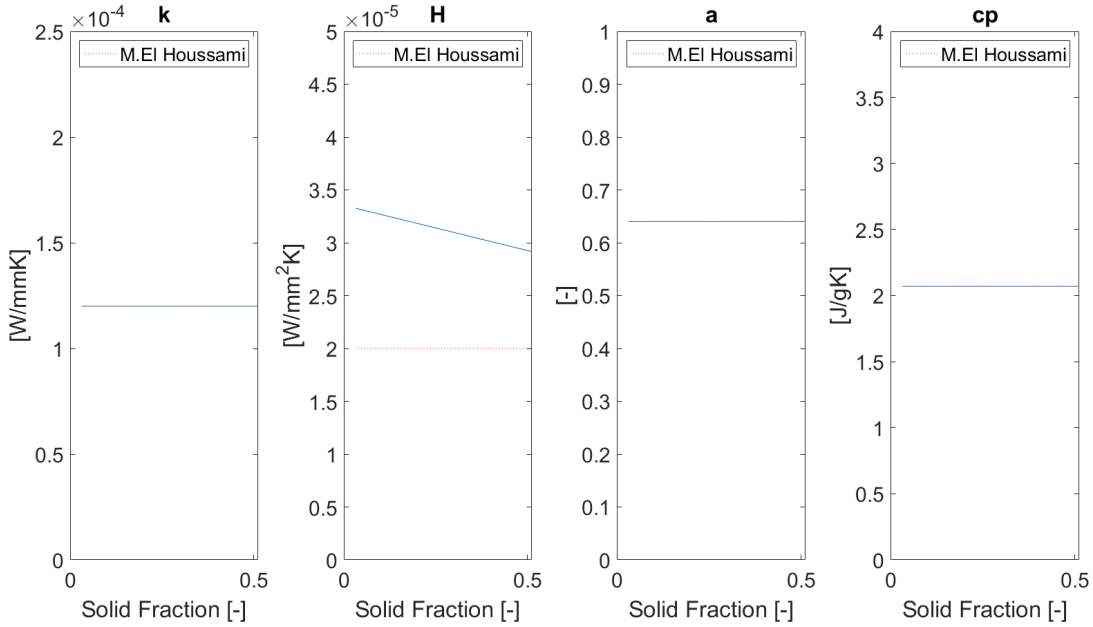

Figure 64: Negative Linear Convection model inputs. Showing, from left to right, the conductivity, total heat transfer coefficient, absorptivity and specific heat capacity as a function of the solid fraction

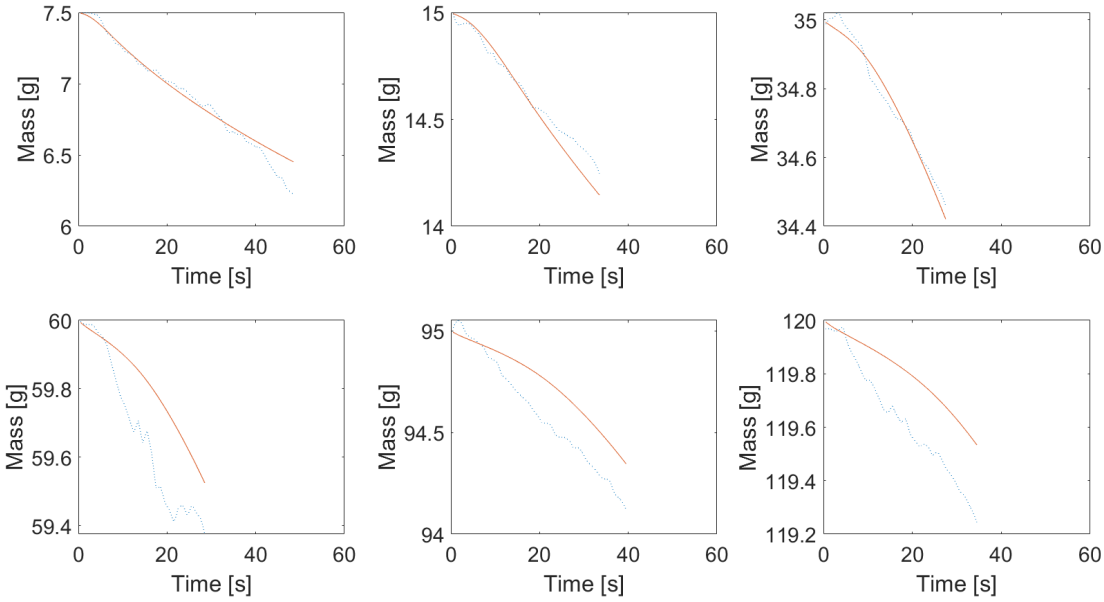

Figure 65: Negative Linear Convection model outputs. Blue line shows experimental mean whilst red line shows the model output. From left to right, top to bottom, the fuel loads shown are 7.5 g, 15 g, 35 g, 60 g, 95 g, 120 g.

5.2.5.4 Positive Linear Storage

The next case is positive linear storage. Here the intention was to represent the increase in heat required to heat the increased fuel load beds. In this way, capturing other potential volumetric heat sink effect such as for example potentially an increase in voids may cause an increase in in-bed convective loss, this would cause the bed to require more heat in order to raise the

temperature of the bed. Optimisation gave the values for c_A and c_B as 3.00 J/gK and 2.95 J/gK respectively and the model inputs as a function of the solid fraction are shown in Figure 66.

The output is shown in Figure 67 and it appears to not fit the experimental data. The high fuel load cases are shown to be underestimated that is to say the heat sink imposed by the increase in the specific heat capacity it too great. This would indicate that the heat capacity of the fuel is not needed to be increased. The physical effect of such a change is that the energy travels slower through the fuel bed as more energy is required to increase the temperature of the fuel at each depth.

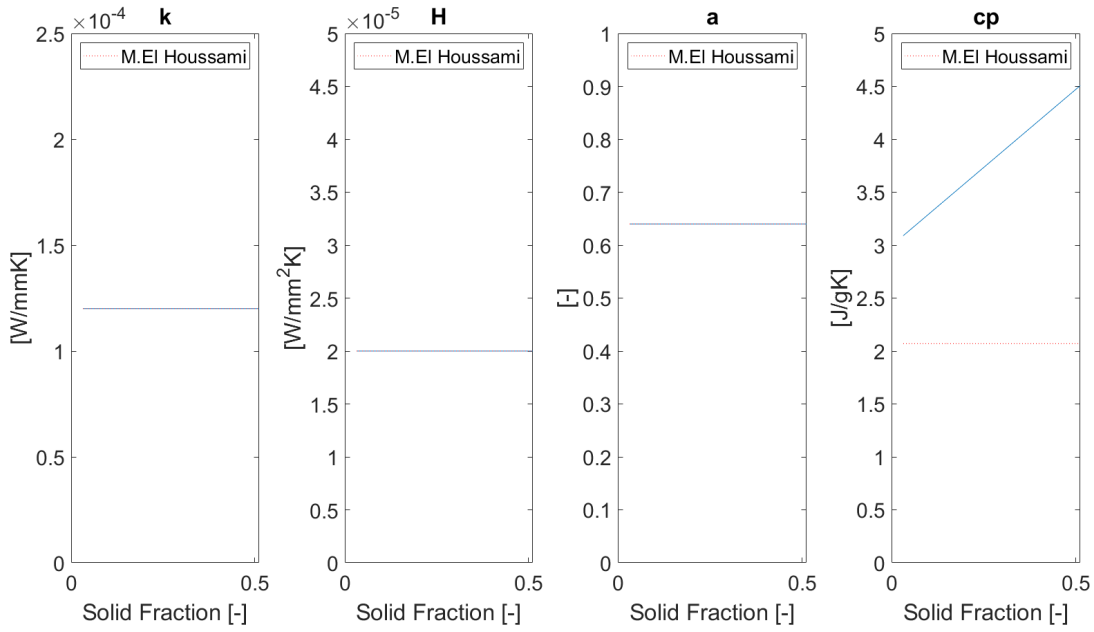

Figure 66: Positive Linear Storage model inputs. Showing, from left to right, the conductivity, total heat transfer coefficient, absorptivity and specific heat capacity as a function of the solid fraction.

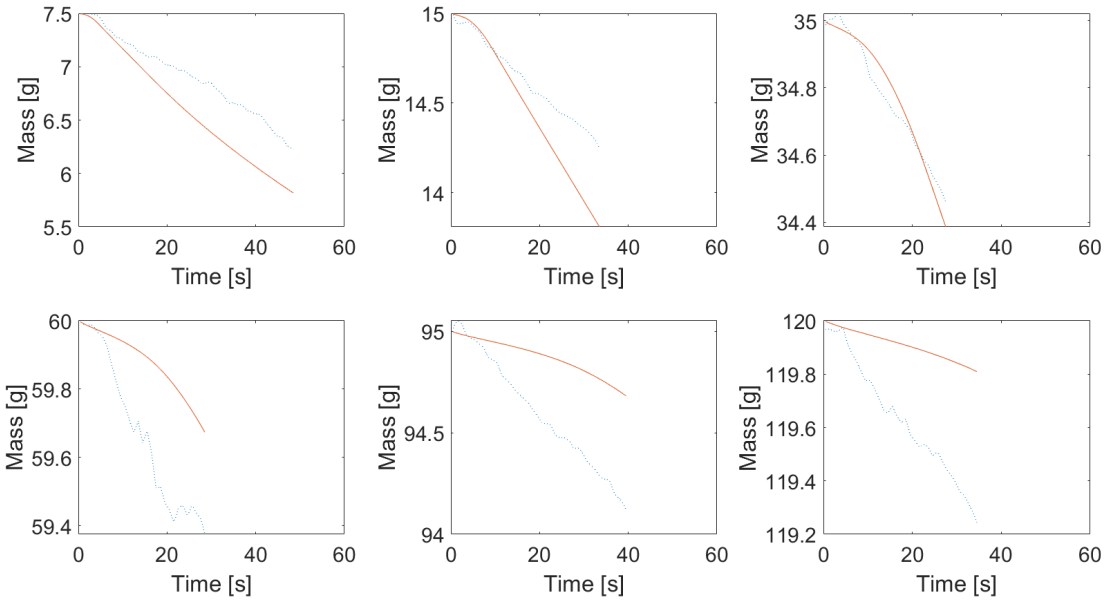

Figure 67: Positive Linear Storage model outputs. Blue line shows experimental mean whilst red line shows the model output. From left to right, top to bottom, the fuel loads shown are 7.5 g, 15 g, 35 g, 60 g, 95g, 120 g.

5.2.5.5 Positive Linear Absorptivity

The next case is positive linear absorbtivity. Here the intention was to represent the increase in heat absorbed at the top surface of the fuel bed due to there being more mass at each depth of the fuel bed. Optimisation gave the values for a_A and a_B as 0.46 and 0.56 respectively and the model inputs as a function of the solid fraction are shown in Figure 68.

The model outputs are shown in Figure 69 and show good agreement between the model and experimental values. However the high fuel loads are seen to have a steeper gradient at longer times. This indicates that the temperature in the system is too high possibly due to the temperature at the surface increasing too rapidly and this not being compensated by high enough heat losses. These heat losses could be achieved with an increase in the conductivity which would distribute the heat in the material or an increase in the convective heat loss that would reduce the amount introduced in the system.

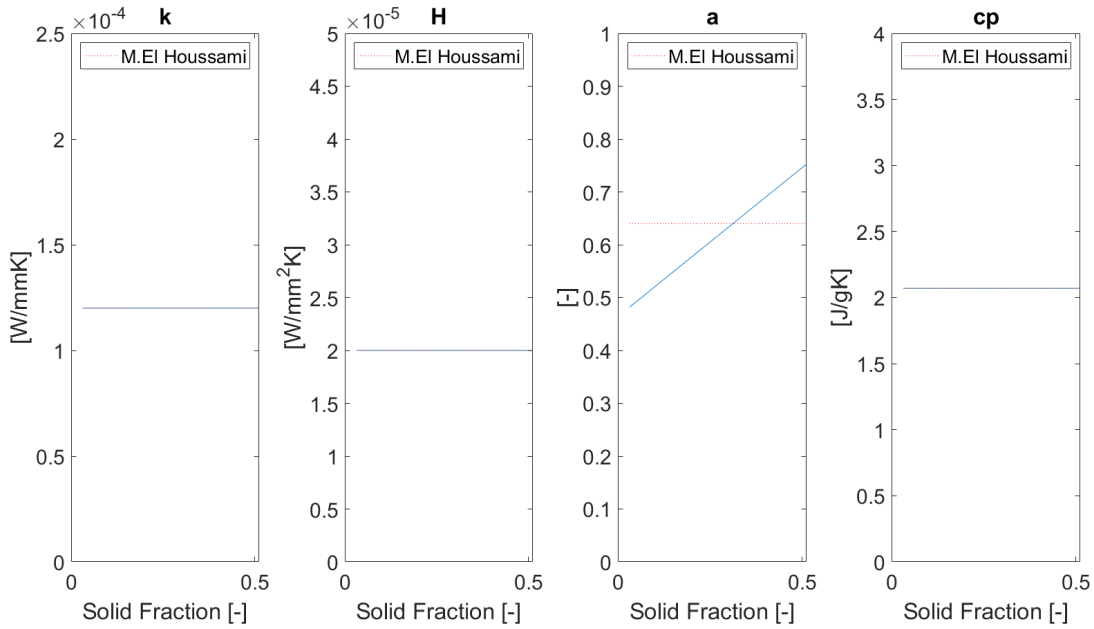

Figure 68: Positive Linear Absorptivity model inputs. Showing, from left to right, the conductivity, total heat transfer coefficient, absorptivity and specific heat capacity as a function of the solid fraction.

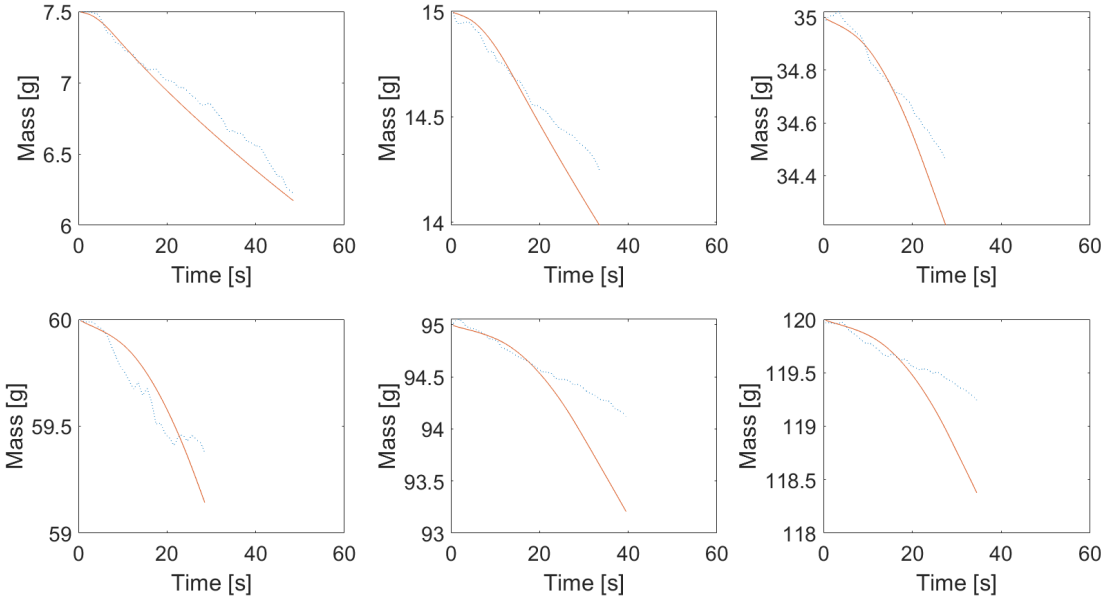

Figure 69: Positive Linear Absorptivity model outputs. Blue line shows experimental mean whilst red line shows the model output. From left to right, top to bottom, the fuel loads shown are 7.5 g, 15 g, 35 g, 60 g, 95 g, 120 g.

5.2.5.6 Positive Linear Conductivity and Negative Linear Convection

The next case is positive linear conductivity and negative linear convection. Here the intention is to capture the assume increased in conductivity as well as the assumed increase in heat losses. Optimisation gave the values for k_A, k_B, H_A and H_B as 1.16e-4 W/mmK, 2.41e-4 W/mmK,

3.33e-5 W/mm$_2$K and -4.44e-6 W/mm$_2$K respectively. The model inputs as a function of the solid fraction are shown in Figure 70

The model outputs are shown in Figure 71. Here there is good agreement in the low fuel load cases but in the high fuel loads is an under estimation of the heating leading to less mass loss than in the experiments. This further indicates that an increase in conductivity is not sufficient to describe the changes in the flammability of the fuel beds.

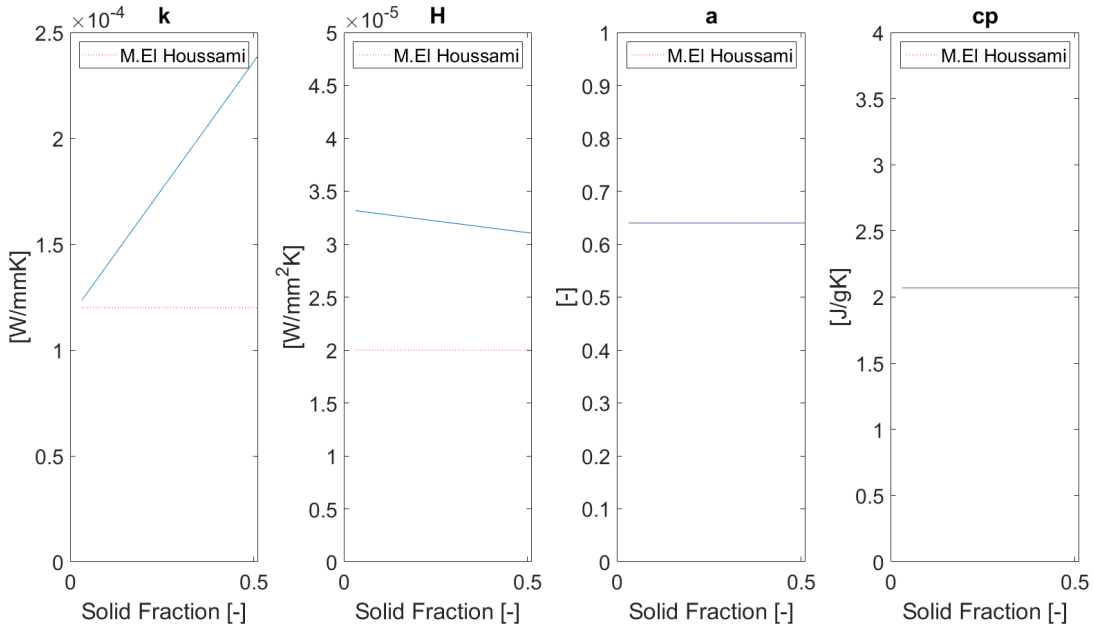

Figure 70: Positive Linear Conductivity and Negative Linear Convection model inputs. Showing, from left to right, the conductivity, total heat transfer coefficient, absorptivity and specific heat capacity as a function of the solid fraction.

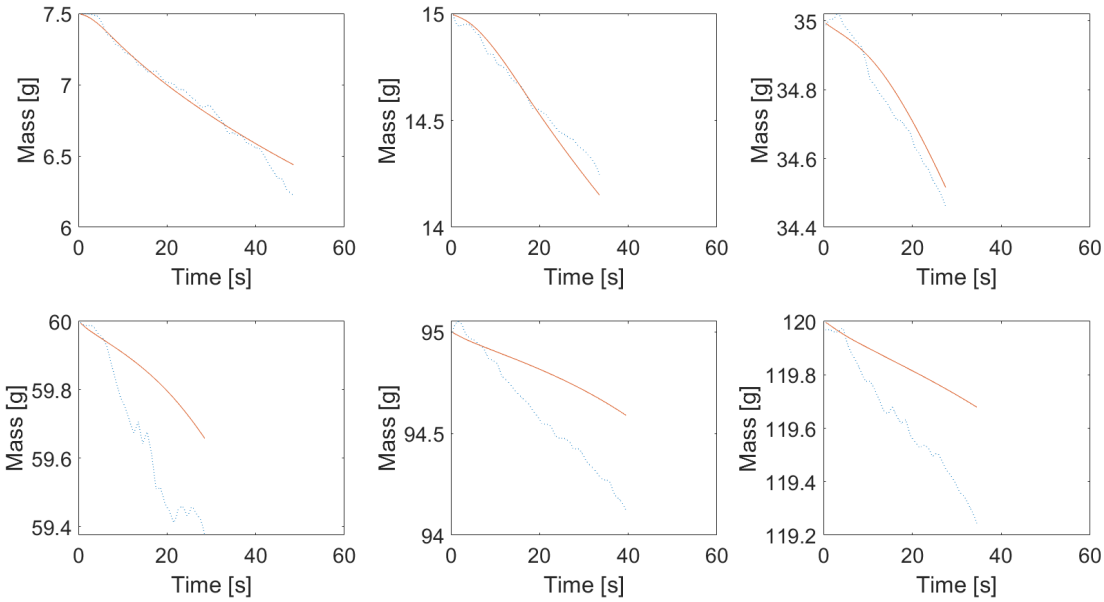

Figure 71: Positive Linear Conductivity and Negative Linear Convection model outputs. Blue line shows experimental mean whilst red line shows the model output. From left to right, top to bottom, the fuel loads shown are 7.5 g, 15 g, 35 g, 60 g, 95 g, 120 g.

5.2.5.7 Positive Linear Absorptivity and Negative Linear Convection

The next case is positive linear absorptivity and negative linear convection. Here the intention is to combine the two cases that have worked the best so far. These would represent a decrease in convection due to the decrease in the permeability of the fuel bed as the solid fraction increases. Where a decrease in permeability should reduce the the influence of fluid flows on the fuel bed and therefore reduce the convective losses. Secondly the increase in the absorptivity is meant to represent an increase in the number of elements projected onto the top surface of the fuel bed as the solid fraction increases. This increase would mean an increase in the number of elements incident with radiation and therefore more points where the heat can enter the fuel bed. Optimisation gave the values for H_A, H_B, a_A and a_B as 3.19e-5 W/mm$_2$K, -2.06e-6 W/mm$_2$K, 0.60 and 0.74 respectively. The model inputs as a function of the solid fraction are shown in Figure 72.

The model outputs are shown in Figure 73. Here the results show that the low fuel loads are adequately represented but the high fuel loads are not. It is also of interest that the convective coefficient does not change much and instead this has been compensated by the absorptivity. What is meant here is that increases in the energy of the system can be achieved in two ways. Either the amount of energy entering the system can be increased i.e. the absorptivity is increased or the amount of energy leaving the system can be reduced i.e. the convective losses are decreased. This underlines the point that these different parameters can balance one another but the changes witnessed are changes due to changes in the energy transport in the fuel bed.

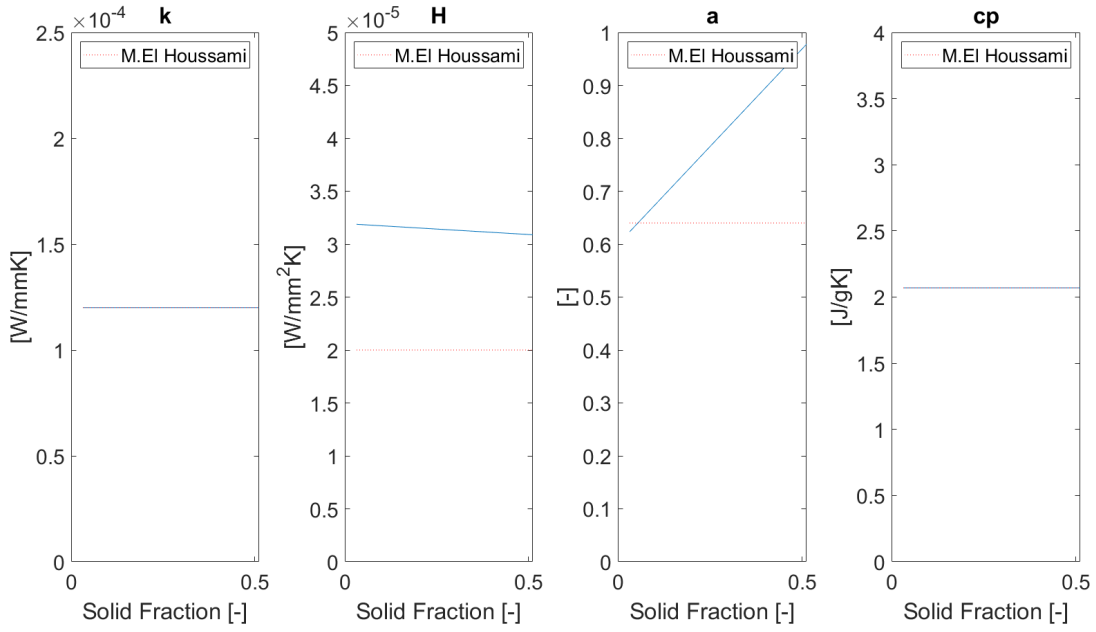

Figure 72: Positive Linear Absorptivity and Negative Linear Convection model inputs. Showing, from left to right, the conductivity, total heat transfer coefficient, absorptivity and specific heat capacity as a function of the solid fraction.

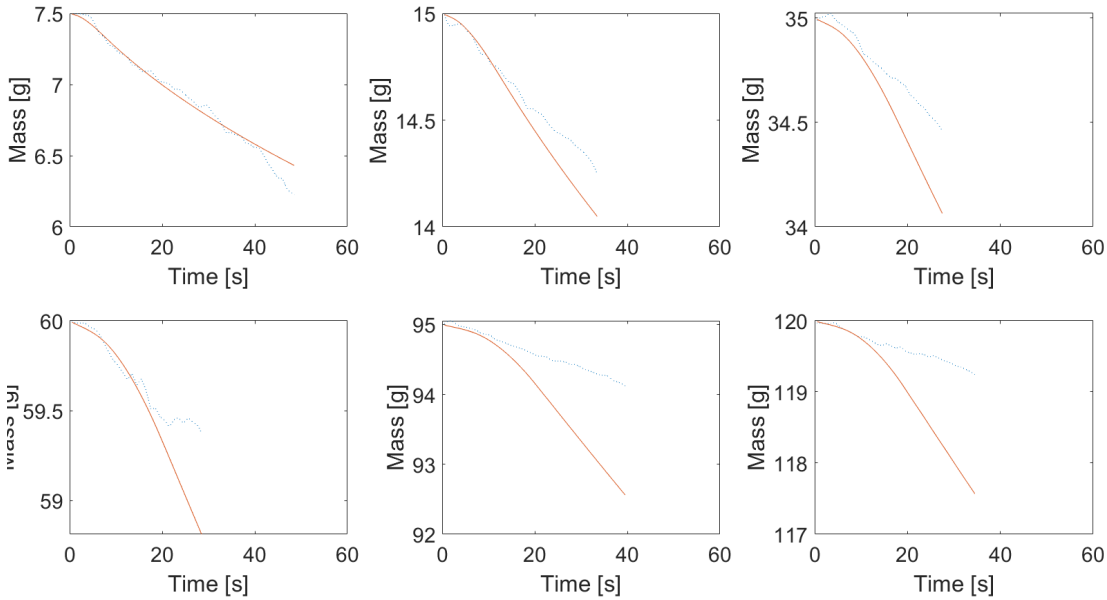

Figure 73: Positive Linear Absorptivity and Negative Linear Convection model outputs. Blue line shows experimental mean whilst red line shows the model output. From left to right, top to bottom, the fuel loads shown are 7.5g, 15g, 35g, 60g, 95g, 120g.

5.2.6 Discussion

5.2.6.1 Trends in Heat Transfer Inputs

The results show that a change in the heat transfer inputs changes the modelled mass loss. The best fit comes with either negative linear convection or positive linear absorptivity. The higher fuel loads require the net heat in the system to be higher either by reducing the heat losses or increasing the energy absorbed by the system. Combining both a negative linear convection with a positive linear absorptivity does not improve the fit due to the competing effects of each. That is to say that an increase in the convective heat losses is balanced by the increase in heat radiation absorbed. Potentially the functional relationships used here are not completely correct and instead a non-linear relationship is more appropriate. The reasoning here would be that the effective properties are a function of the fuel structure up to a point where then they may for example become constant. This point might be represented as transition between a porous fuel to a solid-like fuel. This was an effect seen in the modified ignition temperature model presented in Section 4.5.2.

The experiments modelled here are in closed baskets and as such the flow fields will not change substantially. Furthermore the model is an interpretation of the reality and as such it is in not perfect - it is important to remember that the fuel bed is not simply an effective solid but is a collection of individual elements. Instead this can be thought of as the change in the surface areas involved in each heat transfer mechanism.

As the baskets increase in fuel loading they become more 'closed'. That is to say the surface area wetted and involved in the convective heat transfer reduces. As they become more 'closed' the amount of mass in each layer of the fuel bed increases. That is to say the amount of area incident and involved in the radiative heat transfer increases. These are the effects captured by the effective heat transfer properties where an increase in convective heat transfer coefficient is not simply because there is suddenly an increase in the flow field. Instead its increase accounts for the increase in the wetted surface area. With a similar effect represented by the changes in the absorptivity.

5.2.6.2 Active Region

The negative linear convection is assumed to be representative of the thermal processes occurring in the fuel bed. Using the model the interior of the fuel bed can now be interrogated. Visualisations are depicted in Figure 74. The Figure shows the depths of the material affected active in the ignition reaction. The lowest fuel load (7.5 g) model is shown to be losing mass over a depth of 5 mm whereas the highest fuel load (120 g) shows that the mass is being lost from the top surface. Hence, from the Figure it is clear that the increase in fuel loading reduces the depth of the fuel bed active in the ignition reaction as was suggested in Section 4.1.3. This further underlines that the ignition temperature approximation is not appropriate for porous fuels and that method that considers the whole fuel bed depth is necessary. Such a method has been presented in this work. However, further work is needed in determining an appropriate replacement ignition criteria - potentially one that considers both the integrated mass lost and the rate of mass loss.

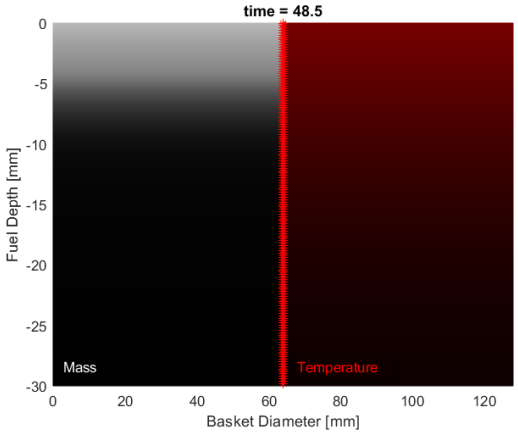

(a) 7.5g

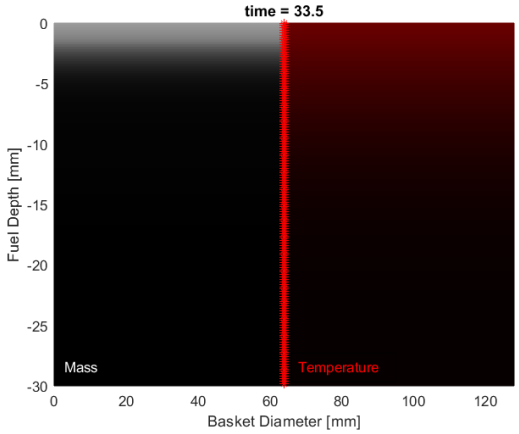

(b) 15g

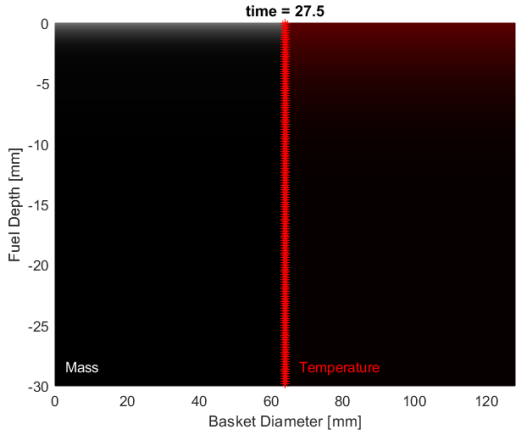

(c) 35g

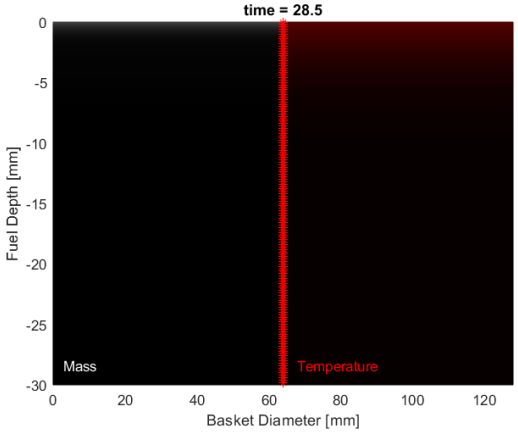

(d) 60g

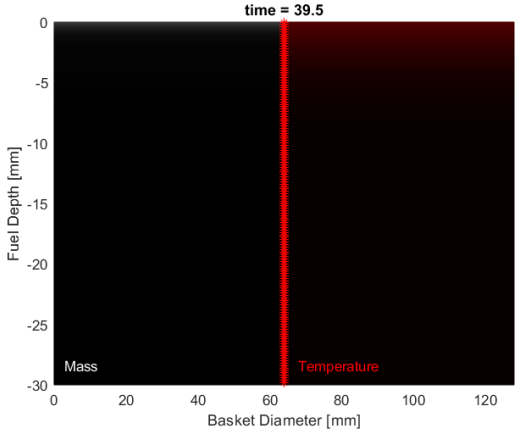

(e) 95g

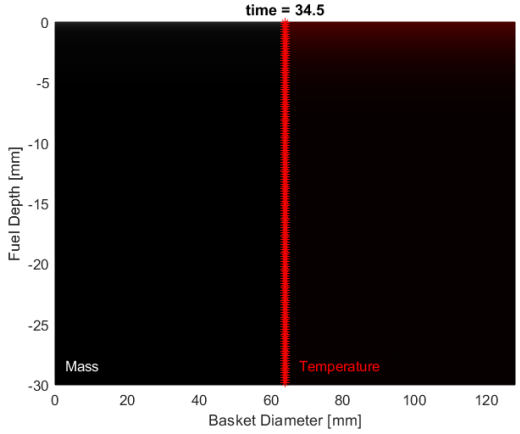

(f) 120g

Figure 74: Visualisation at time to ignition of the negative linear convection model. Each cell is coloured to represent the normalised mass and the temperature. Where 0g is white and 900C is red.

5.2.7 Conclusion

Here, closed basket fuel bed experiments had their temperatures interrogated through the use of measured thermal degradation and the imposition of a semi-infinite temperature distribution. Using a genetic algorithm the effective heat transfer properties were explored in an attempt to match the modelled and experimental mass. In this way it was possible to interpret, with some degree of quantification, how the fuel bed structure affects the heat transfer properties governing the ignition processes.

The results of this analysis suggest that the higher fuel loads require the net heat in the system to be higher either by reducing the heat losses or increasing the heat absorbed by the system. Furthermore there are competing effects, whereby increases in the convective heat losses are faced with increases in the radiation absorbed by the system.

The model presented here is simple. It does not account for how the changes in the mass of each cell will change the energy required to heat up the cell i.e. less mass takes less energy to heat up. It assumes a back face boundary condition that may not comply with the lowest fuel loads i.e. the thermal wave is likely to reach the back in these cases. Nevertheless, it's purpose is to illustrate the difference between porous ignition and solid ignition and that is what has been achieved.

The depth of the active region is not confined to the top surface and as such an interpretation of the ignition process with ignition temperature at its centre is not appropriate. This is only strengthened when one considers that there is no continuous top surface. Especially as in the most porous cases the fuel bed is a collection of individual fuel elements acting in a system. Here this system was postulated as a fuel bed with effective heat transfer properties. In this way the depth of heating was modelled and a mass-based approach was taken. This is the most appropriate method for this fuel type albeit a more difficult measurement to make. A complex fuel, such as wildland fuels, demands a complex experimental method.

The significance of these findings is the need to better understand the heat transfer mechanisms the fuel bed is subject to. Most notably the absorption of radiation and the heat losses of the system. This is important as they have been shown to change with the fuel structure. Due to the large range of fuel structures of wildland fuels it should be an important goal of future work.

Part VI
Conclusion

6.1 Summary

Plants have existed for millions of years. The Pinus genus is one of the most globally distributed and so it represents a good laboratory fuel as it has a widespread application. The pinus genus is globally distributed because it is plastic in its morphology. This results in changes in the leaf shape at a species and a climatic level. As such natural fuels cannot be assumed to be uniform. Furthermore biological process, such as rot, will alter the composition of the fuel. This means that natural fuels are not static materials. They change in both shape and material composition depending on environmental conditions.

Natural fuels are made up of similar molecules leading to similar bonds. Bonds are broken with heat which in turn be represented by temperature. Therefore reaction temperatures are expected to be in similar ranges due to the similarity in bond energy. Natural fuels are composite materials and are not homogeneous. As such, along with the reaction temperature, the proportion of the mass involved in each fire process is of interest. This can be achieved by distilling the material using proximate analysis. However, char oxidation plays its part in a fire and as such oxidative analysis is required.

Ignition is a gas phase reaction. The initial state of the fuel determines the processes required for ignition. Solid fuels must be pyrolysed to produce gaseous fuel. This is a thermal degradation process that is underpinned by heat. As such it can be described by the solid temperature. Part II results suggested that the environment does not have a substantial effect on the proportion of mass available for pyrolysis. In the past heat transfer models have been used to describe the ignition process whereby ignition was approximated as the solid surface reaching of an ignition temperature. This is because the heat described by the temperature is the driving force behind the multiple processes leading to ignition. However in the case of porous fuels there is not a continuous surface leading to questions about the surface temperature approximation.

The fuel loads in wild land fuels lead to different fuel bed structures. It is assumed that there are changes in the system properties as the fuel load changes. Furthermore, the fuel load changes as a function of the fuel element. These changes in the system properties leads to changes in the flammability even though the same material is being considered and as such the material thermal degradation does not change. This leads to the ignition and the burning of the fuel bed to be affected by the morphology of the element. Optimisation can be used to force the models to fit however still the question remains as to how appropriate is it to assume that the system can be defined by its surface temperature when the surface is not continuous?

In order to interrogate the experiments a heat transfer model is used and is paired with a thermal degradation look up table experimentally derived in Part II. This allows for appreciation of the heated depth and region active in the ignition reaction as the fuel load is changed. At low fuel loads the heated depth and active region is large. This means that the region associated to ignition is not confined to the surface as is the case in solid fuels and answers the question as to whether the system can be defined by its surface temperature with a resounding no. Instead a mass based approach is more appropriate as was used here.

In summary, a methodology for the investigation of porous natural fuels has been laid out in this work. This is underpinned by an appreciation of the fuel, heat transfer and thermal degradation. It was found that the fuel beds transition from a high porosity regime to a low porosity regime as the fuel load increases. This strains the usual simplification of the ignition being defined by the surface reaching the ignition temperature. A more holistic approach should be taken in future whereby mass data is used. This requires the coupling of heat and chemistry models which is more complicated than the inert model favoured by fire safety engineering.

6.2 Conclusion

The overarching idea is that the ignition of wildland fuel problem is subject to many complications. There are many species of plants and as such there are a myriad of element geometries and material compositions. Furthermore, natural phenomena such as weathering and rot have their part to play along with the fact that the wildland is not homogenous but is made of mixture of different plant species. Hence, the knowledge of either of these does not amount to much in the grand scheme of things. It is too big a task to know each species at every point of senescence. Instead the complexity must be reduced and that is what is done here. The material composition is reduced to a composition based on generalised fire processes and the fuel beds encapsulated by their fuel bed structure as this defines their bulk properties.

This leads to the next complication. The fuel bed structure is a function of the elemental morphology and the fuel load. Therefore so are the bulk properties. In this work this was tackled by a systematic experimental campaign where the element morphology and the fuel load were changed in tandem, for a singular pinus species - pinus rigida. This was done by changing the element length and filling a known sample volume. This produced a series of different fuel bed structures that had the same thermal degradation chemistry. This meant that effect of the fuel structure on the bulk properties, that dictate the ignition processes, could be analysed without the interference of changes in thermal degradation chemistry. This was done by subjecting the fuel bed structures to the same heating condition. Changes in flammability were presented and it was found that both ignition and burning are affected by the fuel structure. The burning was seen to be improved by an increase in the permeability of the fuel bed. The ignition however showed a more complicated trend.

In order to analyse these changes in the ignition, the experiments were viewed through the lens of mathematical models. Classical ignition theory uses the reaching of a surface temperature to characterise the ignition of a material. However classical ignition theory was postulated for solid materials, where the top surface is the main region active in the ignition processes. On the other hand, wildland fuels are not solid, they are a collection of individual elements, they are porous. Hence, wildland fuels are subject to heat transfer in a different way due to their fuel structure. This amounts to the ignition processes not being restricted to the top surface but instead to a volume as energy is exchanged throughout the bed and as such the surface temperature criteria in wildland fuel is meaningless.

To work around this a method was proposed in this work where the mass is at the centre of the analysis. With this method the experimental mass loss for each fuel structure was modelled using effective bulk properties that were a function of the fuel structure. By optimising these functions to fit the model to the experimental data the effect of the fuel structure on the fuel bed bulk properties could be analysed. The changes in the flammability of the fuel beds must be due to changes in the energy of the system owing to the changes in the fuel bed structure. The most promising rationale is that the convective flow through a porous fuel has a large impact as convective cooling of fine elements by entrained air delays the ignition time. This finding is important for the design of future studies of the burning of wildland fuels as the fuel bed structure is generally not considered, or if it is, over a small range.

6.3 Future Work

Looking forwards, future work in the topic should be considered. Furthermore, investigation into how the element morphology affects the fuel bed it creates. This would involve the question: can element morphology predict the fuel structure in a given volume? Moreover, of interest would be extension of this work to include broad leaf species. The morphology of these species being distinct from pinus species. An extension of the work to consider open basket experiments would also be of interest although caution is needed in the application of the semi-infinite heat diffusion equation in these cases. Additionally, work is needed in mathematically defining ignition in terms of mass. It has been shown that the classical approach of surface temperature is not appropriate at the low fuel loads (high porosities) as, in these cases, a volume is active in the ignition processes. A potential solution to this would be to define the ignition using a combination of the integrated mass lost and the rate of mass loss. The TGA work showed there is also a need to characterise the char oxidation reaction better. This would involve conducting experiments at different heating rates with different flow rates of oxidiser. This is important as char oxidation is a process that provides energy to the fuel bed and as such provides a route to ignition. All in all there are many steps still left to take in understanding the heat transfer, pyrolysis and ignition of wildland fuels nevertheless this work presents a step forward in that endeavour.

References

[1] T. He, C. M. Belcher, B. B. Lamont, and S. L. Lim, "A 350-million-year legacy of fire adaptation among conifers," *Journal of Ecology*, vol. 104, no. 2, pp. 352–363, 2016. [Online]. Available: https://besjournals.onlinelibrary.wiley.com/doi/abs/10.1111/1365-2745.12513

[2] S. H. Doerr and C. Santín, "Global trends in wildfire and its impacts: perceptions versus realities in a changing world," *Philosophical Transactions of the Royal Society B: Biological Sciences*, vol. 371, no. 1696, p. 20150345, 2016. [Online]. Available: https://royalsocietypublishing.org/doi/abs/10.1098/rstb.2015.0345

[3] J. G. Pausas, J. Llovet, A. Rodrigo, and R. Vallejo, "Are wildfires a disaster in the Mediterranean basin? A review," *International Journal of Wildland Fire*, vol. 17, no. 6, pp. 713–723, 2008. [Online]. Available: https://doi.org/10.1071/WF07151

[4] M. R. Coughlan and A. M. Petty, "Linking humans and fire: a proposal for a transdisciplinary fire ecology," *International Journal of Wildland Fire*, vol. 21, no. 5, pp. 477–487, 2012. [Online]. Available: https://doi.org/10.1071/WF11048

[5] J. A. Cardille, S. J. Ventura, and M. G. Turner, "Environmental and social factors influencing wildfires in the upper midwest, united states," *Ecological Applications*, vol. 11, no. 1, pp. 111–127, 2001. [Online]. Available: https://esajournals.onlinelibrary.wiley.com/doi/abs/10.1890/1051-0761%%29011%5B0111%3AEASFIW%5D2.0.CO%3B2

[6] F. Tedim and V. Leone, "The dilemma of wildfire definition: What it reveals and what it implies," *Frontiers in Forests and Global Change*, vol. 3, 2020. [Online]. Available: https://www.frontiersin.org/articles/10.3389/ffgc.2020.553116

[7] J. M. Varner, T. M. Shearman, J. M. Kane, E. M. Banwell, E. S. Jules, and M. C. Stambaugh, "Understanding flammability and bark thickness in the genus Pinus using a phylogenetic approach," *Scientific Reports*, vol. 12, no. 1, p. 7384, 2022. [Online]. Available: https://doi.org/10.1038/s41598-022-11451-x

[8] M. A. Krawchuk, M. A. Moritz, M.-A. Parisien, J. Van Dorn, and K. Hayhoe, "Global pyrogeography: the current and future distribution of wildfire," *PLOS ONE*, vol. 4, no. 4, pp. 1–12, 04 2009. [Online]. Available: https://doi.org/10.1371/journal.pone.0005102

[9] C. Eriksen, "Europe's fiery future: Rethinking wildfire policy," *CSS Policy Perspectives*, vol. 8, no. 12, 10 2020. [Online]. Available: https://css.ethz.ch/content/dam/ethz/special-interest/gess/cis/center-for-securities-studies/pdfs/PP8-12_2020-EN.pdf

[10] S. Solomon, D. Qin, M. Manning, K. Averyt, and M. Marquis, *Climate change 2007-the physical science basis: Working group I contribution to the fourth assessment report of the IPCC*. Cambridge university press, 2007, vol. 4.

[11] E. National Academies of Sciences and Medicine, *Attribution of Extreme Weather Events in the Context of Climate Change*. Washington, DC: The National Academies Press, 2016. [Online]. Available: https://nap.nationalacademies.org/catalog/21852/attribution-of-extreme-weather-events-in-the-context-of-climate-change

[12] J. G. Pausas and J. E. Keeley, "Wildfires and global change," *Frontiers in Ecology and the Environment*, vol. 19, no. 7, pp. 387–395, 2021. [Online]. Available: https://esajournals.onlinelibrary.wiley.com/doi/abs/10.1002/fee.2359

[13] A. Simeoni, *Wildland Fires*. New York, NY: Springer New York, 2016, pp. 3283–3302. [Online]. Available: https://doi.org/10.1007/978-1-4939-2565-0_87

[14] W. J. de Groot, M. D. Flannigan, and A. S. Cantin, "Climate change impacts on future boreal fire regimes," *Forest Ecology and Management*, vol. 294, pp. 35–44, 2013, the Mega-fire reality. [Online]. Available: https://www.sciencedirect.com/science/article/pii/S0378112712005695

[15] C. Potera, "Climate change. challenges of predicting wildfire activity," *Environmental health perspectives*, vol. 117, no. 7, pp. A293–A293, 2009.

[16] D. M. Theobald and W. H. Romme, "Expansion of the us wildland–urban interface," *Landscape and Urban Planning*, vol. 83, no. 4, pp. 340–354, 2007. [Online]. Available: https://www.sciencedirect.com/science/article/pii/S0169204607001491

[17] X. J. Walker, B. M. Rogers, S. Veraverbeke, J. F. Johnstone, J. L. Baltzer, K. Barrett, L. Bourgeau-Chavez, N. J. Day, W. J. de Groot, C. M. Dieleman, S. Goetz, E. Hoy, L. K. Jenkins, E. S. Kane, M.-A. Parisien, S. Potter, E. A. G. Schuur, M. Turetsky, E. Whitman, and M. C. Mack, "Fuel availability not fire weather controls boreal wildfire severity and carbon emissions," *Nature Climate Change*, vol. 10, no. 12, pp. 1130–1136, 2020. [Online]. Available: https://doi.org/10.1038/s41558-020-00920-8

[18] G. H. Donovan and T. C. Brown, "Be careful what you wish for: the legacy of smokey bear," *Frontiers in Ecology and the Environment*, vol. 5, no. 2, pp. 73–79, 2007. [Online]. Available: https://esajournals.onlinelibrary.wiley.com/doi/abs/10.1890/1540-9295%282007%295%5B73%3ABCWYWF%5D2.0.CO%3B2

[19] S. L. Stephens, N. Burrows, A. Buyantuyev, R. W. Gray, R. E. Keane, R. Kubian, S. Liu, F. Seijo, L. Shu, K. G. Tolhurst, and J. W. van Wagtendonk, "Temperate and boreal forest mega-fires: characteristics and challenges," *Frontiers in Ecology and the Environment*, vol. 12, no. 2, pp. 115–122, 2014. [Online]. Available: https://esajournals.onlinelibrary.wiley.com/doi/abs/10.1890/120332

[20] M. A. Moritz, E. Batllori, R. A. Bradstock, A. M. Gill, J. Handmer, P. F. Hessburg, J. Leonard, S. McCaffrey, D. C. Odion, T. Schoennagel, and A. D. Syphard, "Learning to coexist with wildfire," *Nature*, vol. 515, no. 7525, pp. 58–66, 2014. [Online]. Available: https://doi.org/10.1038/nature13946

[21] J. K. Hiers, J. J. O'Brien, J. M. Varner, B. W. Butler, M. Dickinson, J. Furman, M. Gallagher, D. Godwin, S. L. Goodrick, S. M. Hood, A. Hudak, L. N. Kobziar, R. Linn, E. L. Loudermilk, S. McCaffrey, K. Robertson, E. M. Rowell, N. Skowronski, A. C. Watts, and K. M. Yedinak, "Prescribed fire science: the case for a refined research agenda," *Fire Ecology*, vol. 16, no. 1, p. 11, 2020. [Online]. Available: https://doi.org/10.1186/s42408-020-0070-8

[22] W. L. Fons, "Analysis of fire spread in light forest fuels," *Journal of Agricultural Research*, vol. 72, no. 3, pp. 93–121, 1946.

[23] H. Anderson and R. Rothermel, "Influence of moisture and wind upon the characteristics of free-burning fires," *Symposium (International) on Combustion*, vol. 10, no. 1, pp. 1009–1019, 1965, tenth Symposium (International) on Combustion. [Online]. Available: https://www.sciencedirect.com/science/article/pii/S0082078465802430

[24] T. Beer, "The interaction of wind and fire," *Boundary-Layer Meteorology*, vol. 54, no. 3, pp. 287–308, 1991. [Online]. Available: https://doi.org/10.1007/BF00183958

[25] J. L. Dupuy, "Slope and Fuel Load Effects on Fire Behavior: Laboratory Experiments in Pine Needles Fuel Beds," *International Journal of Wildland Fire*, vol. 5, no. 3, pp. 153–164, 1995. [Online]. Available: https://doi.org/10.1071/WF9950153

[26] J. M. C. Mendes-Lopes, J. M. P. Ventura, and J. M. P. Amaral, "Flame characteristics, temperature–time curves, and rate of spread in fires propagating in a bed of <emph type="2">Pinus pinaster</emph> needles," *International*

Journal of Wildland Fire, vol. 12, no. 1, pp. 67–84, 2003. [Online]. Available: https://doi.org/10.1071/WF02063

[27] A. Simeoni, *Experimental Understanding of Wildland Fires*. John Wiley Sons, Ltd, 2013, ch. 3, pp. 35–52. [Online]. Available: https://onlinelibrary.wiley.com/doi/abs/10.1002/9781118529539.ch3

[28] V. Tihay, F. Morandini, P.-A. Santoni, Y. Perez-Ramirez, and T. Barboni, "Combustion of forest litters under slope conditions: Burning rate, heat release rate, convective and radiant fractions for different loads," *Combustion and Flame*, vol. 161, no. 12, pp. 3237–3248, 2014. [Online]. Available: https://www.sciencedirect.com/science/article/pii/S0010218014001801

[29] S. McAllister and M. Finney, "Burning Rates of Wood Cribs with Implications for Wildland Fires," *Fire Technology*, vol. 52, no. 6, pp. 1755–1777, 2016.

[30] F. R. Scarff and M. Westoby, "Leaf litter flammability in some semi-arid Australian woodlands," *Functional Ecology*, vol. 20, no. 5, pp. 745–752, 2006.

[31] D. Schwilk, "Commentary Dimensions of plant flammability," *New Phytologist*, vol. 206, no. 2, pp. 486–8, 2015.

[32] N. Dong, I. C. Prentice, I. J. Wright, B. J. Evans, H. F. Togashi, S. Caddy-Retalic, F. A. McInerney, B. Sparrow, E. Leitch, and A. J. Lowe, "Components of leaf-trait variation along environmental gradients," *New Phytologist*, vol. 228, no. 1, pp. 82–94, 2020. [Online]. Available: https://nph.onlinelibrary.wiley.com/doi/abs/10.1111/nph.16558

[33] R. C. Rothermel, "A mathematical model for predicting fire spread in wildland fuels," *USDA Forest Service Research Paper INT USA*, no. INT-115, p. 40, 1972. [Online]. Available: http://www.srs.fs.usda.gov/pubs/32533

[34] D. P. Incropera, Frank P.; DeWitt, *Fundamentals of heat and mass transfer*, fifth edition. ed. New York ;: Wiley, 2002.

[35] M. J. Hurley, D. T. Gottuk, J. R. Hall Jr., K. Harada, E. D. Kuligowski, M. Puchovsky, J. L. Torero, J. M. Watts Jr., and C. J. WIECZOREK, *SFPE Handbook of Fire Protection Engineering*. New York, NY: Springer New York, 2015.

[36] R. Haberman, *Applied Partial Differential Equations with Fourier Series and Boundary Value Problems*. Harlow: Pearson Education UK, 2013.

[37] "Appendix 5 - transforms of some functions," in *Analytical Heat Diffusion Theory*, J. P. Hartnett and A. LUIKOV, Eds. Academic Press, 1968, pp. 662–668. [Online]. Available: https://www.sciencedirect.com/science/article/pii/B9780124597563500249

[38] W. J. Bond and J. E. Keeley, "Fire as a global 'herbivore': the ecology and evolution of flammable ecosystems," *Trends in Ecology Evolution*, vol. 20, no. 7, pp. 387–394, 2005. [Online]. Available: https://www.sciencedirect.com/science/article/pii/S0169534705001321

[39] D. X. Viegas, A. Rodrigues, A. Abouali, M. Almeida, and J. Raposo, "Fire downwind a flat surface entering a canyon by lateral spread," *Fire Safety Journal*, vol. 122, p. 103349, 2021. [Online]. Available: https://www.sciencedirect.com/science/article/pii/S0379711221000904

[40] H. A. Kramer, B. M. Collins, M. Kelly, and S. L. Stephens, "Quantifying ladder fuels: A new approach using lidar," *Forests*, vol. 5, no. 6, pp. 1432–1453, 2014. [Online]. Available: https://www.mdpi.com/1999-4907/5/6/1432

[41] E. Koo, P. J. Pagni, D. R. Weise, and J. P. Woycheese, "Firebrands and spotting ignition in large-scale fires," *International Journal of Wildland Fire*, vol. 19, no. 7, pp. 818–843, 2010. [Online]. Available: https://doi.org/10.1071/WF07119

[42] J. S. Gould, W. Lachlan McCaw, and N. Phillip Cheney, "Quantifying fine fuel dynamics and structure in dry eucalypt forest (eucalyptus marginata) in western australia for fire management," *Forest Ecology and Management*, vol. 262, no. 3, pp. 531–546, 2011. [Online]. Available: https://www.sciencedirect.com/science/article/pii/S0378112711002374

[43] J. O. Sexton, X.-P. Song, M. Feng, P. Noojipady, A. Anand, C. Huang, D.-H. Kim, K. M. Collins, S. Channan, C. DiMiceli, and J. R. Townshend, "Global, 30-m resolution continuous fields of tree cover: Landsat-based rescaling of modis vegetation continuous fields with lidar-based estimates of error," *International Journal of Digital Earth*, vol. 6, no. 5, pp. 427–448, 2013. [Online]. Available: https://doi.org/10.1080/17538947.2013.786146

[44] J. E. Keeley, "Ecology and evolution of pine life histories," *Annals of forest science.*, vol. 69, no. 4, pp. 445–453, 2012.

[45] W. B. Critchfield and E. L. E. L. Little, *Geographic distribution of the pines of the world.* Washington, D.C. :U.S. Dept. of Agriculture, Forest Service,, vol. no.991, https://www.biodiversitylibrary.org/bibliography/66393. [Online]. Available: https://www.biodiversitylibrary.org/item/133439

[46] G. Caudullo, E. Welk, and J. San-Miguel-Ayanz, "Chorological maps for the main european woody species," *Data in Brief*, vol. 12, pp. 662–666, 2017. [Online]. Available: https://www.sciencedirect.com/science/article/pii/S2352340917301981

[47] U. G. Survey, "Digital representation of "atlas of united states trees" by elbert l. little, jr." 1999. [Online]. Available: http://gec.cr.usgs.gov/data/little

[48] M. P. Nobis, C. Traiser, and A. Roth-Nebelsick, "Latitudinal variation in morphological traits of the genus pinus and its relation to environmental and phylogenetic signals," *Plant Ecology & Diversity*, vol. 5, no. 1, pp. 1–11, 2012. [Online]. Available: https://doi.org/10.1080/17550874.2012.687501

[49] M. Dobbertin, B. Eilmann, P. Bleuler, A. Giuggiola, E. Graf Pannatier, W. Landolt, P. Schleppi, and A. Rigling, "Effect of irrigation on needle morphology, shoot and stem growth in a drought-exposed Pinus sylvestris forest," *Tree Physiology*, vol. 30, no. 3, pp. 346–360, 01 2010. [Online]. Available: https://doi.org/10.1093/treephys/tpp123

[50] R. López, J. Climent, and L. Gil, "From desert to cloud forest: the non-trivial phenotypic variation of canary island pine needles," *Trees (Berlin, West)*, vol. 22, no. 6, pp. 843–849, 2008.

[51] R. E. Keane and L. J. Dickinson, "The photoload sampling technique: Estimating surface fuel loadings from downward-looking photographs of synthetic fuelbeds," *USDA Forest Service - General Technical Report RMRS-GTR*, no. 190 RMRS-GTR, pp. 1–46, 2007.

[52] N. Fernandez-Anez, J. Garcia-Torrent, and L. Medic-Pejic, "Flammability properties of thermally dried sewage sludge," *Fuel*, vol. 134, pp. 636–643, 2014. [Online]. Available: https://www.sciencedirect.com/science/article/pii/S0016236114005638

[53] H. Li, O. Mašek, A. Harper, and R. Ocone, "Kinetic study of pyrolysis of high-density polyethylene (hdpe) waste at different bed thickness in a fixed bed reactor," *The Canadian Journal of Chemical Engineering*, vol. 99, no. 8, pp. 1733–1744, 2021. [Online]. Available: https://onlinelibrary.wiley.com/doi/abs/10.1002/cjce.24123

[54] F. Richter and G. Rein, "The role of heat transfer limitations in polymer pyrolysis at the microscale," *Frontiers in Mechanical Engineering*, vol. 4, p. 18, 2018. [Online]. Available: https://www.frontiersin.org/article/10.3389/fmech.2018.00018

[55] ——, "A multiscale model of wood pyrolysis in fire to study the roles of chemistry and heat transfer at the mesoscale," *Combustion and flame*, vol. 216, pp. 316–325, 2020.

[56] "Hess's law." [Online]. Available: https://www.oxfordreference.com/view/10.1093/oi/authority.20110803095933869

[57] S. J. Blanksby and G. B. Ellison, "Bond dissociation energies of organic molecules," *Accounts of Chemical Research*, vol. 36, no. 4, pp. 255–263, 2003, pMID: 12693923. [Online]. Available: https://doi.org/10.1021/ar020230d

[58] D. Drysdale, *An Introduction to Fire Dynamics*. Chichester, UK: John Wiley & Sons, Ltd, aug 2011, vol. 10, no. 2. [Online]. Available: http://linkinghub.elsevier.com/retrieve/pii/0379711286900469 http://doi.wiley.com/10.1002/9781119975465

[59] S. Bakshi, C. Banik, and D. A. Laird, "Estimating the organic oxygen content of biochar," *Scientific reports*, vol. 10, no. 1, pp. 1–12, 2020.

[60] V. Leroy, D. Cancellieri, and E. Leoni, "Relation between forest fuels composition and energy emitted during their thermal degradation," *Journal of thermal analysis and calorimetry*, vol. 96, no. 1, pp. 293–300, 2009.

[61] M.-S. Safdari, M. Rahmati, E. Amini, J. E. Howarth, J. P. Berryhill, M. Dietenberger, D. R. Weise, and T. H. Fletcher, "Characterization of pyrolysis products from fast pyrolysis of live and dead vegetation native to the southern united states," *Fuel*, vol. 229, pp. 151–166, 2018. [Online]. Available: https://www.sciencedirect.com/science/article/pii/S0016236118308214

[62] A. Simeoni, "On the Role of Bulk Properties and Fuel Species on the Burning Dynamics of Pine Forest Litters," *Fire Safety Science*, vol. 10, no. 3, pp. 459–470, 2011. [Online]. Available: https://iafss.org/publications/fss/10/1401

[63] C. Huggett, "Estimation of rate of heat release by means of oxygen consumption measurements," *Fire and materials*, vol. 4, no. 2, pp. 61–65, 1980.

[64] P. Bartoli, "Thèse présentée pour l ' obtention du grade de DOCTEUR EN BIOLOGIE MARINE Mention : Biologie des populations et écologie Soutenue publiquement par," vol. 6134, 2012.

[65] F. J. Matt, M. A. Dietenberger, and D. R. Weise, "Summative and ultimate analysis of live leaves from southern u.s. forest plants for use in fire modeling," *Energy & Fuels*, vol. 34, no. 4, pp. 4703–4720, 2020. [Online]. Available: https://doi.org/10.1021/acs.energyfuels.9b04107

[66] I. Vermesi, M. J. DiDomizio, F. Richter, E. J. Weckman, and G. Rein, "Pyrolysis and spontaneous ignition of wood under transient irradiation: Experiments and a-priori predictions," *Fire Safety Journal*, vol. 91, pp. 218–225, 2017, fire Safety Science: Proceedings of the 12th International Symposium. [Online]. Available: https://www.sciencedirect.com/science/article/pii/S0379711217301662

[67] X. Huang and G. Rein, "Smouldering combustion of peat in wildfires: Inverse modelling of the drying and the thermal and oxidative decomposition kinetics," *Combustion and Flame*, vol. 161, no. 6, pp. 1633–1644, 2014. [Online]. Available: http://dx.doi.org/10.1016/j.combustflame.2013.12.013

[68] Y. Nishiyama, P. Langan, and H. Chanzy, "Crystal structure and hydrogen-bonding system in cellulose i from synchrotron x-ray and neutron fiber diffraction," *Journal of the American Chemical Society*, vol. 124, no. 31, pp. 9074–9082, 2002.

[69] H. H. Nimz, U. Schmitt, E. Schwab, O. Wittmann, and F. Wolf, *Wood*. American Cancer Society, 2000. [Online]. Available: https://onlinelibrary.wiley.com/doi/abs/10.1002/14356007.a28_305

[70] A. N. Glazer, *Microbial biotechnology : fundamentals of applied microbiology / Alexander N. Glazer, Hiroshi Nikaido.*, second edition. ed. Cambridge: Cambridge University Press, 2007.

[71] G. Dorez, L. Ferry, R. Sonnier, A. Taguet, and J.-M. Lopez-Cuesta, "Effect of cellulose, hemicellulose and lignin contents on pyrolysis and combustion of natural fibers," *Journal of Analytical and Applied Pyrolysis*, vol. 107, pp. 323–331, 2014. [Online]. Available: https://www.sciencedirect.com/science/article/pii/S0165237014000771

[72] G. Alfredsen, T. K. Bader, J. Dibdiakova, T. Filbakk, S. Bollmus, and K. Hofstetter, "Thermogravimetric analysis for wood decay characterisation," *European Journal of Wood and Wood Products*, vol. 70, no. 4, pp. 527–530, 2012.

[73] R. A. Susott, "Characterization of the thermal properties of forest fuels by combustible gas analysis," *Forest Science*, vol. 28, no. 2, pp. 404–420, 1982. [Online]. Available: http://www.ingentaconnect.com/content/saf/fs/1982/00000028/00000002/art00029

[74] P. T. Williams and S. Besler, "The influence of temperature and heating rate on the slow pyrolysis of biomass," *Renewable Energy*, vol. 7, no. 3, pp. 233–250, 1996. [Online]. Available: https://www.sciencedirect.com/science/article/pii/0960148196000067

[75] I. Milosavljevic and E. M. Suuberg, "Cellulose thermal decomposition kinetics: Global mass loss kinetics," *Industrial engineering chemistry research*, vol. 34, no. 4, pp. 1081–1091, 1995.

[76] H. Yang, "Characteristics of hemicellulose , cellulose and lignin pyrolysis," vol. 86, pp. 1781–1788, 2007.

[77] J. Shen, S. Zhu, X. Liu, H. Zhang, and J. Tan, "The prediction of elemental composition of biomass based on proximate analysis," *Energy Conversion and Management*, vol. 51, no. 5, pp. 983–987, 2010. [Online]. Available: http://dx.doi.org/10.1016/j.enconman.2009.11.039

[78] M. G. Grønli, G. Várhegyi, and C. Di Blasi, "Thermogravimetric analysis and devolatilization kinetics of wood," *Industrial engineering chemistry research*, vol. 41, no. 17, pp. 4201–4208, 2002.

[79] V. Tihay, A. Simeoni, P. A. Santoni, L. Rossi, J. P. Garo, and J. P. Vantelon, "Experimental study of laminar flames obtained by the homogenization of three forest fuels," *International Journal of Thermal Sciences*, vol. 48, no. 3, pp. 488–501, 2009. [Online]. Available: http://dx.doi.org/10.1016/j.ijthermalsci.2008.03.018

[80] P. Bartoli, A. Simeoni, H. Biteau, J. L. Torero, and P. A. Santoni, "Determination of the main parameters influencing forest fuel combustion dynamics," *Fire Safety Journal*, vol. 46, no. 1-2, pp. 27–33, 2011. [Online]. Available: http://dx.doi.org/10.1016/j.firesaf.2010.05.002

[81] G.-w. Wang, J.-l. Zhang, J.-g. Shao, H. Sun, and H.-b. Zuo, "Thermogravimetric analysis of coal char combustion kinetics," *Journal of Iron and Steel Research International*, vol. 21, no. 10, pp. 897–904, 2014.

[82] O. Mašek, W. Buss, A. Roy-Poirier, W. Lowe, C. Peters, P. Brownsort, D. Mignard, C. Pritchard, and S. Sohi, "Consistency of biochar properties over time and production scales: A characterisation of standard materials," *Journal of Analytical and Applied Pyrolysis*, vol. 132, pp. 200–210, 2018. [Online]. Available: https://www.sciencedirect.com/science/article/pii/S0165237017311178

[83] W. Han, Y. Chen, F.-J. Zhao, L. Tang, R. Jiang, and F. Zhang, "Floral, climatic and soil ph controls on leaf ash content in china's terrestrial plants," *Global Ecology and Biogeography*, vol. 21, no. 3, pp. 376–382, 2012. [Online]. Available: https://onlinelibrary.wiley.com/doi/abs/10.1111/j.1466-8238.2011.00677.x

[84] "Climate data (based on ecmwf data)." [Online]. Available: https://climate-data.org/

[85] F. X. Jervis and G. Rein, "Experimental study on the burning behaviour of Pinus halepensis needles using small-scale fire calorimetry of live, aged and dead samples," *Fire and Materials*, vol. 40, no. 3, pp. 385–395, apr 2016. [Online]. Available: http://doi.wiley.com/10.1002/fam.2293

[86] C.-Y. Yin, "Prediction of higher heating values of biomass from proximate and ultimate analyses," *Fuel*, vol. 90, no. 3, pp. 1128–1132, 2011.

[87] J. Parikh, S. A. Channiwala, and G. K. Ghosal, "A correlation for calculating HHV from proximate analysis of solid fuels," *Fuel*, vol. 84, no. 5, pp. 487–494, 2005.

[88] *SFPE handbook of fire protection engineering.*, Second edition / editorial staff: Philip j. dinenno [and six others] ed. Quincy, Massachusetts: National Fire Protection Association, 1995 - 1995.

[89] M. G. Zabetakis, "Flammability characteristics of combustible gases and vapors," Bureau of Mines Washington DC, Tech. Rep., 1965.

[90] C. F. Schemel, A. Simeoni, H. Biteau, J. D. Rivera, and J. L. Torero, "A calorimetric study of wildland fuels," *Experimental Thermal and Fluid Science*, vol. 32, no. 7, pp. 1381–1389, 2008.

[91] C. Schemel, "Transport Effects on Calorimetry of Porous Wildland Fuels," Ph.D. dissertation, 2008. [Online]. Available: http://hdl.handle.net/1842/2572

[92] P. Bartoli, A. Simeoni, P. Reszka, J. Torero, and P. Santoni, "A study on forest fuel combustion dynamics using the fire propagation apparatus," in *Proceedings of European Combustion Symposium, Vienna*, 2009, pp. 14–17.

[93] F. Jervis, G. Rein, A. Simeoni, and J. Torero, "The role of moisture in the burning of live and dead pine needles," in *Proceedings of the 6th International Seminar on Fire and Explosion Hazards, Leeds*, 2010.

[94] J. L. Torero and A. Simeoni, "Heat and Mass Transfer in Fires: Scaling Laws, Ignition of Solid Fuels and Application to Forest Fires," *The Open Thermodynamics Journal*, vol. 4, no. 1, pp. 145–155, 2010. [Online]. Available: http://benthamopen.com/ABSTRACT/TOTHERJ-4-145

[95] P. Bartoli, "Feux de forêt : amélioration de la connaissance du couplage combustible-flamme," Ph.D. dissertation, University de Corse-Pascal Paoli; University of Edinburgh, 2011.

[96] P. Mindykowski, A. Fuentes, J. L. Consalvi, and B. Porterie, "Piloted ignition of wildland fuels," *Fire Safety Journal*, vol. 46, no. 1-2, pp. 34–40, 2011. [Online]. Available: http://dx.doi.org/10.1016/j.firesaf.2010.09.003

[97] J. Consalvi, F. Nmira, A. Fuentes, P. Mindykowski, and B. Porterie, "Numerical study of piloted ignition of forest fuel layer," *Proceedings of the Combustion Institute*, vol. 33, no. 2, pp. 2641–2648, 2011.

[98] J. Thomas, A. Simeoni, F. Colella, and J. Torero, "Piloted ignition regimes of wildland fuel beds," in *EGU General Assembly Conference Abstracts*, 2012, p. 12813.

[99] F. X. J. Calle, "Application of fire calorimetry to understand factors affecting flammability of cellulosic material: Pine needles, tree leaves and chipboard," 2012. [Online]. Available: https://www.era.lib.ed.ac.uk/handle/1842/6406

[100] A. Simeoni, J. C. Thomas, P. Bartoli, P. Borowieck, P. Reszka, F. Colella, P. A. Santoni, and J. L. Torero, "Flammability studies for wildland and wildland-urban interface fires applied to pine needles and solid polymers," *Fire Safety Journal*, vol. 54, pp. 203–217, 2012. [Online]. Available: http://dx.doi.org/10.1016/j.firesaf.2012.08.005

[101] A. Fuentes and J. L. Consalvi, "Experimental study of the burning rate of small-scale forest fuel layers," *International Journal of Thermal Sciences*, vol. 74, no. C, pp. 119–125, 2013. [Online]. Available: http://dx.doi.org/10.1016/j.ijthermalsci.2013.06.002

[102] J. Thomas, J. Everett, A. Simeoni, N. Skowronski, and J. Torero, "Flammability study of pine needle beds," in *Proceedings of the 7th International Seminar on Fire and Explosion Hazards*, 2013.

[103] J. Thomas, A. Simeoni, M. Gallagher, and N. Skowronski, "An experimental study evaluating the burning dynamics of pitch pine needle beds using the fpa," *Fire Safety Science*, vol. 11, pp. 1406–1419, 2014.

[104] A. Lamorlette and F. Candelier, "Thermal behavior of solid particles at ignition: Theoretical limit between thermally thick and thin solids," *International Journal of Heat and Mass Transfer*, vol. 82, pp. 117–122, 2015. [Online]. Available: http://dx.doi.org/10.1016/j.ijheatmasstransfer.2014.11.037

[105] M. El Houssami, J. C. Thomas, A. Lamorlette, D. Morvan, M. Chaos, R. Hadden, and A. Simeoni, "Experimental and numerical studies characterizing the burning dynamics of wildland fuels," *Combustion and Flame*, vol. 168, pp. 113–126, 2016.

[106] M. El Houssami, "Development of a numerical and experimental framework to understand and predict the burning dynamics of porous fuel beds," Ph.D. dissertation, 02 2017.

[107] J. Thomas, "Improving the understanding of fundamental mechanisms that influence ignition and burning behavior of porous wildland fuel beds," Ph.D. dissertation, 07 2017.

[108] J. C. Thomas, R. M. Hadden, and A. Simeoni, "Experimental investigation of the impact of oxygen flux on the burning dynamics of forest fuel beds," *Fire Safety Journal*, vol. 91, no. February, pp. 855–863, 2017. [Online]. Available: http://dx.doi.org/10.1016/j.firesaf.2017.03.086

[109] M. El Houssami, A. Lamorlette, D. Morvan, R. M. Hadden, and A. Simeoni, "Framework for submodel improvement in wildfire modeling," *Combustion and Flame*, vol. 190, pp. 12–24, 2018. [Online]. Available: http://linkinghub.elsevier.com/retrieve/pii/S0010218017303760

[110] A. Lamorlette, M. El Houssami, and D. Morvan, "An improved non-equilibrium model for the ignition of living fuel," *International journal of wildland fire*, vol. 27, no. 1, pp. 29–41, 2018.

[111] C. Walker-Ravena, Z. Campbell-Lochrie, and R. M. Hadden, "The influence of structure on the flammability of wildland fuels under radiative heating," in *6th Fire Behavior and Fuels Conference*, 2019.

[112] D. Garg and F. Steward, "Pilot ignition of cellulosic materials containing high void spaces," *Combustion and Flame*, vol. 17, no. 3, pp. 287–294, 1971.

[113] ASTM International, "ASTM E2058-13a Standard Test Methods for Measurement of Material Flammability Using a Fire Propagation Apparatus (FPA)," vol. i, pp. 1–30, 2013. [Online]. Available: www.astm.org

[114] X. Silvani and F. Morandini, "Fire spread experiments in the field: Temperature and heat fluxes measurements," *Fire Safety Journal*, vol. 44, no. 2, pp. 279–285, 2009.

[115] D. Simms, "On the pilot ignition of wood by radiation," *Combustion and Flame*, vol. 7, pp. 253–261, 1963. [Online]. Available: https://www.sciencedirect.com/science/article/pii/0010218063901901

[116] J. P. Hidalgo, P. Pironi, R. M. Hadden, and S. Welch, "A framework for evaluating the thermal behaviour of carbon fibre composite materials," in *2nd IAFSS European Symposium of Fire Safety Science*, 2015, pp. 195–200.

[117] M. Chaos, M. M. Khan, N. Krishnamoorthy, J. L. De Ris, and S. B. Dorofeev, "Evaluation of optimization schemes and determination of solid fuel properties for CFD fire models using bench-scale pyrolysis tests," *Proceedings of the Combustion Institute*, vol. 33, no. 2, pp. 2599–2606, 2011. [Online]. Available: http://dx.doi.org/10.1016/j.proci.2010.07.018

[118] G. Rein, C. Lautenberger, A. C. Fernandez-Pello, J. L. Torero, and D. L. Urban, "Application of genetic algorithms and thermogravimetry to determine the kinetics of polyurethane foam in smoldering combustion," *Combustion and Flame*, vol. 146, no. 1, pp. 95–108, 2006. [Online]. Available: https://www.sciencedirect.com/science/article/pii/S001021800600112X

[119] C. Lautenberger, G. Rein, and C. Fernandez-Pello, "The application of a genetic algorithm to estimate material properties for fire modeling from bench-scale fire test data," *Fire Safety Journal*, vol. 41, no. 3, pp. 204–214, 2006.

[120] E. V. Mueller, N. Skowronski, J. C. Thomas, K. Clark, M. R. Gallagher, R. Hadden, W. Mell, and A. Simeoni, "Local measurements of wildland fire dynamics in a field-scale experiment," *Combustion and Flame*, vol. 194, pp. 452–463, 2018. [Online]. Available: https://www.sciencedirect.com/science/article/pii/S0010218018302281

Part VII
Appendix

A Thermal Degradation - Proximate Analysis

A.1 Temperature Profiles

A.1.1 Pinus

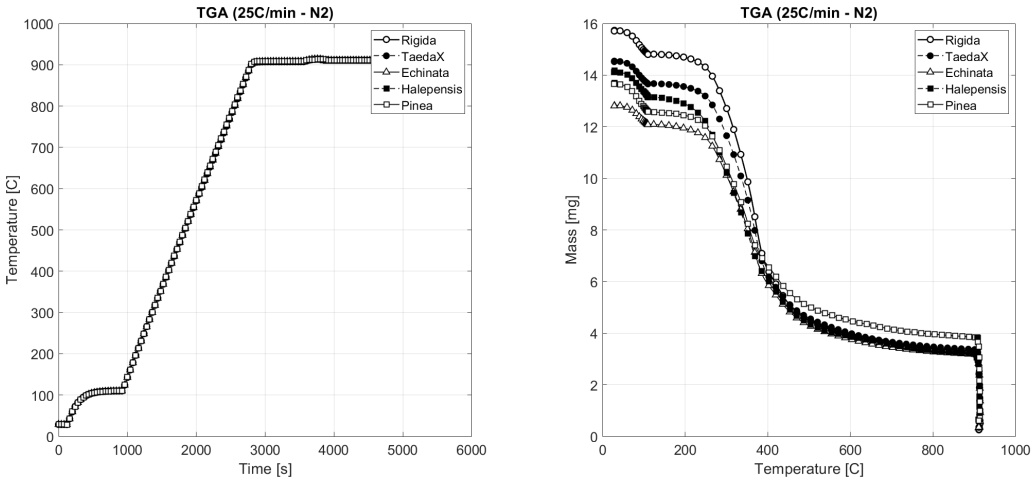

Figure 75: Proximate analysis for pinus samples a) Temperature profiles b) Mass

A.1.2 Broad Leaves

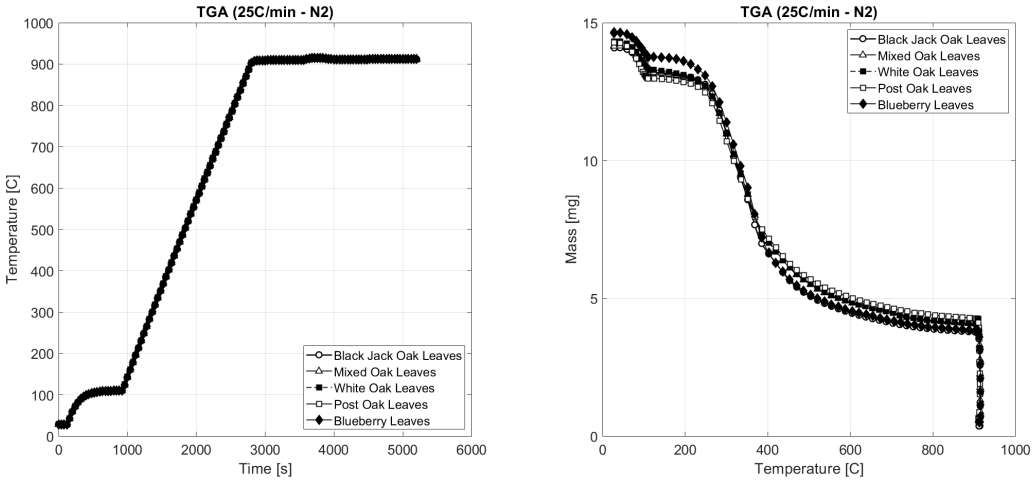

Figure 76: Proximate analysis for broad leaf samples a) Temperature profiles b) Mass

A.1.3 Stems

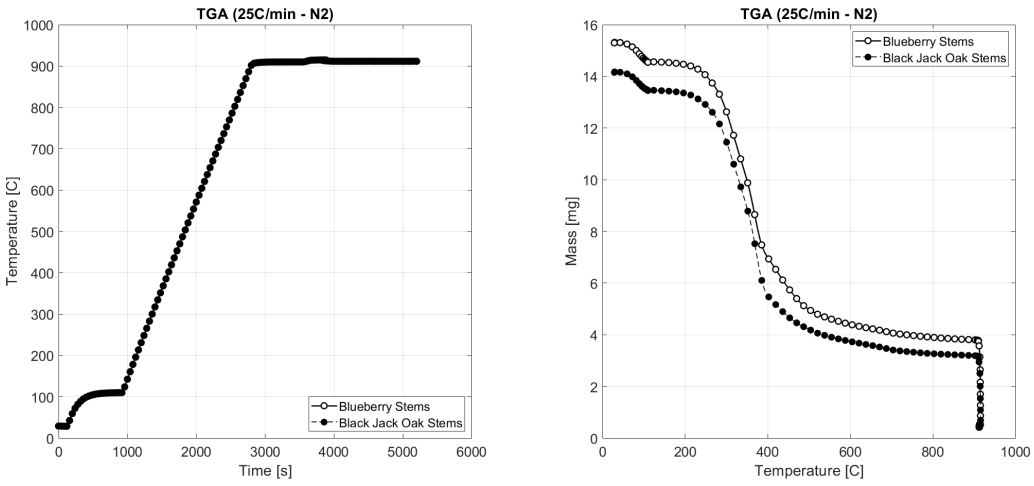

Figure 77: Proximate analysis for stem samples a) Temperature profiles b) Mass

A.2 Reaction Temperature

A.2.1 Pinus

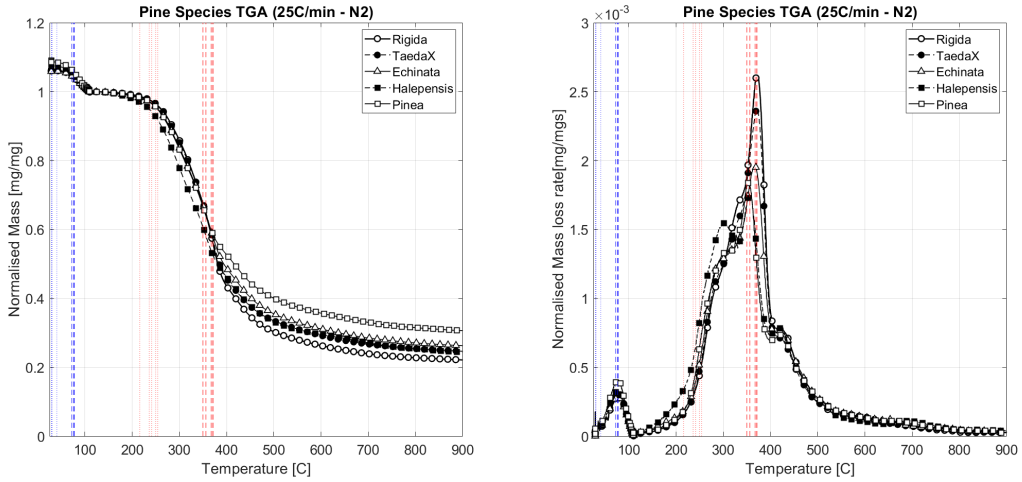

Figure 78: Reaction temperatures from proximate analysis of pinus samples. Dotted lines indicate onset and dashed lines maximum. a) Normalised Mass b) Normalised Mass Loss Rate.

A.2.2 Broad Leaves

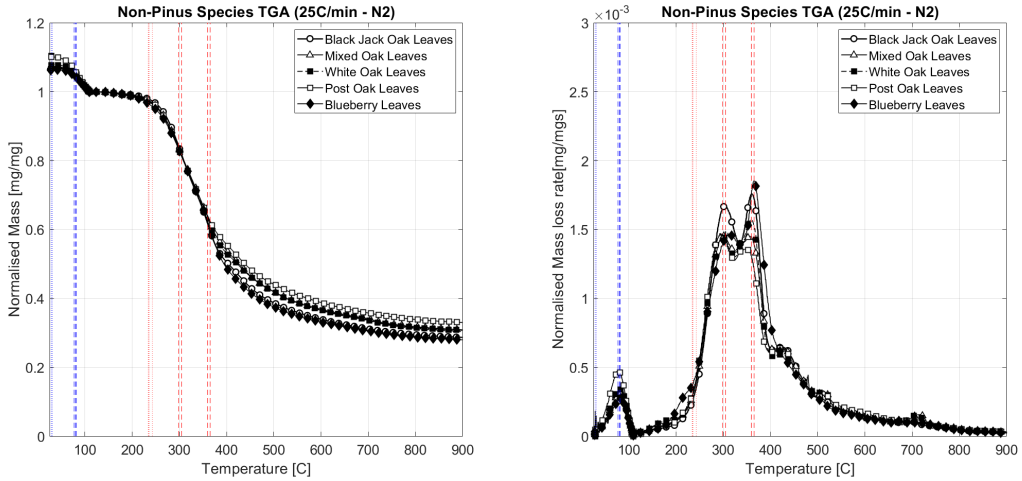

Figure 79: Reaction temperatures from proximate analysis of broad leaf samples. Dotted lines indicate onset and dashed lines maximum. a) Normalised Mass b) Normalised Mass Loss Rate.

A.2.3 Stems

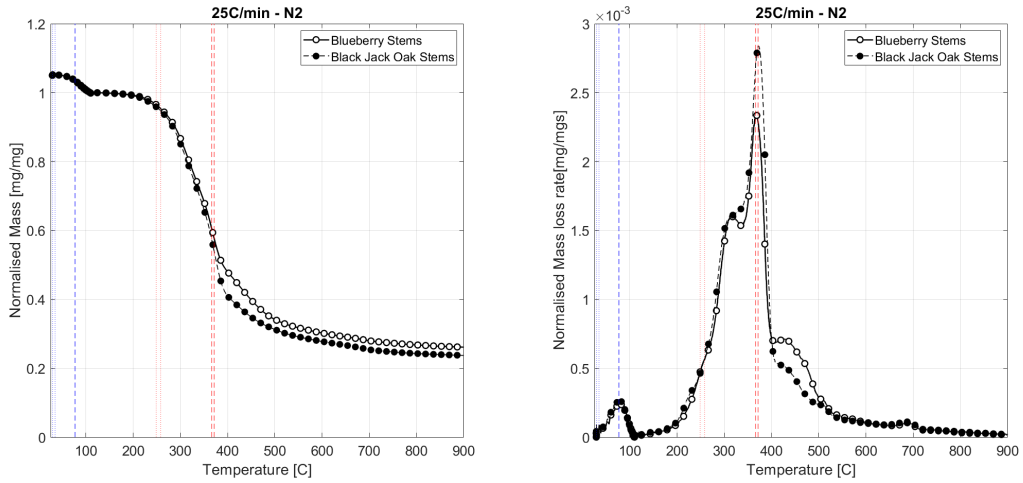

Figure 80: Reaction temperatures from proximate analysis of stem samples. Dotted lines indicate onset and dashed lines maximum. a) Normalised Mass b) Normalised Mass Loss Rate.

A.3 Intra-Specimen Comparison

Here select specimens have been re-plotted to facilitate intra-species graphical comparison.

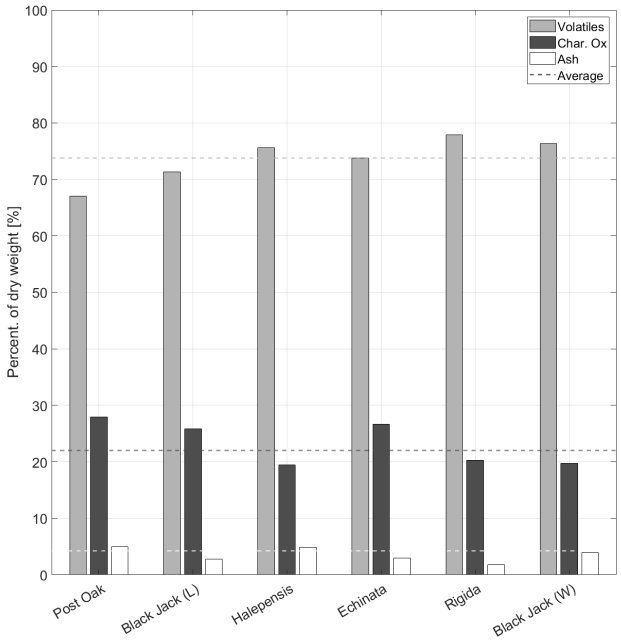

Figure 81: Volatile Matter, Fixed Carbon and Ash Fractions from Proximate Analysis for selected samples.

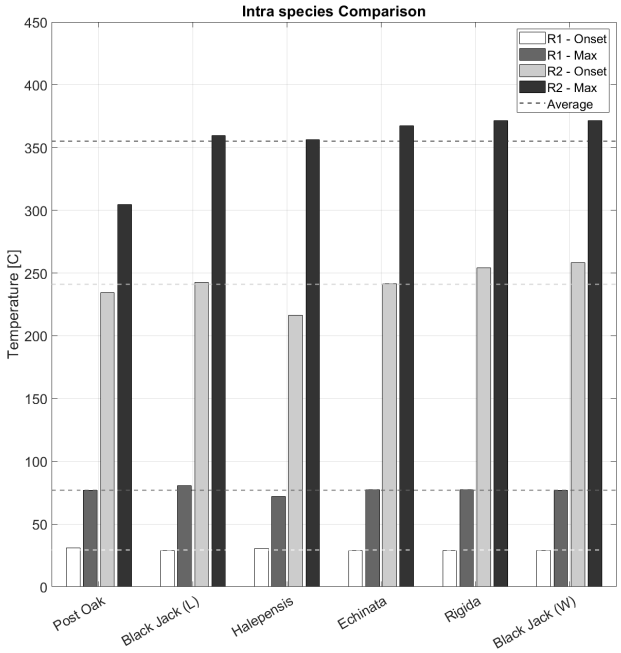

Figure 82: Reaction temperatures from Proximate Analysis for selected samples.

A.3.1 Temperature Profile

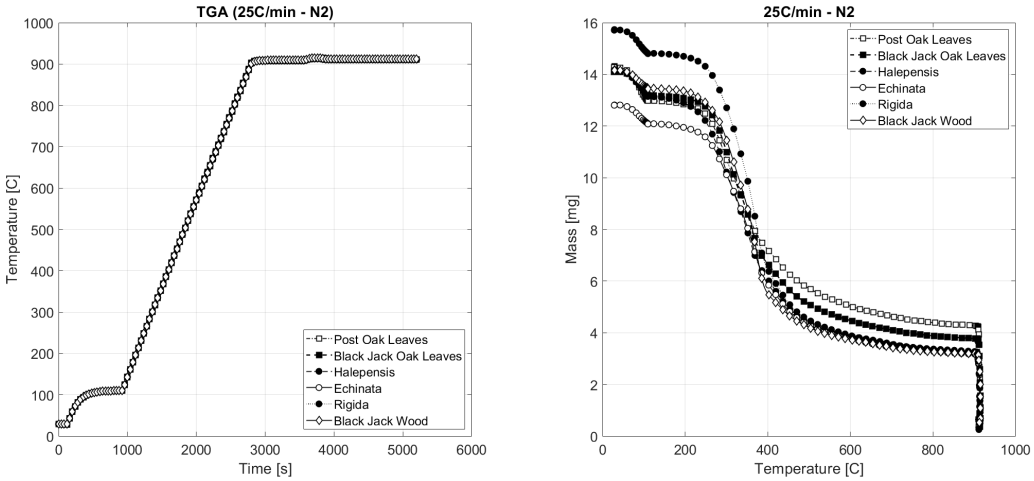

Figure 83: Proximate analysis for selected samples a) Temperature profiles b) Mass

A.3.2 Reaction Temperature

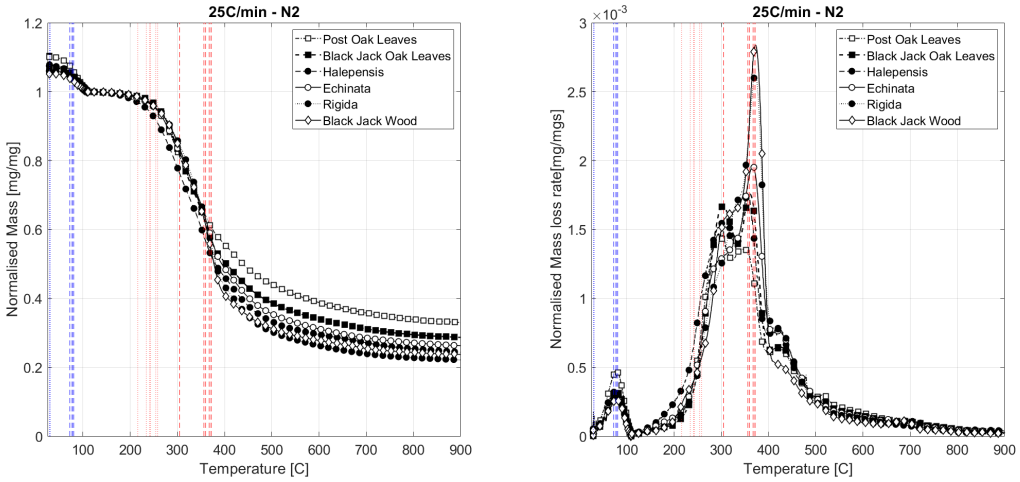

Figure 84: Reaction temperatures from proximate analysis of selected samples. Dotted lines indicate onset and dashed lines maximum. a) Normalised Mass b) Normalised Mass Loss Rate.

B Thermal Degradation - Controlled Combustion

B.1 Change in environment

B.1.1 25°C/min

B.1.1.1 Reaction Temperatures

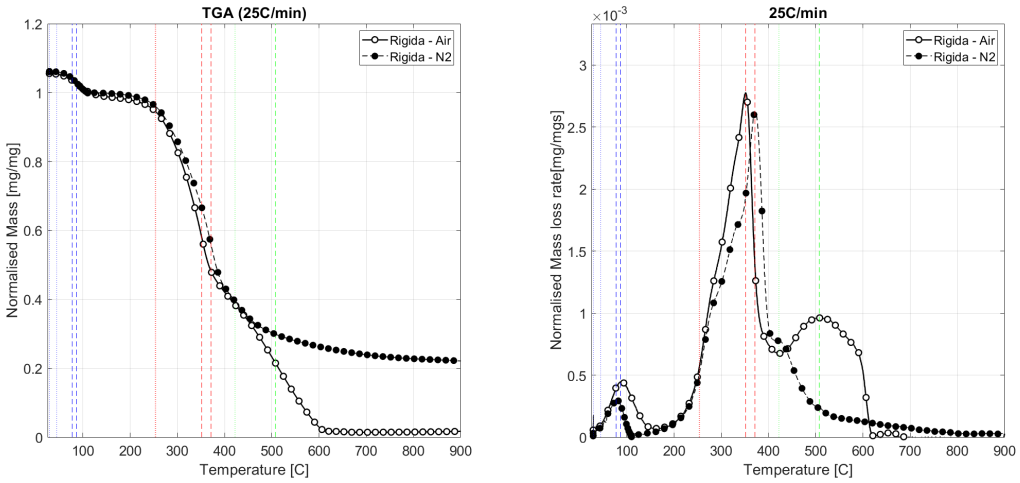

Figure 85: Reaction temperatures from controlled combustion of pinus rigida at 25°C/min. Dotted lines indicate onset and dashed lines maximum. a) Normalised Mass b) Normalised Mass Loss Rate.

B.1.2 15°C/min

B.1.2.1 Reaction Temperatures

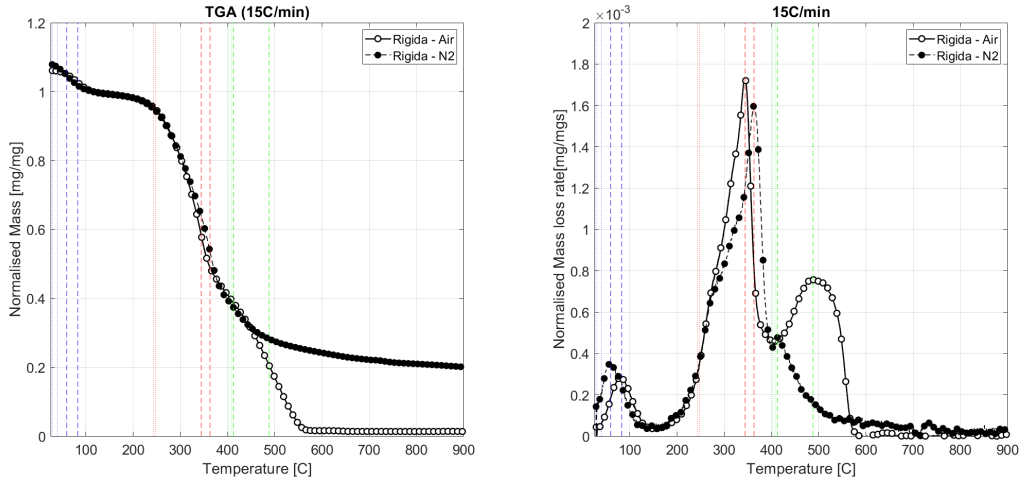

Figure 86: Reaction temperatures from controlled combustion of pinus rigida at 15°C/min. Dotted lines indicate onset and dashed lines maximum. a) Normalised Mass b) Normalised Mass Loss Rate.

B.1.2.2 Bar Chart

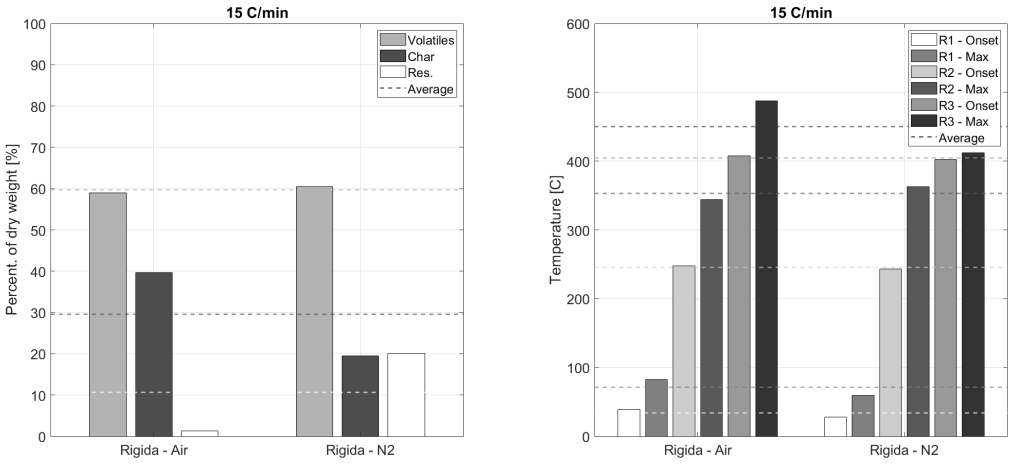

Figure 87: Controlled combustion results for pinus rigida at 15°C/min. Left: Percentage mass. Right: Reaction temperature.

B.1.3 100°C/min

B.1.3.1 Reaction Temperatures

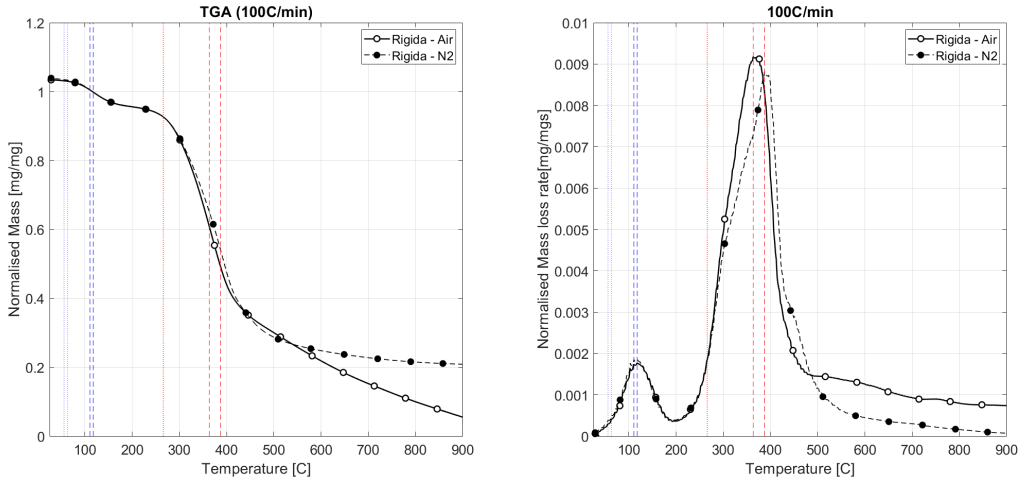

Figure 88: Reaction temperatures from controlled combustion of pinus rigida at 100°C/min. Dotted lines indicate onset and dashed lines maximum. a) Normalised Mass b) Normalised Mass Loss Rate.

B.1.3.2 Bar Chart

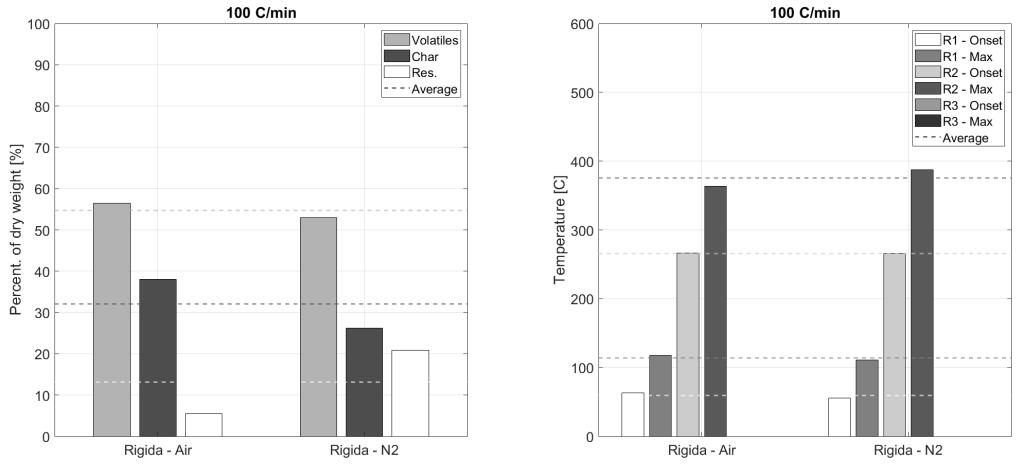

Figure 89: Controlled combustion results for pinus rigida at 100°C/min. Left: Percentage mass. Right: Reaction temperature.

B.2 Conditioning

B.2.0.1 Reaction Temperatures

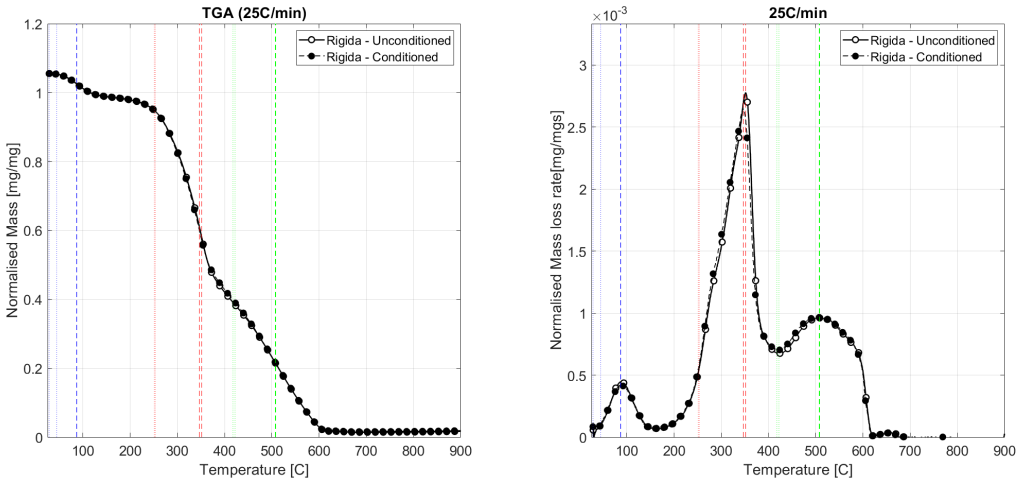

Figure 90: Reaction temperatures from controlled combustion of unconditioned/conditioned pinus rigida at 25°C/min. Dotted lines indicate onset and dashed lines maximum. a) Normalised Mass b) Normalised Mass Loss Rate.

B.3 Low Heating rate

B.3.1 Pinus Tend = 400

B.3.1.1 Reaction Temperatures

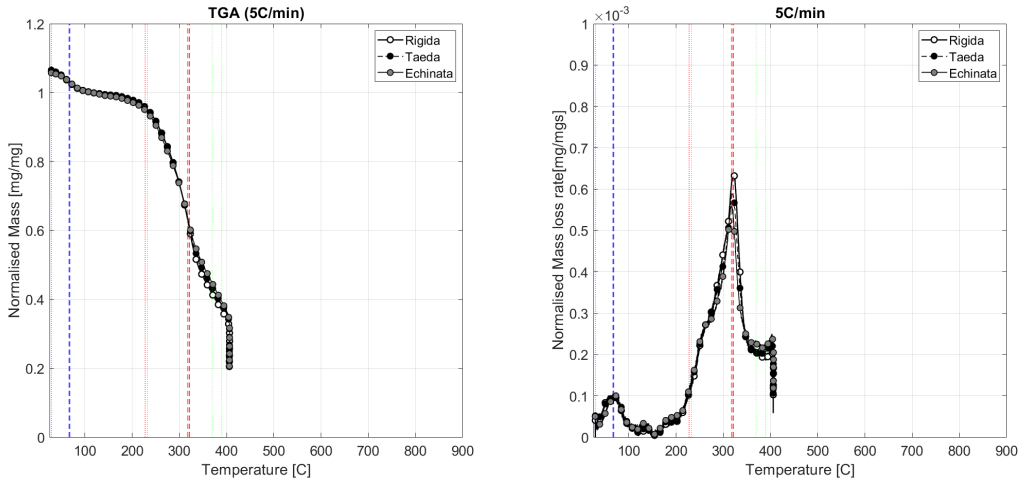

Figure 91: Reaction temperatures from controlled combustion of pinus samples at 5°C/min ending at 400°C. Dotted lines indicate onset and dashed lines maximum. a) Normalised Mass b) Normalised Mass Loss Rate.

B.3.1.2 Bar Chart

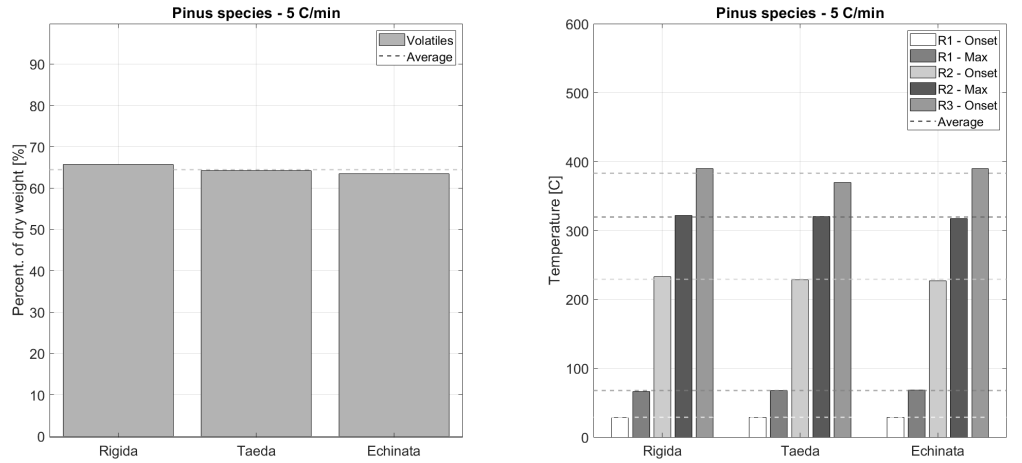

Figure 92: Controlled combustion results for pinus samples at 5°C/min ending at 400°C. Left: Percentage mass. Right: Reaction temperature.

B.3.2 Non-Pinus Tend = 400

B.3.2.1 Reaction Temperatures

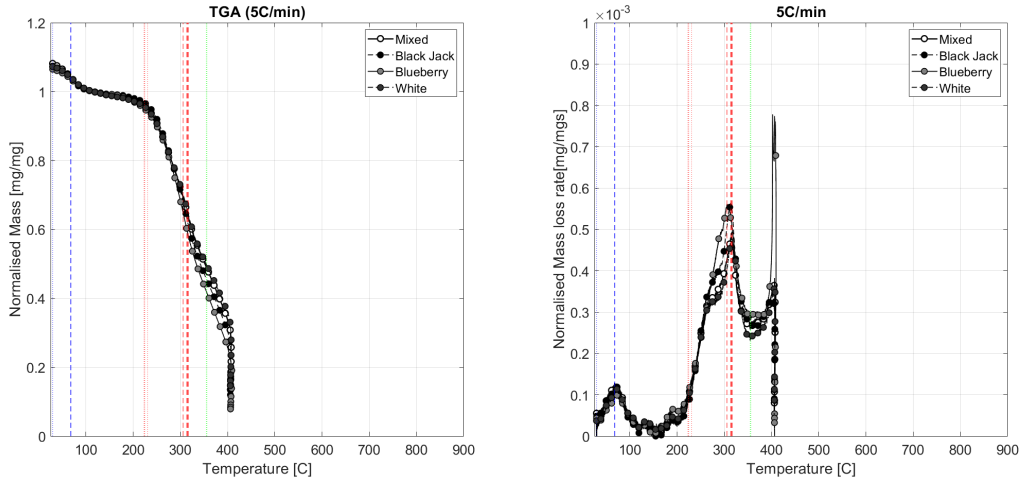

Figure 93: Reaction temperatures from controlled combustion of non-pinus samples at 5°C/min ending at 400°C. Dotted lines indicate onset and dashed lines maximum. a) Normalised Mass b) Normalised Mass Loss Rate.

B.3.2.2 Bar Chart

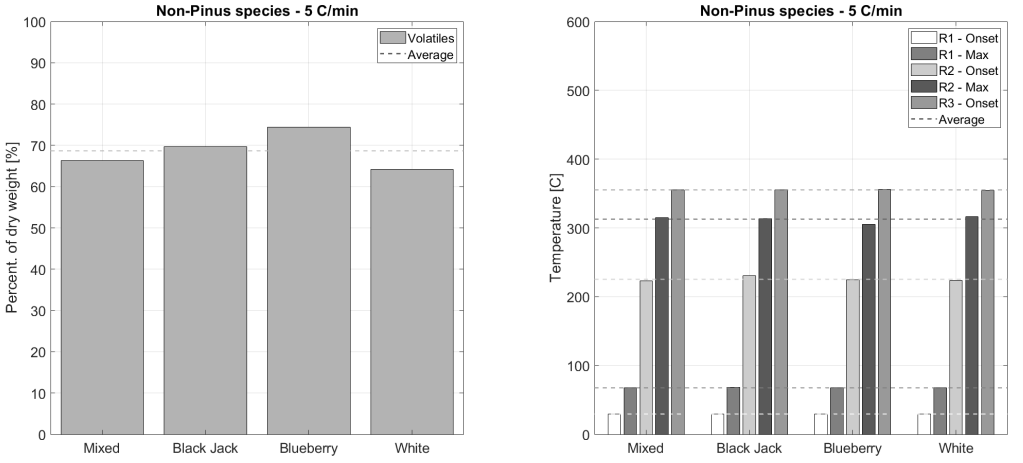

Figure 94: Controlled combustion results for non-pinus samples at 5°C/min ending at 400°C. Left: Percentage mass. Right: Reaction temperature.

B.3.3 Stems Tend = 400

B.3.3.1 Reaction Temperatures

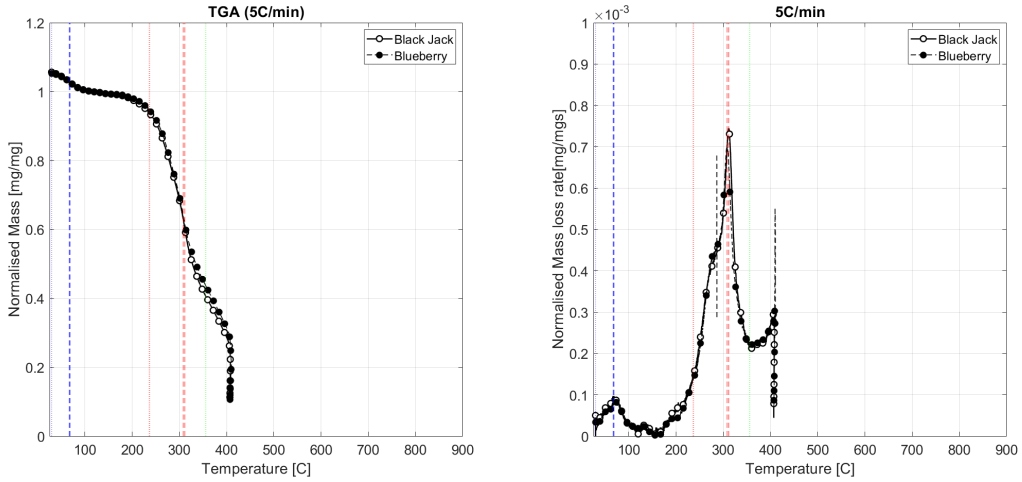

Figure 95: Reaction temperatures from controlled combustion of stems samples at 5°C/min ending at 400°C. Dotted lines indicate onset and dashed lines maximum. a) Normalised Mass b) Normalised Mass Loss Rate.

B.3.3.2 Bar Chart

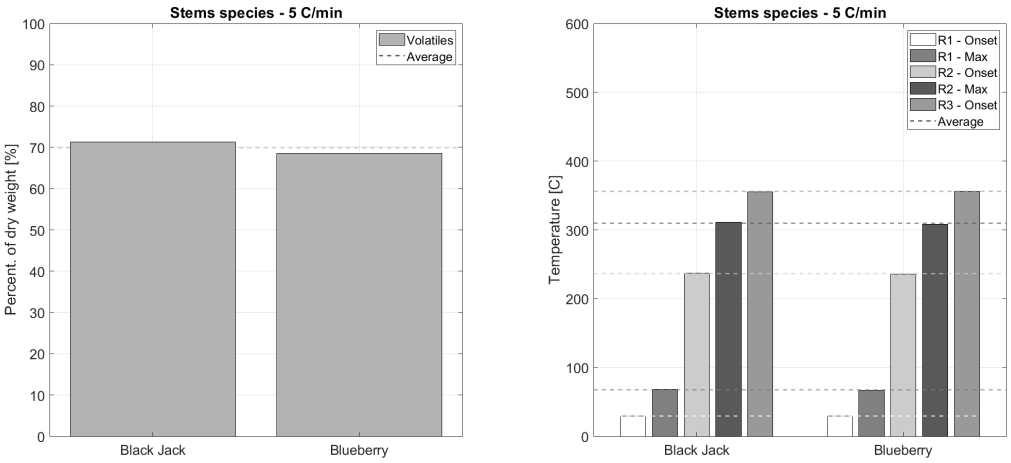

Figure 96: Controlled combustion results for stem samples at 5°C/min ending at 400°C. Left: Percentage mass. Right: Reaction temperature.

	R1	R1 max	R2	R2 max	R3	R3 max
Black Jack - 400	25.08	67.08	233.1	303.7	347.3	NA
Jam Bush - 400	25.08	67	231.6	299.6	347.3	NA

Table 53: Reaction temperatures for controlled combustion of stem samples at 5°C/min ending at 400°C

	Volatile Matter	Char	Residue
Black Jack - 400	66.66	NA	NA
Jam Bush - 400	64.01	NA	NA

Table 54: Volatile matter, fixed carbon, ash fractions for controlled combustion of stem samples at 5°C/min ending at 400°C

B.3.3.3 Table

B.3.4 Pinus Tend = 900

B.3.4.1 Temperature Profile

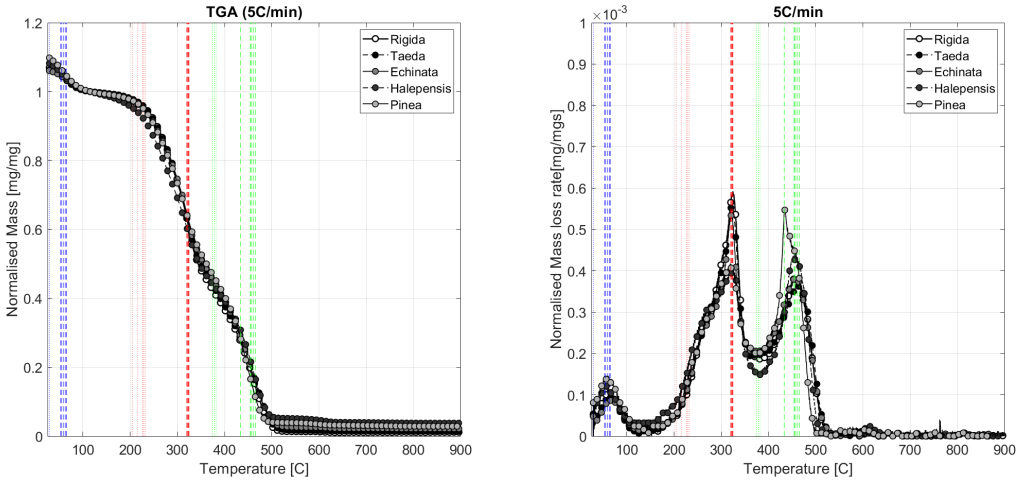

Figure 97: Reaction temperatures from controlled combustion of pinus samples at 5°C/min ending at 900°C. Dotted lines indicate onset and dashed lines maximum. a) Normalised Mass b) Normalised Mass Loss Rate.

B.3.5 Non-Pinus Tend = 900

B.3.5.1 Temperature Profile

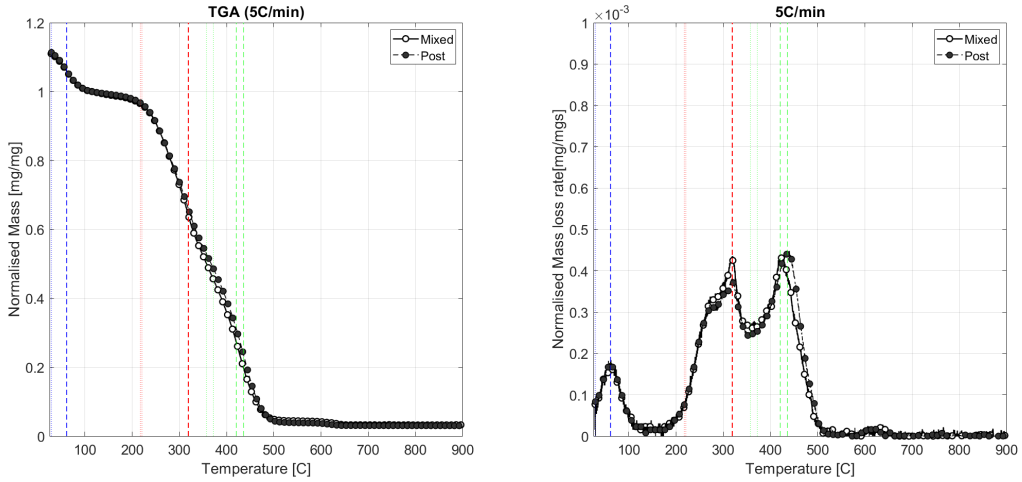

Figure 98: Reaction temperatures from controlled combustion of non-pinus samples at 5°C/min ending at 900°C. Dotted lines indicate onset and dashed lines maximum. a) Normalised Mass b) Normalised Mass Loss

B.4 Medium to High Heating rate

B.4.1 Pinus

B.4.1.1 Temperature Profile

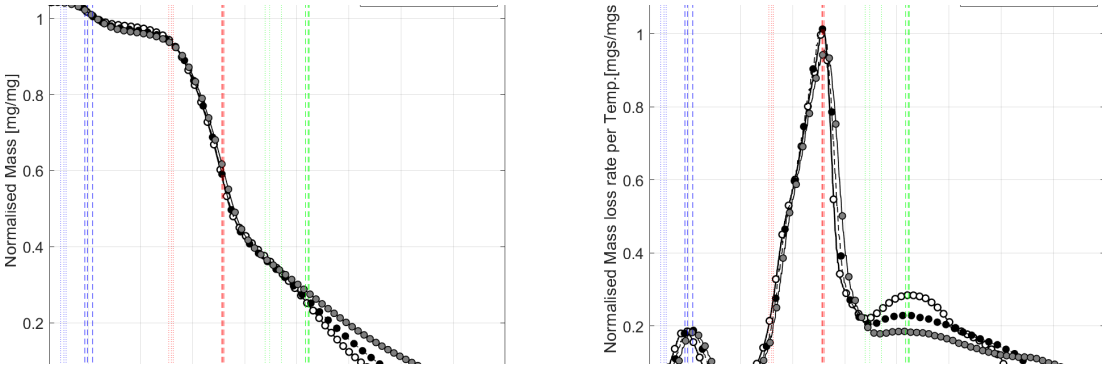

Figure 99: Reaction temperatures from controlled combustion of pinus samples at medium to high heating rates. Dotted lines indicate onset and dashed lines maximum. a) Normalised Mass b) Normalised Mass Loss

B.4.1.2 Bar Chart

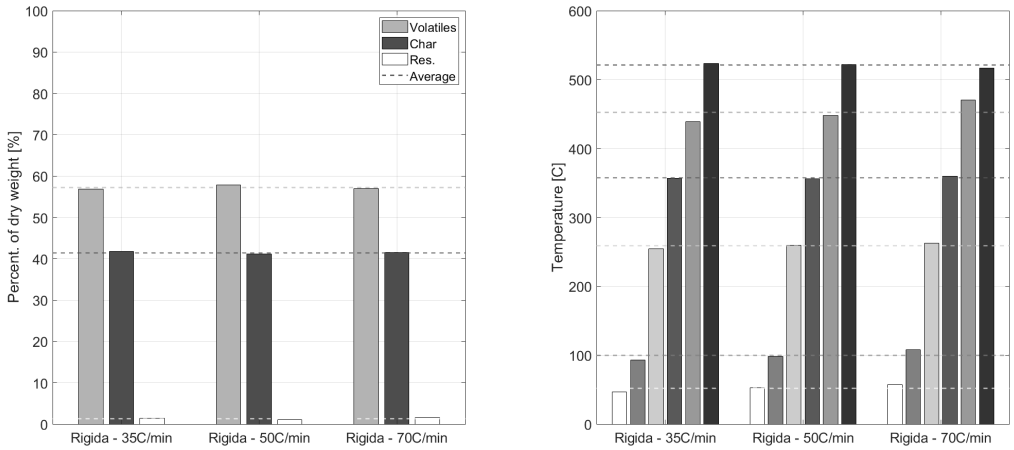

Figure 100: Controlled combustion results for pinus samples at medium to high heating rates. Left: Percentage mass. Right: Reaction temperature.

B.4.1.3 Table

rigida	R1	R1 max	R2	R2 max	R3	R3 max
35	44.83	88.58	246.1	343.5	421.7	507.4
50	48.33	98.33	251.7	341.7	429.2	503.3
70	57.67	109	253.7	343.5	439.2	506.8

Table 55: Reaction temperatures for controlled combustion of pinus rigida at high heating rates.

rigida	Volatile Matter	Char	Residue
35	66.4	32.14	1.46
50	67.43	31.54	1.026
70	66.54	31.3	2.163

Table 56: Volatile matter, fixed carbon and ash fractions for controlled combustion of pinus rigida at high heating rates.

C Fire Propagation Apparatus Experiments

Here are presented all the results for the FPA experiments. They were generated automatically and have had any large jumps removed .

C.1 Tabulated Data

C.1.1 Time

C.1.1.1 Closed Basket Experiments - Pinus Rigida - 25 kW/m^2

	Time to Ignition [s]			
Closed	Average	Minimum	Maximum	Standard Deviation
7.5 g	51.21	48.67	53.74	3.59
15 g	38.28	33.46	41.58	3.64
25 g	30.42	28.39	32.45	2.03
35 g	29.07	27.38	32.45	2.93
60 g	30.76	28.39	34.48	3.26
95 g	47.66	39.55	55.77	11.47
120 g	37.18	34.48	38.53	2.34

Table 57: Time to ignition data for Closed Basket Experiments - Pinus Rigida - 25 kW/m^2

	Time to Flameout [s]			
Closed	Average	Minimum	Maximum	Standard Deviation
7.5 g	96.84	89.23	104.44	10.76
15 g	157.43	145.00	173.40	12.94
25 g	223.08	203.82	235.25	16.88
35 g	370.46	348.83	401.55	27.60
60 g				
95 g	549.08	494.83	603.33	76.72
120 g	235.51	215.44	259.90	22.54

Table 58: Time to Flameout data for Closed Basket Experiments - Pinus Rigida - 25 kW/m^2

	Duration of Flaming [s]			
Closed	Average	Minimum	Maximum	Standard Deviation
7.5 g	45.63	40.56	50.70	7.17
15 g	119.15	107.49	135.88	12.65
25 g	192.66	175.43	204.83	15.34
35 g	341.39	316.38	374.17	29.67
60 g				
95 g	501.42	455.28	547.56	65.25
120 g	198.33	176.91	225.42	24.75

Table 59: Duration of Flaming data for Closed Basket Experiments - Pinus Rigida - 25 kW/m^2

	Test End [s]			
Closed	Average	Minimum	Maximum	Standard Deviation
7.5 g	470.00	456.31	483.70	19.37
15 g	518.16	455.29	612.46	66.68
25 g	604.35	602.32	608.40	3.51
35 g	601.98	601.31	602.32	0.59
60 g	603.00	602.32	604.35	1.17
95 g	605.86	602.31	609.42	5.02
120 g	604.35	602.32	605.36	1.76

Table 60: Test end data for Closed Basket Experiments - Pinus Rigida - 25 kW/m^2

C.1.1.2 Open Basket Experiments - Pinus Rigida - 25 kW/m^2

	Time to Ignition [s]			
Open	Average	Minimum	Maximum	Standard Deviation
10 g	70.98	67.94	74.02	4.30
15 g	76.72	62.87	94.28	16.03
20 g	45.12	43.60	46.64	2.15
25 g	44.62	42.59	48.67	3.51
35 g	42.40	40.00	44.62	2.31
60 g	47.15	44.62	49.69	3.58
90 g	54.42	48.67	63.88	8.26

Table 61: Time to Ignition data for Open Basket Experiments - Pinus Rigida - 25 kW/m^2

	Time to Flameout [s]			
Open	Average	Minimum	Maximum	Standard Deviation
10 g	91.26	88.22	94.30	4.30
15 g	113.57	96.33	122.69	14.94
20 g	88.22	87.20	89.23	1.43
25 g	165.96	158.18	175.42	8.74
35 g	206.26	200.00	210.91	5.63
60 g	464.92	460.36	469.48	6.45
90 g	322.12	247.42	368.09	65.26

Table 62: Time to Flameout data for Open Basket Experiments - Pinus Rigida - 25 kW/m^2

	Duration of Flaming [s]			
Open	Average	Minimum	Maximum	Standard Deviation
10 g	20.28	20.28	20.28	0.00
15 g	36.85	27.41	49.69	11.52
20 g	43.10	42.59	43.60	0.72
25 g	121.34	115.60	132.84	9.95
35 g	163.86	160.00	168.33	4.20
60 g	417.77	410.68	424.87	10.04
90 g	267.70	196.72	304.20	61.48

Table 63: Duration of Flaming data for Open Basket Experiments - Pinus Rigida - 25 kW/m^2

	Test End [s]			
Open	Average	Minimum	Maximum	Standard Deviation
10 g	409.16	388.37	429.96	29.41
15 g	462.05	452.25	471.51	9.64
20 g	332.09	318.40	345.78	19.36
25 g	581.03	561.76	611.46	26.66
35 g	677.35	604.35	771.65	85.66
60 g	2007.75	1913.46	2102.04	133.34
90 g	2961.98	605.36	4379.42	2054.85

Table 64: Test end data for Open Basket Experiments - Pinus Rigida - 25 kW/m^2

C.1.1.3 Open Basket Experiments - Pinus Rigida - 35 kW/m^2

	Time to Ignition [s]			
35 kW/m^2	Average	Minimum	Maximum	Standard Deviation
15 g	20.80	19.28	22.31	2.14
35 g	20.79	20.28	21.29	0.72
90 g	24.95	21.51	28.39	4.87

Table 65: Time to Ignition data for Open Basket Experiments - Pinus Rigida - 35 kW/m^2

	Time to Flameout [s]			
35 kW/m^2	Average	Minimum	Maximum	Standard Deviation
15 g	61.86	61.85	61.87	0.01
35 g	171.37	163.26	179.48	11.47
90 g	270.85	236.26	305.43	48.91

Table 66: Time to Flameout data for Open Basket Experiments - Pinus Rigida - 35 kW/m^2

	Duration of Flaming [s]			
35 kW/m^2	Average	Minimum	Maximum	Standard Deviation
15 g	41.07	39.55	42.59	2.15
35 g	150.58	142.98	158.19	10.76
90 g	245.90	207.87	283.92	53.78

Table 67: Duration of Flaming data for Open Basket Experiments - Pinus Rigida - 35 kW/m^2

	Test End [s]			
35 kW/m^2	Average	Minimum	Maximum	Standard Deviation
15 g	683.96	679.39	688.53	6.46
35 g	1376.01	872.04	1879.99	712.73
90 g	3607.83	3450.78	3764.89	222.11

Table 68: Test End data for Open Basket Experiments - Pinus Rigida - 35 kW/m^2

C.1.1.4 Open Basket Experiments - Pinus Rigida - 50 kW/m^2

	Time to Ignition [s]			
50 kW/m^2	Average	Minimum	Maximum	Standard Deviation
15 g	12.95	11.70	14.20	1.76
35 g	11.37	11.15	11.59	0.31
90 g	11.15	11.15	11.15	0.00

Table 69: Time to Ignition data for Open Basket Experiments - Pinus Rigida - 50 kW/m^2

	Time to Flameout [s]			
50 kW/m^2	Average	Minimum	Maximum	Standard Deviation
15 g	43.60	35.49	51.71	11.47
35 g	160.72	143.99	177.45	23.66
90 g	509.94	353.89	666.00	220.70

Table 70: Time to Flameout data for Open Basket Experiments - Pinus Rigida - 50 kW/m^2

	Duration of Flaming [s]			
50 kW/m^2	Average	Minimum	Maximum	Standard Deviation
15 g	30.65	21.29	40.01	13.24
35 g	149.35	132.83	165.86	23.35
90 g	498.79	342.73	654.85	220.70

Table 71: Duration of Flaming data for Open Basket Experiments - Pinus Rigida - 50 kW/m^2

	Test End [s]			
50 kW/m^2	Average	Minimum	Maximum	Standard Deviation
15 g	400.54	380.26	420.81	28.68
35 g	862.40	730.08	994.73	187.14
90 g	2386.43	1539.28	3233.58	1198.05

Table 72: Test End data for Open Basket Experiments - Pinus Rigida - 50 kW/m^2

C.1.1.5 Open Basket Experiments - Pinus Halepensis, Pinus Pinea, Pinus Pinaster - 25 kW/m^2

	Time to Ignition [s]			
Halepensis	Average	Minimum	Maximum	Standard Deviation
10 g	44.11	31.43	56.78	17.93
15 g	28.90	22.31	35.49	9.32
20 g	23.85	22.31	25.40	2.19
Pinea	Average	Minimum	Maximum	Standard Deviation
10 g	57.29	54.76	59.83	3.59
15 g	40.57	32.45	48.69	11.48
Pinaster	Average	Minimum	Maximum	Standard Deviation
10 g	137.90	137.90	137.90	0.00
15 g	87.71	77.07	98.36	15.06

Table 73: Time to Ignition data for Open Basket Experiments - Pinus Halepensis, Pinus Pinea, Pinus Pinaster - 25 kW/m^2

	Time to Flameout [s]			
Halepensis	Average	Minimum	Maximum	Standard Deviation
10 g	65.91	53.74	78.08	17.21
15 g	62.87	59.83	65.91	4.30
20 g	82.66	70.00	95.32	17.90
Pinea	Average	Minimum	Maximum	Standard Deviation
10 g	77.57	71.99	83.15	7.89
15 g	73.02	63.88	82.15	12.92
Pinaster	Average	Minimum	Maximum	Standard Deviation
10 g	161.23	158.18	164.27	4.30
15 g	112.56	103.43	121.68	12.91

Table 74: Time to Flameout data for Open Basket Experiments - Pinus Halepensis, Pinus Pinea, Pinus Pinaster - 25 kW/m^2

	Duration of Flaming [s]			
Halepensis	Average	Minimum	Maximum	Standard Deviation
10 g	21.80	21.29	22.31	0.72
15 g	33.97	30.42	37.52	5.02
20 g	58.80	44.60	73.01	20.09
Pinea	Average	Minimum	Maximum	Standard Deviation
10 g	20.28	17.24	23.32	4.30
15 g	32.45	31.43	33.46	1.43
Pinaster	Average	Minimum	Maximum	Standard Deviation
10 g	23.32	20.28	26.36	4.30
15 g	24.84	23.32	26.36	2.15

Table 75: Duration of Flaming data for Open Basket Experiments - Pinus Halepensis, Pinus Pinea, Pinus Pinaster - 25 kW/m^2

	Test End [s]			
Halepensis	Average	Minimum	Maximum	Standard Deviation
10 g	332.60	328.54	336.65	5.74
15 g	566.83	421.83	711.83	205.06
20 g	483.68	468.47	498.89	21.51
Pinea	Average	Minimum	Maximum	Standard Deviation
10 g	316.89	304.20	329.57	17.94
15 g	512.60	420.84	604.36	129.76
Pinaster	Average	Minimum	Maximum	Standard Deviation
10 g	23.32	20.28	26.36	4.30
15 g	24.84	23.32	26.36	2.15

Table 76: Test End data for Open Basket Experiments - Pinus Halepensis, Pinus Pinea, Pinus Pinaster - 25 kW/m^2

	Mass Lost during Flaming [g]			
Closed	Average	Minimum	Maximum	Standard Deviation
7.5 g	5.49	5.73	5.25	0.34
15 g	11.38	11.64	11.10	0.23
25 g	18.94	19.05	18.88	0.09
35 g	24.80	24.88	24.69	0.10
60 g				
95 g	34.50	37.27	31.72	3.93
120 g	14.37	16.59	12.88	1.96

Table 80: Mass Lost during flaming data for Closed Basket Experiments - Pinus Rigida - 25 kW/m^2

C.1.2 Mass

C.1.2.1 Closed Basket Experiments - Pinus Rigida - 25 kW/m^2

	Mass Lost at Ignition [g]			
Closed	Average	Minimum	Maximum	Standard Deviation
7.5 g	1.67	1.64	1.70	0.04
15 g	0.79	0.66	1.01	0.17
25 g	0.82	0.62	1.15	0.29
35 g	0.65	0.56	0.75	0.10
60 g	0.72	0.31	1.24	0.47
95 g	1.31	1.00	1.61	0.43
120 g	0.71	0.53	0.89	0.18

Table 77: Mass Lost at ignition data for Closed Basket Experiments - Pinus Rigida - 25 kW/m^2

	Mass Lost at Flameout [g]			
Closed	Average	Minimum	Maximum	Standard Deviation
7.5 g	7.16	6.95	7.37	0.30
15 g	12.17	11.76	12.48	0.30
25 g	19.76	19.56	20.04	0.25
35 g	25.45	25.32	25.63	0.16
60 g				
95 g	35.80	32.72	38.89	4.36
120 g	15.08	13.41	17.29	1.99

Table 78: Mass Lost at flameout data for Closed Basket Experiments - Pinus Rigida - 25 kW/m^2

	Mass Lost at 300 s [g]			
Closed	Average	Minimum	Maximum	Standard Deviation
7.5 g	10.56	10.23	10.88	0.46
15 g	14.16	13.66	14.54	0.39
25 g	21.28	20.88	21.75	0.44
35 g	23.42	22.23	24.30	1.07
60 g	23.81	23.62	23.91	0.17
95 g	21.92	21.87	21.96	0.06
120 g	18.32	17.32	19.55	1.13

Table 79: Mass Lost at 300 s data for Closed Basket Experiments - Pinus Rigida - 25 kW/m^2

C.1.2.2 Open Basket Experiments - Pinus Rigida - 25 kW/m^2

	Mass Lost at Ignition [g]			
Open	Average	Minimum	Maximum	Standard Deviation
10 g	0.72	0.63	0.81	0.13
15 g	1.22	0.91	1.54	0.31
20 g	0.62	0.18	1.07	0.63
25 g	0.88	0.70	0.98	0.16
35 g	0.60	0.12	0.91	0.42
60 g	1.11	1.03	1.19	0.12
90 g	1.29	1.17	1.53	0.21

Table 81: Mass Lost at ignition data for Open Basket Experiments - Pinus Rigida - 25 kW/m^2

	Mass Lost at Flameout [g]			
Open	Average	Minimum	Maximum	Standard Deviation
10 g	7.64	7.55	7.73	0.13
15 g	11.00	9.67	12.30	1.32
20 g	13.40	12.79	14.02	0.87
25 g	21.53	21.07	21.85	0.41
35 g	26.28	25.92	26.55	0.32
60 g	38.87	38.80	38.94	0.10
90 g	25.59	20.71	28.18	4.23

Table 82: Mass Lost at Flameout data for Open Basket Experiments - Pinus Rigida - 25 kW/m^2

	Mass Lost at 300 s [g]			
Open	Average	Minimum	Maximum	Standard Deviation
10 g	10.11	9.84	10.38	0.38
15 g	12.91	11.27	14.18	1.49
20 g	17.27	16.76	17.77	0.71
25 g	24.21	23.41	24.80	0.72
35 g	29.45	28.98	29.81	0.43
60 g	28.68	27.64	29.71	1.46
90 g	24.18	23.82	24.45	0.32

Table 83: Mass Lost at 300 s data for Open Basket Experiments - Pinus Rigida - 25 kW/m^2

	Mass Lost during Flaming [g]			
Open	Average	Minimum	Maximum	Standard Deviation
10 g	6.92	6.92	6.91	0.00
15 g	9.77	11.08	8.76	1.19
20 g	12.78	12.95	12.61	0.24
25 g	20.66	21.15	20.09	0.53
35 g	25.69	26.25	25.01	0.62
60 g	37.76	37.77	37.75	0.01
90 g	24.30	26.71	19.54	4.12

Table 84: Mass Lost during Flaming data for Open Basket Experiments - Pinus Rigida - 25 kW/m^2

C.1.2.3 Open Basket Experiments - Pinus Rigida - 35 kW/m^2

	Mass Lost at Ignition [g]			
35 kW/m^2	Average	Minimum	Maximum	Standard Deviation
15 g	0.27	0.09	0.45	0.26
35 g	0.47	0.46	0.48	0.01
90 g	0.65	0.61	0.69	0.06

Table 85: Mass Lost at Ignition data for Open Basket Experiments - Pinus Rigida - 35 kW/m^2

	Mass Lost at Flameout [g]			
35 kW/m^2	Average	Minimum	Maximum	Standard Deviation
15 g	7.89	7.53	8.25	0.51
35 g	22.24	22.24	22.24	0.00
90 g	26.32	23.66	28.99	3.77

Table 86: Mass Lost at Flameout data for Open Basket Experiments - Pinus Rigida - 35 kW/m^2

	Mass Lost at 300s [g]			
35 kW/m^2	Average	Minimum	Maximum	Standard Deviation
15 g	12.92	11.47	14.38	2.06
35 g	25.79	25.50	26.07	0.40
90 g	28.45	28.35	28.56	0.15

Table 87: Mass Lost at 300 s data for Open Basket Experiments - Pinus Rigida - 35 kW/m^2

	Mass Lost during Flaming [g]			
35 kW/m^2	Average	Minimum	Maximum	Standard Deviation
15 g	7.62	7.80	7.44	0.25
35 g	21.77	21.78	21.76	0.01
90 g	25.68	28.38	22.97	3.83

Table 88: Mass Lost during Flaming data for Open Basket Experiments - Pinus Rigida - 35 kW/m^2

C.1.2.4 Open Basket Experiments - Pinus Rigida - 50 kW/m^2

	Mass Lost at Ignition [g]			
50 kW/m^2	Average	Minimum	Maximum	Standard Deviation
15 g	0.35	0.32	0.37	0.04
35 g	0.26	0.11	0.41	0.21
90 g	0.29	0.22	0.36	0.10

Table 89: Mass Lost at Ignition data for Open Basket Experiments - Pinus Rigida - 50 kW/m^2

	Mass Lost at Flameout [g]			
50 kW/m^2	Average	Minimum	Maximum	Standard Deviation
15 g	2.75	1.68	3.82	1.52
35 g	19.42	18.77	20.08	0.93
90 g	44.61	34.63	54.59	14.11

Table 90: Mass Lost at Flameout data for Open Basket Experiments - Pinus Rigida - 50 kW/m^2

	Mass Lost at 300s [g]			
50 kW/m^2	Average	Minimum	Maximum	Standard Deviation
15 g	7.49	6.16	8.83	1.89
35 g	22.87	22.87	22.87	0.00
90 g	31.25	30.66	31.84	0.83

Table 91: Mass Lost at 300s data for Open Basket Experiments - Pinus Rigida - 50 kW/m^2

	Mass Lost during Flaming [g]			
50 kW/m^2	Average	Minimum	Maximum	Standard Deviation
15 g	2.40	3.50	1.30	1.55
35 g	19.16	19.67	18.65	0.72
90 g	44.32	54.23	34.41	14.02

Table 92: Mass Lost during Flaming data for Open Basket Experiments - Pinus Rigida - 50 kW/m^2

C.1.2.5 Open Basket Experiments - Pinus Halepensis, Pinus Pinea, Pinus Pinaster - 25 kW/m^2

	Mass Lost at Ignition [g]			
Halepensis	Average	Minimum	Maximum	Standard Deviation
10 g	0.73	0.43	1.03	0.42
15 g	0.30	0.27	0.32	0.03
20 g	0.52	0.50	0.54	0.03
Pinea	Average	Minimum	Maximum	Standard Deviation
10 g	0.79	0.69	0.89	0.14
15 g	0.60	0.27	0.92	0.46
Pinaster	Average	Minimum	Maximum	Standard Deviation
10 g	1.08	1.06	1.09	0.02
15 g	1.06	0.92	1.19	0.19

Table 93: Mass Lost at Ignition data for Open Basket Experiments - Pinus Halepensis, Pinus Pinea, Pinus Pinaster - 25 kW/m^2

	Mass Lost at Flameout [g]			
Halepensis	Average	Minimum	Maximum	Standard Deviation
10 g	7.45	7.34	7.57	0.16
15 g	8.82	7.96	9.69	1.22
20 g	10.89	10.14	11.64	1.06
Pinea	Average	Minimum	Maximum	Standard Deviation
10 g	7.57	6.79	8.34	1.10
15 g	10.41	10.07	10.74	0.47
Pinaster	Average	Minimum	Maximum	Standard Deviation
10 g	8.43	8.28	8.58	0.21
15 g	9.90	9.40	10.39	0.70

Table 94: Mass Lost at Flameout data for Open Basket Experiments - Pinus Halepensis, Pinus Pinea, Pinus Pinaster - 25 kW/m^2

	Mass Lost at 300s [g]			
Halepensis	Average	Minimum	Maximum	Standard Deviation
10 g	12.02	11.58	12.46	0.62
15 g	10.86	10.66	11.05	0.27
20 g	14.44	13.85	15.04	0.84
Pinea	Average	Minimum	Maximum	Standard Deviation
10 g	9.24	8.77	9.70	0.65
15 g	13.57	12.87	14.26	0.99
Pinaster	Average	Minimum	Maximum	Standard Deviation
10 g	9.02	8.89	9.14	0.18
15 g	11.41	10.63	12.20	1.11

Table 95: Mass Lost at 300s data for Open Basket Experiments - Pinus Halepensis, Pinus Pinea, Pinus Pinaster - 25 kW/m^2

	Mass Lost during Flaming [g]			
Halepensis	Average	Minimum	Maximum	Standard Deviation
10 g	6.72	6.90	6.54	0.26
15 g	8.53	9.37	7.69	1.19
20 g	10.37	11.11	9.64	1.04
Pinea	Average	Minimum	Maximum	Standard Deviation
10 g	6.77	7.45	6.10	0.96
15 g	9.81	9.82	9.80	0.01
Pinaster	Average	Minimum	Maximum	Standard Deviation
10 g	7.35	7.49	7.22	0.19
15 g	8.84	9.20	8.48	0.51

Table 96: Mass Lost during Flaming data for Open Basket Experiments - Pinus Halepensis, Pinus Pinea, Pinus Pinaster - 25 kW/m^2

C.1.3 Mass Loss Rate

C.1.3.1 Closed Basket Experiments - Pinus Rigida - 25 kW/m^2

	Mass Loss Rate at Ignition [g/s]			
Closed	Average	Minimum	Maximum	Standard Deviation
7.5 g	0.050	0.040	0.059	0.014
15 g	0.054	0.037	0.095	0.028
25 g	0.048	0.022	0.076	0.027
35 g	0.055	0.035	0.072	0.019
60 g	0.064	0.014	0.090	0.043
95 g	0.095	0.084	0.105	0.014
120 g	0.079	0.046	0.130	0.045

Table 97: Mass Loss Rate at ignition data for Closed Basket Experiments - Pinus Rigida - 25 kW/m^2

	Average Mass Loss Rate During Flaming [g/s]			
Closed	Average	Minimum	Maximum	Standard Deviation
7.5 g	0.12	0.10	0.14	0.027
15 g	0.10	0.08	0.11	0.010
25 g	0.10	0.09	0.11	0.0078
35 g	0.073	0.066	0.079	0.0064
60 g				
95 g	0.069	0.068	0.070	0.0011
120 g	0.072	0.071	0.074	0.0014

Table 100: Average Mass Loss Rate during Flaming data for Closed Basket Experiments - Pinus Rigida - 25 kW/m^2

	Mass Loss Rate at Flameout [g/s]			
Closed	Average	Minimum	Maximum	Standard Deviation
7.5 g	0.049	0.013	0.085	0.051
15 g	0.016	0.004	0.022	0.008
25 g	0.014	-0.004	0.038	0.022
35 g	0.025	-0.005	0.066	0.037
60 g				
95 g	0.025	0.020	0.030	0.007
120 g	0.059	0.031	0.090	0.029

Table 98: Mass Loss Rate at flameout data for Closed Basket Experiments - Pinus Rigida - 25 kW/m^2

	Peak Mass Loss Rate [g/s]			
Closed	Average	Minimum	Maximum	Standard Deviation
7.5 g	0.34	0.33	0.36	0.021
15 g	0.43	0.36	0.54	0.087
25 g	0.37	0.33	0.39	0.030
35 g	0.36	0.28	0.47	0.096
60 g	0.29	0.28	0.30	0.014
95 g	0.27	0.25	0.28	0.018
120 g	0.26	0.23	0.31	0.045

Table 99: Peak Mass Loss Rate data for Closed Basket Experiments - Pinus Rigida - 25 kW/m^2

C.1.3.2 Open Basket Experiments - Pinus Rigida - 25 kW/m^2

	Mass Loss Rate at Ignition [g/s]			
Open	Average	Minimum	Maximum	Standard Deviation
10 g	0.020	0.008	0.033	0.018
15 g	0.068	-0.014	0.165	0.091
20 g	0.036	-0.010	0.082	0.065
25 g	0.036	0.020	0.064	0.025
35 g	0.041	0.032	0.051	0.010
60 g	0.051	0.047	0.055	0.005
90 g	0.045	0.028	0.067	0.020

Table 101: Mass Loss Rate at ignition data for Open Basket Experiments - Pinus Rigida - 25 kW/m^2

	Mass Loss Rate at Flameout [g/s]			
Open	Average	Minimum	Maximum	Standard Deviation
10 g	0.076	0.051	0.10	0.036
15 g	0.071	-0.001	0.12	0.063
20 g	0.087	0.040	0.13	0.066
25 g	0.059	0.042	0.07	0.014
35 g	0.060	0.012	0.11	0.049
60 g	0.031	0.022	0.04	0.013
90 g	0.055	0.042	0.08	0.021

Table 102: Mass Loss Rate at flameout data for Open Basket Experiments - Pinus Rigida - 25 kW/m^2

	Peak Mass Loss Rate [g/s]			
Open	Average	Minimum	Maximum	Standard Deviation
10 g	0.62	0.61	0.63	0.02
15 g	0.64	0.50	0.76	0.13
20 g	0.98	0.60	1.37	0.55
25 g	0.43	0.39	0.45	0.03
35 g	0.44	0.30	0.61	0.16
60 g	0.36	0.30	0.41	0.080
90 g	0.27	0.25	0.29	0.019

Table 103: Peak Mass Loss Rate data for Open Basket Experiments - Pinus Rigida - 25 kW/m^2

	Average Mass Loss Rate During Flaming [g/s]			
Open	Average	Minimum	Maximum	Standard Deviation
10 g	0.34	0.34	0.34	0.00021
15 g	0.28	0.22	0.35	0.063
20 g	0.30	0.30	0.30	0.00063
25 g	0.17	0.16	0.18	0.010
35 g	0.16	0.15	0.16	0.0072
60 g	0.090	0.089	0.09	0.0022
90 g	0.092	0.088	0.10	0.0066

Table 104: Average Mass Loss Rate During Flaming data for Open Basket Experiments - Pinus Rigida - 25 kW/m^2

C.1.3.3 Open Basket Experiments - Pinus Rigida - 35 kW/m^2

	Mass Loss Rate at Ignition [g/s]			
35 kW/m^2	Average	Minimum	Maximum	Standard Deviation
15 g	0.0053	-0.012	0.023	0.025
35 g	0.020	-0.007	0.046	0.038
90 g	0.062	0.057	0.068	0.007

Table 105: Mass Loss Rate at Ignition data for Open Basket Experiments - Pinus Rigida - 35 kW/m^2

	Mass Loss Rate at Flameout [g/s]			
35 kW/m^2	Average	Minimum	Maximum	Standard Deviation
15 g	0.066	0.066	0.066	0.00026
35 g	0.026	0.021	0.030	0.0066
90 g	0.089	0.081	0.096	0.0102

Table 106: Mass Loss Rate at Flameout data for Open Basket Experiments - Pinus Rigida - 35 kW/m^2

	Peak Mass Loss Rate [g/s]			
35 kW/m^2	Average	Minimum	Maximum	Standard Deviation
15 g	0.50	0.47	0.52	0.033
35 g	0.33	0.30	0.36	0.042
90 g	0.34	0.30	0.39	0.066

Table 107: Peak Mass Loss Rate data for Open Basket Experiments - Pinus Rigida - 35 kW/m^2

	Average Mass Loss Rate During Flaming [g/s]			
35 kW/m^2	Average	Minimum	Maximum	Standard Deviation
15 g	0.19	0.18	0.19	0.0036
35 g	0.14	0.14	0.15	0.0104
90 g	0.11	0.10	0.11	0.0075

Table 108: Average Mass Loss Rate during Flaming data for Open Basket Experiments - Pinus Rigida - 35 kW/m^2

C.1.3.4 Open Basket Experiments - Pinus Rigida - 50 kW/m^2

	Mass Loss Rate at Ignition [g/s]			
50 kW/m^2	Average	Minimum	Maximum	Standard Deviation
15 g	0.0092	0.0091	0.0093	0.00016
35 g	0.0215	-0.00077	0.044	0.032
90 g	0.0057	-0.0018	0.013	0.011

Table 109: Mass Loss Rate at Ignition data for Open Basket Experiments - Pinus Rigida - 50 kW/m^2

	Mass Loss Rate at Flameout [g/s]			
50 kW/m^2	Average	Minimum	Maximum	Standard Deviation
15 g	0.10	0.035	0.16	0.090
35 g	0.044	0.042	0.045	0.0021
90 g	0.045	0.031	0.060	0.020

Table 110: Mass Loss Rate at Flameout data for Open Basket Experiments - Pinus Rigida - 50 kW/m^2

	Peak Mass Loss Rate [g/s]			
50 kW/m^2	Average	Minimum	Maximum	Standard Deviation
15 g	0.32	0.28	0.36	0.05
35 g	0.48	0.30	0.66	0.25
90 g	0.31	0.28	0.33	0.04

Table 111: Peak Mass Loss Rate data for Open Basket Experiments - Pinus Rigida - 50 kW/m^2

	Mass Loss Rate at Flameout [g/s]			
Halepensis	Average	Minimum	Maximum	Standard Deviation
10 g	0.12	0.12	0.12	0.00033
15 g	0.071	0.068	0.074	0.0045
20 g	0.094	0.033	0.16	0.087
Pinea	Average	Minimum	Maximum	Standard Deviation
10 g	0.13	0.13	0.13	0.00081
15 g	0.17	0.14	0.19	0.036
Pinaster	Average	Minimum	Maximum	Standard Deviation
10 g	0.11	0.091	0.12	0.021
15 g	0.073	0.044	0.10	0.041

Table 114: Mass Loss Rate at Flameout data for Open Basket Experiments - Pinus Halepensis, Pinus Pinea, Pinus Pinaster - 25 kW/m^2

	Average Mass Loss Rate During Flaming [g/s]			
50 kW/m^2	Average	Minimum	Maximum	Standard Deviation
15 g	0.074	0.061	0.087	0.018
35 g	0.13	0.12	0.14	0.015
90 g	0.092	0.083	0.10	0.012

Table 112: Average Mass Loss Rate during Flaming data for Open Basket Experiments - Pinus Rigida - 50 kW/m^2

C.1.3.5 Open Basket Experiments - Pinus Halepensis, Pinus Pinea, Pinus Pinaster - 25 kW/m^2

	Mass Loss Rate at Ignition [g/s]			
Halepensis	Average	Minimum	Maximum	Standard Deviation
10 g	0.11	0.016	0.21	0.13
15 g	0.042	0.024	0.060	0.025
20 g	0.011	0.000	0.023	0.017
Pinea	Average	Minimum	Maximum	Standard Deviation
10 g	0.032	0.017	0.047	0.021
15 g	0.038	0.018	0.058	0.028
Pinaster	Average	Minimum	Maximum	Standard Deviation
10 g	0.0064	0.0056	0.0073	0.0012
15 g	0.022	0.0027	0.041	0.027

Table 113: Mass Loss Rate at Ignition data for Open Basket Experiments - Pinus Halepensis, Pinus Pinea, Pinus Pinaster - 25 kW/m^2

	Peak Mass Loss Rate [g/s]			
Halepensis	Average	Minimum	Maximum	Standard Deviation
10 g	0.58	0.58	0.59	0.010
15 g	0.55	0.44	0.65	0.15
20 g	0.41	0.37	0.44	0.045
Pinea	Average	Minimum	Maximum	Standard Deviation
10 g	0.68	0.61	0.76	0.11
15 g	0.79	0.60	0.97	0.26
Pinaster	Average	Minimum	Maximum	Standard Deviation
10 g	0.75	0.71	0.78	0.048
15 g	0.77	0.75	0.79	0.027

Table 115: Peak Mass Loss Rate data for Open Basket Experiments - Pinus Halepensis, Pinus Pinea, Pinus Pinaster - 25 kW/m^2

	Average Mass Loss Rate During Flaming [g/s]			
Halepensis	Average	Minimum	Maximum	Standard Deviation
10 g	0.31	0.31	0.31	0.0016
15 g	0.26	0.20	0.31	0.073
20 g	0.18	0.15	0.22	0.045
Pinea	Average	Minimum	Maximum	Standard Deviation
10 g	0.34	0.32	0.35	0.024
15 g	0.30	0.29	0.31	0.013
Pinaster	Average	Minimum	Maximum	Standard Deviation
10 g	0.32	0.28	0.36	0.051
15 g	0.36	0.32	0.39	0.052

Table 116: Average Mass Loss Rate During Flaming for Open Basket Experiments - Pinus Halepensis, Pinus Pinea, Pinus Pinaster - 25 kW/m^2

C.1.4 Heat Release Rate

C.1.4.1 Closed Basket Experiments - Pinus Rigida - 25 kW/m^2

	Peak Heat Release Rate - O2 [kW]				Peak Heat Release Rate - CO2 [kW]			
Closed	Average	Min.	Max.	Standard Deviation	Average	Min.	Max.	Standard Deviation
7.5 g	2.87	2.63	3.11	0.34	1.80	1.67	1.94	0.19
15 g	3.04	2.80	3.17	0.16	1.60	1.21	2.04	0.38
25 g	3.40	3.15	3.74	0.31	2.51	1.96	3.03	0.53
35 g	2.67	2.45	2.97	0.27	2.48	2.23	2.68	0.23
60 g	3.14	2.74	3.40	0.35	1.77	1.51	1.98	0.24
95 g	3.07	3.05	3.10	0.03	1.16	1.13	1.19	0.04
120 g	2.05	1.69	2.61	0.49	1.32	1.20	1.44	0.12

Table 117: Peak Heat Release data for Closed Basket Experiments - Pinus Rigida - 25 kW/m^2

	Peak Heat Release Rate - O2 [kW]				Peak Heat Release Rate - CO2 [kW]			
Open	Average	Min	Max	Standard Deviation	Average	Min	Max	Standard Deviation
10 g	6.15	5.95	6.35	0.28	0.96	0.92	0.99	0.05
15 g	5.29	4.50	5.76	0.69	1.18	0.71	1.43	0.41
20 g	6.31	6.01	6.60	0.42	2.12	1.99	2.25	0.18
25 g	4.13	3.05	4.72	0.93	1.71	1.29	2.16	0.43
35 g	3.94	3.50	4.30	0.41	1.90	1.63	2.24	0.32
60 g	2.88	2.72	3.03	0.22	1.12	0.94	1.29	0.25
90 g	2.63	2.10	2.94	0.46	0.80	0.64	0.99	0.17

Table 118: Peak Heat Release Rate at ignition data for Open Basket Experiments - Pinus Rigida - 25 kW/m^2

C.1.4.2 Open Basket Experiments - Pinus Rigida - 25 kW/m^2

C.1.4.3 Open Basket Experiments - Pinus Rigida - 35 kW/m^2

	Peak Heat Release Rate - O2 [kW]				Peak Heat Release Rate - CO2 [kW]			
35 kW/m^2	Average	Min.	Max.	Standard Deviation	Average	Min.	Max.	Standard Deviation
15 g	4.93	4.01	5.85	1.31	1.19	0.90	1.49	0.42
35 g	3.61	3.24	3.98	0.52	1.42	1.22	1.62	0.28
90 g	2.50	2.05	2.95	0.63	0.85	0.67	1.02	0.25

Table 119: Peak Heat Release Rate at ignition data for Open Basket Experiments - Pinus Rigida - 35 kW/m^2

C.1.4.4 Open Basket Experiments - Pinus Rigida - 50 kW/m^2

	Peak Heat Release Rate - O2 [kW]				Peak Heat Release Rate - CO2 [kW]			
35 kW/m^2	Average	Min.	Max.	Standard Deviation	Average	Min.	Max.	Standard Deviation
15 g	5.35	4.56	6.15	1.12	1.46	1.31	1.61	0.21
35 g	3.95	3.57	4.34	0.55	1.98	1.88	2.08	0.14
90 g	4.16	3.62	4.69	0.75	1.51	1.45	1.56	0.07

Table 120: Peak Heat Release Rate at ignition data for Open Basket Experiments - Pinus Rigida - 50 kW/m^2

C.1.4.5 Open Basket Experiments - Pinus Halepensis, Pinus Pinea, Pinus Pinaster - 25 kW/m^2

	Peak Heat Release Rate - O2 [kW]				Peak Heat Release Rate - CO2 [kW]			
Halepensis	Average	Min.	Max.	Standard Deviation	Average	Min.	Max.	Standard Deviation
10 g	5.65	5.47	5.84	0.26	1.27	1.26	1.28	0.02
15 g	5.79	4.30	7.28	2.10	0.98	0.91	1.05	0.10
20 g	5.00	4.70	5.30	0.42	2.66	2.36	2.97	0.43
Pinea	Average	Min.	Max.	Standard Deviation	Average	Min.	Max.	Standard Deviation
10 g	5.30	5.29	5.31	0.01	1.49	1.25	1.73	0.34
15 g	4.59	3.83	5.35	1.08	0.96	0.94	0.97	0.02
Pinaster	Average	Min.	Max.	Standard Deviation	Average	Min.	Max.	Standard Deviation
10 g	6.64	6.52	6.76	0.17	2.07	1.92	2.23	0.21
15 g	6.81	6.41	7.21	0.56	1.05	0.94	1.16	0.15

Table 121: Peak Heat Release Rate data for Open Basket Experiments - Pinus Halepensis, Pinus Pinea, Pinus Pinaster - 25 kW/m^2

C.2 Extracted Literature Data

C.2.1 Time to Ignition

Experimentalist	Mass [g]	Heat Flux [kW/m^2]	Species	Fuel Condition	Basket Condition	Time To Ignition [s]
Jervis	8	25	Halepensis	Wet	Open	25.19
Jervis	8	25	Nigra	Wet	Open	47.01
Jervis	8	25	Pinaster	Wet	Open	53.73
Jervis	8	25	Halepensis	Dry	Open	21.27
Jervis	8	25	Nigra	Dry	Open	36.38
Jervis	8	25	Pinaster	Dry	Open	57.09
Jervis	8	25	Halepensis	Wet	Open with Flow	87.31
Jervis	8	25	Nigra	Wet	Open with Flow	95.71
Jervis	8	25	Pinaster	Wet	Open with Flow	175.19
Jervis	8	25	Halepensis	Dry	Open with Flow	38.06
Jervis	8	25	Nigra	Dry	Open with Flow	51.49
Jervis	8	25	Pinaster	Dry	Open with Flow	302.80
Jervis	8	35	Halepensis	Wet	Open	13.84
Jervis	8	35	Nigra	Wet	Open	18.99
Jervis	8	35	Pinaster	Wet	Open	29.81
Jervis	8	35	Halepensis	Wet	Open with Flow	28.70
Jervis	8	35	Nigra	Wet	Open with Flow	31.90
Jervis	8	35	Pinaster	Wet	Open with Flow	41.52
Jervis	8	50	Halepensis	Wet	Open	10.61
Jervis	8	50	Nigra	Wet	Open	17.07
Jervis	8	50	Pinaster	Wet	Open	18.91
Jervis	8	50	Halepensis	Dry	Open	9.36
Jervis	8	50	Nigra	Dry	Open	14.76
Jervis	8	50	Pinaster	Dry	Open	17.27
Jervis	8	50	Halepensis	Wet	Open with Flow	12.83
Jervis	8	50	Nigra	Wet	Open with Flow	25.08

Experimentalist	Mass [g]	Heat Flux [kW/m^2]	Species	Fuel Condition	Basket Condition	Time To Ignition [s]
Jervis	8	50	Pinaster	Wet	Open with Flow	29.61
Jervis	8	50	Halepensis	Dry	Open with Flow	12.35
Jervis	8	50	Nigra	Dry	Open with Flow	16.78
Jervis	8	50	Pinaster	Dry	Open with Flow	26.33
Jervis	3	50	Halepensis	Wet	Open	14.04
Jervis	5	50	Halepensis	Wet	Open	11.96
Jervis	8	50	Halepensis	Wet	Open	12.95
Jervis	10	50	Halepensis	Wet	Open	9.97
Jervis	12	50	Halepensis	Wet	Open	10.95
Jervis	15	50	Halepensis	Wet	Open	10.98
Jervis	20	50	Halepensis	Wet	Open	11.98
Jervis	3	50	Nigra	Wet	Open	15.03
Jervis	5	50	Nigra	Wet	Open	11.01
Jervis	8	50	Nigra	Wet	Open	11.01
Jervis	10	50	Nigra	Wet	Open	10.02
Jervis	12	50	Nigra	Wet	Open	10.05
Jervis	15	50	Nigra	Wet	Open	12.04
Jervis	20	50	Nigra	Wet	Open	11.03
Jervis	3	50	Pinaster	Wet	Open	20.83
Jervis	5	50	Pinaster	Wet	Open	17.87
Jervis	8	50	Pinaster	Wet	Open	19.86
Jervis	10	50	Pinaster	Wet	Open	16.89
Jervis	12	50	Pinaster	Wet	Open	16.86
Jervis	15	50	Pinaster	Wet	Open	15.83
Jervis	20	50	Pinaster	Wet	Open	15.88
Jervis	3	50	Halepensis	Wet	Open with Flow	15.96
Jervis	5	50	Halepensis	Wet	Open with Flow	12.03
Jervis	8	50	Halepensis	Wet	Open with Flow	12.03
Jervis	10	50	Halepensis	Wet	Open with Flow	12.99
Jervis	12	50	Halepensis	Wet	Open with Flow	7.99
Jervis	15	50	Halepensis	Wet	Open with Flow	7.99
Jervis	20	50	Halepensis	Wet	Open with Flow	12.01
Mindykowski	5	15	Pinaster	Dry	Open	172.77
Mindykowski	5	17.5	Pinaster	Dry	Open	93.96
Mindykowski	5	20	Pinaster	Dry	Open	69.23
Mindykowski	5	22.5	Pinaster	Dry	Open	50.71
Mindykowski	5	25	Pinaster	Dry	Open	35.92
Mindykowski	5	27.5	Pinaster	Dry	Open	30.88
Mindykowski	5	30	Pinaster	Dry	Open	25.90
Mindykowski	10	13.8	Pinaster	Dry	Open	250.44
Mindykowski	10	15	Pinaster	Dry	Open	165.25
Mindykowski	10	17.5	Pinaster	Dry	Open	96.84
Mindykowski	10	20	Pinaster	Dry	Open	63.66
Mindykowski	10	22.5	Pinaster	Dry	Open	40.88
Mindykowski	10	25	Pinaster	Dry	Open	34.99
Mindykowski	10	27.5	Pinaster	Dry	Open	27.02
Mindykowski	10	30	Pinaster	Dry	Open	23.91
Mindykowski	20	12.5	Pinaster	Dry	Open	202.53
Mindykowski	20	15	Pinaster	Dry	Open	102.67
Mindykowski	20	17.5	Pinaster	Dry	Open	72.72
Mindykowski	20	20	Pinaster	Dry	Open	42.64
Mindykowski	20	22.5	Pinaster	Dry	Open	34.87

Experimentalist	Mass [g]	Heat Flux [kW/m^2]	Species	Fuel Condition	Basket Condition	Time To Ignition [s]
Mindykowski	20	25	Pinaster	Dry	Open	26.91
Mindykowski	20	27.5	Pinaster	Dry	Open	23.92
Mindykowski	20	30	Pinaster	Dry	Open	22.00
Bartoli	20	25	Halepensis	Wet	Closed	20.73
Bartoli	15	25	Halepensis	Wet	Closed	25.46
Bartoli	12	25	Halepensis	Wet	Closed	21.32
Bartoli	10	25	Halepensis	Wet	Closed	29.12
Bartoli	17	25	Laricio	Wet	Closed	27.21
Bartoli	15	25	Laricio	Wet	Closed	39.86
Bartoli	13	25	Laricio	Wet	Closed	34.47
Bartoli	11	25	Laricio	Wet	Closed	37.66
Bartoli	20	25	Pinaster	Wet	Closed	42.76
Bartoli	15	25	Pinaster	Wet	Closed	61.55
Bartoli	13	25	Pinaster	Wet	Closed	43.43
Bartoli	11	25	Pinaster	Wet	Closed	55.40
Bartoli	20	25	Halepensis	Wet	Open	21.38
Bartoli	15	25	Halepensis	Wet	Open	22.56
Bartoli	12	25	Halepensis	Wet	Open	21.96
Bartoli	10	25	Halepensis	Wet	Open	20.98
Bartoli	17	25	Laricio	Wet	Open	33.22
Bartoli	15	25	Laricio	Wet	Open	46.73
Bartoli	13	25	Laricio	Wet	Open	33.35
Bartoli	11	25	Laricio	Wet	Open	37.19
Bartoli	20	25	Pinaster	Wet	Open	45.58
Bartoli	15	25	Pinaster	Wet	Open	38.45
Bartoli	13	25	Pinaster	Wet	Open	55.41
Bartoli	11	25	Pinaster	Wet	Open	57.40
Bartoli	20	25	Halepensis	Wet	Open with Flow	22.34
Bartoli	15	25	Halepensis	Wet	Open with Flow	50.79
Bartoli	12	25	Halepensis	Wet	Open with Flow	53.15
Bartoli	10	25	Halepensis	Wet	Open with Flow	45.56
Bartoli	17	25	Laricio	Wet	Open with Flow	61.15
Bartoli	15	25	Laricio	Wet	Open with Flow	89.41
Bartoli	13	25	Laricio	Wet	Open with Flow	70.77
Bartoli	11	25	Laricio	Wet	Open with Flow	76.61
Bartoli	20	25	Pinaster	Wet	Open with Flow	84.29
Bartoli	15	25	Pinaster	Wet	Open with Flow	93.39
Bartoli	13	25	Pinaster	Wet	Open with Flow	90.79
Bartoli	11	25	Pinaster	Wet	Open with Flow	88.66
Thomas	15	20	Rigida	Wet	Open	108.68
Thomas	15	30	Rigida	Wet	Open	38.90
Thomas	15	35	Rigida	Wet	Open	25.13
Thomas	15	40	Rigida	Wet	Open	20.50
Thomas	15	45	Rigida	Wet	Open	16.50
Thomas	15	50	Rigida	Wet	Open	13.67
Thomas	15	55	Rigida	Wet	Open	11.43
Thomas	15	60	Rigida	Wet	Open	10.76
Thomas	15	25	Rigida	Wet	Open with Flow	211.27
Thomas	15	30	Rigida	Wet	Open with Flow	54.40
Thomas	15	35	Rigida	Wet	Open with Flow	37.94
Thomas	15	40	Rigida	Wet	Open with Flow	24.58
Thomas	15	45	Rigida	Wet	Open with Flow	17.01

Experimentalist	Mass [g]	Heat Flux [kW/m^2]	Species	Fuel Condition	Basket Condition	Time To Ignition [s]
Thomas	15	50	Rigida	Wet	Open with Flow	12.83
Thomas	15	55	Rigida	Wet	Open with Flow	11.64
Thomas	15	60	Rigida	Wet	Open with Flow	9.66
Thomas	15	27.5	Rigida	Wet	Open with 'High' Flow	438.71
Thomas	15	30	Rigida	Wet	Open with 'High' Flow	105.36
Thomas	15	35	Rigida	Wet	Open with 'High' Flow	55.27
Thomas	15	40	Rigida	Wet	Open with 'High' Flow	32.26
Thomas	15	45	Rigida	Wet	Open with 'High' Flow	17.43
Thomas	15	50	Rigida	Wet	Open with 'High' Flow	15.31
Thomas	15	55	Rigida	Wet	Open with 'High' Flow	13.69
Thomas	15	60	Rigida	Wet	Open with 'High' Flow	10.07
Thomas	15	20	Strobus	Wet	Open	45.25
Thomas	15	30	Strobus	Wet	Open	19.24
Thomas	15	35	Strobus	Wet	Open	12.84
Thomas	15	40	Strobus	Wet	Open	11.70
Thomas	15	45	Strobus	Wet	Open	8.92
Thomas	15	50	Strobus	Wet	Open	8.28
Thomas	15	55	Strobus	Wet	Open	7.69
Thomas	15	60	Strobus	Wet	Open	5.89
Thomas	15	22.5	Strobus	Wet	Open with Flow	137.38
Thomas	15	25	Strobus	Wet	Open with Flow	82.27
Thomas	15	30	Strobus	Wet	Open with Flow	28.12
Thomas	15	35	Strobus	Wet	Open with Flow	19.94
Thomas	15	40	Strobus	Wet	Open with Flow	11.52
Thomas	15	45	Strobus	Wet	Open with Flow	8.48
Thomas	15	50	Strobus	Wet	Open with Flow	7.92
Thomas	15	55	Strobus	Wet	Open with Flow	6.52
Thomas	15	60	Strobus	Wet	Open with Flow	5.55
Thomas	15	25	Strobus	Wet	Open with 'High' Flow	282.29
Thomas	15	30	Strobus	Wet	Open with 'High' Flow	49.18
Thomas	15	35	Strobus	Wet	Open with 'High' Flow	29.65
Thomas	15	40	Strobus	Wet	Open with 'High' Flow	10.11
Thomas	15	45	Strobus	Wet	Open with 'High' Flow	9.24
Thomas	15	50	Strobus	Wet	Open with 'High' Flow	8.74
Thomas	15	55	Strobus	Wet	Open with 'High' Flow	7.42
Thomas	15	60	Strobus	Wet	Open with 'High' Flow	5.90

Table 122: Extracted Literature Time to Ignition Data

C.2.2 Mass at Ignition

Author	Mass [g]	Heat Flux [kW/m^2]	Species	Fuel Condition	Basket Condition	Mass at Ignition [g]
Jervis	8	25	Halepensis	Wet	Open	0.67
Jervis	8	25	Nigra	Wet	Open	1.50
Jervis	8	25	Pinaster	Wet	Open	1.51
Jervis	8	25	Halepensis	Dry	Open	1.40
Jervis	8	25	Nigra	Dry	Open	1.65
Jervis	8	25	Pinaster	Dry	Open	1.75
Jervis	8	25	Halepensis	Wet	Open with Flow	0.57
Jervis	8	25	Nigra	Wet	Open with Flow	0.84
Jervis	8	25	Pinaster	Wet	Open with Flow	0.94
Jervis	8	25	Halepensis	Dry	Open with Flow	0.88
Jervis	8	25	Nigra	Dry	Open with Flow	0.71
Jervis	8	25	Pinaster	Dry	Open with Flow	1.86
Jervis	8	35	Halepensis	Wet	Open	0.80
Jervis	8	35	Nigra	Wet	Open	1.22
Jervis	8	35	Pinaster	Wet	Open	1.34
Jervis	8	35	Halepensis	Wet	Open with Flow	1.06
Jervis	8	35	Nigra	Wet	Open with Flow	1.97
Jervis	8	35	Pinaster	Wet	Open with Flow	1.48
Jervis	8	50	Halepensis	Wet	Open	0.88
Jervis	8	50	Nigra	Wet	Open	1.79
Jervis	8	50	Pinaster	Wet	Open	0.84
Jervis	8	50	Halepensis	Dry	Open	0.67
Jervis	8	50	Nigra	Dry	Open	1.17
Jervis	8	50	Pinaster	Dry	Open	1.66
Jervis	8	50	Halepensis	Wet	Open with Flow	0.53
Jervis	8	50	Nigra	Wet	Open with Flow	0.84
Jervis	8	50	Pinaster	Wet	Open with Flow	1.06
Jervis	8	50	Halepensis	Dry	Open with Flow	0.64
Jervis	8	50	Nigra	Dry	Open with Flow	0.94
Jervis	8	50	Pinaster	Dry	Open with Flow	1.72
Jervis	3	50	Halepensis	Wet	Open	0.75
Jervis	5	50	Halepensis	Wet	Open	0.41
Jervis	8	50	Halepensis	Wet	Open	0.32
Jervis	10	50	Halepensis	Wet	Open	0.19
Jervis	12	50	Halepensis	Wet	Open	0.22
Jervis	15	50	Halepensis	Wet	Open	0.17
Jervis	20	50	Halepensis	Wet	Open	0.19
Jervis	3	50	Nigra	Wet	Open	0.52
Jervis	5	50	Nigra	Wet	Open	0.36
Jervis	8	50	Nigra	Wet	Open	0.28
Jervis	10	50	Nigra	Wet	Open	0.22
Jervis	12	50	Nigra	Wet	Open	0.18
Jervis	15	50	Nigra	Wet	Open	0.20
Jervis	20	50	Nigra	Wet	Open	0.18
Jervis	3	50	Pinaster	Wet	Open	0.68
Jervis	5	50	Pinaster	Wet	Open	0.36
Jervis	8	50	Pinaster	Wet	Open	0.35
Jervis	10	50	Pinaster	Wet	Open	0.24
Jervis	12	50	Pinaster	Wet	Open	0.32
Jervis	15	50	Pinaster	Wet	Open	0.31

Author	Mass [g]	Heat Flux [kW/m^2]	Species	Fuel Condition	Basket Condition	Mass at Ignition [g]
Jervis	20	50	Pinaster	Wet	Open	0.21
Jervis	3	50	Halepensis	Wet	Open with Flow	0.75
Jervis	5	50	Halepensis	Wet	Open with Flow	0.32
Jervis	8	50	Halepensis	Wet	Open with Flow	0.44
Jervis	10	50	Halepensis	Wet	Open with Flow	0.34
Jervis	12	50	Halepensis	Wet	Open with Flow	0.17
Jervis	15	50	Halepensis	Wet	Open with Flow	0.22
Jervis	20	50	Halepensis	Wet	Open with Flow	0.24
Consalvi	20	12.5	Pinaster	Dry	Open	1.01
Consalvi	20	15	Pinaster	Dry	Open	0.88
Consalvi	20	17.5	Pinaster	Dry	Open	0.80
Consalvi	20	20	Pinaster	Dry	Open	0.65
Consalvi	20	22.5	Pinaster	Dry	Open	0.54
Consalvi	20	25	Pinaster	Dry	Open	0.48
Consalvi	20	27.5	Pinaster	Dry	Open	0.40
Consalvi	20	30	Pinaster	Dry	Open	0.37
Consalvi	10	15	Pinaster	Dry	Open	1.35
Consalvi	10	17.5	Pinaster	Dry	Open	0.98
Consalvi	10	20	Pinaster	Dry	Open	0.59
Consalvi	10	22.5	Pinaster	Dry	Open	0.53
Consalvi	10	25	Pinaster	Dry	Open	0.51
Consalvi	10	27.5	Pinaster	Dry	Open	0.45
Consalvi	10	30	Pinaster	Dry	Open	0.40

Table 123: Extracted Literature Mass at Ignition Data

C.2.3 Mass Loss Rate at Ignition

Author	Mass [g]	Heat Flux [kW/m^2]	Species	Fuel Condition	Basket Condition	Mass Loss Rate at Ignition [g/s]
Jervis	8	25	Halepensis	Wet	Open	0.14
Jervis	8	25	Nigra	Wet	Open	0.16
Jervis	8	25	Pinaster	Wet	Open	0.18
Jervis	8	25	Halepensis	Dry	Open	0.15
Jervis	8	25	Nigra	Dry	Open	0.18
Jervis	8	25	Pinaster	Dry	Open	0.14
Jervis	8	25	Halepensis	Wet	Open with Flow	0.16
Jervis	8	25	Nigra	Wet	Open with Flow	0.13
Jervis	8	25	Pinaster	Wet	Open with Flow	0.11
Jervis	8	25	Halepensis	Dry	Open with Flow	0.21
Jervis	8	25	Nigra	Dry	Open with Flow	0.13
Jervis	8	25	Pinaster	Dry	Open with Flow	0.12
Jervis	8	35	Halepensis	Wet	Open	0.15
Jervis	8	35	Nigra	Wet	Open	0.23
Jervis	8	35	Pinaster	Wet	Open	0.21
Jervis	8	35	Halepensis	Wet	Open with Flow	0.21
Jervis	8	35	Nigra	Wet	Open with Flow	0.31
Jervis	8	35	Pinaster	Wet	Open with Flow	0.16
Jervis	8	50	Halepensis	Wet	Open	0.19
Jervis	8	50	Nigra	Wet	Open	0.24
Jervis	8	50	Pinaster	Wet	Open	0.21
Jervis	8	50	Halepensis	Dry	Open	0.24

Author	Mass [g]	Heat Flux [kW/m^2]	Species	Fuel Condition	Basket Condition	Mass Loss Rate at Ignition [g/s]
Jervis	8	50	Nigra	Dry	Open	0.24
Jervis	8	50	Pinaster	Dry	Open	0.25
Jervis	8	50	Halepensis	Wet	Open with Flow	0.24
Jervis	8	50	Nigra	Wet	Open with Flow	0.12
Jervis	8	50	Pinaster	Wet	Open with Flow	0.21
Jervis	8	50	Halepensis	Dry	Open with Flow	0.29
Jervis	8	50	Nigra	Dry	Open with Flow	0.19
Jervis	8	50	Pinaster	Dry	Open with Flow	0.23
Jervis	3	50	Halepensis	Wet	Open	0.11
Jervis	5	50	Halepensis	Wet	Open	0.21
Jervis	8	50	Halepensis	Wet	Open	0.21
Jervis	10	50	Halepensis	Wet	Open	0.21
Jervis	12	50	Halepensis	Wet	Open	0.24
Jervis	15	50	Halepensis	Wet	Open	0.24
Jervis	20	50	Halepensis	Wet	Open	0.26
Jervis	3	50	Nigra	Wet	Open	0.15
Jervis	5	50	Nigra	Wet	Open	0.20
Jervis	8	50	Nigra	Wet	Open	0.25
Jervis	10	50	Nigra	Wet	Open	0.25
Jervis	12	50	Nigra	Wet	Open	0.22
Jervis	15	50	Nigra	Wet	Open	0.28
Jervis	20	50	Nigra	Wet	Open	0.27
Jervis	3	50	Pinaster	Wet	Open	0.16
Jervis	5	50	Pinaster	Wet	Open	0.15
Jervis	8	50	Pinaster	Wet	Open	0.22
Jervis	10	50	Pinaster	Wet	Open	0.16
Jervis	12	50	Pinaster	Wet	Open	0.25
Jervis	15	50	Pinaster	Wet	Open	0.24
Jervis	20	50	Pinaster	Wet	Open	0.26
Jervis	3	50	Halepensis	Wet	Open with Flow	0.07
Jervis	5	50	Halepensis	Wet	Open with Flow	0.22
Jervis	8	50	Halepensis	Wet	Open with Flow	0.26
Jervis	10	50	Halepensis	Wet	Open with Flow	0.30
Jervis	12	50	Halepensis	Wet	Open with Flow	0.25
Jervis	15	50	Halepensis	Wet	Open with Flow	0.29
Jervis	20	50	Halepensis	Wet	Open with Flow	0.36

Table 124: Extracted Literature Mass Loss Rate at Ignition Data

C.2.4 Mass Loss rate at Flameout

Author	Mass [g]	Heat Flux [kW/m^2]	Species	Fuel Condition	Basket Condition	Mass Loss Rate at Flameout [g/s]
Jervis	8	25	Halepensis	Wet	Open	0.078
Jervis	8	25	Nigra	Wet	Open	0.112
Jervis	8	25	Pinaster	Wet	Open	0.199
Jervis	8	25	Halepensis	Dry	Open	0.048
Jervis	8	25	Nigra	Dry	Open	0.189
Jervis	8	25	Pinaster	Dry	Open	0.176
Jervis	8	25	Halepensis	Wet	Open with Flow	0.153
Jervis	8	25	Nigra	Wet	Open with Flow	0.187
Jervis	8	25	Pinaster	Wet	Open with Flow	0.182

Author	Mass [g]	Heat Flux [kW/m^2]	Species	Fuel Condition	Basket Condition	Mass Loss Rate at Flameout [g/s]
Jervis	8	25	Halepensis	Dry	Open with Flow	0.208
Jervis	8	25	Nigra	Dry	Open with Flow	0.220
Jervis	8	25	Pinaster	Dry	Open with Flow	0.134
Jervis	8	35	Halepensis	Wet	Open	0.063
Jervis	8	35	Nigra	Wet	Open	0.190
Jervis	8	35	Pinaster	Wet	Open	0.137
Jervis	8	35	Halepensis	Wet	Open with Flow	0.163
Jervis	8	35	Nigra	Wet	Open with Flow	0.163
Jervis	8	35	Pinaster	Wet	Open with Flow	0.196
Jervis	8	50	Halepensis	Wet	Open	0.088
Jervis	8	50	Nigra	Wet	Open	0.160
Jervis	8	50	Pinaster	Wet	Open	0.166
Jervis	8	50	Halepensis	Dry	Open	0.093
Jervis	8	50	Nigra	Dry	Open	0.185
Jervis	8	50	Pinaster	Dry	Open	0.261
Jervis	8	50	Halepensis	Wet	Open with Flow	0.179
Jervis	8	50	Nigra	Wet	Open with Flow	0.244
Jervis	8	50	Pinaster	Wet	Open with Flow	0.256
Jervis	8	50	Halepensis	Dry	Open with Flow	0.298
Jervis	8	50	Nigra	Dry	Open with Flow	0.306
Jervis	8	50	Pinaster	Dry	Open with Flow	0.210
Jervis	3	50	Halepensis	Wet	Open	0.116
Jervis	5	50	Halepensis	Wet	Open	0.111
Jervis	8	50	Halepensis	Wet	Open	0.041
Jervis	10	50	Halepensis	Wet	Open	0.058
Jervis	12	50	Halepensis	Wet	Open	0.052
Jervis	15	50	Halepensis	Wet	Open	0.089
Jervis	20	50	Halepensis	Wet	Open	0.047
Jervis	3	50	Nigra	Wet	Open	0.094
Jervis	5	50	Nigra	Wet	Open	0.095
Jervis	8	50	Nigra	Wet	Open	0.096
Jervis	10	50	Nigra	Wet	Open	0.093
Jervis	12	50	Nigra	Wet	Open	0.067
Jervis	15	50	Nigra	Wet	Open	0.080
Jervis	20	50	Nigra	Wet	Open	0.055
Jervis	3	50	Pinaster	Wet	Open	0.156
Jervis	5	50	Pinaster	Wet	Open	0.112
Jervis	8	50	Pinaster	Wet	Open	0.117
Jervis	10	50	Pinaster	Wet	Open	0.084
Jervis	12	50	Pinaster	Wet	Open	0.129
Jervis	15	50	Pinaster	Wet	Open	0.130
Jervis	20	50	Pinaster	Wet	Open	0.107
Jervis	3	50	Halepensis	Wet	Open with Flow	0.072
Jervis	5	50	Halepensis	Wet	Open with Flow	0.148
Jervis	8	50	Halepensis	Wet	Open with Flow	0.311
Jervis	10	50	Halepensis	Wet	Open with Flow	0.229
Jervis	12	50	Halepensis	Wet	Open with Flow	0.086
Jervis	15	50	Halepensis	Wet	Open with Flow	0.075
Jervis	20	50	Halepensis	Wet	Open with Flow	0.055

Table 125: Extracted Literature Mass Loss Rate at Flameout Data

C.2.5 Peak Mass Loss Rate

Author	Mass [g]	Heat Flux [kW/m^2]	Species	Fuel Condition	Basket Condition	Peak Mass Loss Rate [g/s]
Jervis	8	25	Halepensis	Wet	Open	0.34
Jervis	8	25	Nigra	Wet	Open	0.34
Jervis	8	25	Pinaster	Wet	Open	0.40
Jervis	8	25	Halepensis	Dry	Open	0.29
Jervis	8	25	Nigra	Dry	Open	0.40
Jervis	8	25	Pinaster	Dry	Open	0.40
Jervis	8	25	Halepensis	Wet	Open with Flow	0.40
Jervis	8	25	Nigra	Wet	Open with Flow	0.33
Jervis	8	25	Pinaster	Wet	Open with Flow	0.30
Jervis	8	25	Halepensis	Dry	Open with Flow	0.44
Jervis	8	25	Nigra	Dry	Open with Flow	0.39
Jervis	8	25	Pinaster	Dry	Open with Flow	0.23
Jervis	8	35	Halepensis	Wet	Open	0.29
Jervis	8	35	Nigra	Wet	Open	0.36
Jervis	8	35	Pinaster	Wet	Open	0.38
Jervis	8	35	Halepensis	Wet	Open with Flow	0.46
Jervis	8	35	Nigra	Wet	Open with Flow	0.38
Jervis	8	35	Pinaster	Wet	Open with Flow	0.36
Jervis	8	50	Halepensis	Wet	Open	0.31
Jervis	8	50	Nigra	Wet	Open	0.44
Jervis	8	50	Pinaster	Wet	Open	0.46
Jervis	8	50	Halepensis	Dry	Open	0.45
Jervis	8	50	Nigra	Dry	Open	0.48
Jervis	8	50	Pinaster	Dry	Open	0.50
Jervis	8	50	Halepensis	Wet	Open with Flow	0.53
Jervis	8	50	Nigra	Wet	Open with Flow	0.54
Jervis	8	50	Pinaster	Wet	Open with Flow	0.51
Jervis	8	50	Halepensis	Dry	Open with Flow	0.56
Jervis	8	50	Nigra	Dry	Open with Flow	0.53
Jervis	8	50	Pinaster	Dry	Open with Flow	0.51
Jervis	3	50	Halepensis	Wet	Open	0.13
Jervis	5	50	Halepensis	Wet	Open	0.32
Jervis	8	50	Halepensis	Wet	Open	0.31
Jervis	10	50	Halepensis	Wet	Open	0.38
Jervis	12	50	Halepensis	Wet	Open	0.38
Jervis	15	50	Halepensis	Wet	Open	0.39
Jervis	20	50	Halepensis	Wet	Open	0.39
Jervis	3	50	Nigra	Wet	Open	0.20
Jervis	5	50	Nigra	Wet	Open	0.30
Jervis	8	50	Nigra	Wet	Open	0.41
Jervis	10	50	Nigra	Wet	Open	0.47
Jervis	12	50	Nigra	Wet	Open	0.48
Jervis	15	50	Nigra	Wet	Open	0.51
Jervis	20	50	Nigra	Wet	Open	0.49
Jervis	3	50	Pinaster	Wet	Open	0.19
Jervis	5	50	Pinaster	Wet	Open	0.32
Jervis	8	50	Pinaster	Wet	Open	0.36
Jervis	10	50	Pinaster	Wet	Open	0.48
Jervis	12	50	Pinaster	Wet	Open	0.41
Jervis	15	50	Pinaster	Wet	Open	0.42

Author	Mass [g]	Heat Flux [kW/m^2]	Species	Fuel Condition	Basket Condition	Peak Mass Loss Rate [g/s]
Jervis	20	50	Pinaster	Wet	Open	0.46
Jervis	3	50	Halepensis	Wet	Open with Flow	0.07
Jervis	5	50	Halepensis	Wet	Open with Flow	0.36
Jervis	8	50	Halepensis	Wet	Open with Flow	0.38
Jervis	10	50	Halepensis	Wet	Open with Flow	0.49
Jervis	12	50	Halepensis	Wet	Open with Flow	0.55
Jervis	15	50	Halepensis	Wet	Open with Flow	0.51
Houssami	6.4	50	Rigida	Wet	Open	0.74
Houssami	8.7	50	Rigida	Wet	Open	0.81
Houssami	11.4	50	Rigida	Wet	Open	0.82
Houssami	15	50	Rigida	Wet	Open	0.84
Bartoli	15	25	Halepensis	Wet	Closed	0.36

Table 126: Extracted Literature Peak Mass Loss Rate Data

C.2.6 Peak Heat Release Rate

Author	Mass [g]	Heat Flux [kW/m^2]	Species	Fuel Condition	Basket Condition	Peak Heat Release Rate [kW]
Jervis	8	25	Halepensis	Wet	Open	4.26
Jervis	8	25	Nigra	Wet	Open	6.61
Jervis	8	25	Pinaster	Wet	Open	7.47
Jervis	8	25	Halepensis	Dry	Open	1.41
Jervis	8	25	Nigra	Dry	Open	1.97
Jervis	8	25	Pinaster	Dry	Open	7.01
Jervis	8	25	Halepensis	Wet	Open with Flow	6.66
Jervis	8	25	Nigra	Wet	Open with Flow	7.08
Jervis	8	25	Pinaster	Wet	Open with Flow	7.56
Jervis	8	25	Halepensis	Dry	Open with Flow	2.45
Jervis	8	25	Nigra	Dry	Open with Flow	2.25
Jervis	8	25	Pinaster	Dry	Open with Flow	6.58
Jervis	8	35	Halepensis	Wet	Open	4.58
Jervis	8	35	Nigra	Wet	Open	6.99
Jervis	8	35	Pinaster	Wet	Open	6.72
Jervis	8	35	Halepensis	Wet	Open with Flow	7.29
Jervis	8	35	Nigra	Wet	Open with Flow	7.27
Jervis	8	35	Pinaster	Wet	Open with Flow	6.98
Jervis	8	50	Halepensis	Wet	Open	6.23
Jervis	8	50	Nigra	Wet	Open	7.41
Jervis	8	50	Pinaster	Wet	Open	6.84
Jervis	8	50	Halepensis	Dry	Open	4.62
Jervis	8	50	Nigra	Dry	Open	8.07
Jervis	8	50	Pinaster	Dry	Open	7.87
Jervis	8	50	Halepensis	Wet	Open with Flow	8.44
Jervis	8	50	Nigra	Wet	Open with Flow	5.73
Jervis	8	50	Pinaster	Wet	Open with Flow	6.88
Jervis	8	50	Halepensis	Dry	Open with Flow	6.05
Jervis	8	50	Nigra	Dry	Open with Flow	9.04
Jervis	8	50	Pinaster	Dry	Open with Flow	8.46
Jervis	3	50	Halepensis	Wet	Open	2.30
Jervis	5	50	Halepensis	Wet	Open	4.55
Jervis	8	50	Halepensis	Wet	Open	5.19

Author	Mass [g]	Heat Flux [kW/m^2]	Species	Fuel Condition	Basket Condition	Peak Heat Release Rate [kW]
Jervis	10	50	Halepensis	Wet	Open	5.66
Jervis	12	50	Halepensis	Wet	Open	6.33
Jervis	15	50	Halepensis	Wet	Open	6.65
Jervis	20	50	Halepensis	Wet	Open	6.47
Jervis	3	50	Nigra	Wet	Open	2.76
Jervis	5	50	Nigra	Wet	Open	4.73
Jervis	8	50	Nigra	Wet	Open	6.71
Jervis	10	50	Nigra	Wet	Open	8.00
Jervis	12	50	Nigra	Wet	Open	8.25
Jervis	15	50	Nigra	Wet	Open	8.42
Jervis	20	50	Nigra	Wet	Open	8.58
Jervis	3	50	Pinaster	Wet	Open	2.72
Jervis	5	50	Pinaster	Wet	Open	4.70
Jervis	8	50	Pinaster	Wet	Open	6.17
Jervis	10	50	Pinaster	Wet	Open	6.77
Jervis	12	50	Pinaster	Wet	Open	7.21
Jervis	15	50	Pinaster	Wet	Open	8.94
Jervis	20	50	Pinaster	Wet	Open	8.32
Jervis	3	50	Halepensis	Wet	Open with Flow	2.01
Jervis	5	50	Halepensis	Wet	Open with Flow	5.17
Jervis	8	50	Halepensis	Wet	Open with Flow	7.02
Jervis	10	50	Halepensis	Wet	Open with Flow	9.41
Jervis	12	50	Halepensis	Wet	Open with Flow	11.08
Jervis	15	50	Halepensis	Wet	Open with Flow	11.90
Jervis	20	50	Halepensis	Wet	Open with Flow	12.32
Houssami	6.4	50	Rigida	Wet	Open	5.34
Houssami	8.7	50	Rigida	Wet	Open	6.25
Houssami	11.4	50	Rigida	Wet	Open	7.30
Houssami	15	50	Rigida	Wet	Open	7.76
Bartoli	10	25	Halepensis	Wet	Open	7.79
Bartoli	12	25	Halepensis	Wet	Open	6.11
Bartoli	15	25	Halepensis	Wet	Open	7.21
Bartoli	11	25	Laricio	Wet	Open	7.27
Bartoli	13	25	Laricio	Wet	Open	6.72
Bartoli	17	25	Laricio	Wet	Open	8.36
Bartoli	13	25	Pinaster	Wet	Open	7.58
Bartoli	15	25	Pinaster	Wet	Open	9.23
Bartoli	20	25	Pinaster	Wet	Open	7.90
Bartoli	10	25	Halepensis	Wet	Open with Flow	11.93
Bartoli	12	25	Halepensis	Wet	Open with Flow	12.71
Bartoli	15	25	Halepensis	Wet	Open with Flow	11.32
Bartoli	11	25	Laricio	Wet	Open with Flow	10.62
Bartoli	13	25	Laricio	Wet	Open with Flow	11.51
Bartoli	17	25	Laricio	Wet	Open with Flow	10.52
Bartoli	13	25	Pinaster	Wet	Open with Flow	10.38
Bartoli	15	25	Pinaster	Wet	Open with Flow	9.37
Bartoli	20	25	Pinaster	Wet	Open with Flow	8.91

Table 127: Extracted Literature Peak Heat Release Rate Data

C.3 Closed Basket Experiments - 25 kW/m^2 - Pinus Rigida

C.3.1 7.5g Fuel Load

C.3.1.1 Mass

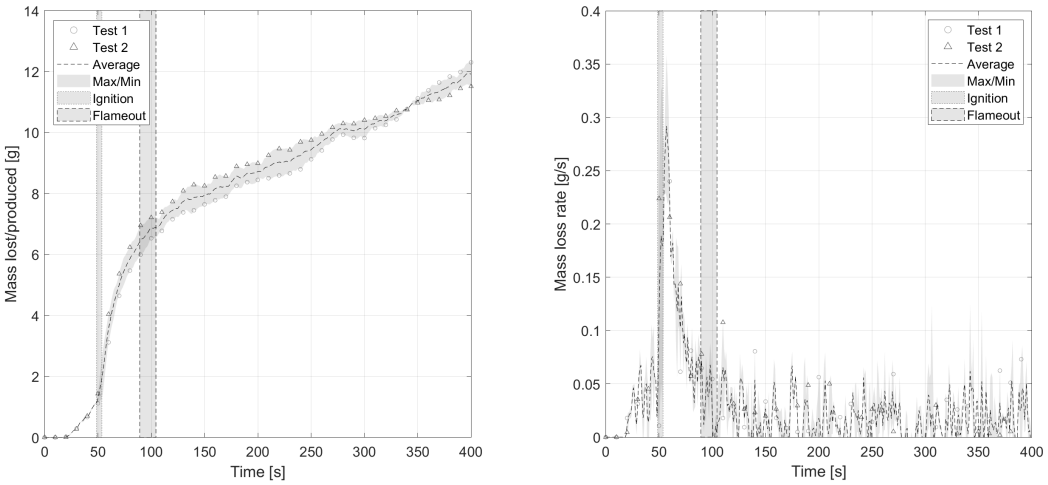

Figure 101: Closed Basket Experiments - Pinus Rigida - 7.5g Fuel Load: a)Mass b)Mass loss rate

C.3.1.2 Mass Loss Rate at Ignition and Flameout

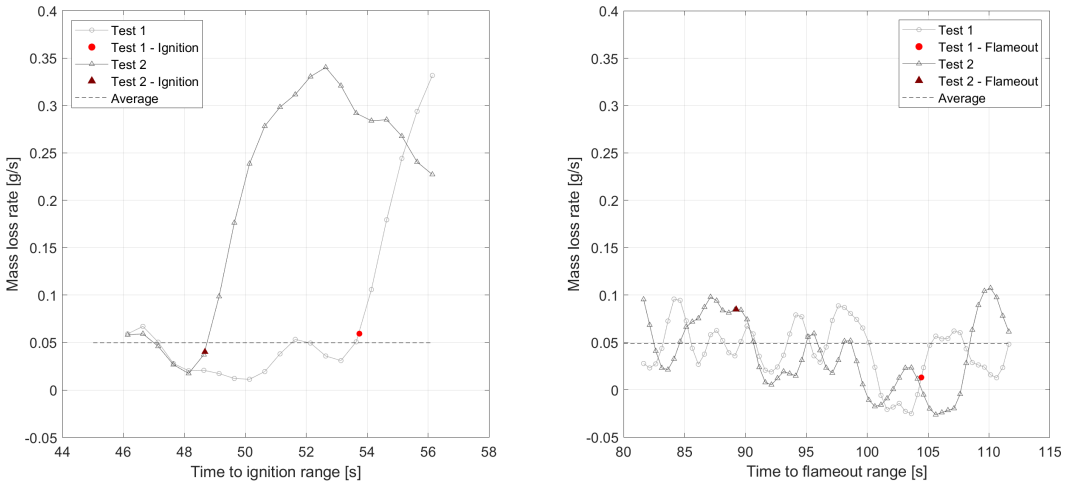

Figure 102: Closed Basket Experiments - Pinus Rigida - 7.5g Fuel Load: a)Mass loss rate at ignition b)Mass loss rate at flame out

C.3.1.3 Heat Release Rate

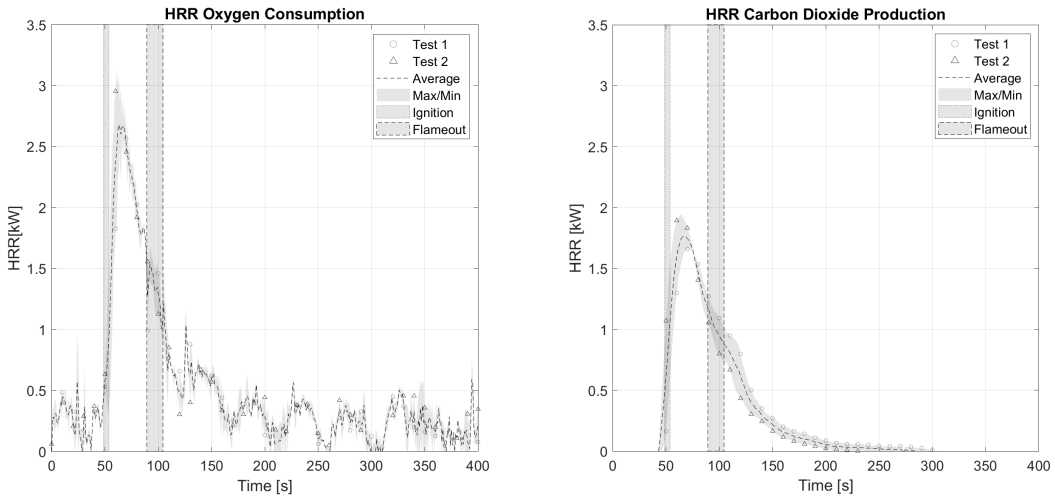

Figure 103: Closed Basket Experiments - Pinus Rigida - 7.5g Fuel Load: a)Heat release rate - Oxygen Consumption b)Heat release rate - CO2 Production

C.3.1.4 CO2 and CO

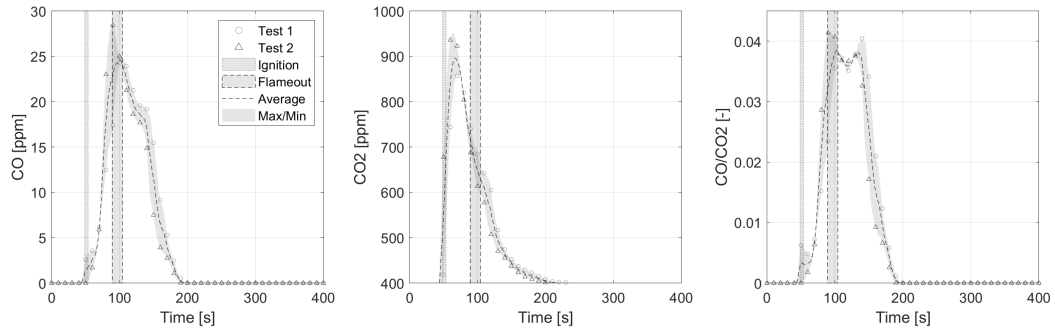

Figure 104: Closed Basket Experiments - Pinus Rigida - 7.5g Fuel Load: a)CO production b)CO2 production c)CO/CO2

C.3.2 15g Fuel Load

C.3.2.1 Mass

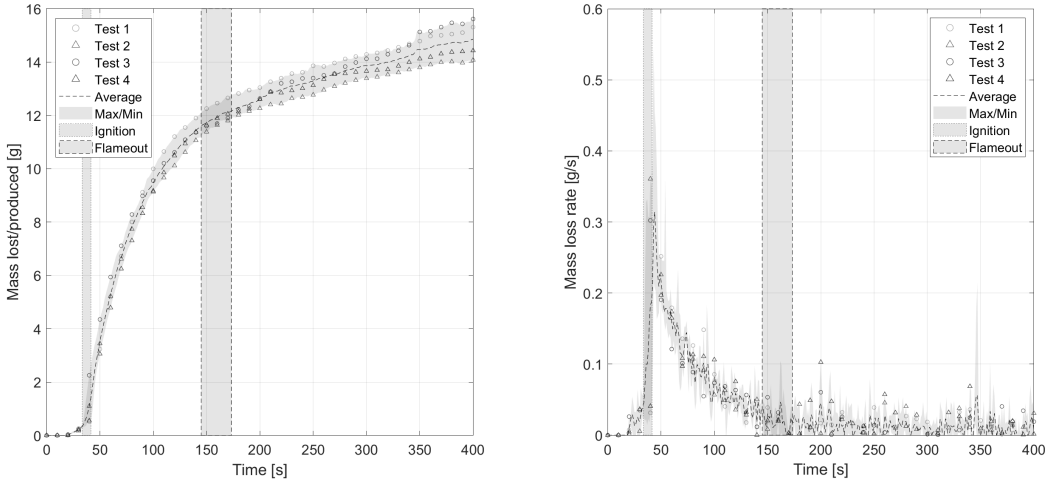

Figure 105: Closed Basket Experiments - Pinus Rigida - 15g Fuel Load: a)Mass b)Mass loss rate

C.3.2.2 Mass Loss Rate at Ignition and Flameout

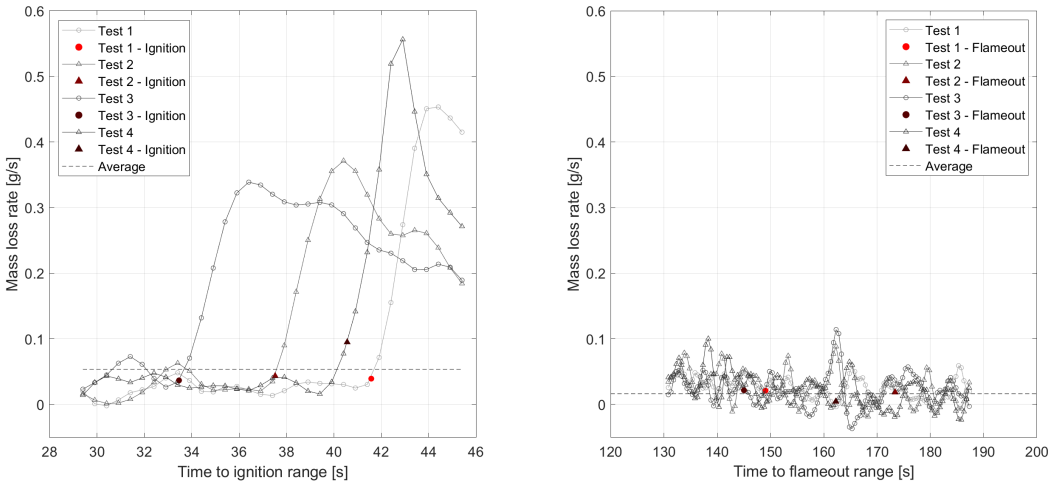

Figure 106: Closed Basket Experiments - Pinus Rigida - 15g Fuel Load: a)Mass loss rate at ignition b)Mass loss rate at flame out

C.3.2.3 Heat Release Rate

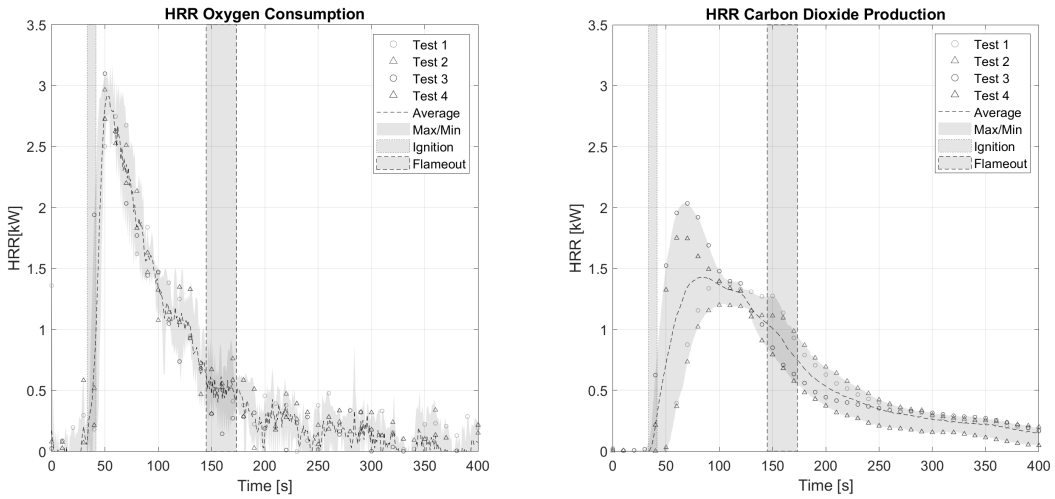

Figure 107: Closed Basket Experiments - Pinus Rigida - 15g Fuel Load: a)Heat release rate - Oxygen Consumption b)Heat release rate - CO2 Production

C.3.2.4 CO2 and CO

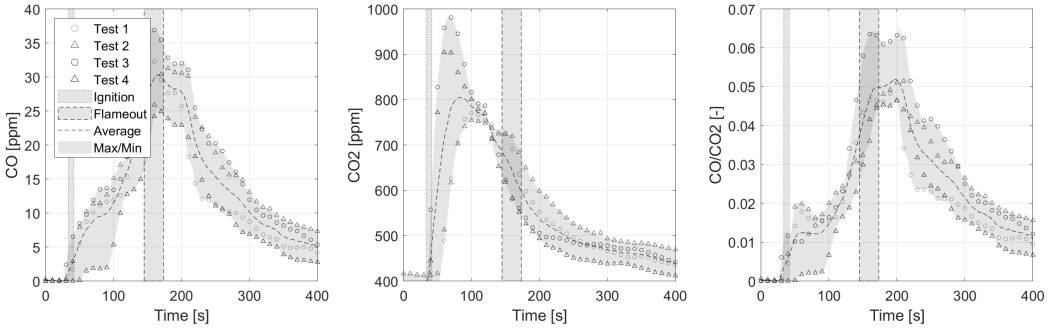

Figure 108: Closed Basket Experiments - Pinus Rigida - 15g Fuel Load: a)CO production b)CO2 production c)CO/CO2

C.3.3 25g Fuel Load

C.3.3.1 Mass

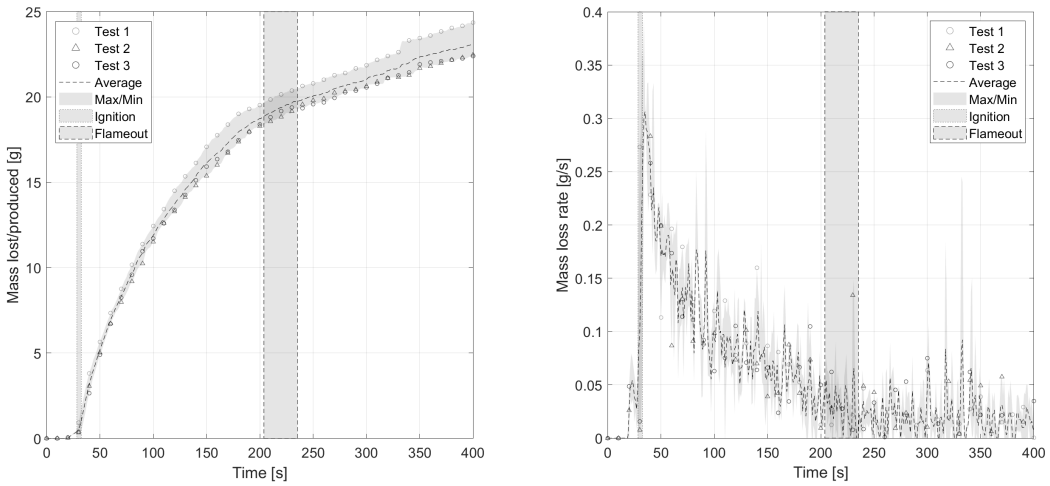

Figure 109: Closed Basket Experiments - Pinus Rigida - 25g Fuel Load: a)Mass b)Mass loss rate

C.3.3.2 Mass Loss Rate at Ignition and Flameout

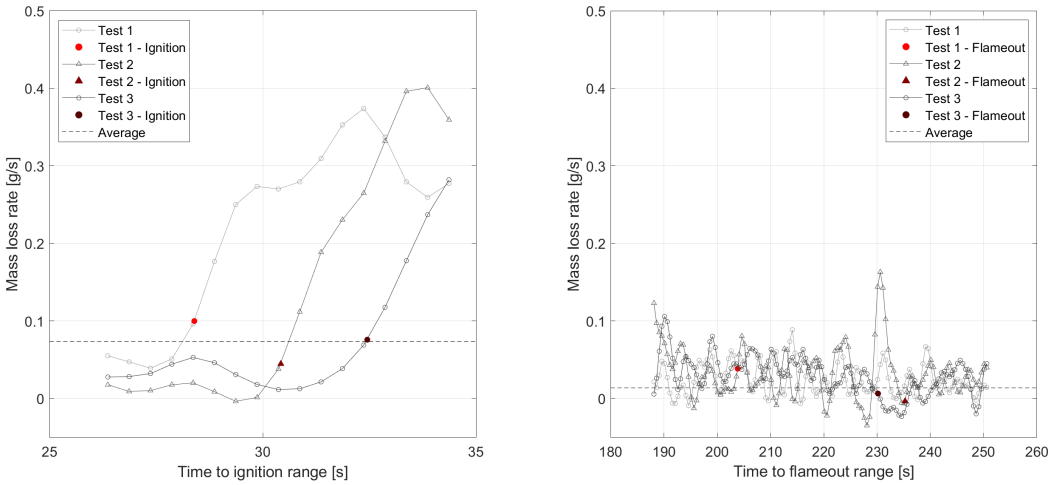

Figure 110: Closed Basket Experiments - Pinus Rigida - 25g Fuel Load: a)Mass loss rate at ignition b)Mass loss rate at flame out

C.3.3.3 Heat Release Rate

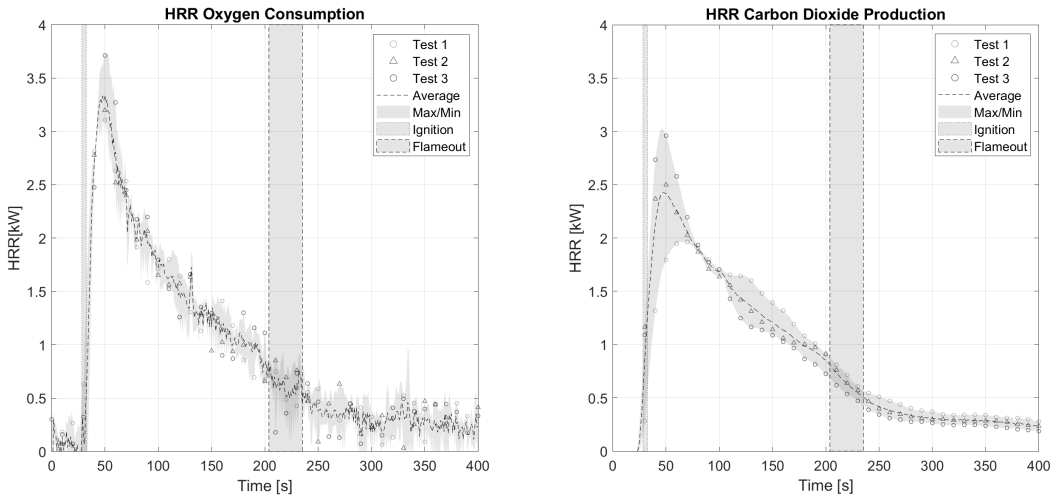

Figure 111: Closed Basket Experiments - Pinus Rigida - 25g Fuel Load: a)Heat release rate - Oxygen Consumption b)Heat release rate - CO2 Production

C.3.3.4 CO2 and CO

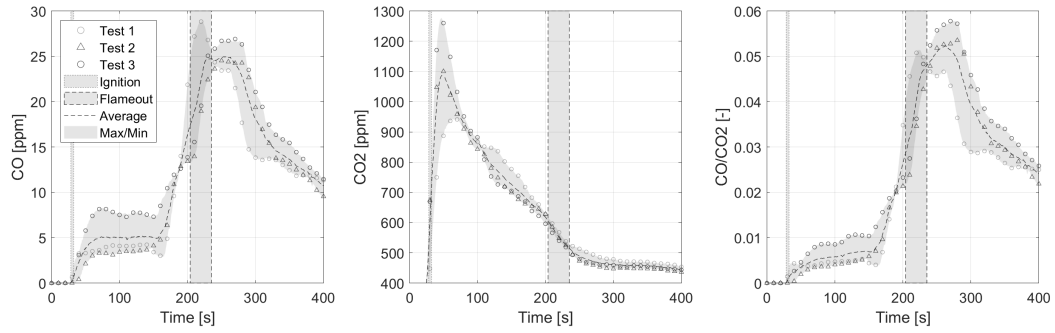

Figure 112: Closed Basket Experiments - Pinus Rigida - 25g Fuel Load: a)CO production b)CO2 production c)CO/CO2

C.3.4 35g Fuel Load

C.3.4.1 Mass

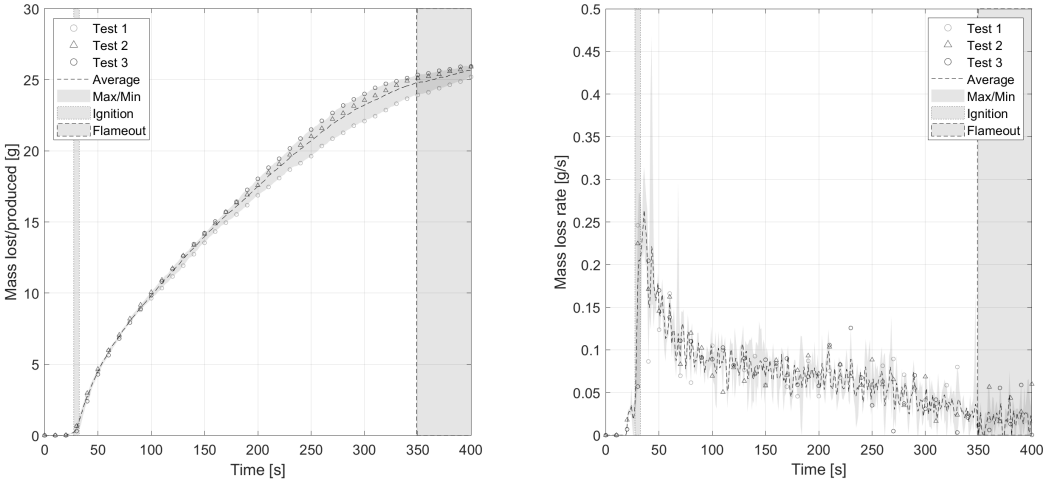

Figure 113: Closed Basket Experiments - Pinus Rigida - 35g Fuel Load: a)Mass b)Mass loss rate

C.3.4.2 Mass Loss Rate at Ignition and Flameout

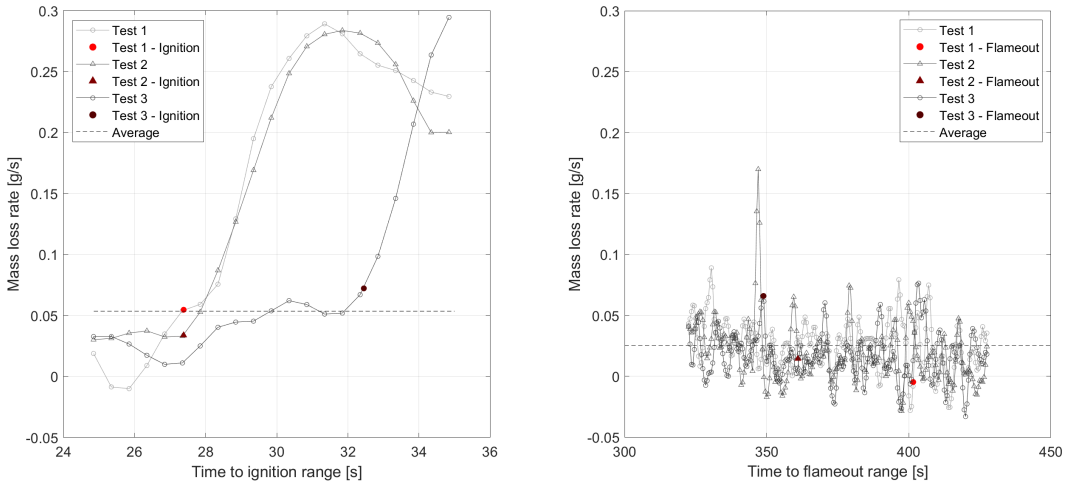

Figure 114: Closed Basket Experiments - Pinus Rigida - 35g Fuel Load: a)Mass loss rate at ignition b)Mass loss rate at flame out

C.3.4.3 Heat Release Rate

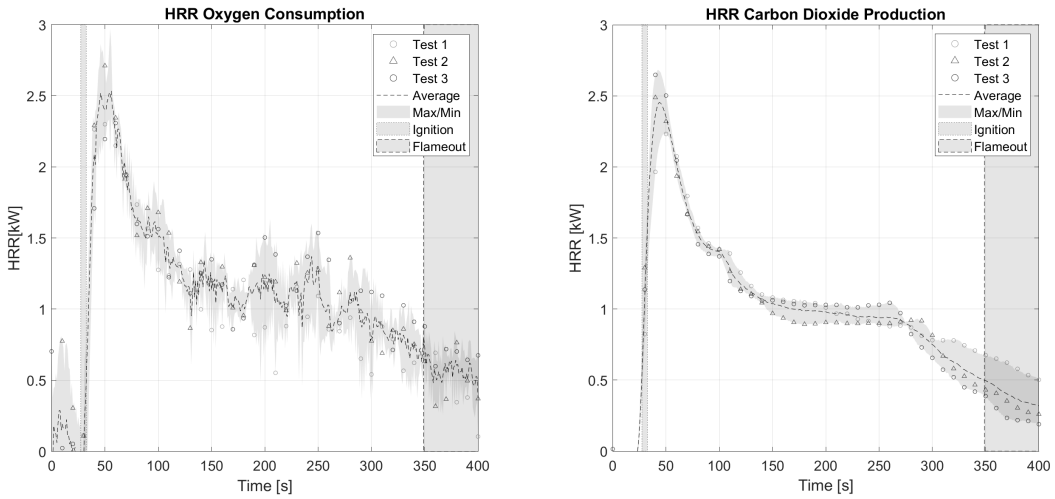

Figure 115: Closed Basket Experiments - Pinus Rigida - 35g Fuel Load: a)Heat release rate - Oxygen Consumption b)Heat release rate - CO2 Production

C.3.4.4 CO2 and CO

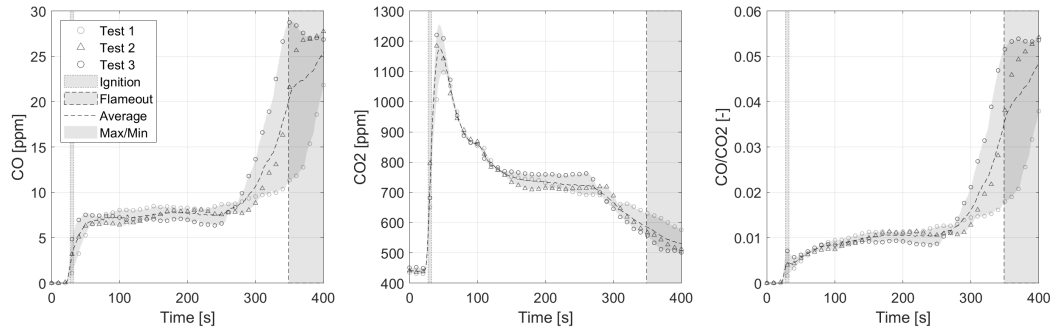

Figure 116: Closed Basket Experiments - Pinus Rigida - 35g Fuel Load: a)CO production b)CO2 production c)CO/CO2

C.3.5 60g Fuel Load

C.3.5.1 Mass

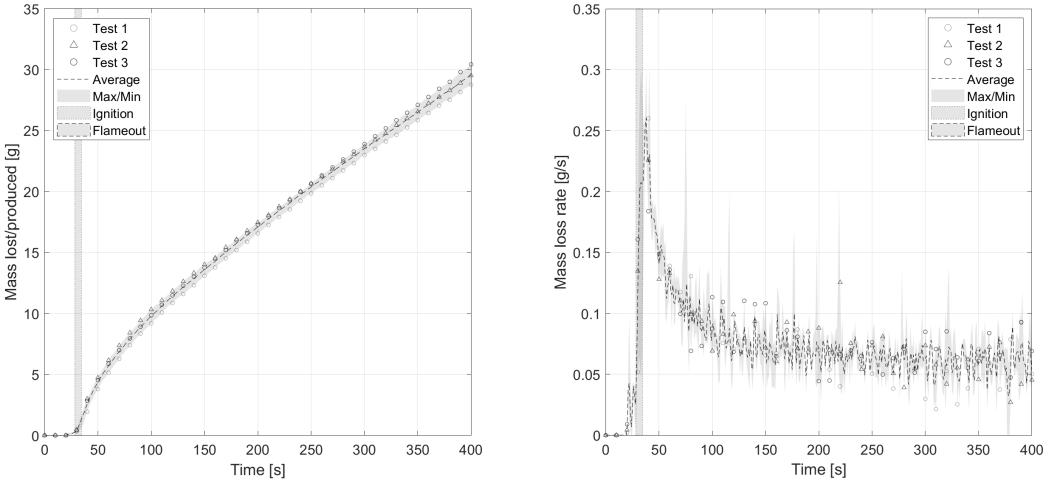

Figure 117: Closed Basket Experiments - Pinus Rigida - 60g Fuel Load: a)Mass b)Mass loss rate

C.3.5.2 Mass Loss Rate at Ignition and Flameout

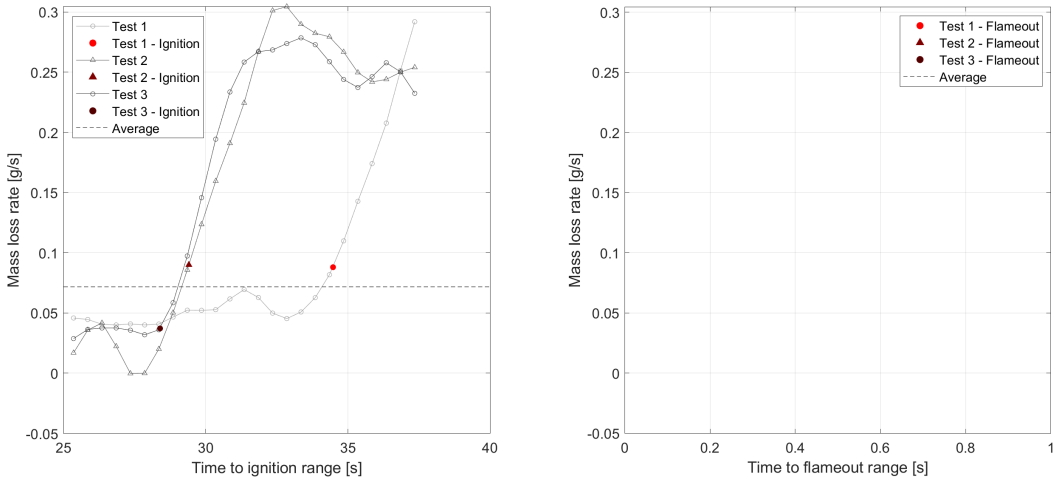

Figure 118: Closed Basket Experiments - Pinus Rigida - 60g Fuel Load: a)Mass loss rate at ignition b)Mass loss rate at flame out

C.3.5.3 Heat Release Rate

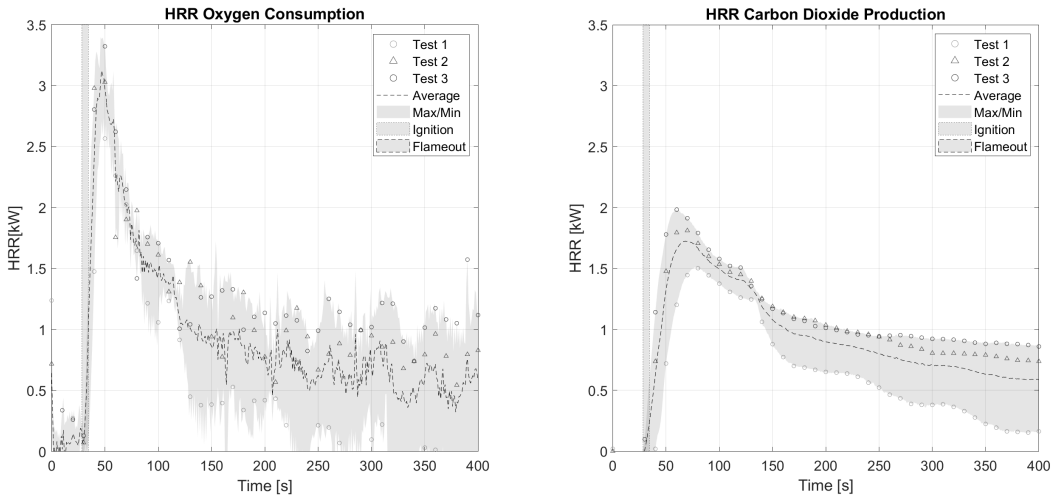

Figure 119: Closed Basket Experiments - Pinus Rigida - 60g Fuel Load: a)Heat release rate - Oxygen Consumption b)Heat release rate - CO2 Production

C.3.5.4 CO2 and CO

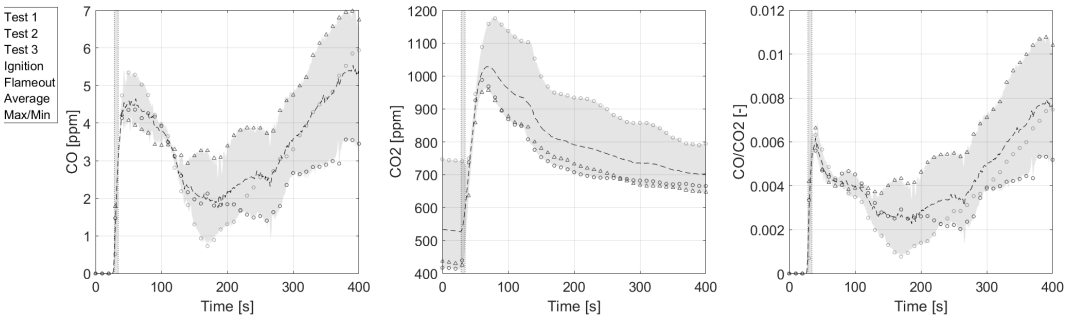

Figure 120: Closed Basket Experiments - Pinus Rigida - 60g Fuel Load: a)CO production b)CO2 production c)CO/CO2

C.3.6 95g Fuel Load

C.3.6.1 Mass

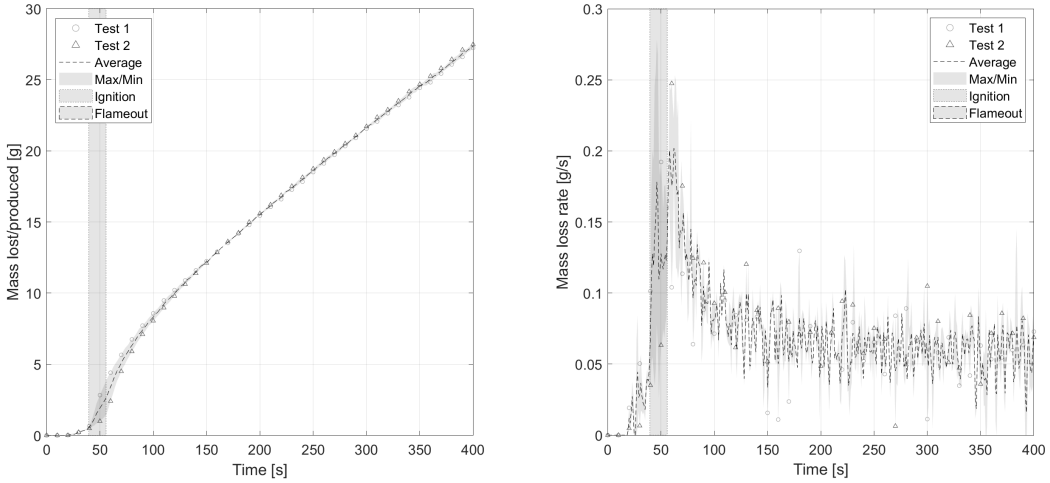

Figure 121: Closed Basket Experiments - Pinus Rigida - 95g Fuel Load: a)Mass b)Mass loss rate

C.3.6.2 Mass Loss Rate at Ignition and Flameout

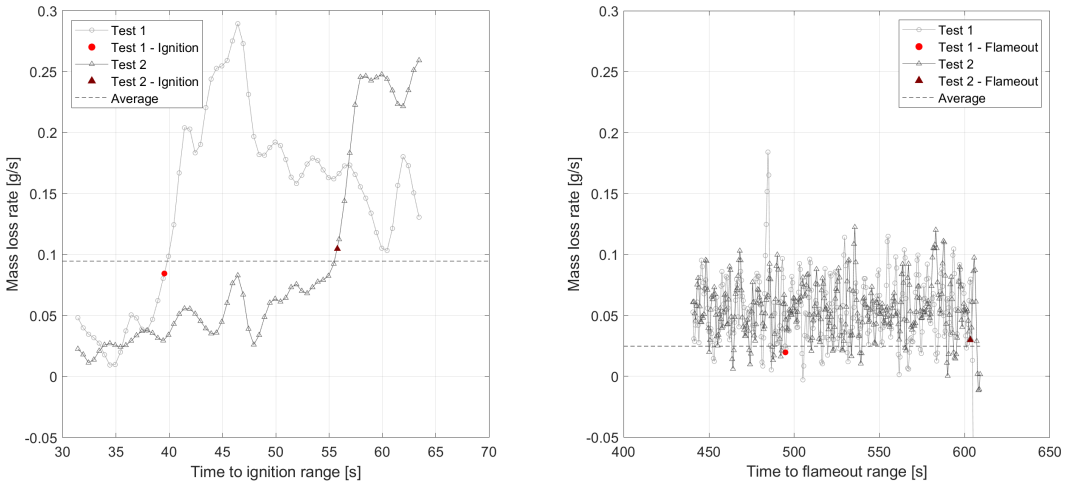

Figure 122: Closed Basket Experiments - Pinus Rigida - 95g Fuel Load: a)Mass loss rate at ignition b)Mass loss rate at flame out

C.3.6.3 Heat Release Rate

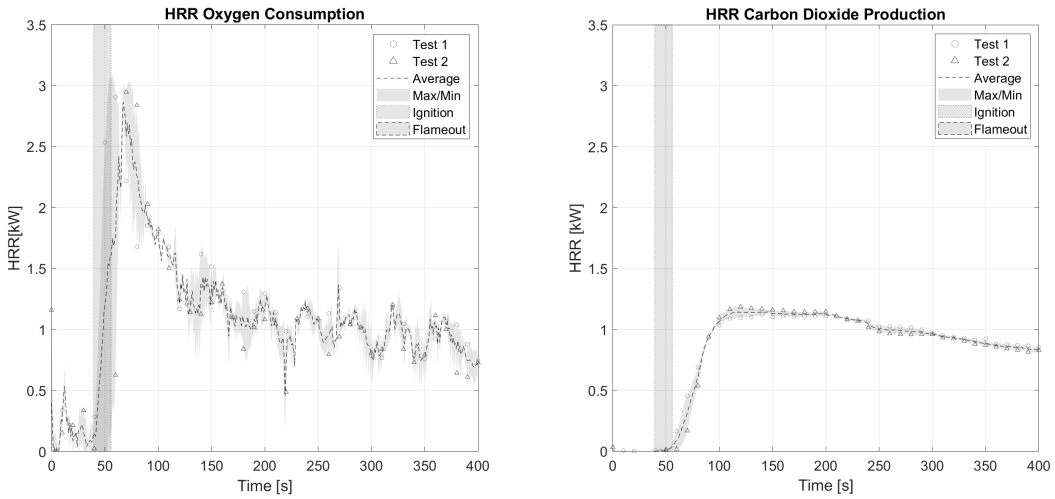

Figure 123: Closed Basket Experiments - Pinus Rigida - 95g Fuel Load: a)Heat release rate - Oxygen Consumption b)Heat release rate - CO2 Production

C.3.6.4 CO2 and CO

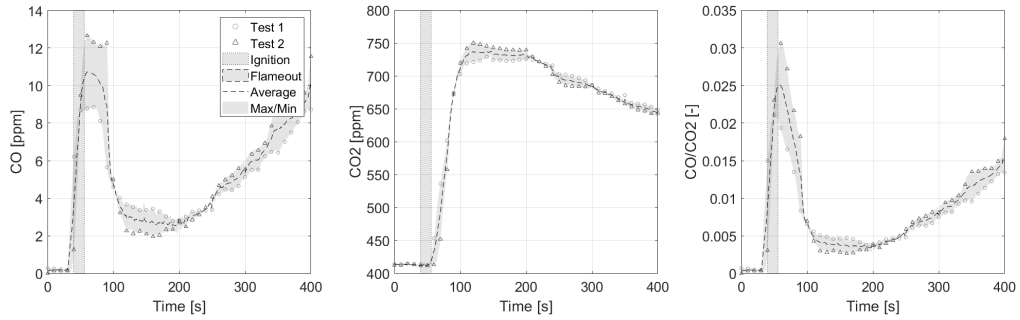

Figure 124: Closed Basket Experiments - Pinus Rigida - 95g Fuel Load: a)CO production b)CO2 production c)CO/CO2

C.3.7 120g Fuel Load

C.3.7.1 Mass

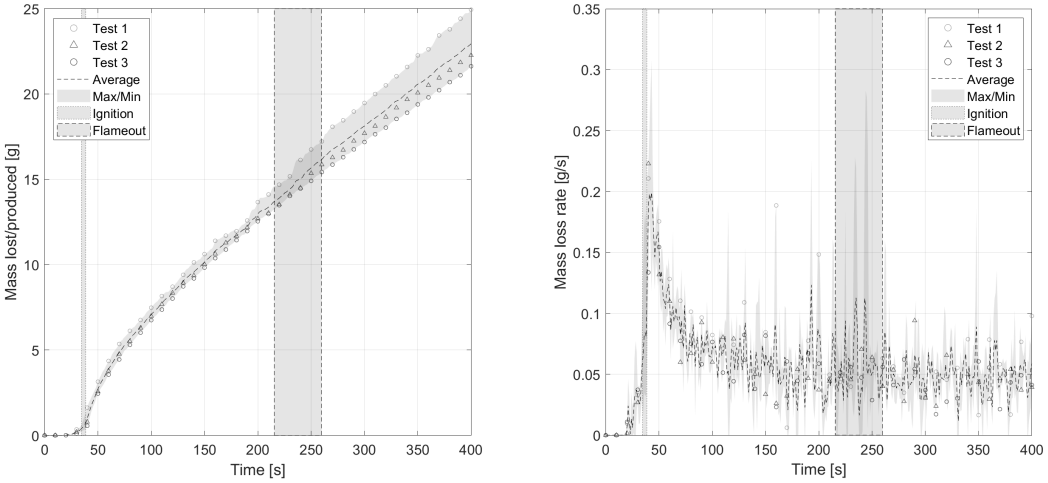

Figure 125: Closed Basket Experiments - Pinus Rigida - 120g Fuel Load: a)Mass b)Mass loss rate

C.3.7.2 Mass Loss Rate at Ignition and Flameout

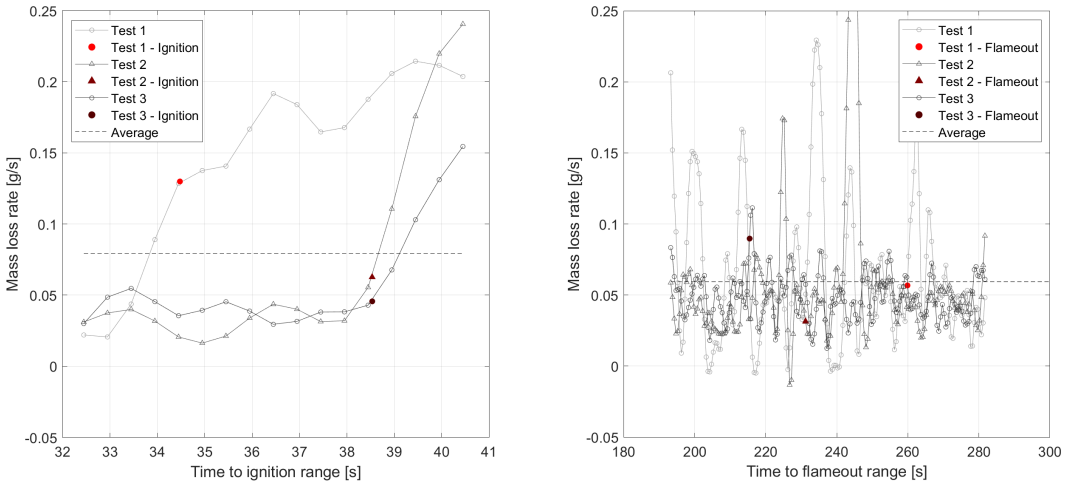

Figure 126: Closed Basket Experiments - Pinus Rigida - 120g Fuel Load: a)Mass loss rate at ignition b)Mass loss rate at flame out

C.3.7.3 Heat Release Rate

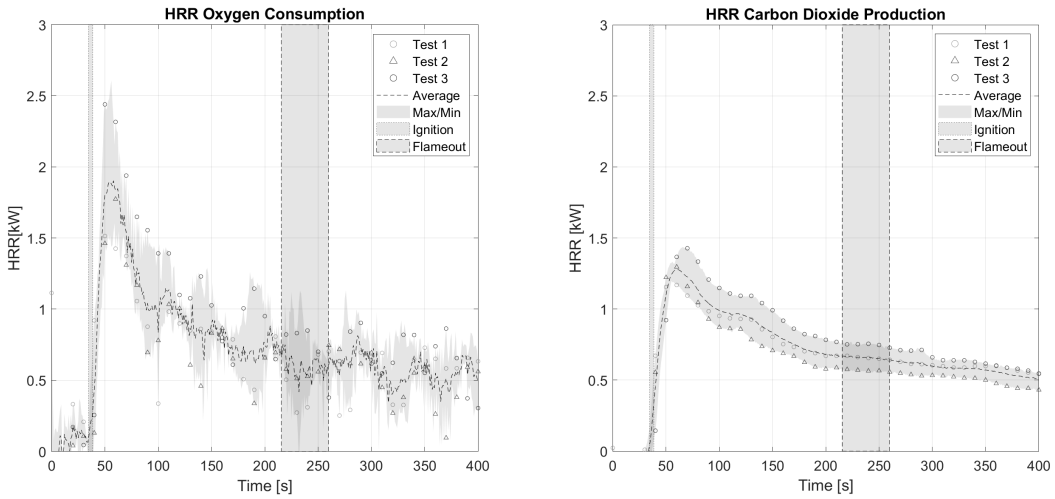

Figure 127: Closed Basket Experiments - Pinus Rigida - 120g Fuel Load: a)Heat release rate - Oxygen Consumption b)Heat release rate - CO2 Production

C.3.7.4 CO2 and CO

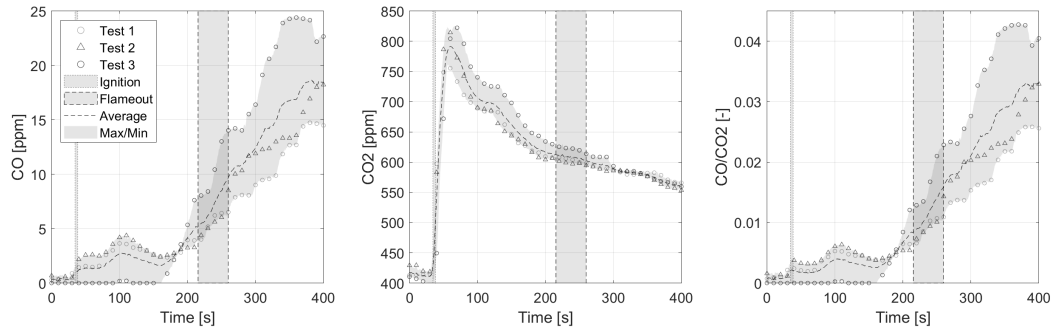

Figure 128: Closed Basket Experiments - Pinus Rigida - 120g Fuel Load: a)CO production b)CO2 production c)CO/CO2

C.4 Open Basket Experiments - 25 kW/m^2 - Pinus Rigida

C.4.1 10g Fuel Load

C.4.1.1 Mass

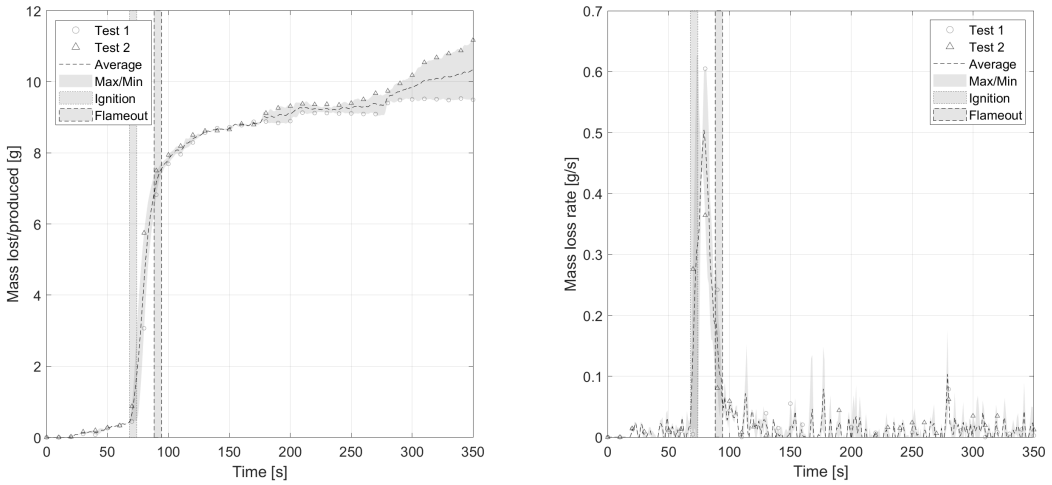

Figure 129: Open Basket Experiments - 25 kW/m^2 - Pinus Rigida - 10g Fuel Load: a)Mass b)Mass loss rate

C.4.1.2 Mass Loss Rate at Ignition and Flameout

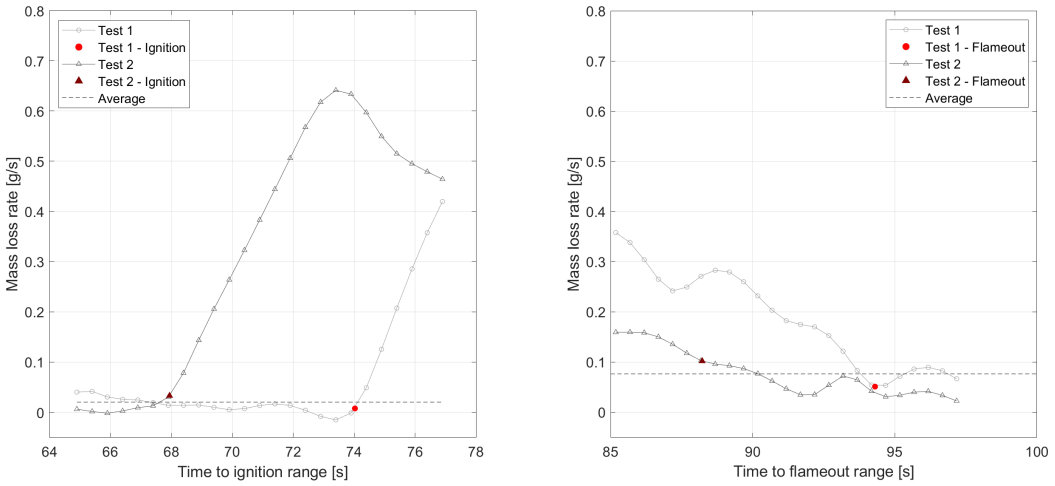

Figure 130: a)Mass loss rate at ignition b)Mass loss rate at flame out

C.4.1.3 Heat Release Rate

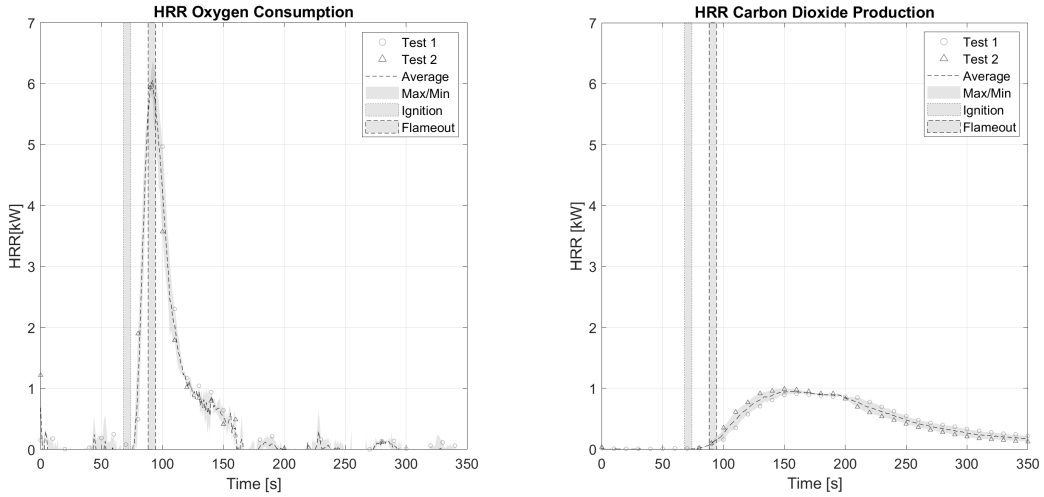

Figure 131: a)Heat release rate - Oxygen Consumption b)Heat release rate - CO2 Production

C.4.1.4 CO2 and CO

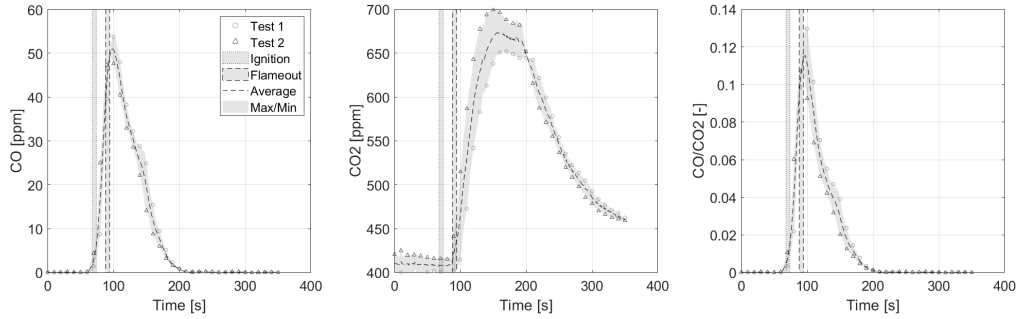

Figure 132: a)CO production b)CO2 production c)CO/CO2

C.4.2 15g Fuel Load

C.4.2.1 Mass

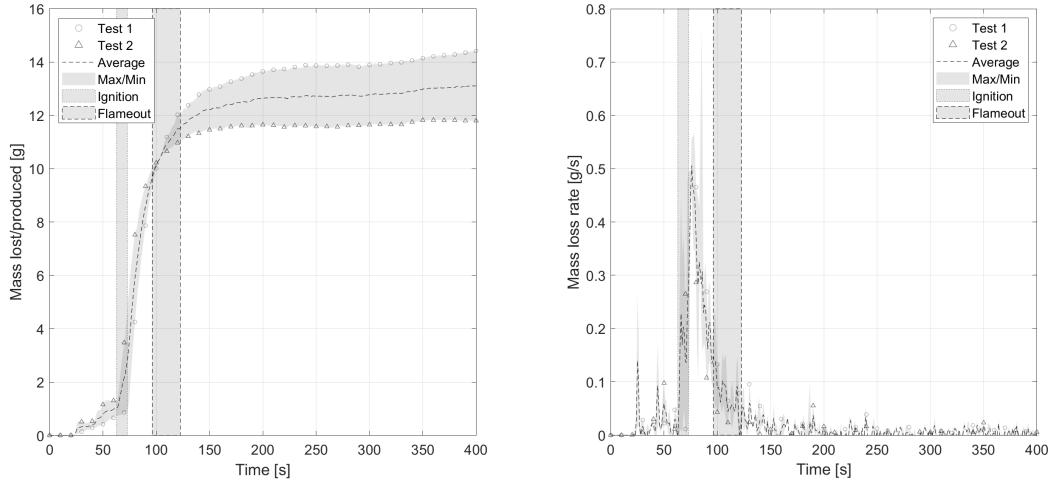

Figure 133: a)Mass b)Mass loss rate

C.4.2.2 Mass Loss Rate at Ignition and Flameout

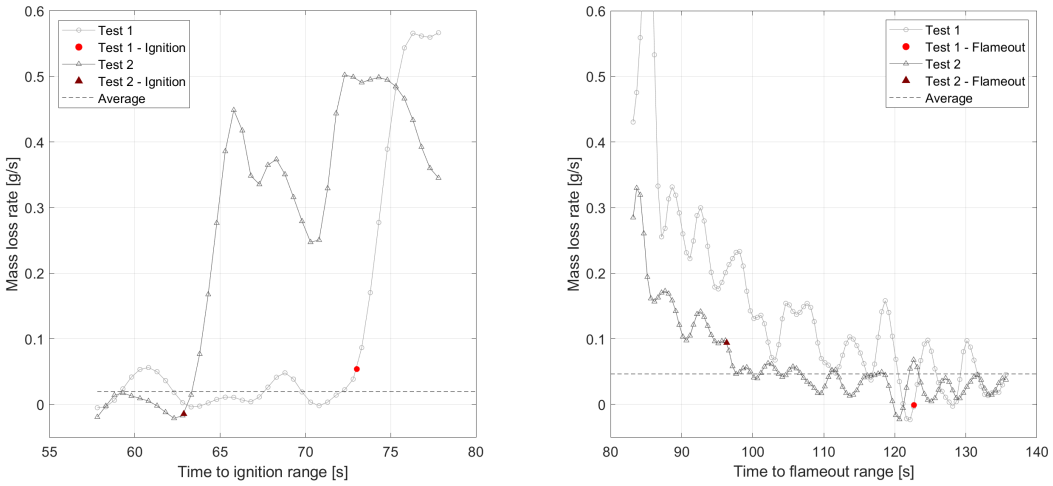

Figure 134: a)Mass loss rate at ignition b)Mass loss rate at flame out

C.4.2.3 Heat Release Rate

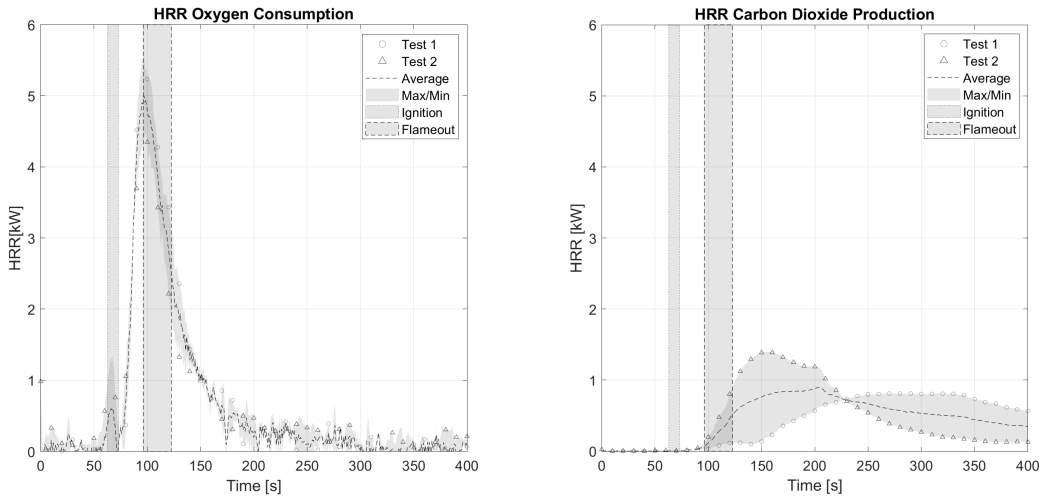

Figure 135: a)Heat release rate - Oxygen Consumption b)Heat release rate - CO2 Production

C.4.2.4 CO2 and CO

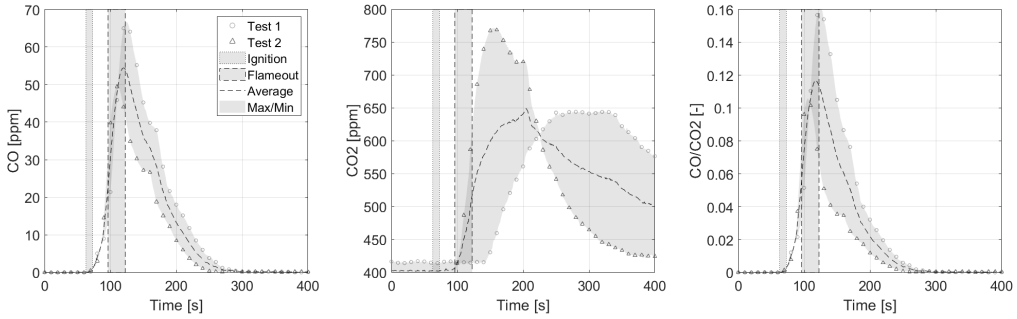

Figure 136: a)CO production b)CO2 production c)CO/CO2

C.4.3 20g Fuel Load

C.4.3.1 Mass

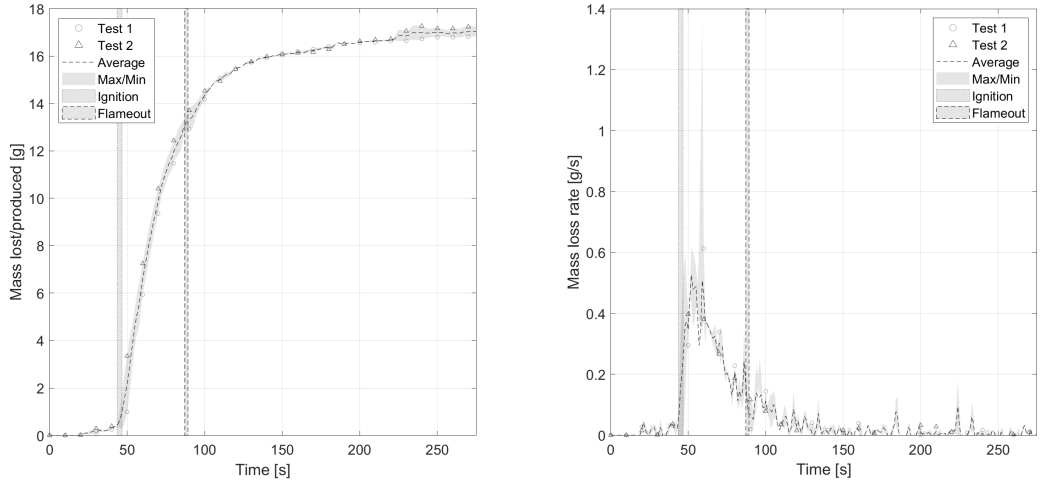

Figure 137: a)Mass b)Mass loss rate

C.4.3.2 Mass Loss Rate at Ignition and Flameout

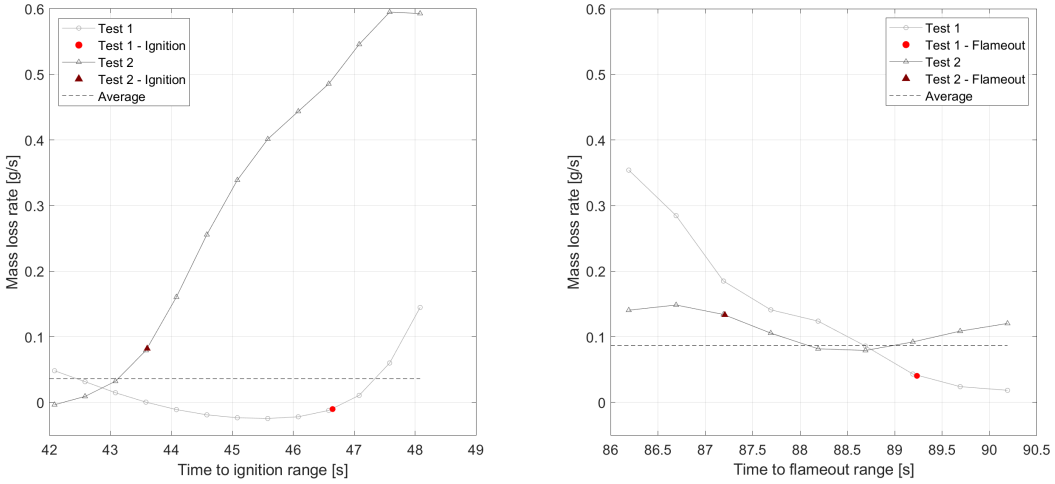

Figure 138: a)Mass loss rate at ignition b)Mass loss rate at flame out

C.4.3.3 Heat Release Rate

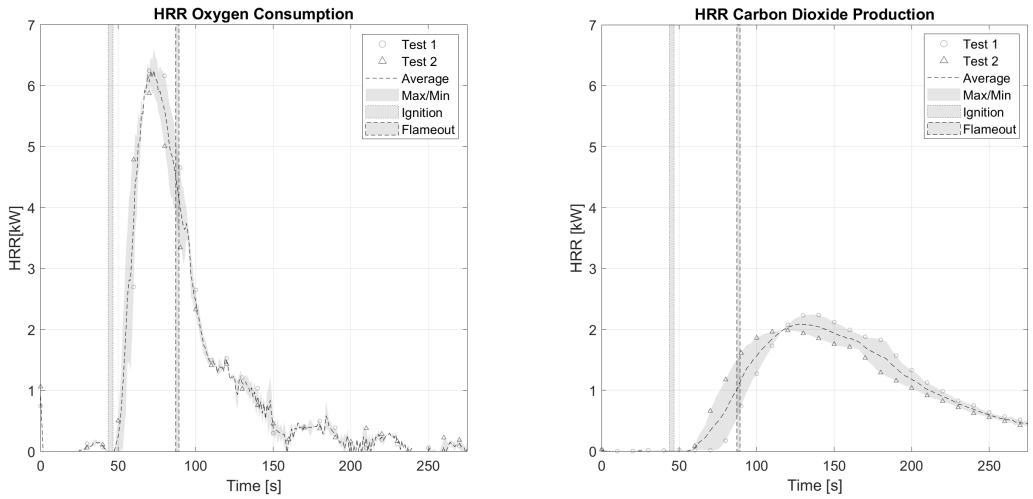

Figure 139: a)Heat release rate - Oxygen Consumption b)Heat release rate - CO2 Production

C.4.3.4 CO2 and CO

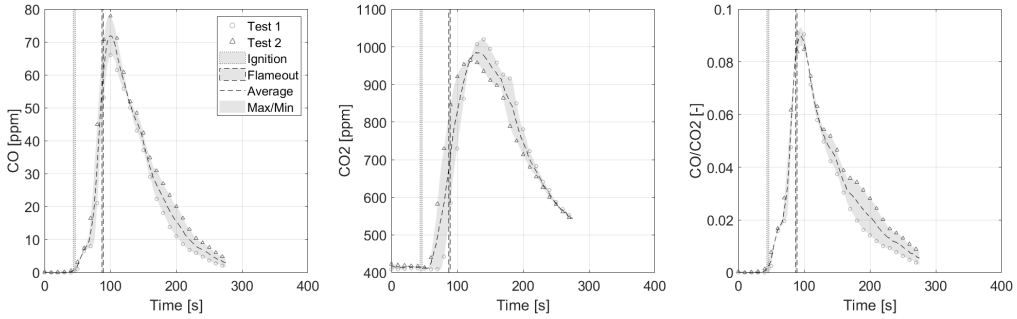

Figure 140: a)CO production b)CO2 production c)CO/CO2

C.4.4 25g Fuel Load

C.4.4.1 Mass

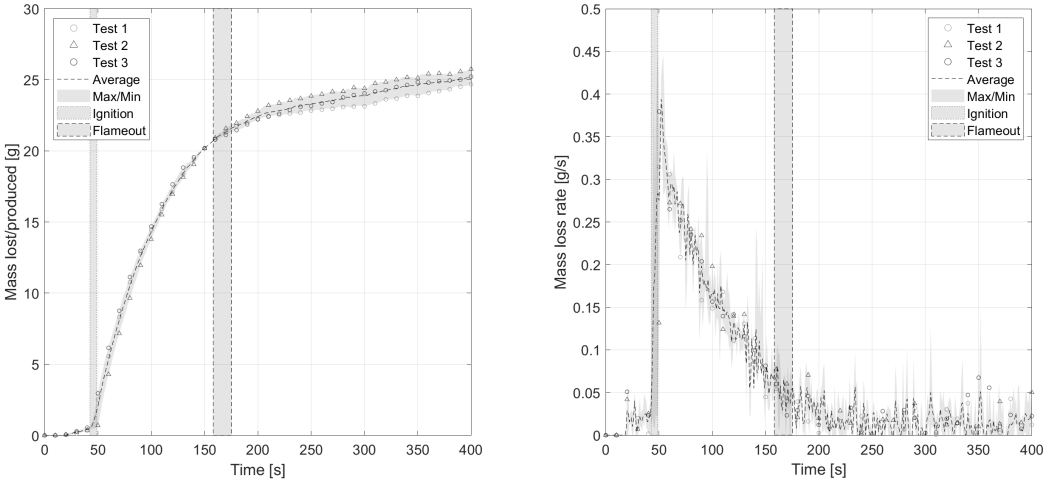

Figure 141: a)Mass b)Mass loss rate

C.4.4.2 Mass Loss Rate at Ignition and Flameout

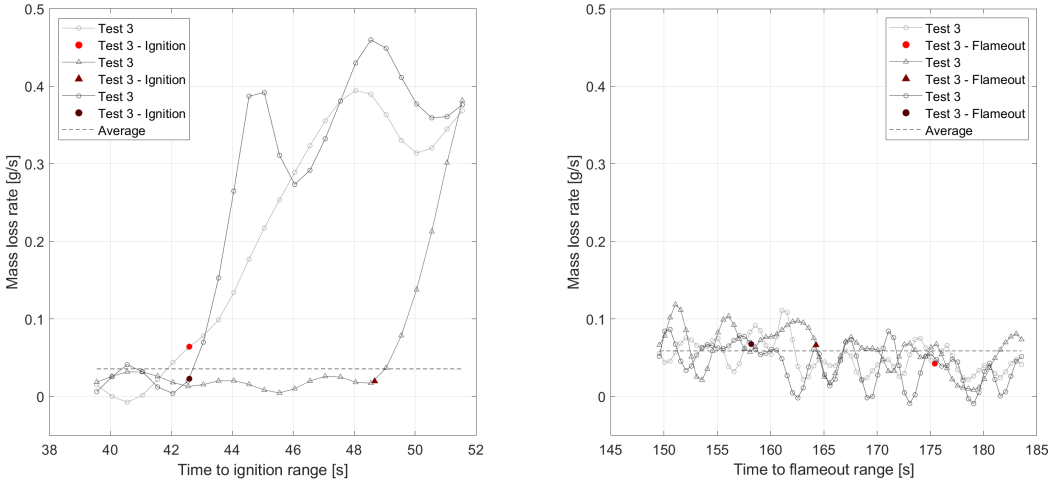

Figure 142: a)Mass loss rate at ignition b)Mass loss rate at flame out

C.4.4.3 Heat Release Rate

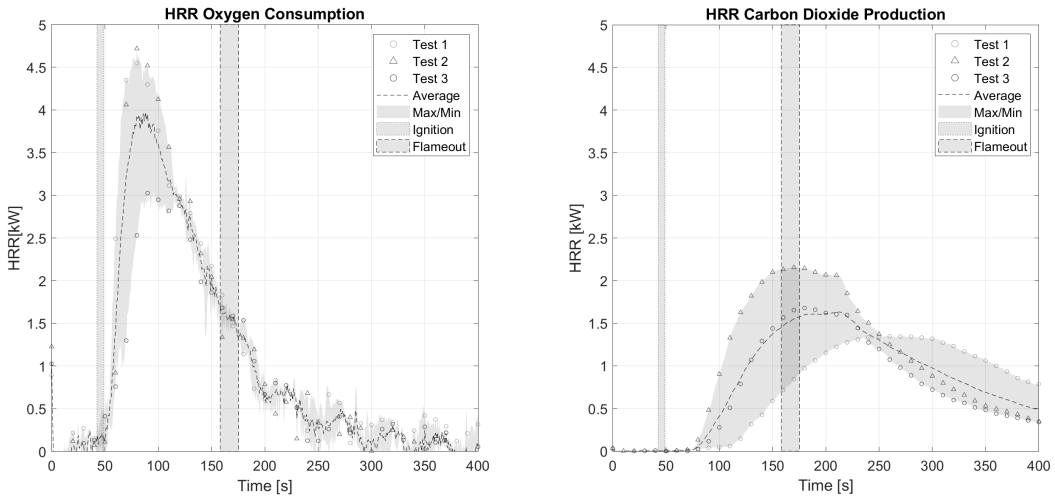

Figure 143: a)Heat release rate - Oxygen Consumption b)Heat release rate - CO2 Production

C.4.4.4 CO2 and CO

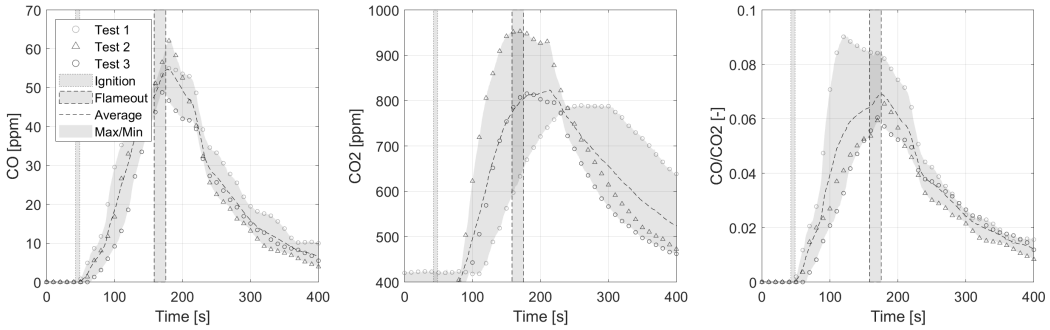

Figure 144: a)CO production b)CO2 production c)CO/CO2

C.4.5 35g Fuel Load

C.4.5.1 Mass

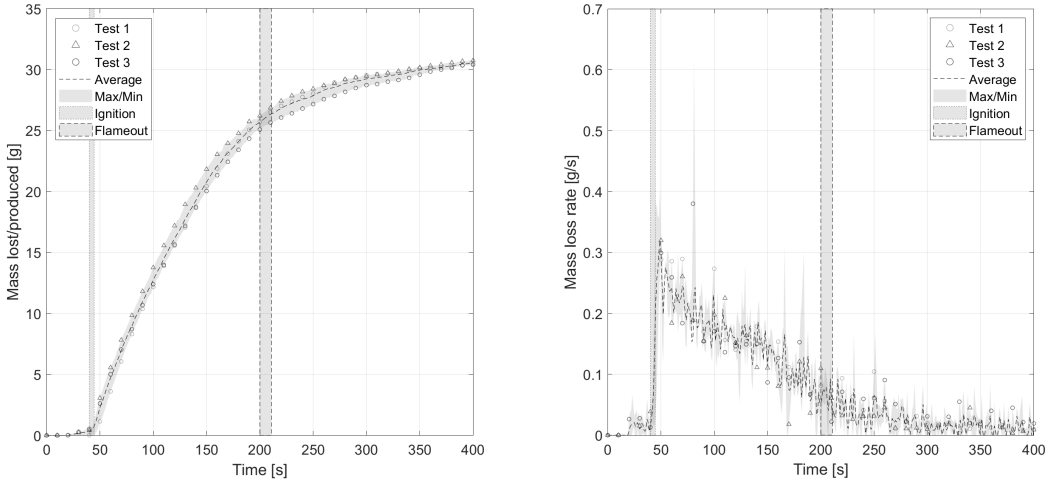

Figure 145: a)Mass b)Mass loss rate

C.4.5.2 Mass Loss Rate at Ignition and Flameout

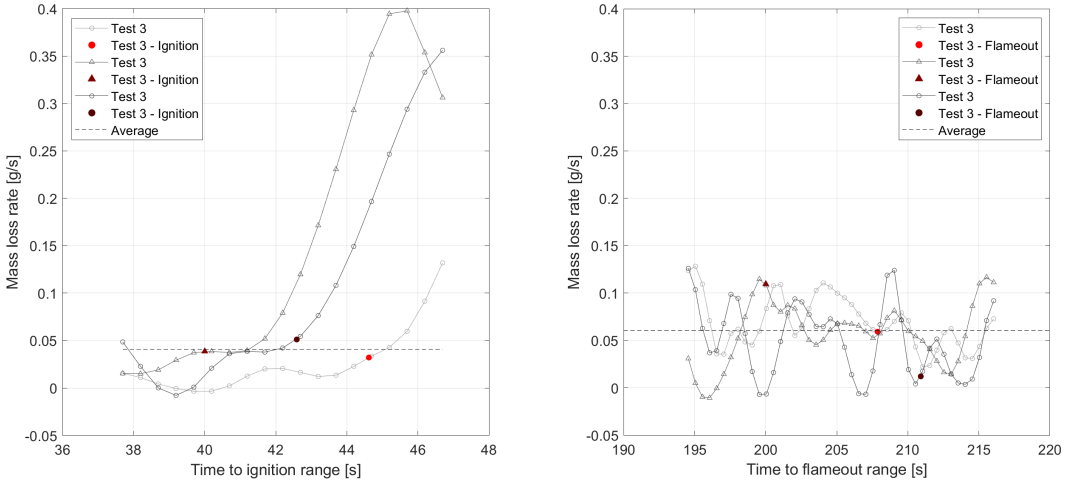

Figure 146: a)Mass loss rate at ignition b)Mass loss rate at flame out

C.4.5.3 Heat Release Rate

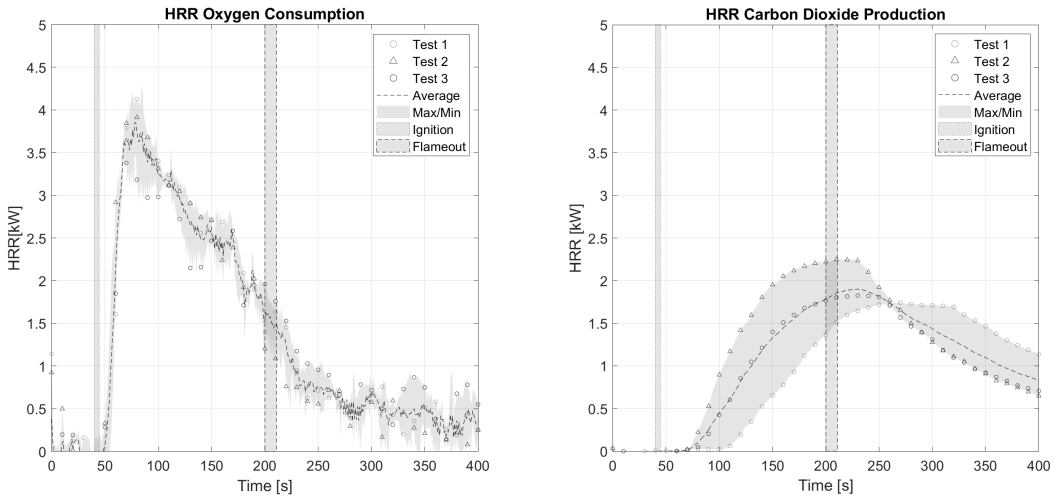

Figure 147: a)Heat release rate - Oxygen Consumption b)Heat release rate - CO2 Production

C.4.5.4 CO2 and CO

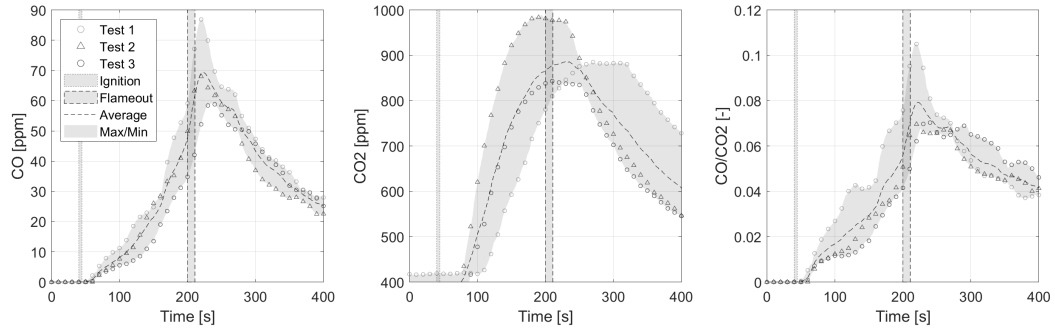

Figure 148: a)CO production b)CO2 production c)CO/CO2

C.4.6 60g Fuel Load

C.4.6.1 Mass

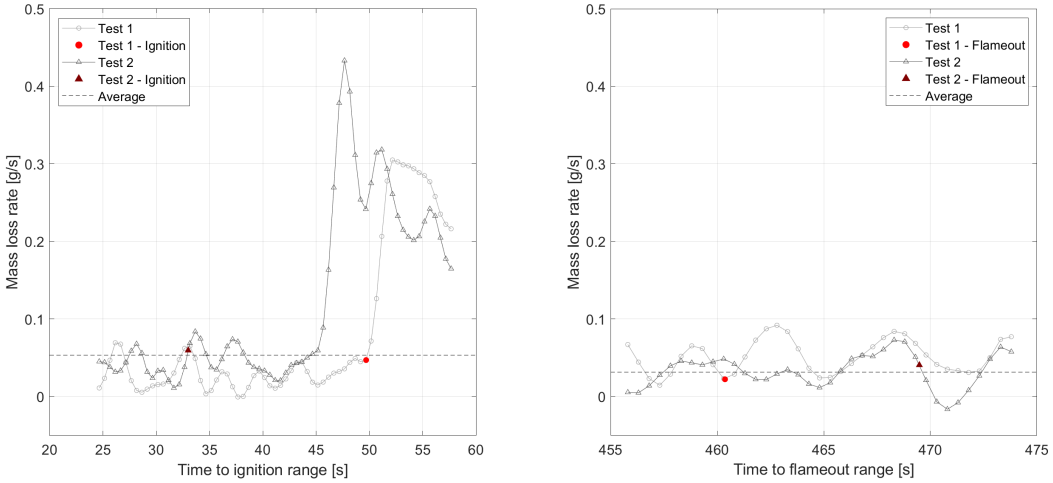

Figure 149: a)Mass b)Mass loss rate

C.4.6.2 Mass Loss Rate at Ignition and Flameout

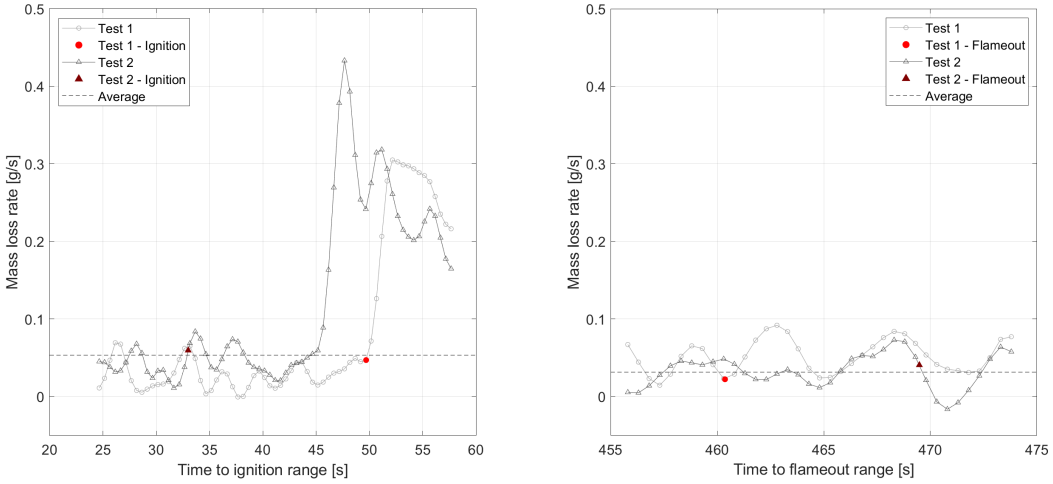

Figure 150: a)Mass loss rate at ignition b)Mass loss rate at flame out

C.4.6.3 Heat Release Rate

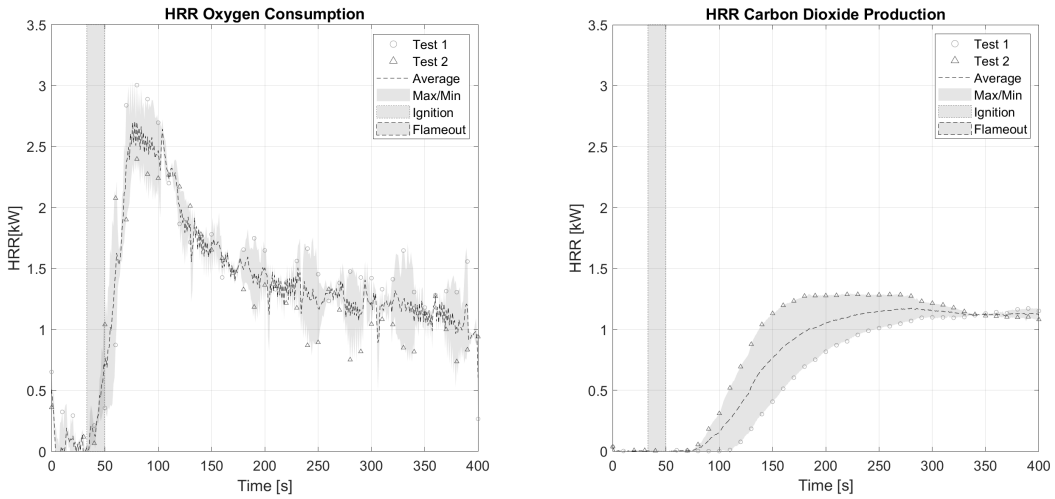

Figure 151: a)Heat release rate - Oxygen Consumption b)Heat release rate - CO2 Production

C.4.6.4 CO2 and CO

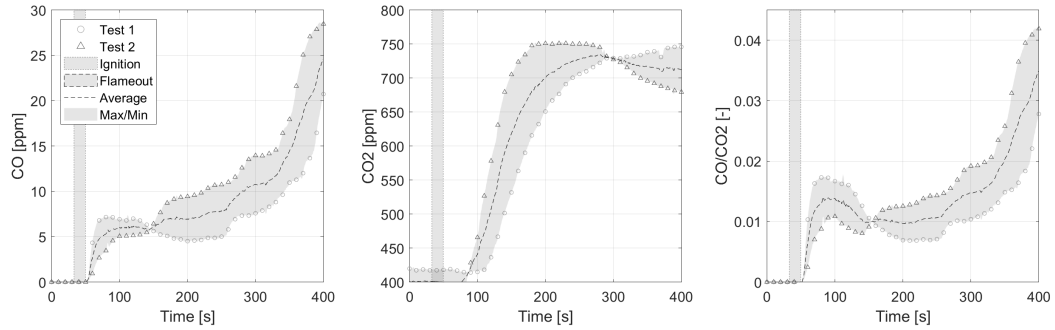

Figure 152: a)CO production b)CO2 production c)CO/CO2

C.4.7 90g Fuel Load

C.4.7.1 Mass

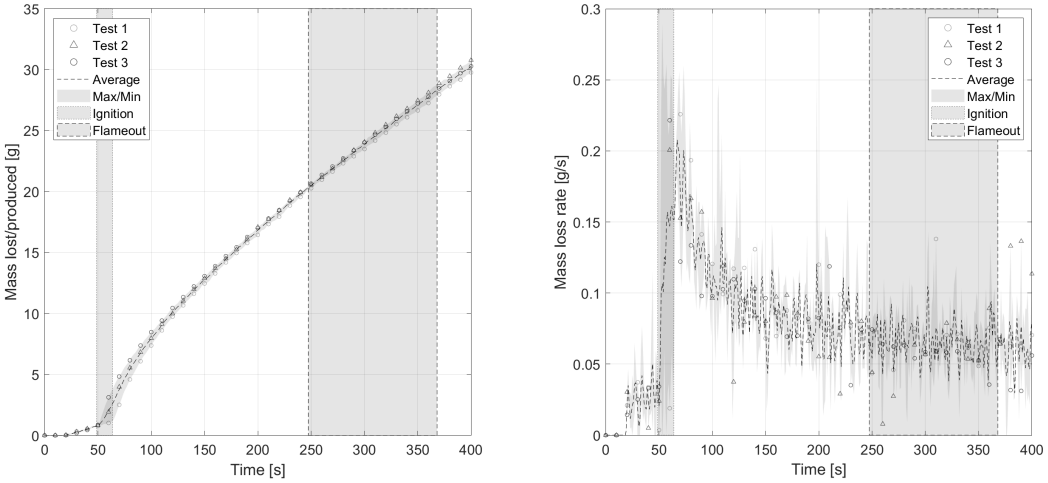

Figure 153: a)Mass b)Mass loss rate

C.4.7.2 Mass Loss Rate at Ignition and Flameout

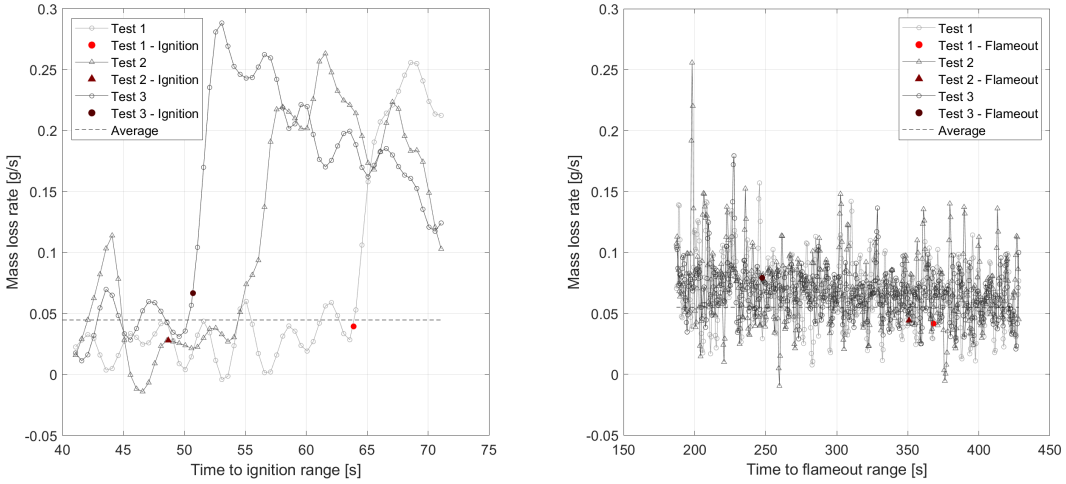

Figure 154: a)Mass loss rate at ignition b)Mass loss rate at flame out

C.4.7.3 Heat Release Rate

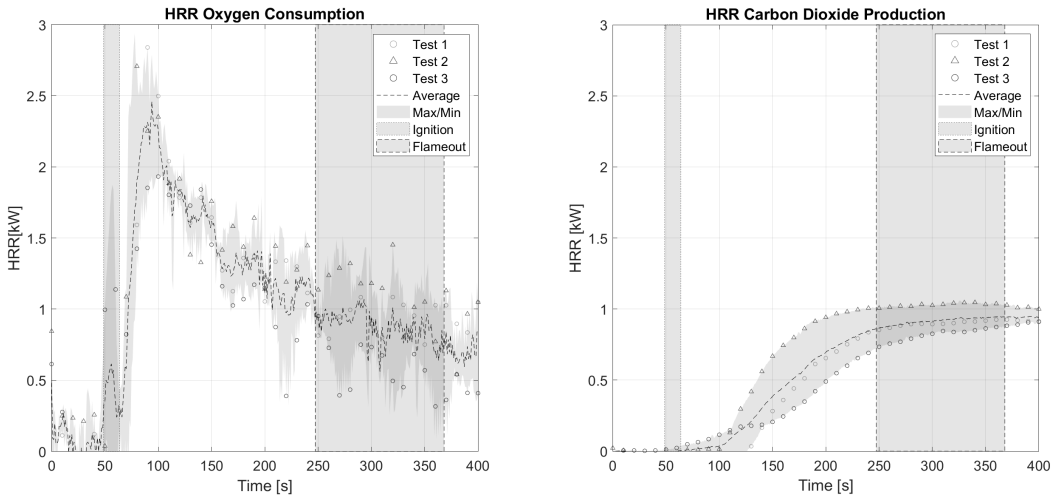

Figure 155: a)Heat release rate - Oxygen Consumption b)Heat release rate - CO2 Production

C.4.7.4 CO2 and CO

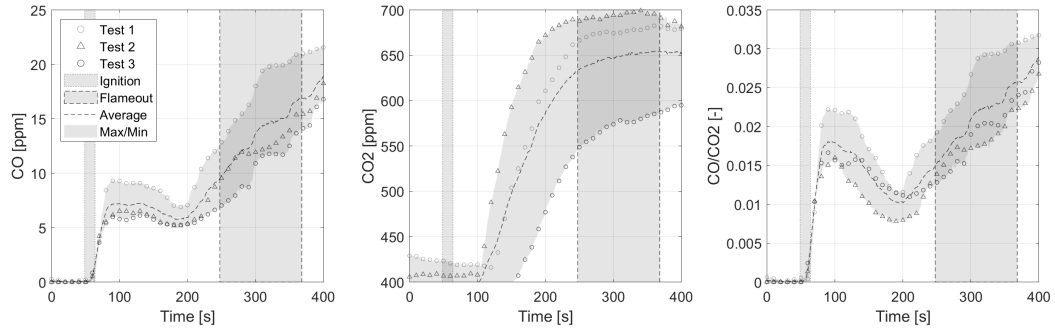

Figure 156: a)CO production b)CO2 production c)CO/CO2

C.5 Open Basket Experiments - 35 kW/m^2 - Pinus Rigida

C.5.1 15g Fuel Load

C.5.1.1 Mass

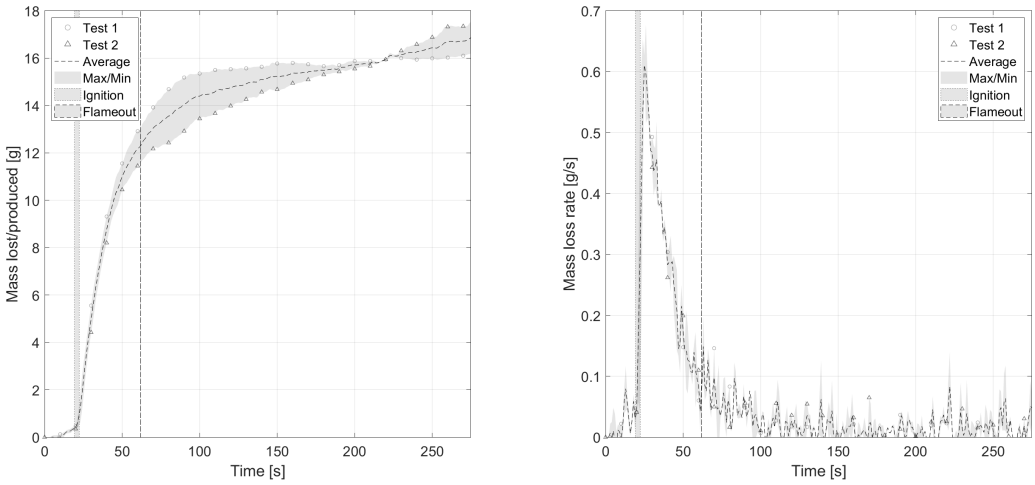

Figure 157: a)Mass b)Mass loss rate

C.5.1.2 Mass Loss Rate at Ignition and Flameout

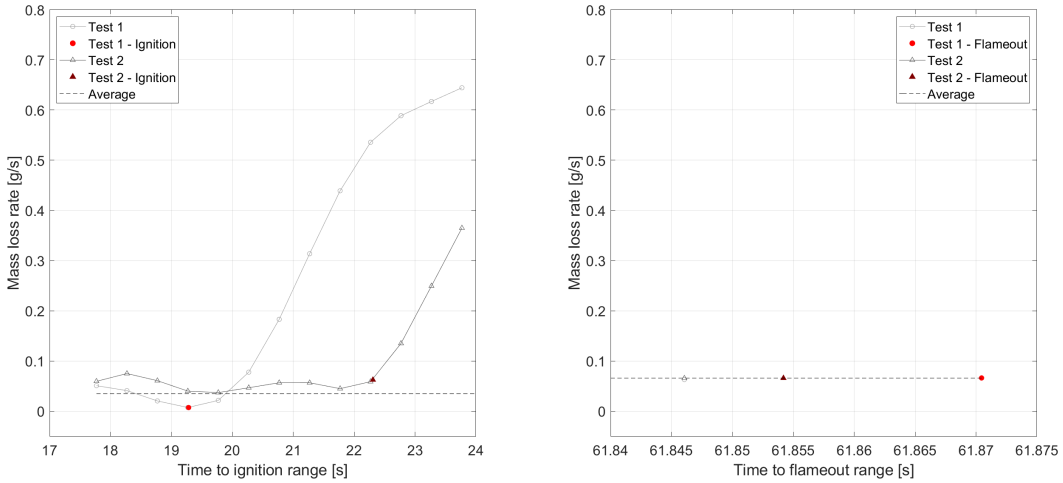

Figure 158: a)Mass loss rate at ignition b)Mass loss rate at flame out

C.5.1.3 Heat Release Rate

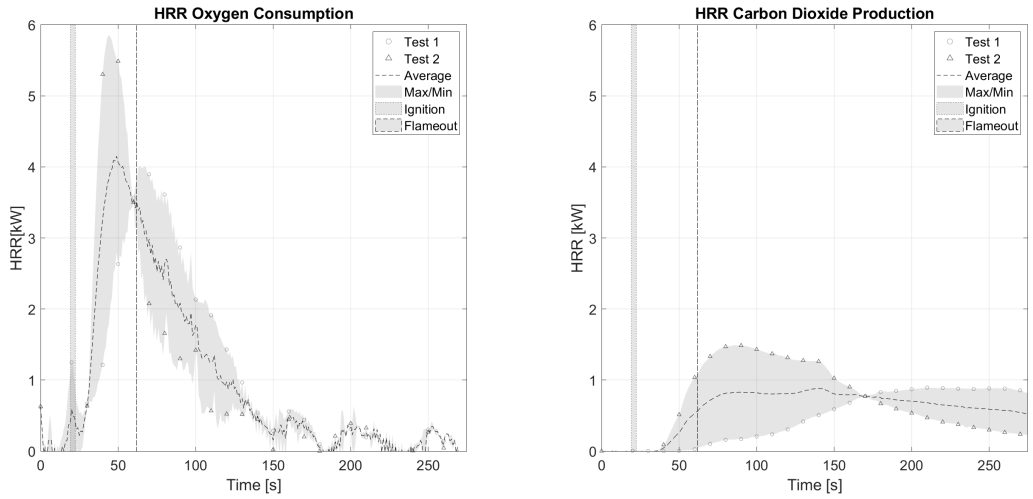

Figure 159: a)Heat release rate - Oxygen Consumption b)Heat release rate - CO2 Production

C.5.1.4 CO2 and CO

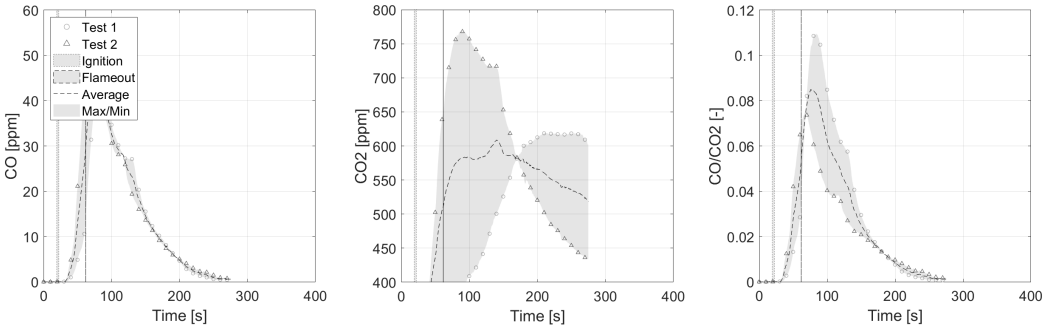

Figure 160: a)CO production b)CO2 production c)CO/CO2

C.5.2 35g Fuel Load

C.5.2.1 Mass

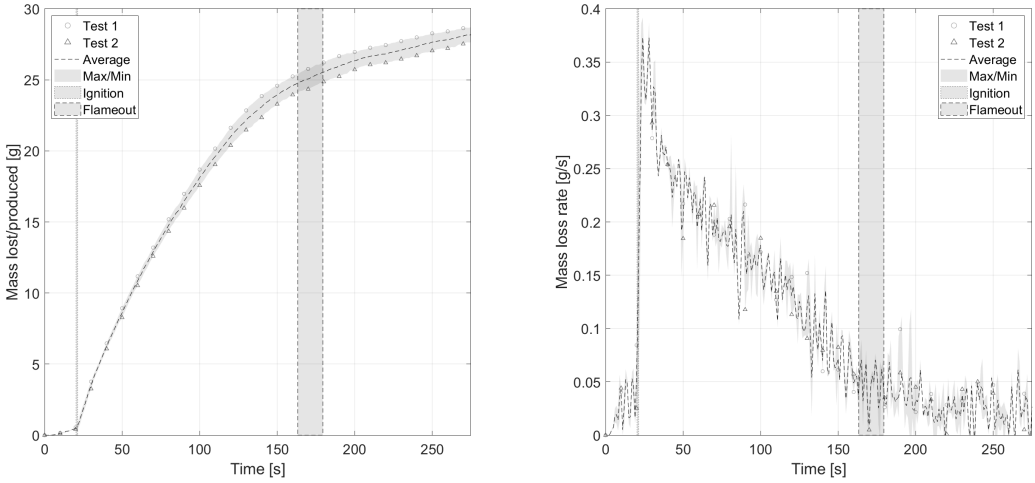

Figure 161: a)Mass b)Mass loss rate

C.5.2.2 Mass Loss Rate at Ignition and Flameout

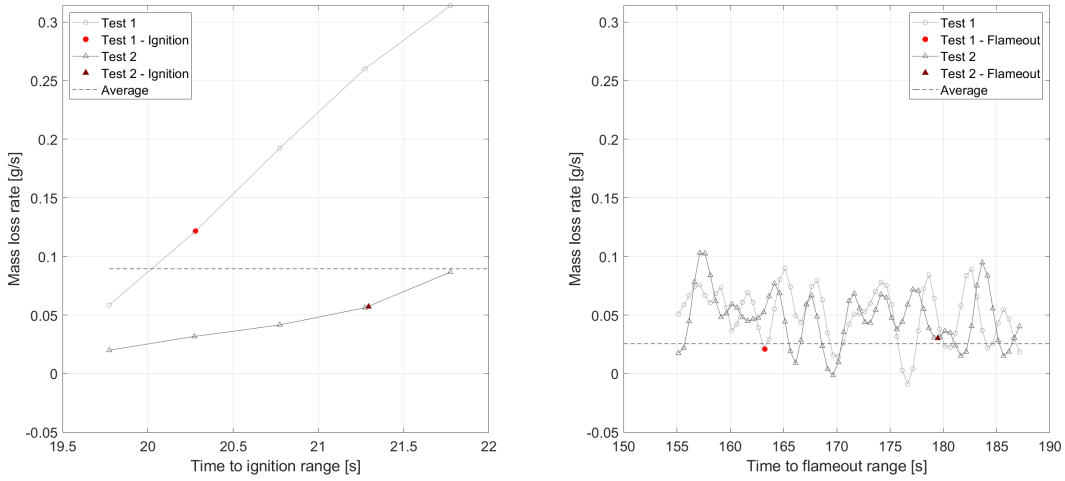

Figure 162: a)Mass loss rate at ignition b)Mass loss rate at flame out

C.5.2.3 Heat Release Rate

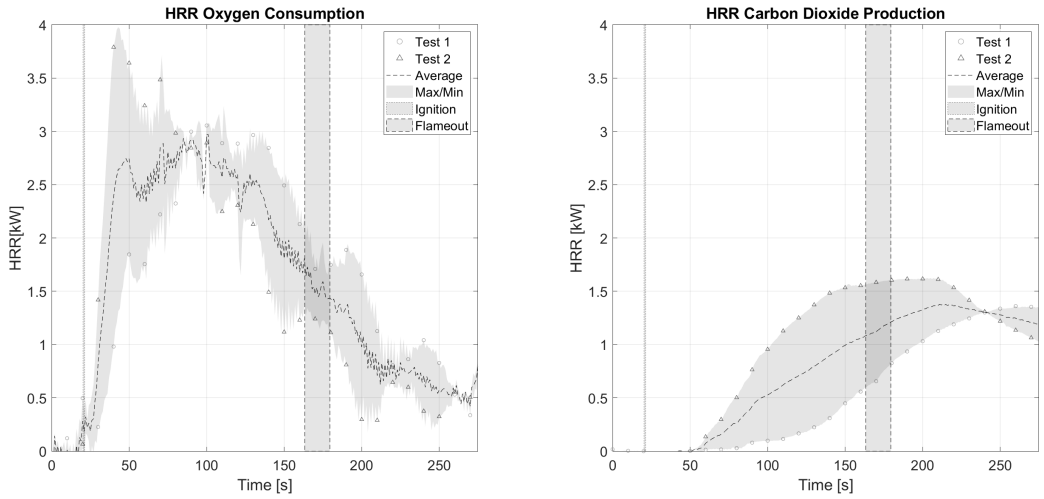

Figure 163: a)Heat release rate - Oxygen Consumption b)Heat release rate - CO2 Production

C.5.2.4 CO2 and CO

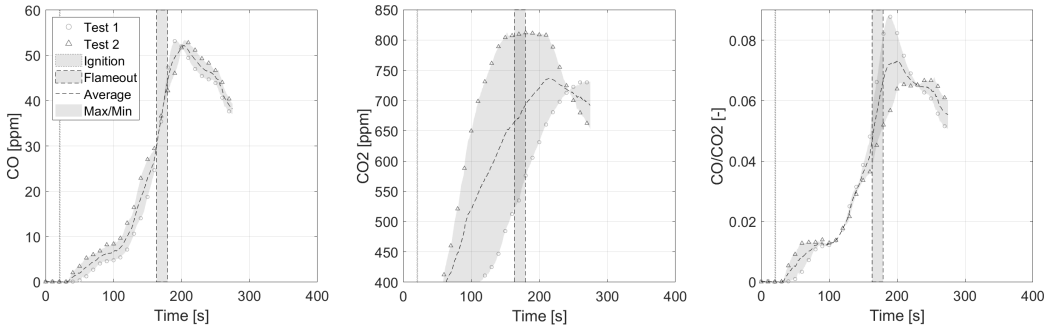

Figure 164: a)CO production b)CO2 production c)CO/CO2

C.5.3 90g Fuel Load

C.5.3.1 Mass

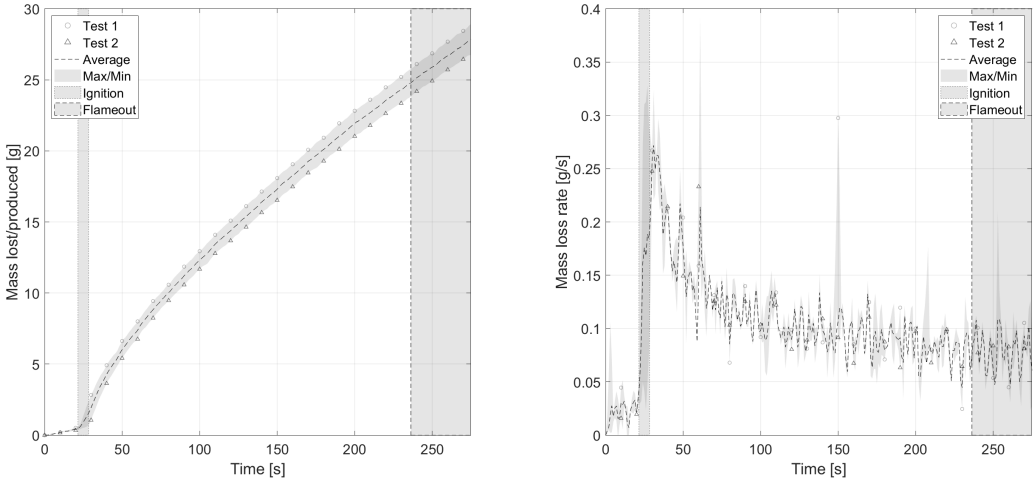

Figure 165: a)Mass b)Mass loss rate

C.5.3.2 Mass Loss Rate at Ignition and Flameout

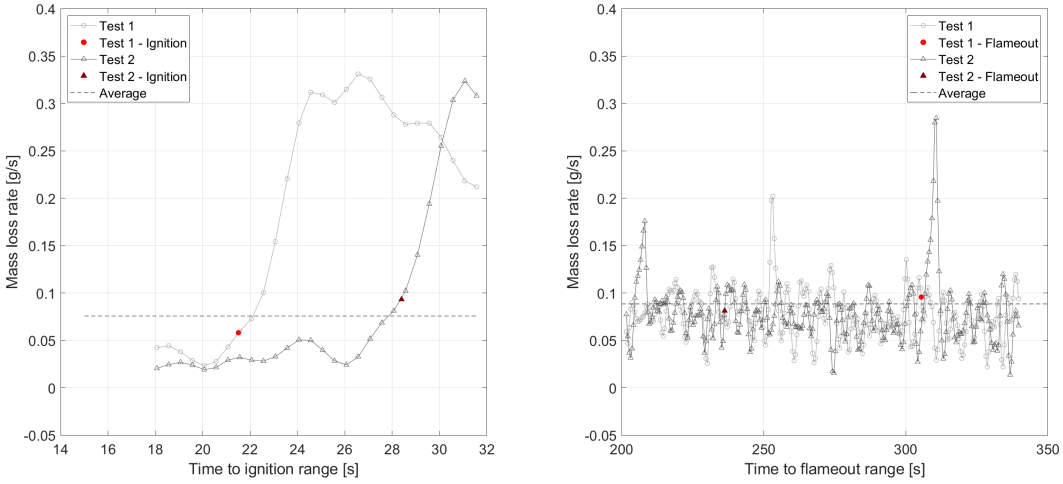

Figure 166: a)Mass loss rate at ignition b)Mass loss rate at flame out

C.5.3.3 Heat Release Rate

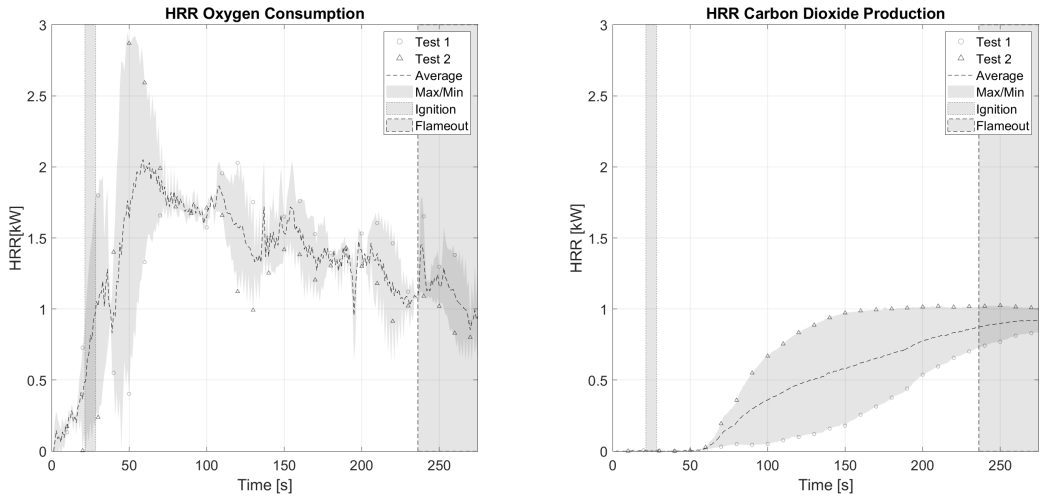

Figure 167: a)Heat release rate - Oxygen Consumption b)Heat release rate - CO2 Production

C.5.3.4 CO2 and CO

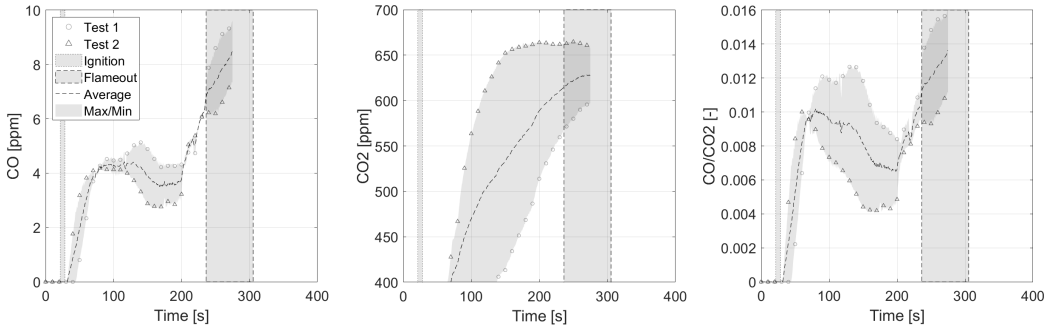

Figure 168: a)CO production b)CO2 production c)CO/CO2

C.6 Open Basket Experiments - 50 kW/m^2 - Pinus Rigida

C.6.1 15g Fuel Load

C.6.1.1 Mass

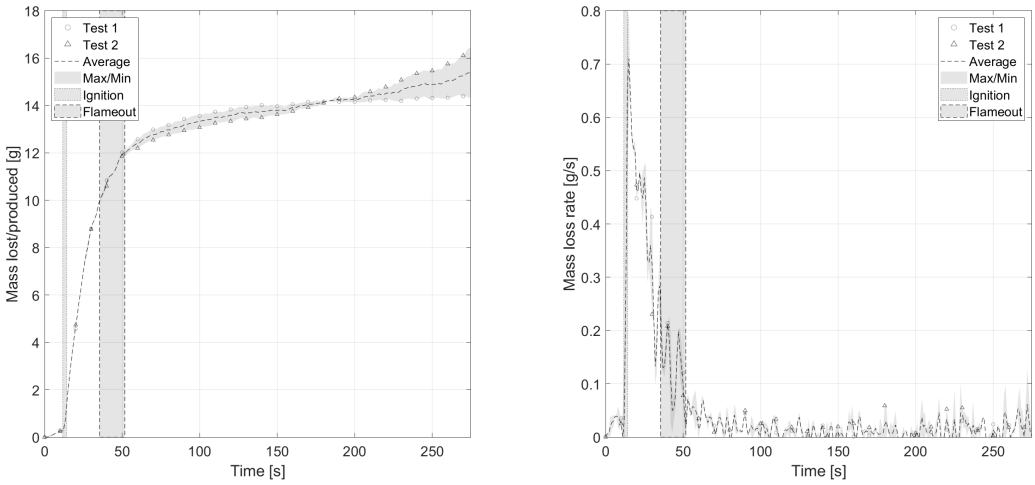

Figure 169: a)Mass b)Mass loss rate

C.6.1.2 Mass Loss Rate at Ignition and Flameout

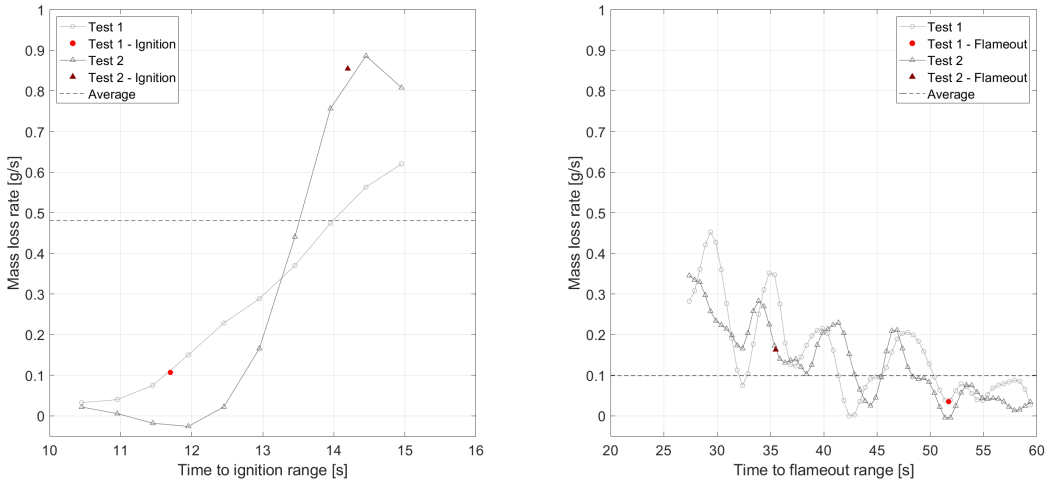

Figure 170: a)Mass loss rate at ignition b)Mass loss rate at flame out

C.6.1.3 Heat Release Rate

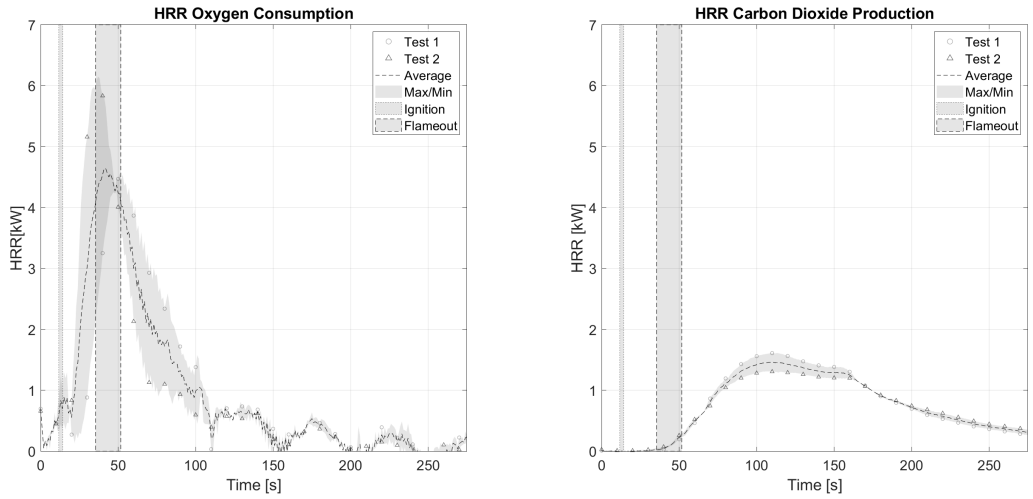

Figure 171: a)Heat release rate - Oxygen Consumption b)Heat release rate - CO2 Production

C.6.1.4 CO2 and CO

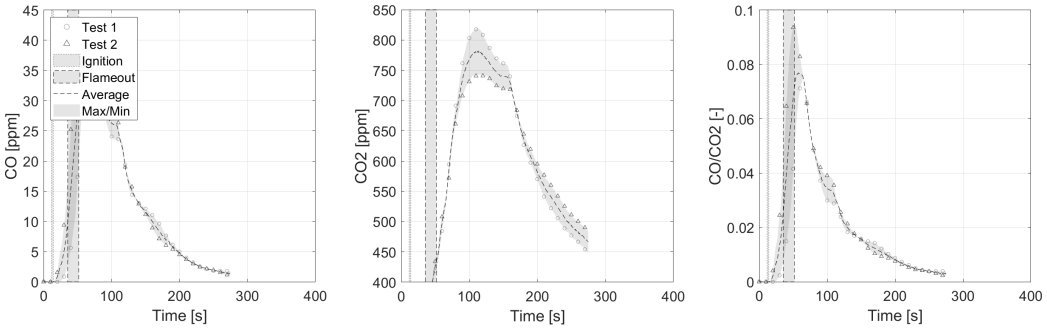

Figure 172: a)CO production b)CO2 production c)CO/CO2

C.6.2 35g Fuel Load

C.6.2.1 Mass

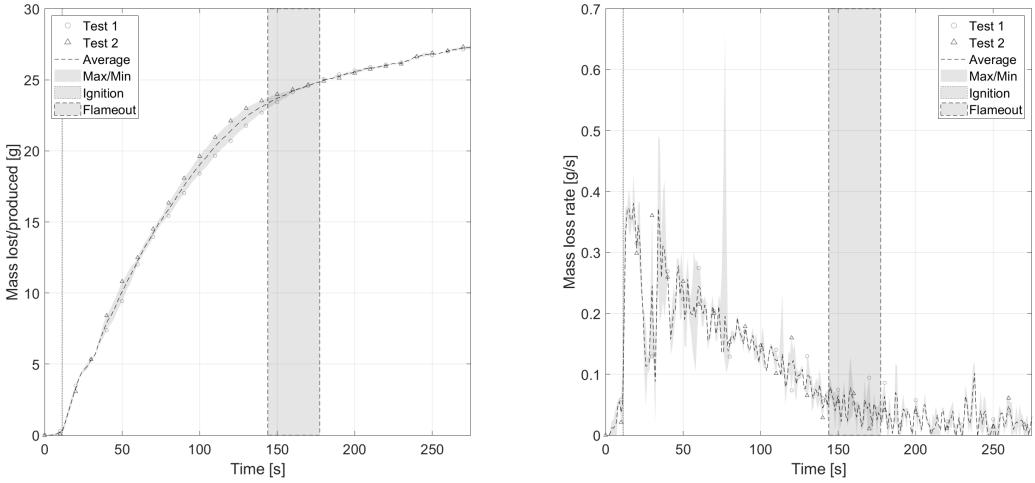

Figure 173: a)Mass b)Mass loss rate

C.6.2.2 Mass Loss Rate at Ignition and Flameout

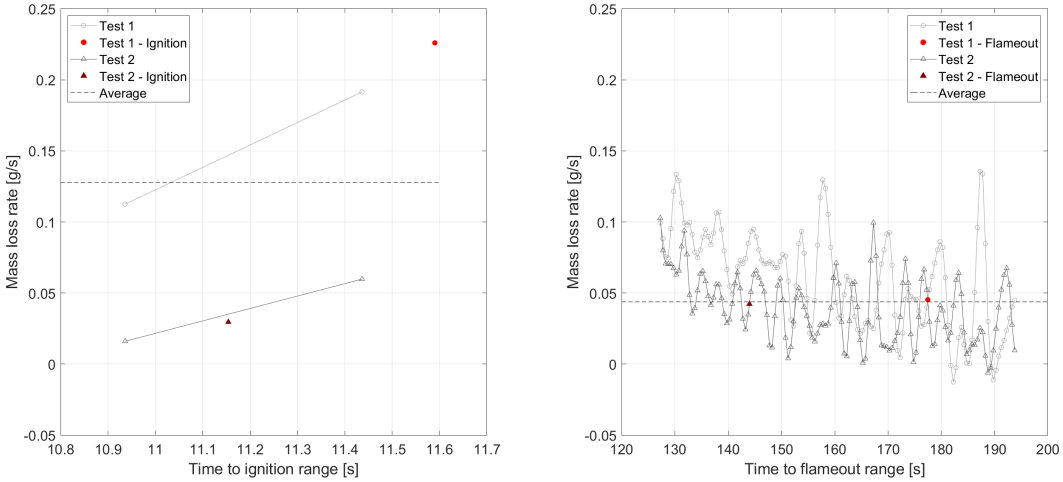

Figure 174: a)Mass loss rate at ignition b)Mass loss rate at flame out

C.6.2.3 Heat Release Rate

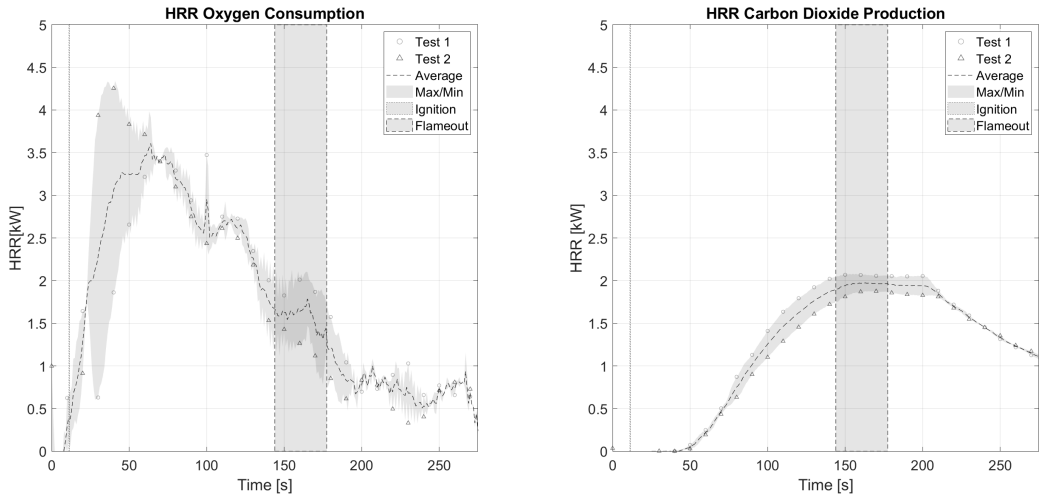

Figure 175: a)Heat release rate - Oxygen Consumption b)Heat release rate - CO2 Production

C.6.2.4 CO2 and CO

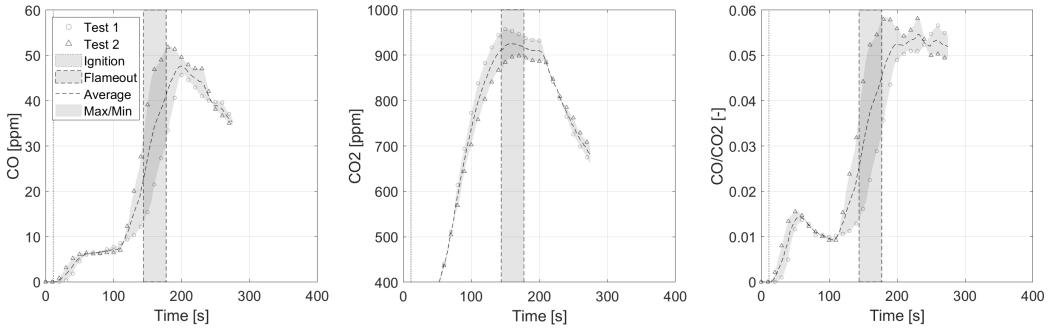

Figure 176: a)CO production b)CO2 production c)CO/CO2

C.6.3 90g Fuel Load

C.6.3.1 Mass

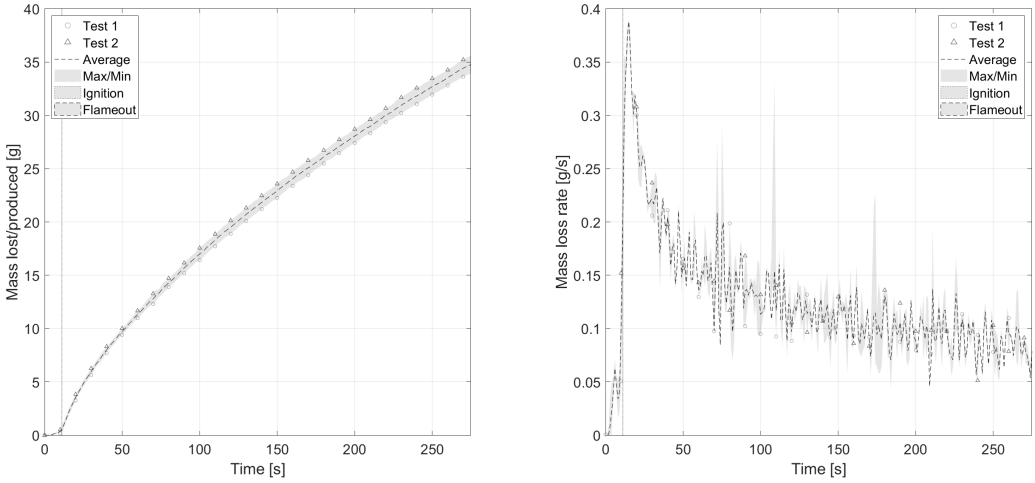

Figure 177: a)Mass b)Mass loss rate

C.6.3.2 Mass Loss Rate at Ignition and Flameout

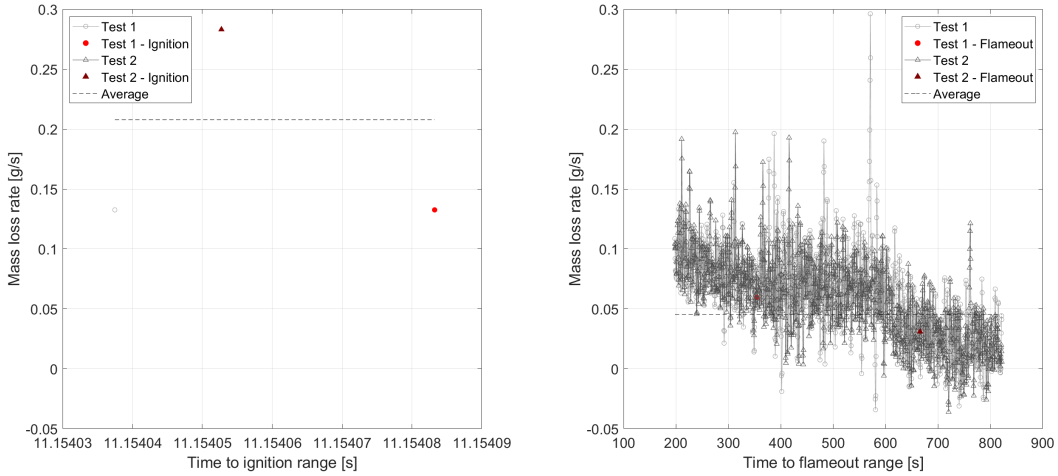

Figure 178: a)Mass loss rate at ignition b)Mass loss rate at flame out

C.6.3.3 Heat Release Rate

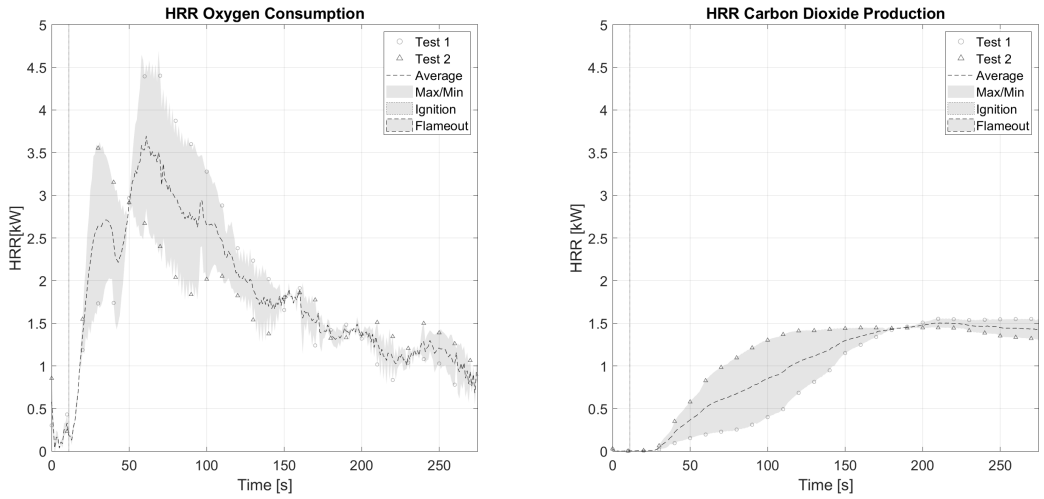

Figure 179: a)Heat release rate - Oxygen Consumption b)Heat release rate - CO2 Production

C.6.3.4 CO2 and CO

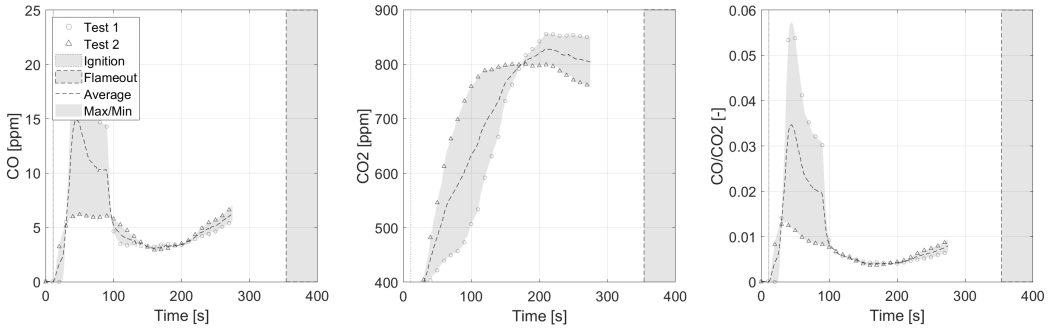

Figure 180: a)CO production b)CO2 production c)CO/CO2

C.7 Open Basket Experiments - 25 kW/m^2 - Pinus Halepensis

C.7.1 10g Fuel Load

C.7.1.1 Mass

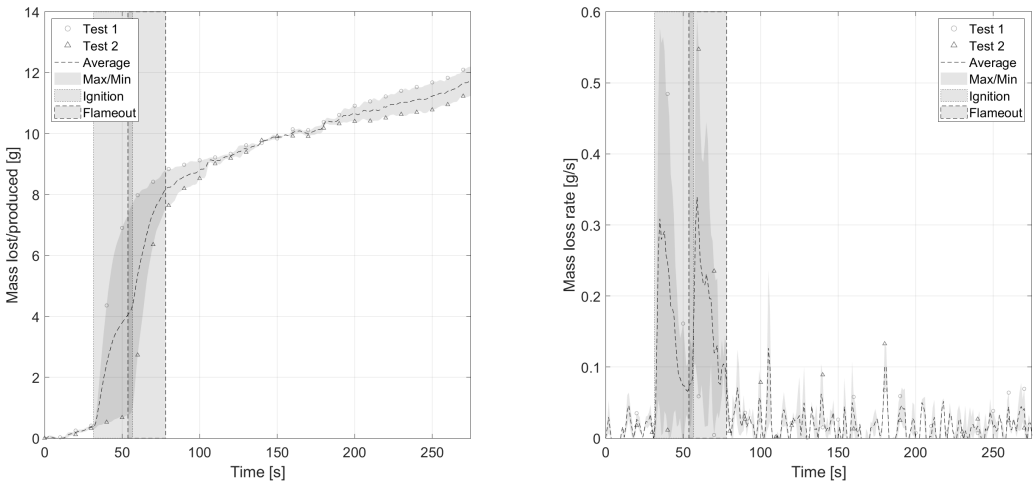

Figure 181: a)Mass b)Mass loss rate

C.7.1.2 Mass Loss Rate at Ignition and Flameout

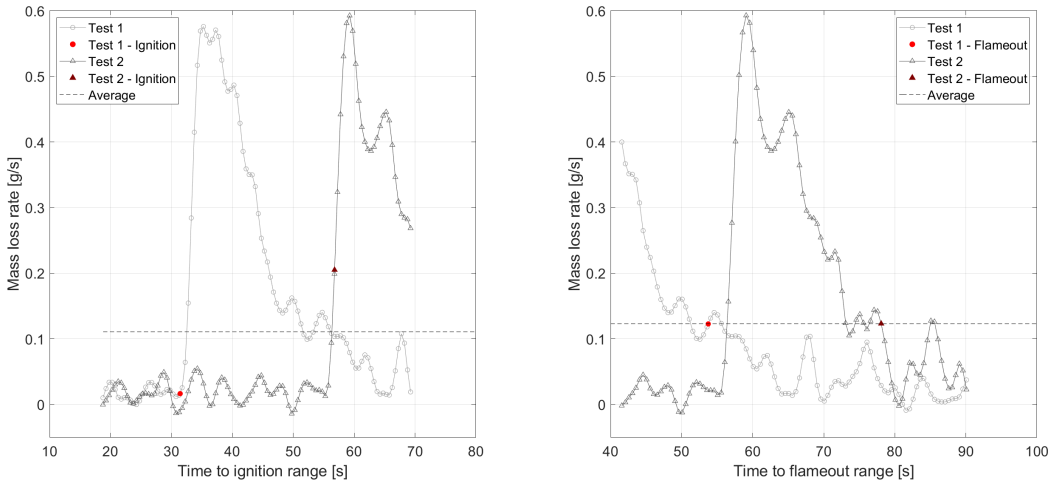

Figure 182: a)Mass loss rate at ignition b)Mass loss rate at flame out

C.7.1.3 Heat Release Rate

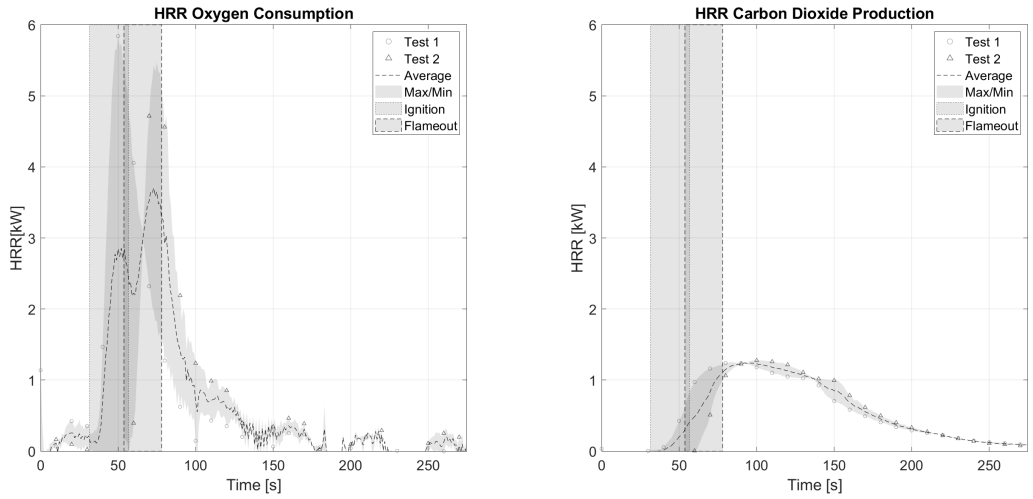

Figure 183: a)Heat release rate - Oxygen Consumption b)Heat release rate - CO2 Production

C.7.1.4 CO2 and CO

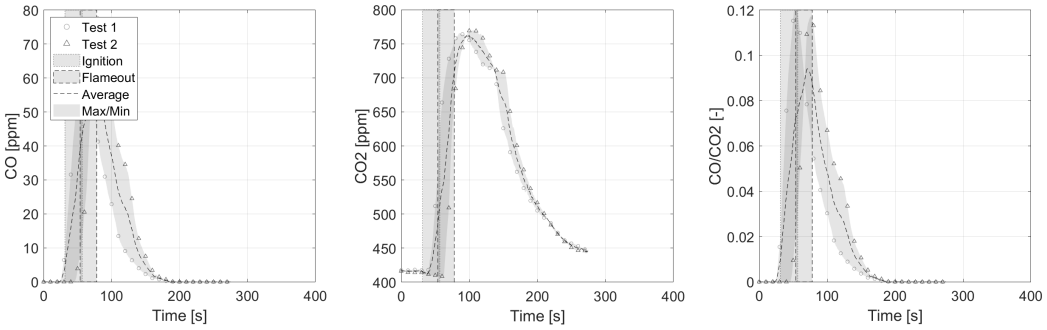

Figure 184: a)CO production b)CO2 production c)CO/CO2

C.7.2 15g Fuel Load

C.7.2.1 Mass

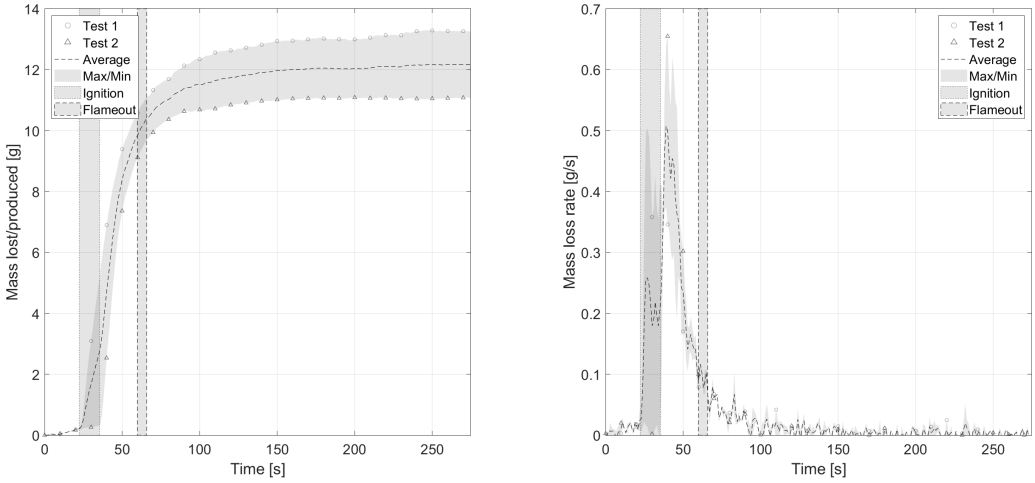

Figure 185: a)Mass b)Mass loss rate

C.7.2.2 Mass Loss Rate at Ignition and Flameout

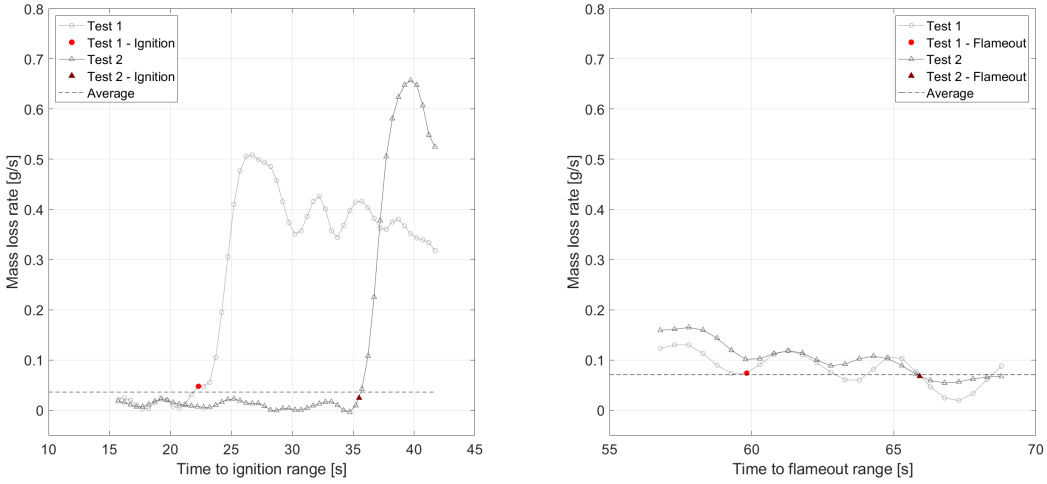

Figure 186: a)Mass loss rate at ignition b)Mass loss rate at flame out

C.7.2.3 Heat Release Rate

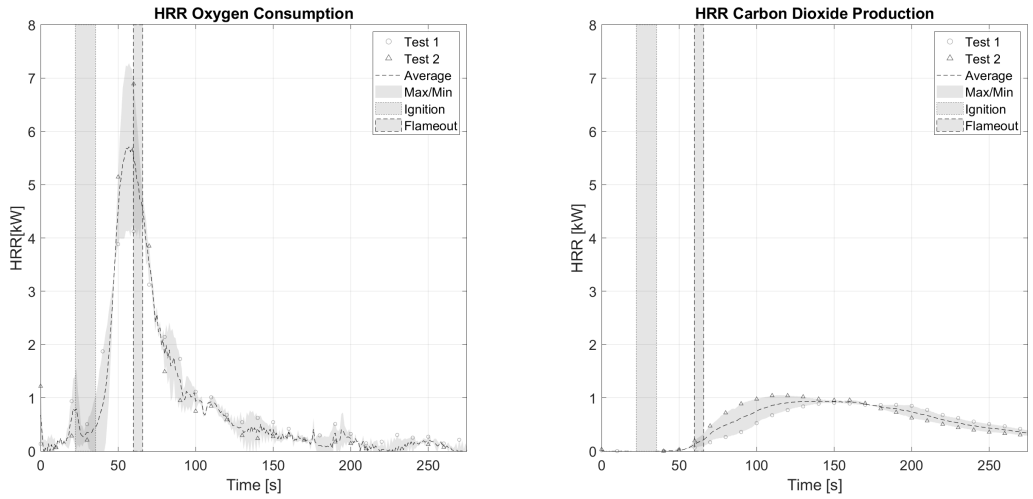

Figure 187: a)Heat release rate - Oxygen Consumption b)Heat release rate - CO2 Production

C.7.2.4 CO2 and CO

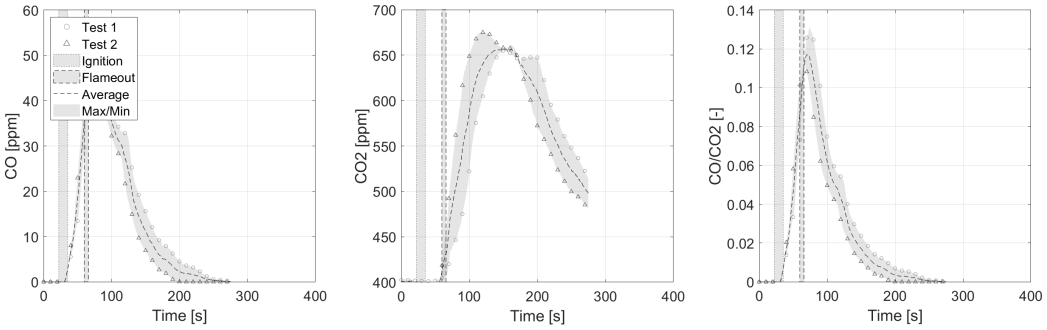

Figure 188: a)CO production b)CO2 production c)CO/CO2

C.7.3 20g Fuel Load

C.7.3.1 Mass

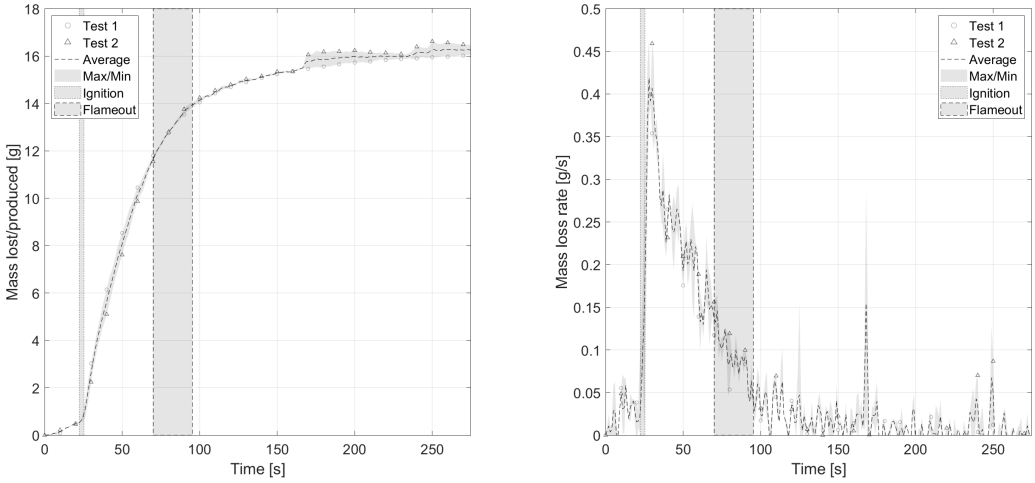

Figure 189: a)Mass b)Mass loss rate

C.7.3.2 Mass Loss Rate at Ignition and Flameout

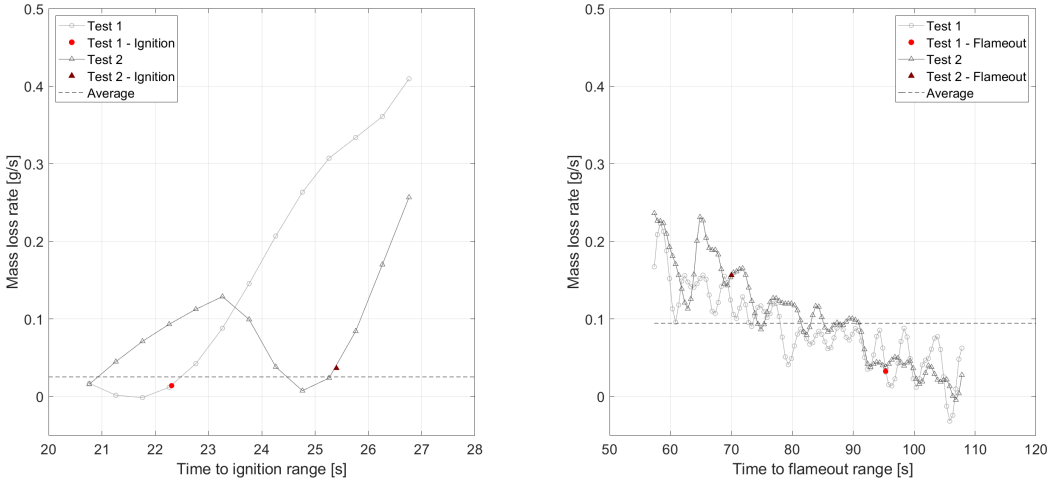

Figure 190: a)Mass loss rate at ignition b)Mass loss rate at flame out

C.7.3.3 Heat Release Rate

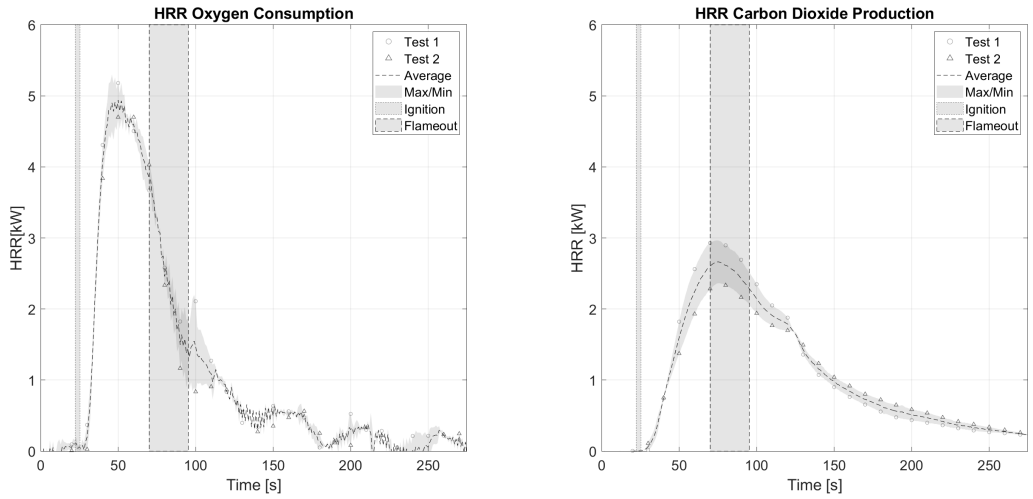

Figure 191: a)Heat release rate - Oxygen Consumption b)Heat release rate - CO2 Production

C.7.3.4 CO2 and CO

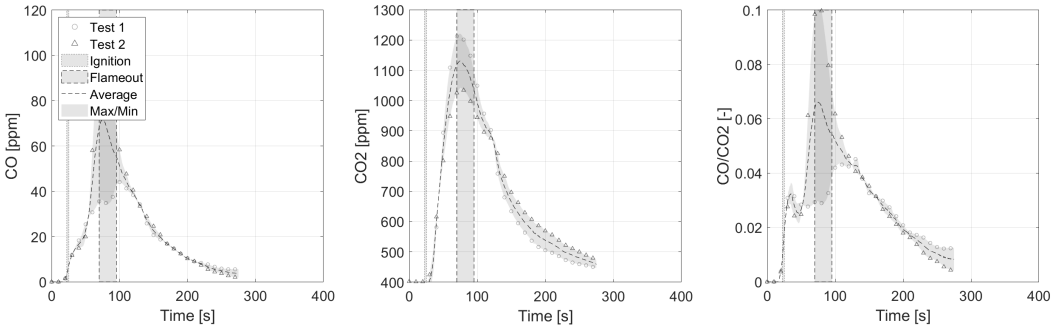

Figure 192: a)CO production b)CO2 production c)CO/CO2

C.8 Open Basket Experiments - 25 kW/m^2 - Pinus Pinea

C.8.1 10g Fuel Load

C.8.1.1 Mass

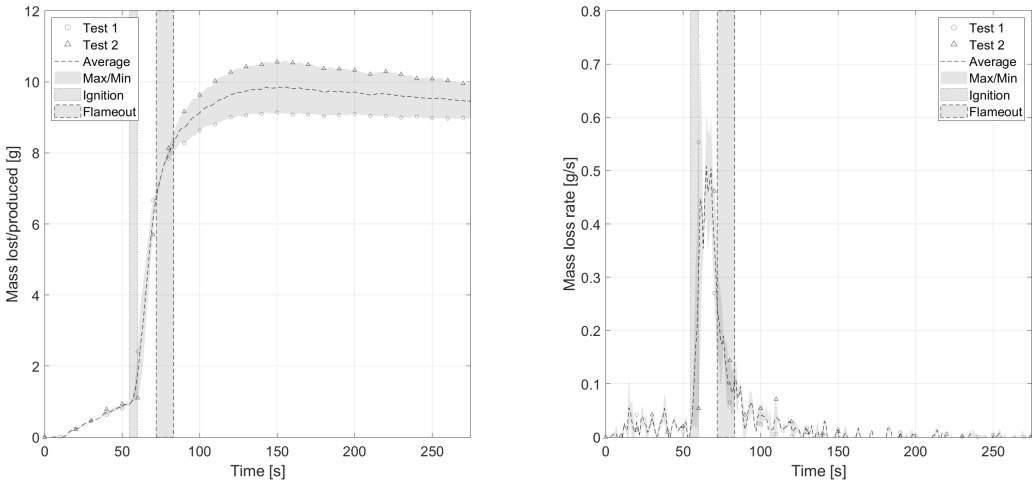

Figure 193: a)Mass b)Mass loss rate

C.8.1.2 Mass Loss Rate at Ignition and Flameout

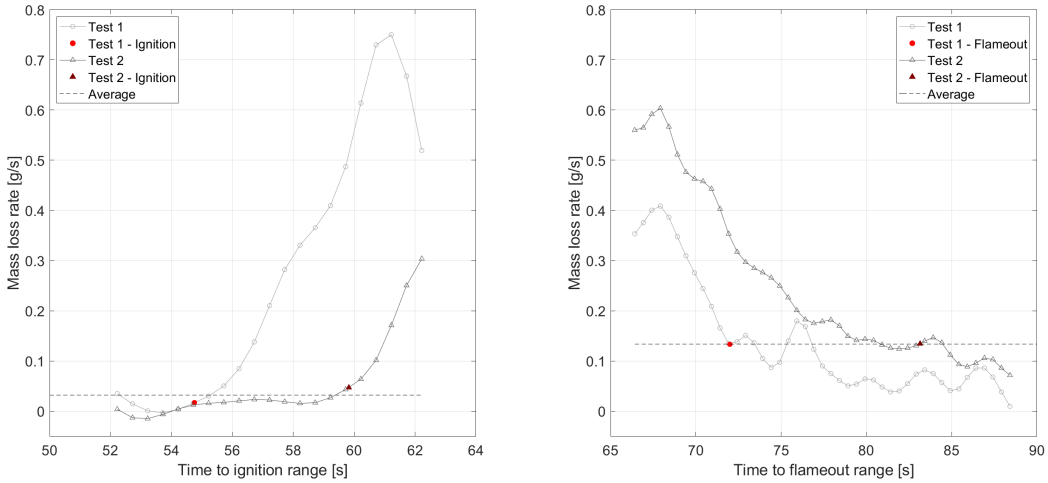

Figure 194: a)Mass loss rate at ignition b)Mass loss rate at flame out

C.8.1.3 Heat Release Rate

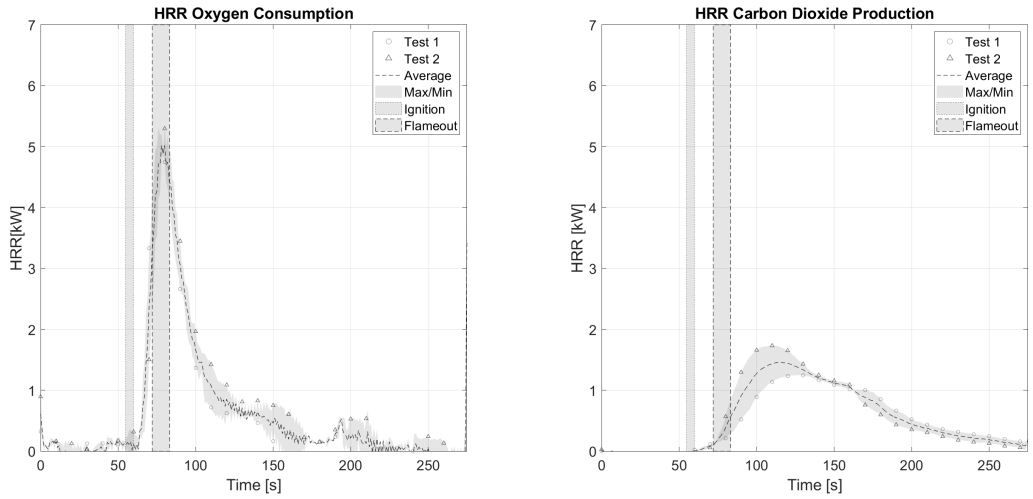

Figure 195: a)Heat release rate - Oxygen Consumption b)Heat release rate - CO2 Production

C.8.1.4 CO2 and CO

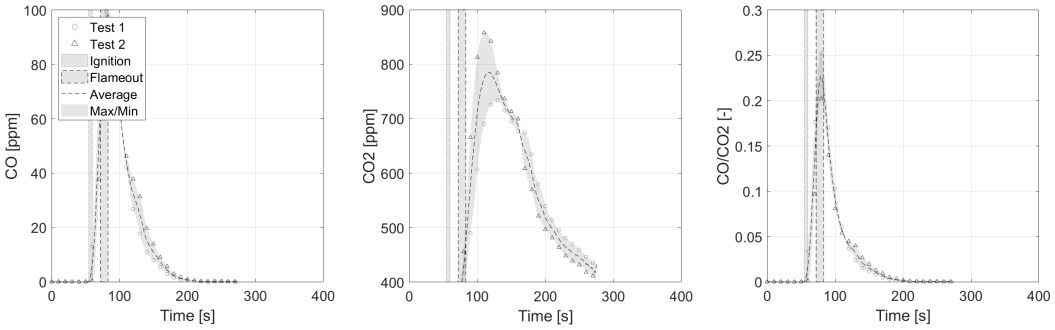

Figure 196: a)CO production b)CO2 production c)CO/CO2

C.8.2 15g Fuel Load

C.8.2.1 Mass

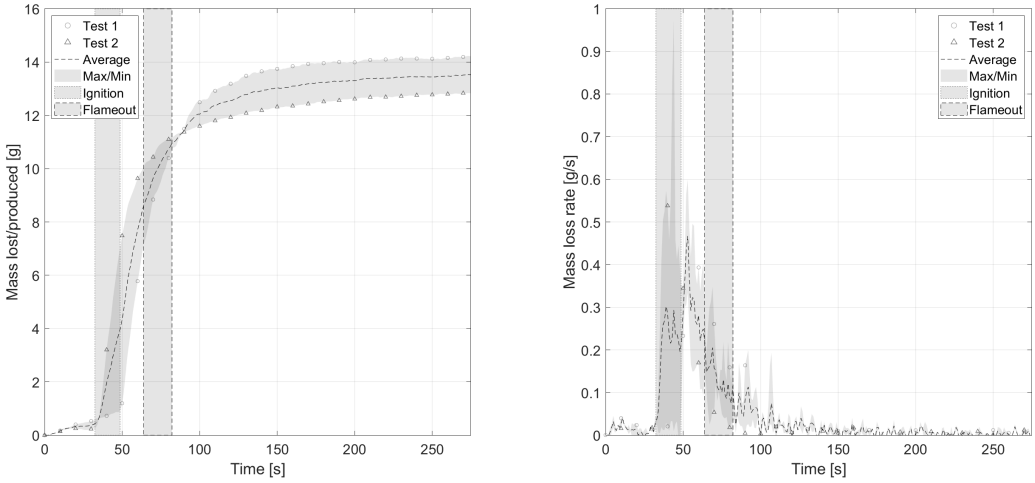

Figure 197: a)Mass b)Mass loss rate

C.8.2.2 Mass Loss Rate at Ignition and Flameout

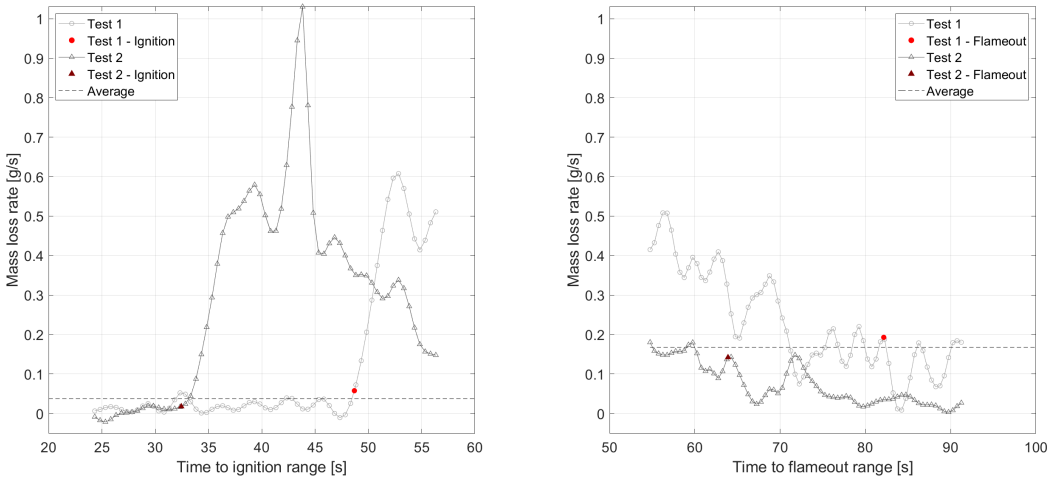

Figure 198: a)Mass loss rate at ignition b)Mass loss rate at flame out

C.8.3 20g Fuel Load

C.8.3.1 Mass

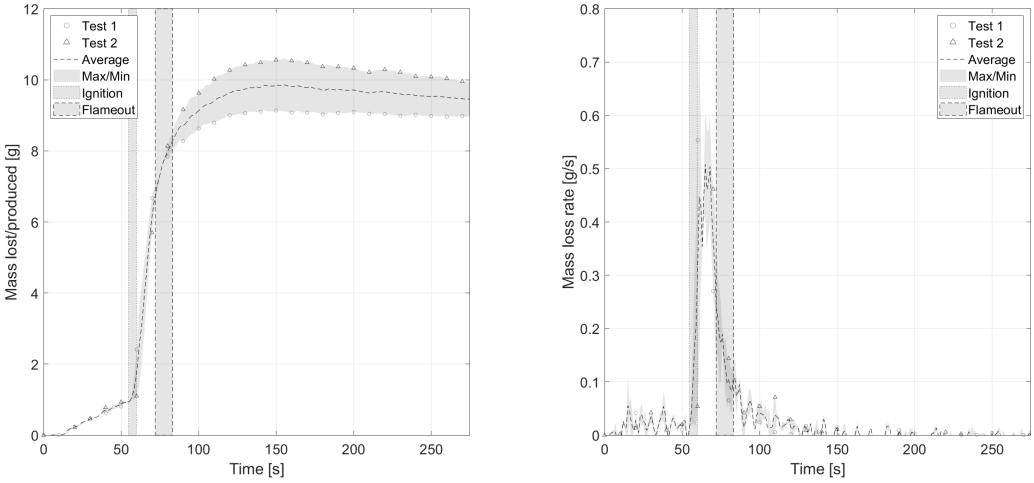

Figure 199: a)Mass b)Mass loss rate

C.8.3.2 Mass Loss Rate at Ignition and Flameout

C.8.3.3 Heat Release Rate

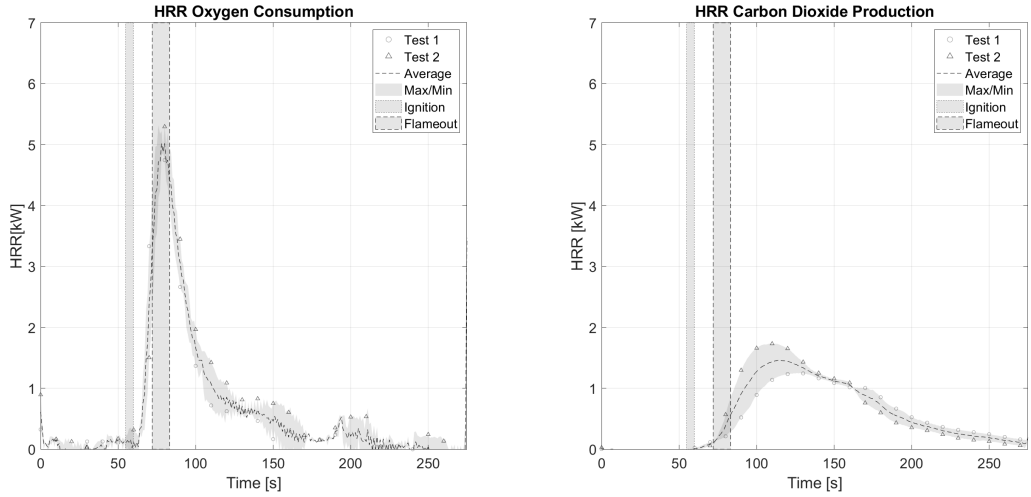

Figure 200: a)Heat release rate - Oxygen Consumption b)Heat release rate - CO2 Production

C.8.3.4 CO2 and CO

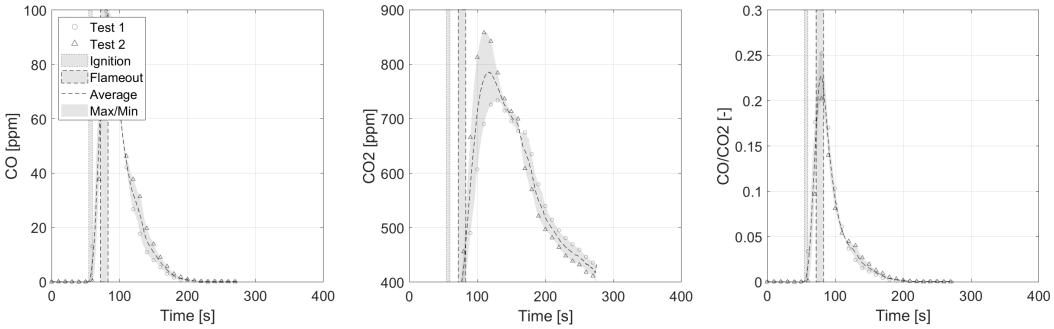

Figure 201: a)CO production b)CO2 production c)CO/CO2

C.9 Open Basket Experiments - 25 kW/m^2 - Pinus Pinaster

C.9.1 10g Fuel Load

C.9.1.1 Mass

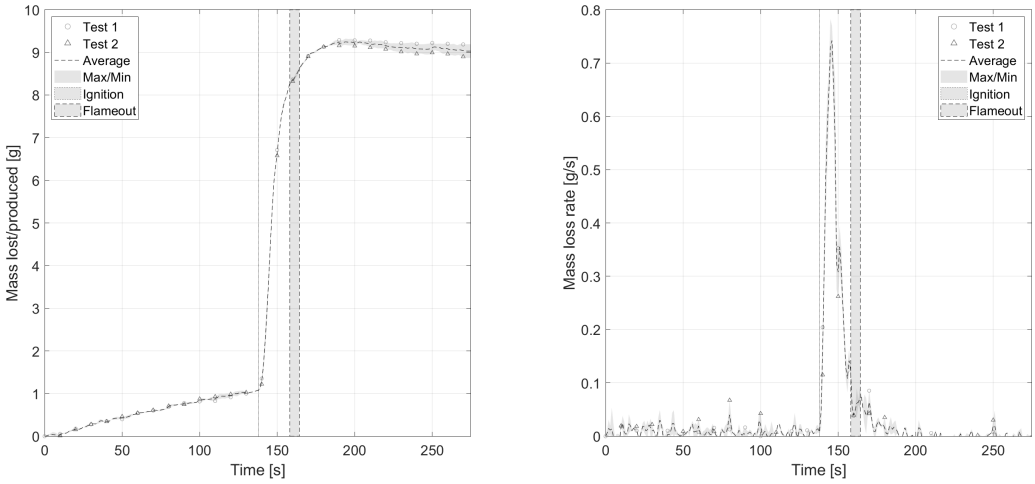

Figure 202: a)Mass b)Mass loss rate

C.9.1.2 Mass Loss Rate at Ignition and Flameout

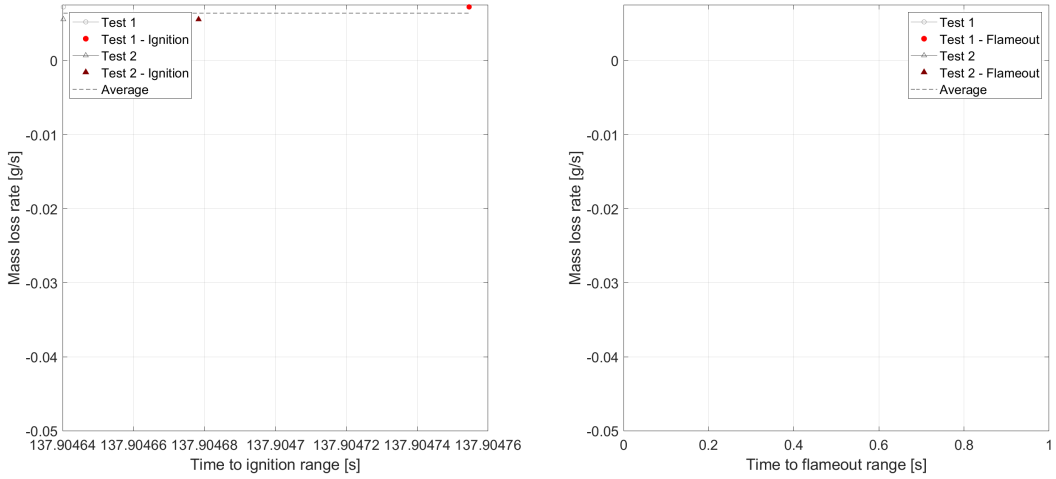

Figure 203: a)Mass loss rate at ignition b)Mass loss rate at flame out

C.9.2 15g Fuel Load

C.9.2.1 Mass

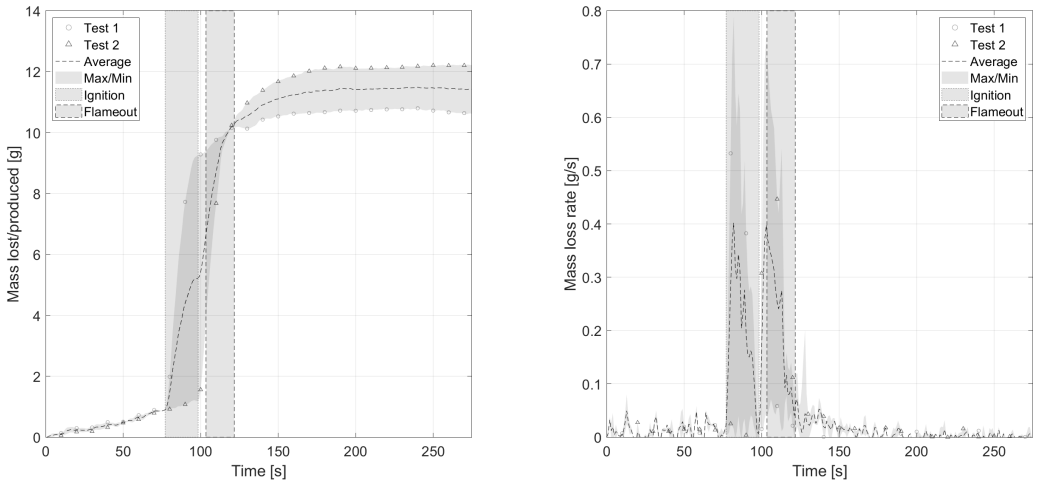

Figure 204: a)Mass b)Mass loss rate

C.9.2.2 Mass Loss Rate at Ignition and Flameout

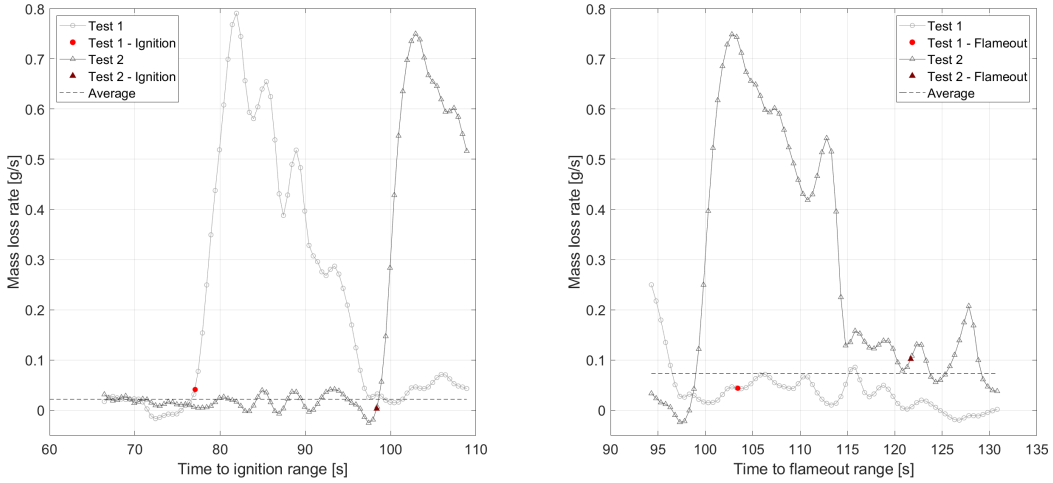

Figure 205: a)Mass loss rate at ignition b)Mass loss rate at flame out

C.9.2.3 Heat Release Rate

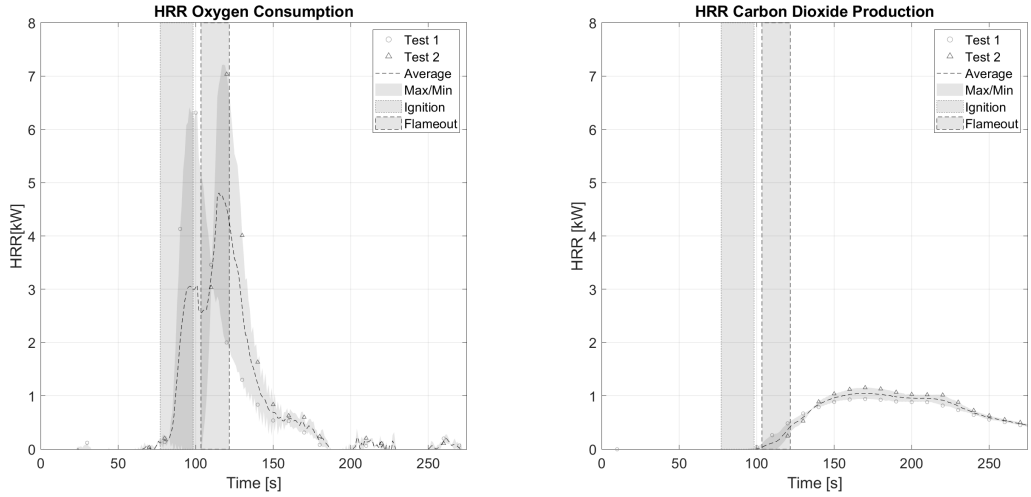

Figure 206: a)Heat release rate - Oxygen Consumption b)Heat release rate - CO2 Production

C.9.2.4 CO2 and CO

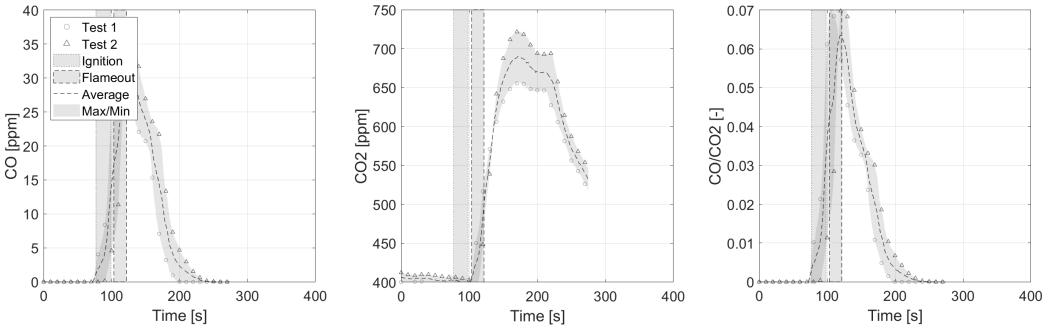

Figure 207: a)CO production b)CO2 production c)CO/CO2

C.10 Open Basket Experiments - Critical Heat Flux - 15g Pinus Rigida (≈7% FMC)

C.10.1 15 kW/m²

C.10.1.1 Mass

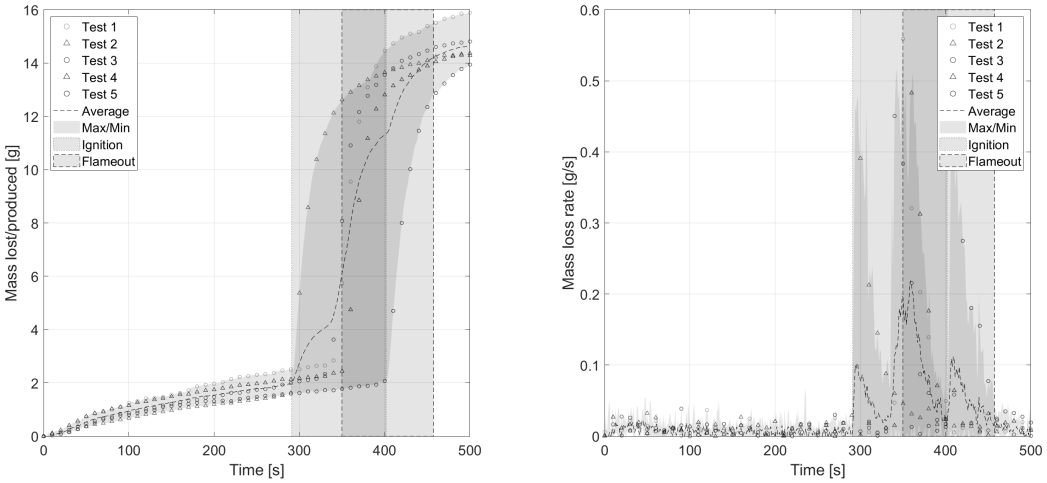

Figure 208: a)Mass b)Mass loss rate

C.10.1.2 Mass Loss Rate at Ignition and Flameout

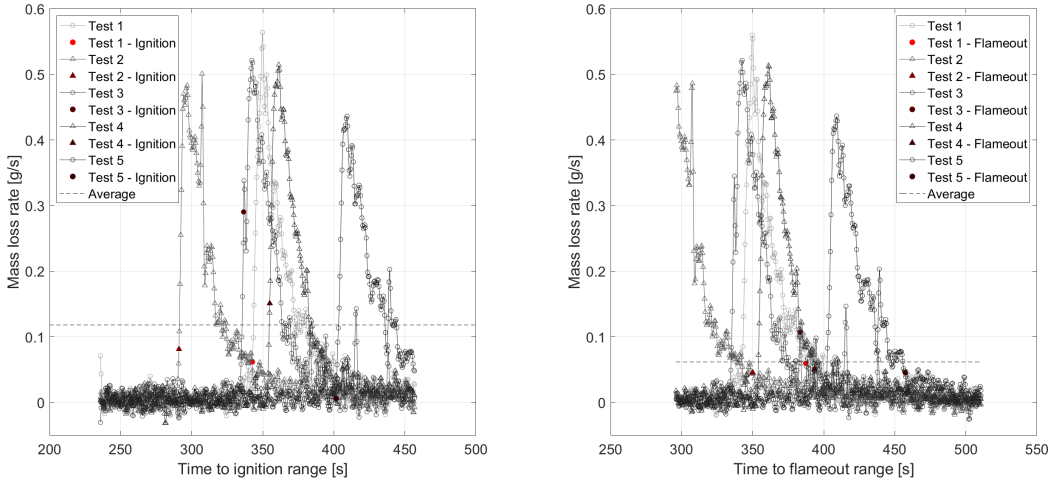

Figure 209: a)Mass loss rate at ignition b)Mass loss rate at flame out

C.10.1.3 Heat Release Rate

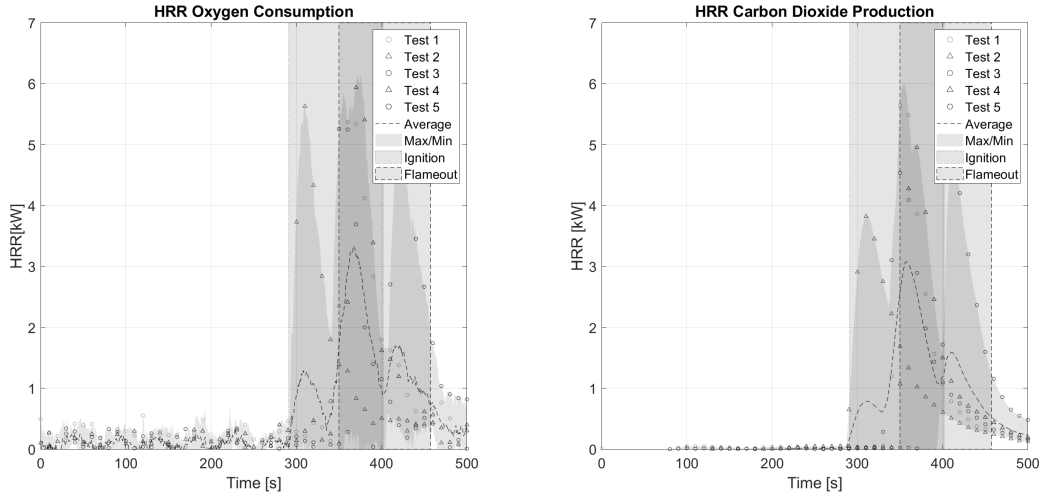

Figure 210: a)Heat release rate - Oxygen Consumption b)Heat release rate - CO2 Production

C.10.2 17 kW/m²

C.10.2.1 Mass

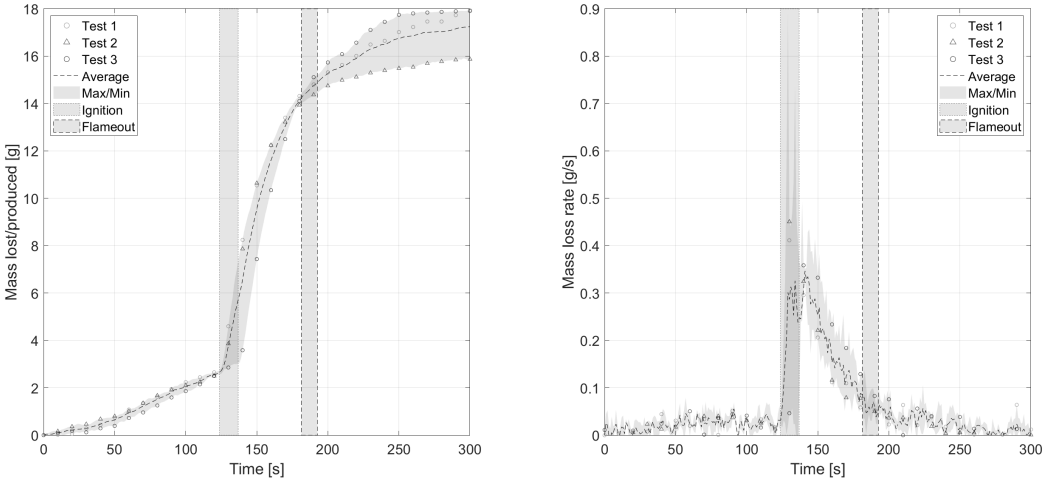

Figure 211: a)Mass b)Mass loss rate

C.10.2.2 Mass Loss Rate at Ignition and Flameout

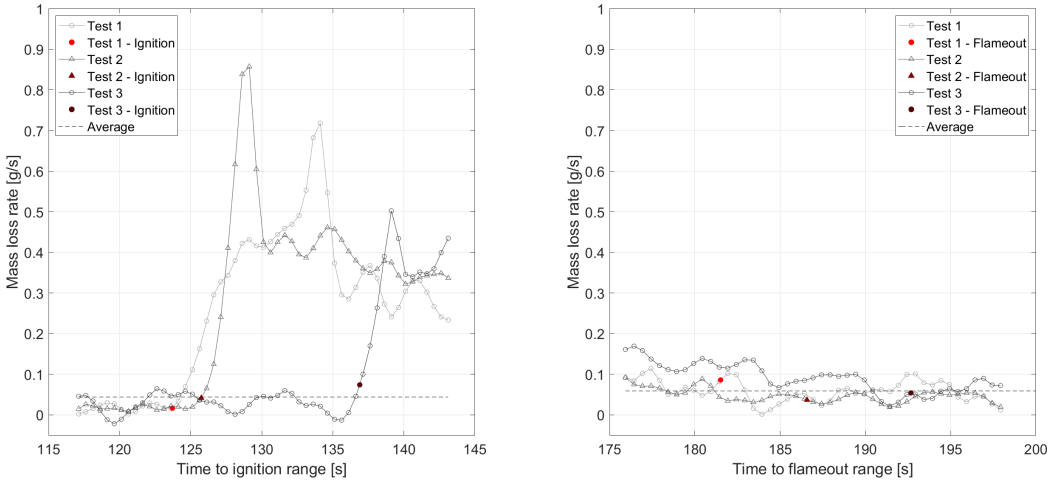

Figure 212: a)Mass loss rate at ignition b)Mass loss rate at flame out

C.10.2.3 Heat Release Rate

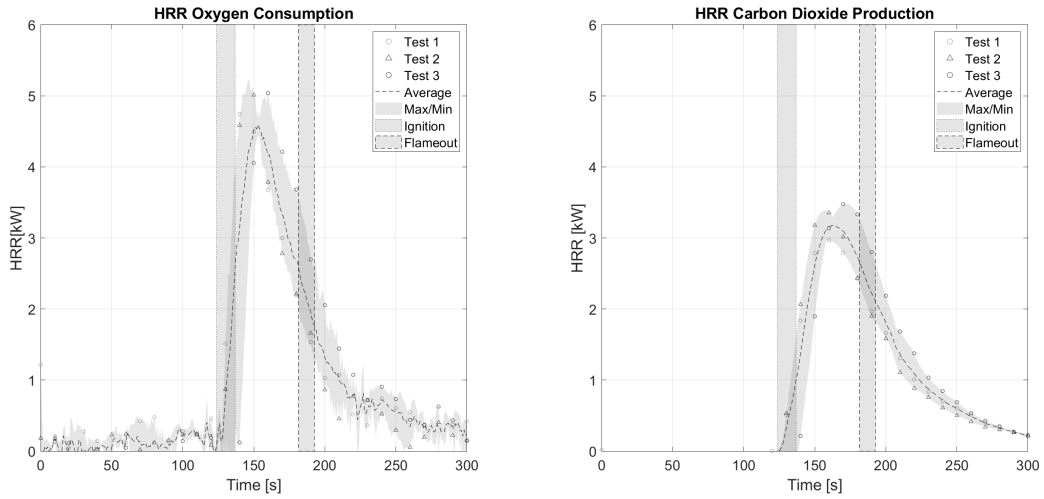

Figure 213: a)Heat release rate - Oxygen Consumption b)Heat release rate - CO2 Production

C.10.2.4 CO2 and CO

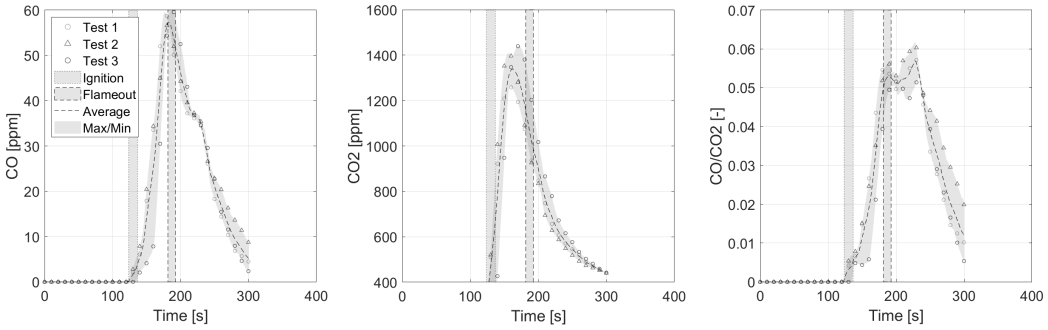

Figure 214: a)CO production b)CO2 production c)CO/CO2

C.10.3 20 kW/m²

C.10.3.1 Mass

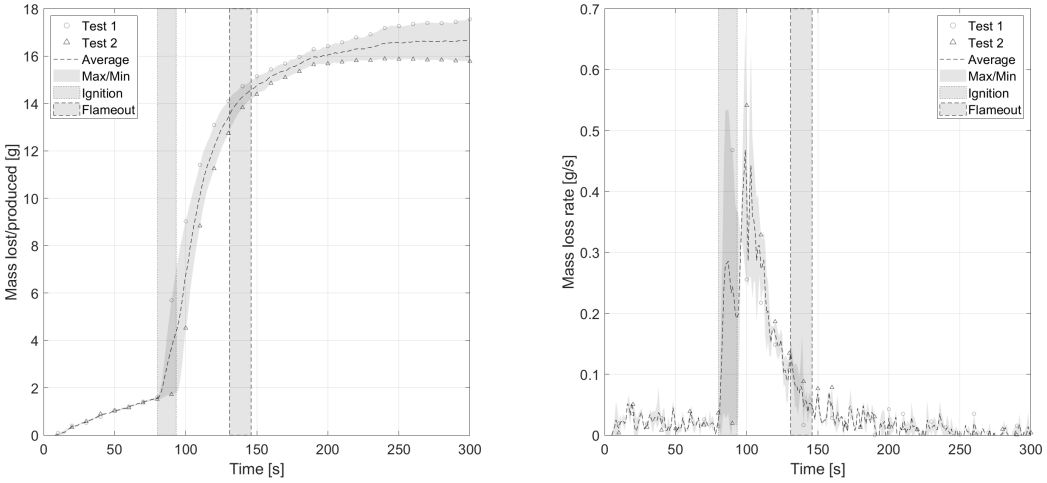

Figure 215: a)Mass b)Mass loss rate

C.10.3.2 Mass Loss Rate at Ignition and Flameout

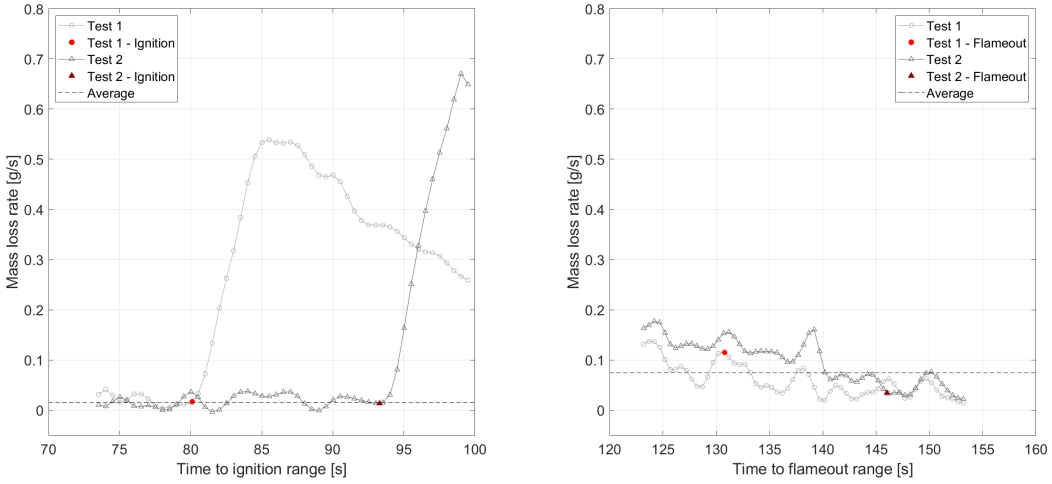

Figure 216: a)Mass loss rate at ignition b)Mass loss rate at flame out

C.10.4 25 kW/m²

C.10.4.1 Mass

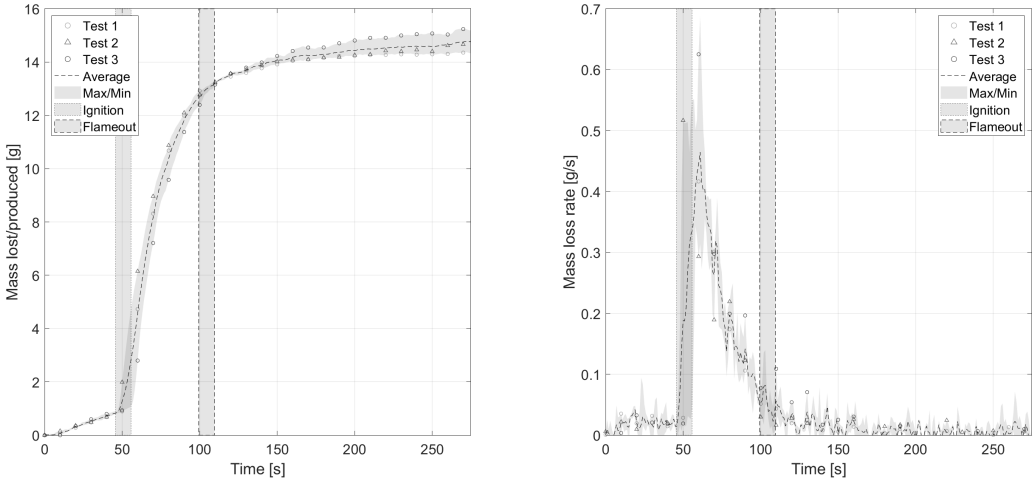

Figure 217: a)Mass b)Mass loss rate

C.10.4.2 Mass Loss Rate at Ignition and Flameout

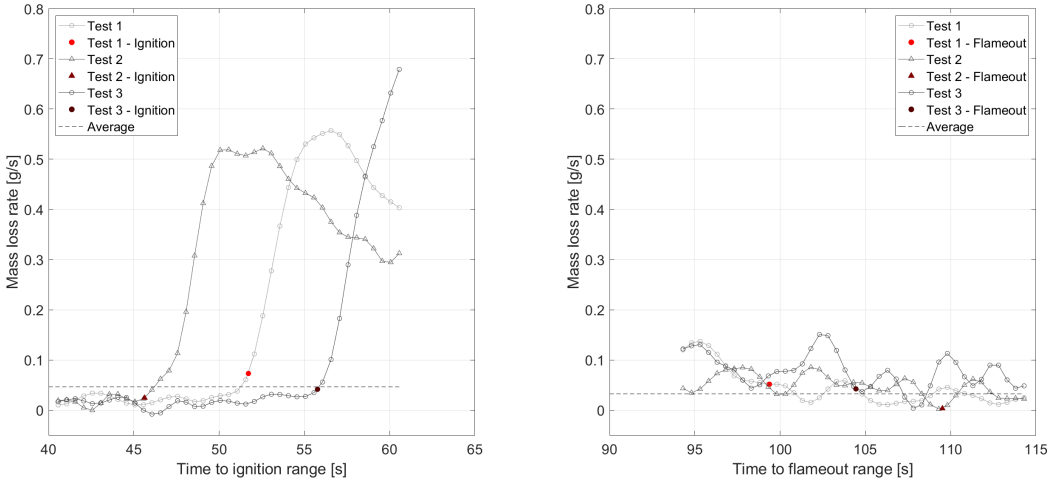

Figure 218: a)Mass loss rate at ignition b)Mass loss rate at flame out

C.10.4.3 Heat Release Rate

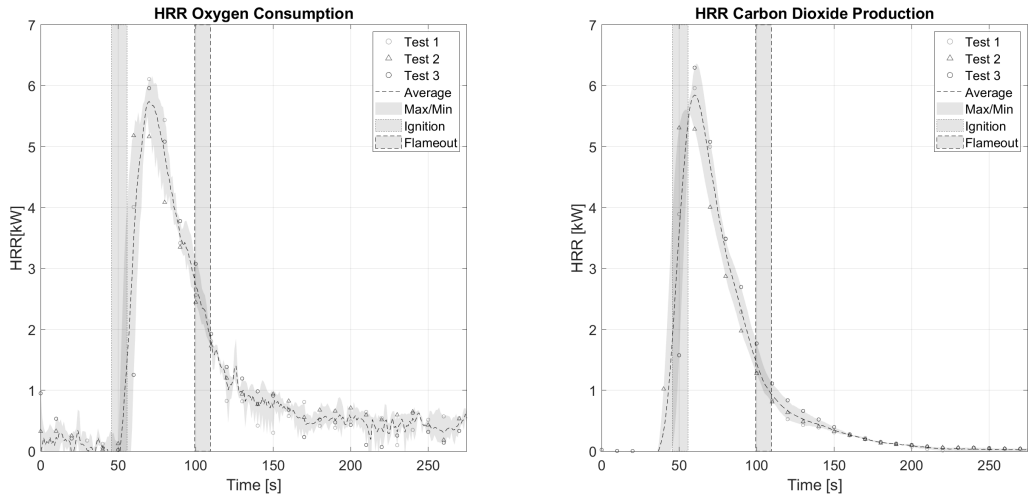

Figure 219: a)Heat release rate - Oxygen Consumption b)Heat release rate - CO2 Production

C.10.4.4 CO2 and CO

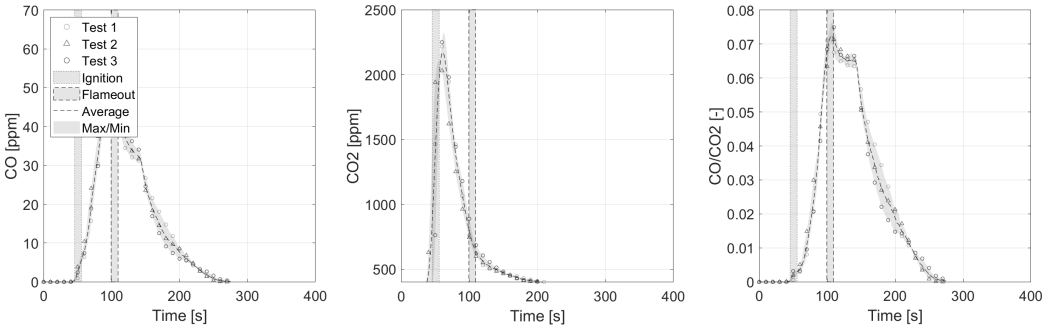

Figure 220: a)CO production b)CO2 production c)CO/CO2

C.10.5 30 kW/m²

C.10.5.1 Mass

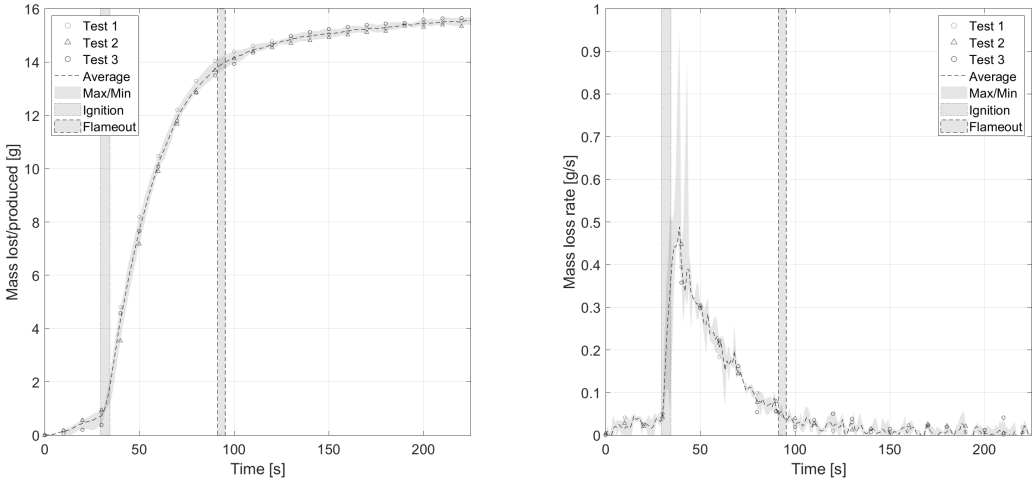

Figure 221: a)Mass b)Mass loss rate

C.10.5.2 Mass Loss Rate at Ignition and Flameout

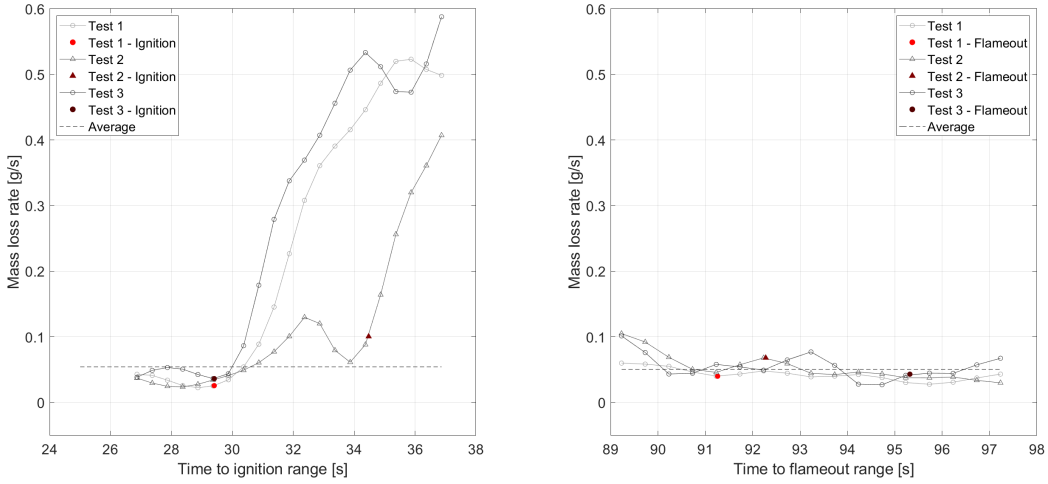

Figure 222: a)Mass loss rate at ignition b)Mass loss rate at flame out

C.10.5.3 Heat Release Rate

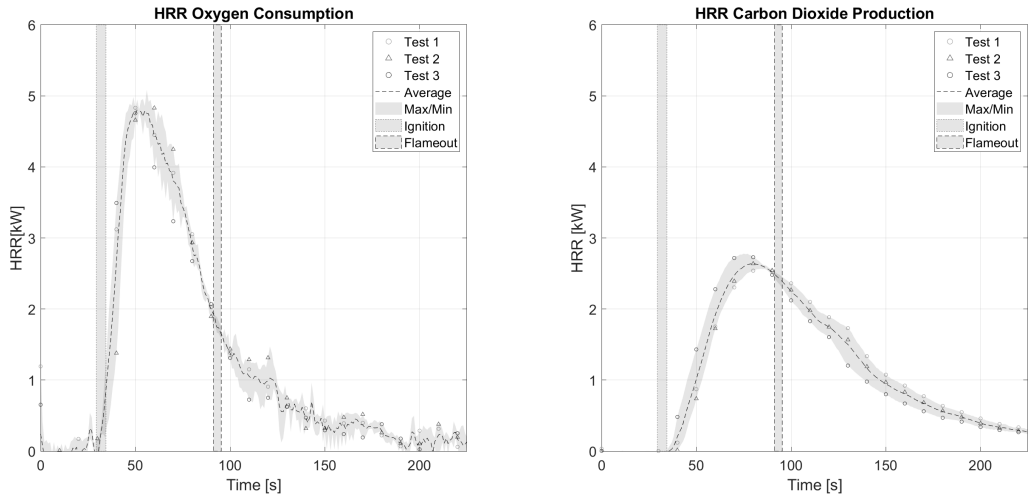

Figure 223: a)Heat release rate - Oxygen Consumption b)Heat release rate - CO2 Production

C.10.5.4 CO2 and CO

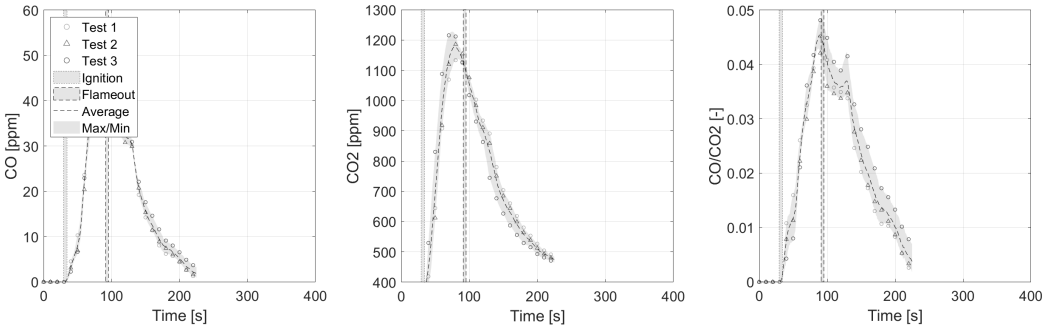

Figure 224: a)CO production b)CO2 production c)CO/CO2

D Pine Needles

D.1 Pinus Rigida

Figure 225: Pinus Rigida needles

D.1.1 Hand Measurements

	L [mm]	w [mm]			t [mm]			wi _avg	ti_avg	m [g]
1	76.0	1.6	1.3	1.1	0.3	0.5	0.6	1.3	0.4	0.01874
2	108.0	1.5	1.3	1.3	0.4	0.4	0.5	1.4	0.4	0.03124
3	112.5	1.4	1.3	1.4	0.4	0.4	0.5	1.4	0.5	0.03356
4	81.0	0.9	1.0	1.1	0.4	0.4	0.3	1.0	0.4	0.02210
5	105.5	0.9	1.3	1.2	0.6	0.5	0.4	1.1	0.5	0.02896
6	78.0	0.9	1.1	0.9	0.2	0.3	0.4	1.0	0.3	0.01564
7	104.0	1.1	1.2	1.2	0.4	0.5	0.4	1.1	0.4	0.02623
8	76.5	1.3	1.2	1.0	0.4	0.5	0.4	1.1	0.4	0.01862
9	103.0	1.2	1.5	1.4	0.6	0.5	0.6	1.4	0.6	0.02711
10	102.5	1.2	1.3	1.2	0.5	0.4	0.4	1.2	0.4	0.02961
11	97.0	1.2	1.4	1.3	0.6	0.6	0.5	1.3	0.6	0.03533
12	92.5	1.2	1.5	1.3	0.6	0.4	0.4	1.3	0.5	0.03215
13	117.5	1.1	1.3	1.3	0.6	0.5	0.5	1.2	0.5	0.04039
14	78.5	0.9	1.0	0.8	0.4	0.4	0.3	0.9	0.4	0.01663
15	89.5	1.4	1.2	1.2	0.6	0.4	0.5	1.3	0.5	0.02502
16	116.0	1.0	1.2	1.2	0.6	0.5	0.5	1.2	0.5	0.04058
17	90.0	1.2	1.2	1.1	0.5	0.6	0.5	1.2	0.5	0.02305
18	121.5	1.3	1.3	1.3	0.4	0.5	0.5	1.3	0.5	0.03421
Average	97.2	-	-	-	-	-	-	1.2	0.5	0.02773

Table 128: Hand measurements of pine needles shown in Figure 225. Numbered from left to right, top to bottom.

D.2 Pinus Halepensis

Figure 226: Pinus Halepensis needles

D.3 Pinus Pinaster

Figure 227: Pinus Pinaster needles

D.4 Pinus Pinea

Figure 228: Pinus Pinea needles

E Arduino Data-Logger

E.1 Temperature Method

One way to interrogate this is to measure the temperature in the fuel bed. This creates more experimental data points to compare with the modelled data. Therefore reducing the degrees of freedom of the solution and enhancing the uniqueness of the optimisation. An approach taken is to use thermocouples to measure the temperature of the fuel bed. Unfortunately, this results in the sacrifice of the mass measurements due to interference of the measuring techniques [107].

In this work a novel proof-of-concept device is presented. Instead of using an external data-logger, a micro-controller (Arduino) data-logger was developed. Similar devices have been used in field work for the characterisation of wildfires [120]. Here instead it is used to improve laboratory equipment. The device is attached to the load cell pedestal directly and as such mitigates the disturbances that disables mass measurements.

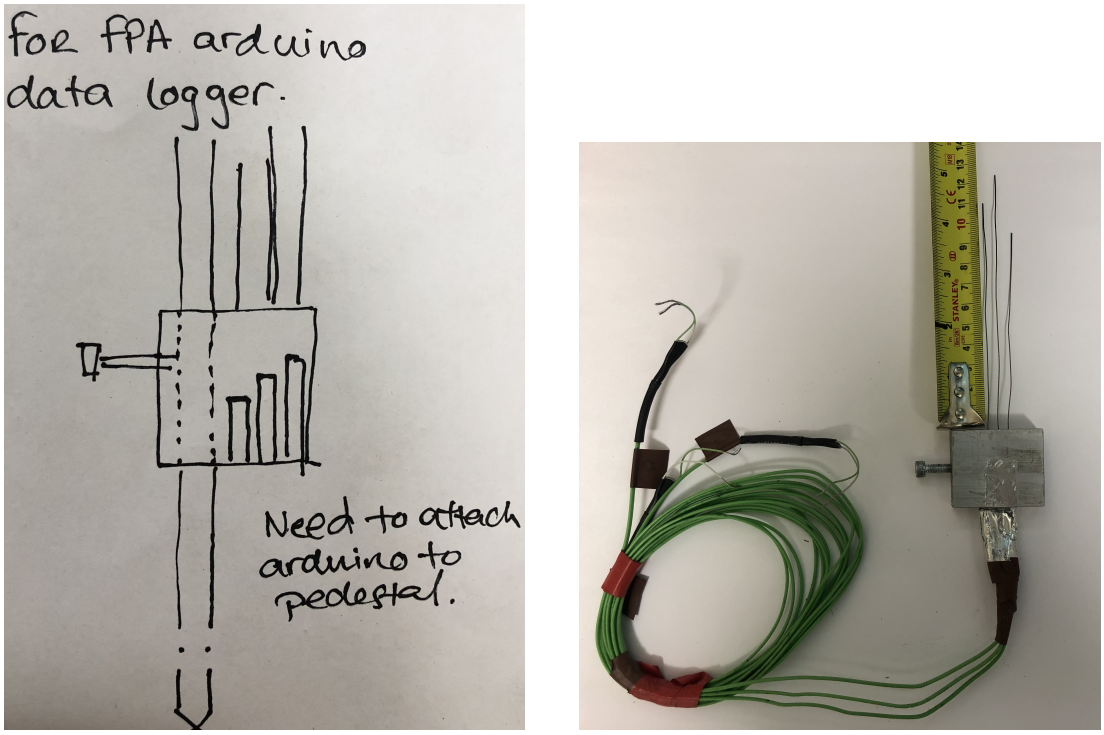

(a) Drawing of device (b) Photo of device

Figure 229: Proof-of-concept device

The device is shown in Figure 229 and code for the data-logger is presented in Appendix E.

However, due to unforeseen circumstances experimental work involving this did not advance beyond initial stages. Nevertheless, on reflection this might not be the most appropriate for porous fuels. This is because of the unresolved questions of precisely what temperature is being measured. Is the thermocouple in contact with a pine needle; in a pore or somewhere in between? How then can the temperature measured inform our model? When our model assumes an effective fuel bed? Nevertheless, one use is to know the location of the fire. A binary 'hot' or 'cold' measurement can be understood but as a measurement of fuel bed temperature...not so much. As such an alternative method for interrogating the fuel bed temperature is sought.

```
// Adafruit Writing libraries
#include <Adafruit_I2CDevice.h>
#include <Adafruit_I2CRegister.h>
#include <Adafruit_SPIDevice.h>
#include <Adafruit_BusIO_Register.h>
#include "Adafruit_MAX31855.h"
// Adafruit library setup
#ifdef __avr__
#include <avr/pgmspace.h>
#include <util/delay.h>
#endif
#ifdef __arm__
#define _delay_ms(ms) delayMicroseconds((ms) * 1000)
#endif

// Standard Arduino libraries
#include <stdlib.h>
#include <SPI.h>
#include <SD.h>

// SD Card Pin
#define cardSelect 4

// Thermocouple
#define MAXDO   10 // Data Output Pin
#define MAXCLK  9 // Clock Pin

#define MAXCS_1   13 // Click Selector Pin
#define MAXCS_2   12 // Click Selector Pin
#define MAXCS_3   11 // Click Selector Pin

Adafruit_MAX31855 thermocouple_1(MAXCLK, MAXCS_1, MAXDO); // ...
    Initialise Thermocouple object
Adafruit_MAX31855 thermocouple_2(MAXCLK, MAXCS_2, MAXDO); // ...
    Initialise Thermocouple object
Adafruit_MAX31855 thermocouple_3(MAXCLK, MAXCS_3, MAXDO); // ...
    Initialise Thermocouple object

// Logfile
File logfile;

// Blink out an error code
void error(uint8_t errno) {
  while (1) {
    uint8_t i;
    for (i = 0; i < errno; i++) {
      digitalWrite(13, HIGH);
      delay(100);
      digitalWrite(13, LOW);
      delay(100);
    }
    for (i = errno; i < 10; i++) {
      delay(200);
    }
  }
```

```
53 }
54
55 // Setup
56 void setup() {
57
58   // connect at 115200
59   // also spit it out
60   Serial.begin(115200);
61   Serial.println("\r\nAnalog logger test");
62   pinMode(13, OUTPUT);
63   pinMode(11, INPUT); // Set pin 11 input logger
64
65   // See if the card is present and can be initialized:
66   if (!SD.begin(cardSelect)) {
67     Serial.println("Card init. failed!");
68     error(2);
69   }
70   char filename[15];
71   strcpy(filename, "/ANALOG00.TXT");
72   for (uint8_t i = 0; i < 100; i++) {
73     filename[7] = '0' + i / 10;
74     filename[8] = '0' + i % 10;
75     // Create if does not exist, do not open existing, write, ...
          sync after write
76     if (! SD.exists(filename)) {
77       break;
78     }
79   }
80
81   // Start logfile
82   logfile = SD.open(filename, FILE_WRITE);
83   if ( ! logfile ) {
84     Serial.print("Couldnt create ");
85     Serial.println(filename);
86     error(3);
87   }
88   Serial.print("Writing to ");
89   Serial.println(filename);
90
91   pinMode(13, OUTPUT);
92   pinMode(8, OUTPUT);
93   Serial.println("Ready!");
94 }
95
96 // Loop
97 uint8_t i = 0;
98 void loop() {
99
100   // SD Card Out
101   digitalWrite(8, HIGH);
102
103   // Output
104   Serial.println(String(millis()) +",it" + String(i) + ",");
105   logfile.println(String(millis()) +",it" + String(i) + ",");
106
107   Serial.print("T_1int = ");
```

```
  logfile.print("T_1int = ");

  Serial.println(String(thermocouple_1.readInternal())+ ",");
  logfile.print(String(thermocouple_1.readInternal())+ ",");

    Serial.print("T_2int = ");
  logfile.print("T_2int = ");

  Serial.println(String(thermocouple_2.readInternal())+ ",");
  logfile.print(String(thermocouple_2.readInternal())+ ",");

  Serial.print("T_3int = ");
  logfile.print("T_3int = ");

  Serial.println(String(thermocouple_3.readInternal())+ ",");
  logfile.print(String(thermocouple_3.readInternal())+ ",");

  // SD Card out
  digitalWrite(8, LOW);

  // Read temp
  double c1 = thermocouple_1.readCelsius();
  double c2 = thermocouple_2.readCelsius();
  double c3 = thermocouple_3.readCelsius();
  if (isnan(c1)||isnan(c2)||isnan(c3)) {
    Serial.println("Something wrong with thermocouple!");
     logfile.println("Something wrong with thermocouple!");
  } else {
    Serial.print(" C1 = ");
    logfile.print(" C1 = ");
    Serial.print(String(c1) + ",");
    logfile.print(String(c1) + ",");

    Serial.print(" C2 = ");
    logfile.print(" C2 = ");
    Serial.print(String(c2) + ",");
    logfile.print(String(c2) + ",");

    Serial.print(" C3 = ");
    logfile.print(" C3 = ");
    Serial.println(String(c3) + ",");
    logfile.println(String(c3) + ",");
  }

  if (i % 100) { // Flush file every 100 iterations
    logfile.flush();
  }

  // Sleep
  delay(100);

  // Update Counter
  i++;
```

F Genetic Algorithm

```
clear all
close all

% M. El Houssami pitch pine properties.
% SVR       = 7296      %m-1
% rho       = 607       %kg/m3
% lambda    = 0.12      %W/mK
% a         = 0.64      %
% chi       = 10 - 20   %W/m2K
% cp        = 2069.7    %J/kgK

sv = 1                  %saving parameter.
%% Initialise
%Mass data.
m_wet           = [7.5 15 35 60 95 120]; %   [g]
cond            = 1;
n_cond         = length(m_wet);

%Experiment geometric prop.
D               = 128;                      % [mm] Diameter
thickness       = 30;                       % [mm] Thickness

%Discretisation of depth
x               = linspace(0,thickness,151);% [mm]
x               = x(1:end-1);               %Define cell position as the top face.

%t is defined per condition so it is in the while loop below.

Area            = 0.25*pi()*D^2;            %   [mm2]
Vol             = Area * thickness;         %   [mm3]
dVol            = Area*diff(x(1:2));        %   [mm3] Cell volume

%% Genes definition
n = 8;  %genes
N = 100; %individuals
lastgen = 500;
chi = 3;

% Define limits of the search space for each gene.

k_A_max =   1.2*10^-4;      % [W/mmK]
k_A_min =   k_A_max;
k_B_max =   0;
k_B_min =   0;
h_A_max =   4*10^-5;        % [W/mm2K]
h_A_min =   2*10^-5;
h_B_max =   0;
h_B_min =   -2*10^-5;
a_A_max =   0.64;           % [-]
a_A_min =   a_A_max;
a_B_max =   0;              % Be careful this does not cause a>1
a_B_min =   0;
c_A_max =   2.0697;         % [J/gK]
c_A_min =   c_A_max;
c_B_max =   0;
c_B_min =   0;

a_bounds = [k_A_max, k_B_max, h_A_max, h_B_max,...
    a_A_max, a_B_max, c_A_max, c_B_max;...
    k_A_min, k_B_min, h_A_min, h_B_min,...
    a_A_min, a_B_min, c_A_min, c_B_min];

amax = max(a_bounds);
amin = min(a_bounds);


```

```
%Initialise variables:
A       = zeros(N,n);    % Parent population
B       = zeros(N,n);    % Sorted population
C       = zeros(N,n);    % Selected Individuals
D       = zeros(N,n);    % Off-Spring
R       = zeros(N,n_cond);  % Residual
e       = zeros(1,n_cond);  % Solid fraction
R_tot   = zeros(N,1);       % Total residual

%% Generation 1 Parents
r1 = rand(N,n);
A = amin + r1.*(amax-amin); % Each row in A represents a set of input ...
    parameters for the model.

%% Genetic Algorithm
for generation = 2:lastgen
    generation
    individual = 1;
    while individual ≤N % Considering each individual.
        if individual == 0
            individual = 1; % This is to ensure the index is correct.
        end
        %% model
        %constants
        while cond ≤ n_cond %Each individual is subjected to all conditions.
            m                = m_wet(cond);
            [exp, exp_mean]  = assignMass(m);            % exp values.
            t                = [0.5:0.5:exp_mean(end,1)]'; %time discretised ...
                using the average time to ignition.

            FMC              = 0; % [%] % reality = 1%. However exp data is ...
                m_exp = m_wet + mass loss rate;

            m_dry            = m/(1+FMC);        % [g]
            rho_bulk         = m_dry/Vol;        % Bulk density
            rho              = 607 *10^-6;       % Material density [M El H]
            e(cond)          = m_dry/(rho*Vol);  % Solid fraction

            I                = 0.025;            % [W/mm2]
            Tamb             = 25;               % [ C ]

            k_A = A(individual,1); % Conductive gene - Function param 1
            k_B = A(individual,2); % Conductive gene - Function param 2
            H_A = A(individual,3); % Convective gene - Function param 1
            H_B = A(individual,4); % Convective gene - Function param 2
            a_A = A(individual,5); % Absorbtivity gene - Function param 1
            a_B = A(individual,6); % Absorbtivity gene - Function param 2
            c_A = A(individual,7); % Storage gene - Function param 1
            c_B = A(individual,8); % Storage gene - Function param 2

            %Calculation of effective parameters at each experimental condition.
            k    = k_A + k_B*e(cond);
            H    = H_A + H_B*e(cond);
            a    = a_A + a_B*e(cond);
            cp   = c_A + c_B*e(cond);

            [T_S, m_S] = SimmsDist(x, t,dVol, I, Tamb, rho_bulk, cp, k, H, a );

            sum_m_S = sum(m_S,2)';

            R(individual,cond) = ResProDeriv(exp, exp_mean, ...
                sum_m_S);%proportional and derivative residual.
            cond = cond +1 ; % consider next condition
        end

        R_tot(individual) = sum(R(individual),2);  %Total residual for each ...
            individual. i.e. residual at each condition summed.
        individual = individual + 1; % consider next individual
        cond = 1; % consider first condition

```

```
132
133     end
134
135     %% Selection -> Parent Matrix
136
137     [R_sorted, Rss] = sort(R_tot,'descend');
138     B = A(Rss,:); % sorting population
139
140     if generation ==2
141         R_best       = R_sorted(1);
142         R_best(1)    = R_sorted(1);
143         A_best(1,:)  = B(1,:);
144         G_best(1)    = generation;
145     end
146
147     if R_sorted(1) > R_best(end)
148         R_best(end+1)    = R_sorted(1);
149         A_best(end+1,:)  = B(1,:);
150         G_best(end+1)    = generation;
151     end
152
153     p_sel   = R_sorted./sum(R_tot);   % Probability of selection
154     q       = cumsum(p_sel,'reverse');% Cumulative
155
156
157     counter     = zeros(N,1);%counter for each individual
158     S           = 5; % Repeat Parent Limit
159     individualC = 1; % C is the Selected Parent Matrix. An individual can be ...
            be a parent S times.
160
161
162     bst = 5;                                % Force 5 best candidates.
163     C(1:bst,:)      = B(1:bst,:);           % Selection of 5 best candidates
164     counter(1:bst)  = counter(1:bst) +1;    % Best 5 selected +1
165     indiviudalC     = bst+1;                % Considering 6th individual for ...
            parent matrix
166
167     while individualC  ≤ N
168         r2          = 0.90 + 0.2*(rand()-0.5);  % Randomly select candidates ...
                above 0.8
169         selection   = find(r2<q, 1,'last');
170
171         while counter(selection)≥S
172             r2          = rand();               % If selected more than S ...
                    times. Then randomly select any candidate.
173             selection   = find(r2<q, 1,'last');
174         end
175         counter(selection) = counter(selection) + 1; % If selected increase ...
                individuals counter +1
176
177         if counter(selection) < S %if less than the Parent limit
178             C(individualC,:) = B(selection,:);
179             individualC = individualC +1; % Move onto the next individual in C ...
                    nb size(C)=size(B)
180         end
181
182     end
183
184     %% Offspring Matrix
185     shuffleC = randperm(N);
186     C(shuffleC,:) = C(:,:);
187     r3 = rand(N/2,n)-0.5;
188
189     D(1:2:end,:) = r3.*C(1:2:end,:)+(1-r3).*C(2:2:end,:);
190     D(2:2:end,:) = r3.*C(2:2:end,:)+(1-r3).*C(1:2:end,:);
191
192     %% Mutation
193     pmut = 0.015;   % mutation probability
194     vmut = 0.1;     %mutation factor
195     r4 = rand(N,n);
```

```
196
197     for i = 1:N % Each individual
198         for j = 1:n % Each gene
199             if pmut≥r4(N,n)
200                 if rand≥0.5
201                     D(i,j) = amin(j) + rand.*(amax(j)-amin(j)); % re-roll
202                 else
203                     D(i,j) = D(i,j) + (rand-0.5)*vmut*(amax(j)-amin(j)); % ...
                            excursion
204                 end
205             end
206
207             if D(i,j)<amin(j) || D(i,j)>amax(j) % If outside search bounds.
208                 D(i,j) = amin(j) + rand.*(amax(j)-amin(j)); % re-roll
209             end
210         end
211     end
212
213     %% Replacement
214     A = D;
215     stor(sv,:) = [R_sorted(1),B(1,:)]; % Save best.
216     sv = sv+1;
217
218 end
```